PATHOPHYSIOLOGICAL ROLE OF MICRORNA-29

IN PANCREATIC DUCTAL ADENOCARCINOMA

Jason Jae-Hyuk Kwon

Submitted to the faculty of the University Graduate School
in partial fulfillment of the requirements
for the degree
Doctor of Philosophy
in the Department of Medical and Molecular Genetics,
Indiana University

July 2018

Accepted by the Graduate Faculty of Indiana University, in partial fulfillment of the requirements for the degree of Doctor of Philosophy.

Doctoral Committee

_____
Janaiah Kota, Ph.D., Chair

_____
Murray Korc, M.D.

May 23, 2018

_____
Yunlong Liu, Ph.D.

_____
Ronald Wek, Ph.D.

DEDICATION

This dissertation is dedicated to all those who have suffered the loss of a loved one due to cancer. I humbly hope that the findings of this dissertation provide even the minutest contribution towards finding a cure.

ACKNOWLEDGEMENT

I express my sincerest appreciation to all of the faculty members and administrative staff of the Indiana University School of Medicine, including the Indiana Biomedical Gateway Program and Medical and Molecular Genetics Department. To my committee members, Dr. Ronald Wek, Dr. Yunlong Liu, and Dr. Murray Korc, I am especially thankful for all of their time, intellectual input, resource sharing, and efforts in providing countless letters of recommendations, all of which has provided invaluable support to my research work, academic growth and career development. To Dr. Janaiah Kota, I am eternally grateful for his belief in me, and putting forth the patience and effort to train me. None of this work would have been possible without his guidance and the intellectual support he has provided. Dr. Kota has taught me that due diligence and hard work always prevails in the end and that science is nothing without a sincere desire to contribute towards bettering humanity. In addition to the scientific training, his wisdom and personal advice he has shared with me will stay with me for the rest of my life.

Finally, I have been blessed with family and friends who love and support me in all the ways that one could ever hope for. To my mother, father, sisters, and Christine, I am eternally grateful for their sacrifices, unwavering patience, and constant support throughout my life. To all of my friends, I am appreciative for all the times they have helped me decompress and provided a counterpoint of balance to my life.

Jason Jae-Hyuk Kwon

PATHOPHYSIOLOGICAL ROLE OF MICRORNA-29

IN PANCREATIC DUCTAL ADENOCARCINOMA

Pancreatic ductal adenocarcinoma (PDAC) is a highly lethal malignancy and responds poorly to current therapies. Thus, it is imperative to develop novel treatments for PDAC. Dense fibrotic stroma associated with PDAC abrogates drug perfusion into the tumor, and pancreatic stellate cells (PSCs) are the major stromal cells responsible for fibrosis. Activated PSCs produce pro-inflammatory factors and secrete an excessive amount of extracellular matrix (ECM) proteins, the major stromal proteins in PDAC.

MicroRNAs (miRNAs) are conserved small non-coding RNAs that regulate gene expression by binding to the 3′UTR of target mRNA transcripts, causing translational repression or degradation. A single miRNA regulates several targets within intracellular networks and can have a profound impact on normal physiology.

miR-29 has been previously reported to have anti-fibrotic and tumor suppressive roles in various cancers. We found miR-29 expression was significantly decreased in activated PSCs and pancreatic cancer cells *in vitro*, *in vivo* models, as well as in PDAC patient biopsies. Through *in vitro* studies in activated PSC, we found that miR-29 inhibited the expression of ECM proteins and reduced cancer growth when co-cultured with pancreatic cancer cells. miR-29 overexpression in pancreatic cancer cells decreased their invasive potential and sensitized chemoresistant cancer cells to gemcitabine treatment by inhibiting autophagy through the direct targeting of two essential, autophagy related genes, TFEB and ATG9A.

In developing therapies and for *in vivo* functional studies, viral-based gene delivery is a powerful tool to target the pancreas. We tested various self-complementary recombinant adeno-associated virus (scAAV) serotypes in normal mice (C57BL/6) and in a $Kras^{G12D}$-driven pancreatic cancer mouse model via systemic and intraductal delivery methods. We found that retrograde intraductal delivery of scAAV6 safely targeted the pancreas/neoplasm with the greatest efficiency.

Our findings provide a better understanding of miR-29 in pancreatic cancer and demonstrates its potential therapeutic use to target PDAC.

Janaiah Kota, Ph.D., Chair

TABLE OF CONTENTS

List of Tables ix
List of Figures x
List of Abbreviations xiii
Chapter 1: Introduction 1
1.1 The Current State of Pancreatic Cancer: Prognosis and Treatment Strategies 1
1.2 Tumor Stroma and its Role in PDAC Progression 2
1.3 Autophagy in Pancreatic Cancer 7
1.4 miRNA Biology and the miR-29 Family 8
1.5 In Vivo Function of miR-29 13
1.6 Statement of Purpose 14
Chapter 2: Pathophysiological Role of miR-29 in Pancreatic Cancer Stroma 17
2.1 Introduction 17
2.2 Materials and Methods 19
2.3 Results 27
2.4 Discussion 66
Chapter 3: Novel Role of miR-29a in Pancreatic Cancer Autophagy and its Therapeutic Potential 72
3.1 Introduction 72
3.2 Materials and Methods 74
3.3 Results 79
3.4 Discussion 115
Chapter 4: Safety and Efficacy of AAV Retrograde Pancreatic Ductal Gene Delivery in Normal and Pancreatic Cancer Mice 121
4.1 Introduction 121
4.2 Materials and Methods 124
4.3 Results 129
4.4 Discussion 149
Chapter 5: Summary and Future Directions 155
5.1 The Role of miR-29 in PDAC Stroma 155
5.2 The Role of miR-29 in PDAC Autophagy 156
5.3 Mechanisms of miR-29 in Pancreatic Cancer Cell Migration Potential 157
5.4 The Need for miR-29 *In Vivo* Validation 159
5.5 The Pragmatism of miRNA-Based Therapies 160
5.6 Controversies of miR-29 in Cancer 161
5.7 Concluding Remarks 163
References 164
Curriculum Vitae

LIST OF TABLES

Table 1. Clinical PDAC Patient Data 40
Table 2. Clinical Sample ID and Information.....41
Table 3. Comparison of scAAV6 and scAAV9 pancreatic transduction efficiency via retrograde intraductal delivery (vector genomes/nuclei) 139
Table 4. Percentage Long-term GFP expression Retrograde Pancreatic Intraductal Delivery of scAAV6 143
Table 5. Histological analysis of B cell activation (B220) in retrograde pancreatic intraductally infused KC mice. 147

LIST OF FIGURES

Figure 1. Pathogenesis of Pancreatic Cancer and its Associated Stroma 6
Figure 2. Schematic representation of the miR-29 family members: miR-29a, -29b, and -29c 12
Figure 3. miR-29 studies in cancer pathogenesis.....16
Figure 4. TGF-β1-mediated activation of PSCs leads to downregulation of miR-29 and increases ECM protein expression.....29
Figure 5. miR-29 expression analysis in an additional mouse PSC cell line.....31
Figure 6. TGF-β1 mediated activation of human PSCs leads to an increase in pSMAD2/3 expression levels. 32
Figure 7. TGF-β1 activated PSCs exhibit increased expression of ECM components at the mRNA and protein level. Current miR-29 studies in cancer.....33
Figure 8. TGF-β1 downregulates miR-29 in human fibroblasts and cancer associated fibroblasts. 35
Figure 9. Global loss of miR-29 is a common phenomenon of KrasG12D-activated murine pancreata and human PDAC tumors with increased collagen deposition. 37
Figure 10. Pancreatic tissues from PDAC patient samples display a high degree of fibrosis.....39
Figure 11. miR-29a is the most abundantly expressed miR-29 family member in pancreatic stellate cells, pancreatic ductal epithelial cells, and the whole pancreas.....44
Figure 12. PSC and epithelial cell specific miR-29 loss of expression in human PDAC tumors.....45
Figure 13. miR-29a is decreased in GFAP-positive PSCs in KC mice 46
Figure 14. miR-29a is decreased in CK19-positive epithelial cells in KC mice 47
Figure 15. Mouse and human PSCs transfected with miR-29 mimics have increased exogenous miR-29a and miR-29b 50
Figure 16. Physiological role of miR-29 in PSC-mediated stromal ECM protein accumulation.....51
Figure 17. Ectopic expression of miR-29 mimics reduce ECM components in TGF-β1 activated mouse PSCs.....53
Figure 18. miR-29 suppresses SMAD2 activation in mouse PSCs 54
Figure 19. LNA-miR-29 efficiently knockdown all endogenous miR-29 family members (miR-29a, miR-29b, and miR-29c) in mouse and human PSCs. 55
Figure 20. miR-29 knockdown increases direct miR-29 ECM target proteins in mouse PSCs 56
Figure 21. Ectopic expression of miR-29 in PSCs reduces cancer cells viability and cancer colony growth in co-culture.....59
Figure 22. Ectopic expression of miR-29 in PSCs causes reduced cancer colony formation and stromal deposition in direct co-cultures 60
Figure 23. Ectopic miR-29 expression does not affect PSC viability.....61
Figure 24. miR-29 decreases the effect of PSCs on anchorage independent growth of pancreatic cancer cells.....62
Figure 25. TGF-β1-mediated downregulation of miR-29 expression in PSCs is SMAD3 dependent.....64
Figure 26. miR-29a increased sensitivity of chemoresistant PDAC cells to

gemcitabine treatment 82
Figure 27. miR-29a is the most abundantly expressed miR-29 family member in human pancreatic normal epithelial cell line 84
Figure 28. Effect of miR-29a overexpression and gemcitabine treatment on COLO 357 cell viability 85
Figure 29. LDH release in MIA PaCa-2 cells treated with gemcitabine in combination with miR-29a. 86
Figure 30: Caspase3/7 activity and activated caspase 3 levels in MIA PaCa-2 cells treated with gemcitabine in combination with miR-29a 87
Figure 31. miR-29a overexpression causes blockage in autophagy flux 91
Figure 32. miR-29a overexpression inhibits autophagic flux in MIA PaCa-2 and COLO 357 cells 92
Figure 33. p62 transcriptional expression is unaltered by miR-29a overexpression in Panc-1 and COLO 357 cells 93
Figure 34. Effect of CQ and BafA1 on Panc-1 and MIA PaCa-2 autophagy 94
Figure 35. Effect of miR-29a, CQ, and BafA1 on sensitization of MIA PaCa-2 cells to gemcitabine treatment 95
Figure 36. miR-29a blocks gemcitabine induced autophagy in Panc-1 and MIA PaCa-2 96
Figure 37. miR-29a inhibits autophagosome-lysosome fusion 98
Figure 38: LC3B puncta quantification in miR-29a overexpressing Panc-1 cells 99
Figure 39: 2D representative images of LC3B and LAMP-2 colocalization in miR-29a overexpressing Panc-1 cells 100
Figure 40. miR-29a downregulates TFEB and ATG9A to inhibit autophagy 104
Figure 41. Effect of miR-29a overexpression on TFEB and ATG9A expression in MIA PaCa-2 and COLO 357 cells 106
Figure 42. ATG9A and TFEB expression in HPNE, Panc-1, MIA PaCa-2, and AsPC-1 107
Figure 43. Effect of TFEB and ATG9A knockdown on autophagy of MIA PaCa-2 cells 108
Figure 44. Knockdown of TFEB and ATG9A results in decreased autophagosomal-lysosomal fusion 109
Figure 45. miR-29a inhibits invasive potential of PDAC cells 112
Figure 46. Effect of miR-29a overexpression on migration and invasion of MIA PaCa-2 cells 113
Figure 47. Effect of miR-29a overexpression on anchorage independent growth of MIA PaCa-2 cells 114
Figure 48. Schematic diagram representing the role of miR-29a in PDAC autophagy and metastasis 120
Figure 49. Comparison of scAAV8 and AAV9 to Target the Pancreas via Systemic Delivery 131
Figure 50. Assessment of off-target effects for AAV9 systemic delivery and AAV6 retrograde pancreatic intraductal delivery 132
Figure 51. Optimization of Retrograde Intraductal Infusion via Catheterizing the Common Bile Duct through the Gallbladder and Cystic Duct 136
Figure 52. scAAV6 Has Increased Specificity in Transducing the Pancreas

Compared with scAAV9 C57BL/6 mice were dosed with scAAV6.GFP or scAAV9.GFP at 5 x 10^{11} vg/animal....138
Figure 53. Retrograde pancreatic intraductal delivery of scAAV6 targets KC mice pancreata at early timepoint (3 weeks post-injection)....141
Figure 54. Retrograde Pancreatic Intraductal Delivery of scAAV6 Targets Acinar, Epithelial, and Stromal Cells and Shows Long-Term Gene Expression in PDAC Mice....142
Figure 55. Retrograde Pancreatic Intraductal Delivery is Safe and Does Not Induce Chronic Pancreatitis....146
Figure 56. Retrograde Pancreatic Intraductal Delivery has No Effect on PDAC Progression in KC mice....148

LIST OF ABBREVIATIONS

α-SMA	alpha smooth muscle actin
AAHRPP	Accreditation of Human Research Protection Programs
AAV	adeno-associated virus
AGO	Argonaut
AMY2	amylase
ANOVA	analysis of variance
ATG9A	autophagy-related protein 9A
BafA1	bafilomycinA1
BVDV	bovine diarrhea virus
CAF	cancer associated fibroblast
Cal	calcipotriol
CCK8	Cell Counting Kit-8
CK19	cytokeratin 19
CMV	cytomegalovirus
COL1A1	collagen 1a1
COL3A1	collagen 3a1
CRISPR	clustered regularly interspaced short palindromic repeats
CTCF	corrected total cell fluorescence
CTGF	connective tissue growth factor
CTRL	control
DAPI	4',6-Diamidino-2-Phenylindole, Dihydrochloride
DMEM	Dulbecco's Modified Eagle's Medium

dsAAV	double-stranded adeno-associated virus
ECM	extracellular matrix
EMT	epithelial-mesenchymal transition
ERCP	endoscopic retrograde cholangiopancreatography
FBS	fetal bovine serum
FDA	Food and Drug Administration
FFPE	formalin fixed paraffin embedded
FN1	fibronectin
FOLFIRINOX	folinic acid, 5-fluorouracil, irinotecan and oxaliplatin
GEM	gemcitabine
GEMM	genetically engineered mouse model
GFAP	glial fibrillary acidic protein
GFP	green fluorescent protein
H&E	Hematoxylin and Eosin
HCQ	hydroxychloroquine
HDAC4	histone deacetylase 4
HIER	heat-induced epitope retrieval
hPSC	human pancreatic stellate cell
IgG	immunoglobulin G
IHC	immunohistochemistry
IL	interleukin
INS	insulin
IRB	Institutional Review Board

ITGB1	integrin beta 1
KC	*Kras*^{G12D}; *Pdx1-Cre*
KO	knockout
LAMC1	laminin
LAMP-2	lysosomal-associated membrane protein 2
LC3	microtubule-associated protein 1 light chain 3
LDH	lactate dehydrogenase
LNA	locked nucleic acids
MET	mesenchymal-epithelial transition
miR-29	microRNA-29
miRNA	microRNA
MMP2	matrix metallopeptidase 2
mPSC	mouse pancreatic stellate cell
MUC1	mucin 1
NLS	nuclear localization sequence
PanIN	pancreatic intraepithelial neoplasia
PAS	phagophore assembly sites
PDAC	pancreatic ductal adenocarcinoma
PDGF	platelet-derived growth factor
PEGPH20	PEGylated recombinant hyaluronidase
PIP2	phosphatidylinositol 2-phosphate
PIP3	phosphatidylinositol 3-phosphate
PPIB	cyclophilin B

PSC	pancreatic stellate cell
qCLASH	quick cross-linking, ligation, and sequencing of hybrids
qPCR	quantitative polymerase chain reaction
rAAV	recombinant adeno-associated virus
rAd	recombinant adenovirus
RPMI	Roswell Park Memorial Institute
SEM	standard error of the mean
Smo	smoothened
SQSTM1	sequestome-1
ssAAV	single-stranded adeno-associated virus
TCGA	The Cancer Genome Atlas
TFEB	transcription factor EB
TGF-β1	transforming growth factor β1
TH2	T helper 2
TNFα	tumor necrosis factor alpha
TuD	Tough Decoys
ULK	UNC51-like kinase
UTR	untranslated region
vg	viral genome
WIPI	WD-repeat protein interacting with phosphoinositides
WT	wildtype

Chapter 1: Introduction

1.1 The Current State of Pancreatic Cancer: Prognosis and Treatment Strategies

Pancreatic cancer is one of the leading causes of cancer deaths in western societies, with the worst prognosis (1). In the United States, it is the third leading cause of cancer deaths**,** and projected to become the second leading cause of cancer related deaths in just over a decade (2). Pancreatic cancer originates from exocrine cells of the pancreas, and among all exocrine tumors, PDAC is the most common type of pancreatic neoplasm, accounting for more than 90% of pancreatic tumors (3). In spite of intense research efforts and the development of numerous new cancer drugs and treatment strategies over the past four decades, there has been no significant improvement in overall patient survival for pancreatic cancer and death rates are almost equivalent to incidence rates (4).

Surgery, radiation, and chemotherapy are treatment options that may extend patient survival or reduce symptoms, but they seldom produce a cure. Surgical resection or surgery in combination with adjuvant therapy is the only potentially curative therapy that improves overall patient survival (5). However, only a minority of PDAC patients are candidates for surgery due to the typical timing of diagnosis at late stages of progression, where the cancer has metastasized to other parts of the body, and the tumors are not amenable to current therapeutic modalities (6, 7).

For the past several decades, gemcitabine (difluorodeoxycytidine) has remained the standard of care for chemotherapy of pancreatic cancer. Gemcitabine is a cytotoxic nucleoside analog that is phosphorylated within the cell by deoxycytidine kinase (8), and the reaction product then competes with endogenous cytosine triphosphate during DNA

synthesis (9). Once incorporated into the synthesizing strand of DNA, masked chain termination is induced, triggering apoptosis (9). In recent years, combination treatments involving folinic acid, 5-fluorouracil, irinotecan and oxaliplatin (FOLFIRINOX) or Gemcitabine/Nab-paclitaxel have received FDA approval for pancreatic cancer, but these therapies may be associated with severe toxicity issues and each only modestly improve patient survival (10). Unfortunately recent improvements in combination chemotherapy and patient selection for targeted therapies have moderately improved outcomes for PDAC patients, with an average overall 5-year survival rate of less than 8% (11). Overall, pancreatic cancer is still refractory to most therapeutic strategies. Therefore, a better understanding of the mechanistic underpinnings of pancreatic cancer is needed to generate new strategies for more effective treatments.

1.2 Tumor Stroma and its Role in PDAC Progression

Dense fibrotic stromal reaction, called desmoplasia, is a histopathological hallmark of PDAC. The stroma surrounding pancreatic cancer cells is composed of both cellular (e.g. pancreatic stellate cells, fibroblasts, vascular, and immune cells) and acellular (e.g. extracellular matrix [ECM] proteins, cytokines, and growth factors) components (12, 13) (Figure 1). Dynamic interactions between stromal components and pancreatic cancer cells is an integral part of PDAC progression and metastasis.

In the normal pancreas, a resident subclass of fibroblasts, consisting of pancreatic stellate cells (PSCs), immune cells, and vascular cells, play a critical role in tissue repair and wound healing. In response to pancreatic tissue damage, injured acinar cells secrete pro-inflammatory and pro-angiogenic growth factors/cytokines, and induced immune

cells, PSCs/fibroblasts, and endothelial cells to engage immune surveillance, synthesize connective tissue, and generate blood vessels, respectively, which collectively restore normal pancreatic function (14). However, chronic inflammatory responses involving pancreatic cancer cells have been known to alter the properties of PSCs, immune cells, and vascular cells, creating a favorable microenvironment for tumor progression (14, 15).

In the PDAC tumor microenvironment, cancer cells secrete pro-inflammatory growth factors/cytokines, including TGF-β1, PDGF, TNFα, and IL-1/6, that activate PSCs and pancreatic fibroblasts. Activated PSCs/fibroblasts transform into a myofibroblast-like cells that secrete large amounts of extracellular matrix (ECM) proteins, comprised of collagens, fibronectins, and laminins, that form fibrous tissues situated in the periacinar regions of the organ (16, 17). Furthermore, activated PSCs/fibroblasts produce pro-inflammatory growth factors/chemokines that act in an autocrine fashion to maintain their sustained stimulation, leading to the production of fibrotic stromal ECM proteins (18, 19) (Figure 1). Excessive ECM deposition in periacinar regions distorts normal parenchyma, causing compression of the vasculature that leads to hypovascularity and hypoxia in the tumors (20, 21). Tumor hypoxia is also known to activate PSCs that maintain and perpetuate the hypoxia-fibrosis cycle (22). In addition, dense fibrotic stroma causes dysfunctions in the vasculature, impairing drug delivery to the cancer cells that as a consequence reduce therapeutic efficacy (21). Pancreatic cancer cells also suppress tumor immune surveillance by decreasing cytotoxic CD8 T cells and increasing the presence of immunosuppressive macrophages (M2), neutrophils (N2), and T-regulatory cells (Th2) (23, 24). Dense fibrotic stroma, in combination with immune suppression and neo-angiogenesis, creates a more favorable

environment for pancreatic cancer progression and metastasis (25). PSCs are also known to closely interact with pancreatic cancer cells to promote metastasis and have even been shown to co-migrate to distant metastatic sites, establishing stromal abundant tumors beyond the pancreas (26-28).

Developing therapies for advanced PDAC is much more complicated than simply targeting pancreatic cancer cells, as the associated tumor stroma plays an important role in progression, drug resistance, and metastasis (20, 21). In fact, stromal biology and targeted therapies are currently under intense investigation in an attempt to improve the efficacy of chemotherapy and patient survival. Tuveson and colleagues were one of the first to report the therapeutic efficacy of targeting stroma in pancreatic cancer (21). Utilizing a small molecule inhibitor of smoothened (Smo) (IPI-926) to inhibit hedgehog pathway and lead to stromal ablation, gemcitabine treatment in combination with IPI-926 led to a significant increase in intratumoral vascularization, drug perfusion, and overall survival in a genetically engineered mouse model of pancreatic cancer (21). Similar results were observed with various other similar anti-stromal approaches in PDAC pre-clinical settings, such as utilizing enzyme-based ECM protein depletion strategy by targeting hyaluronan via PEGylated recombinant hyaluronidase (PEGPH20) (29-31) or treating with anti-fibrotic drug pirfenidone (32, 33).

Based on these findings, IPI-926 was tested in combination with gemcitabine in PDAC clinical trials. Unfortunately, long-term Phase II/III clinical trials not only failed to show treatment benefit, the IPI-926/gemcitabine combination cohort actually fared worse than the cohort that received gemcitabine alone (34). In contradiction to previous reports, recent paradoxical evidence suggests that pancreatic stroma acts to restrain tumor growth,

not promote it (35, 36). Two independent research groups depleted the stroma through different means in PDAC mice using genetic (thymidine kinase mediated PSC depletion) or pharmacological (IPI-926) approaches and found that stromal ablation induces a de-differentiated cancer phenotype, enhances disease progression, and reduces survival (35, 36). However within the same year, Ronald Evan's group demonstrated that a more subtle approach of reverting activated PSCs to quiescence led to a more promising therapeutic approach in contrast to complete stromal ablation (37). Treatment with vitamin D analog, calcipotriol (Cal) in combination with gemcitabine administration reprogrammed PSCs to a less fibrotic/inflammatory state that enhanced drug efficacy and improved survival of genetically engineered mouse models of PDAC (37). Based on these preclinical studies, this novel stromal reprogramming therapeutic strategy is currently being evaluated in PDAC patients with advanced disease in combination with PD1 Inhibitor, Pembrolizumab (ClinicalTrials.gov; NCT03331562).

The culmination of these studies indicates that PDAC stroma is a heterogeneous and complex tissue, and different components of the stroma potentially have diverse roles that can promote or inhibit tumor growth. Given the failure of stromal ablation therapeutic strategies in clinic and the potential of the stroma to restrain tumor growth, efforts are now focused on developing novel stromal-targeted therapies that appropriately modulate the stroma and avoid the extremes of ablation versus abundance (25, 37).

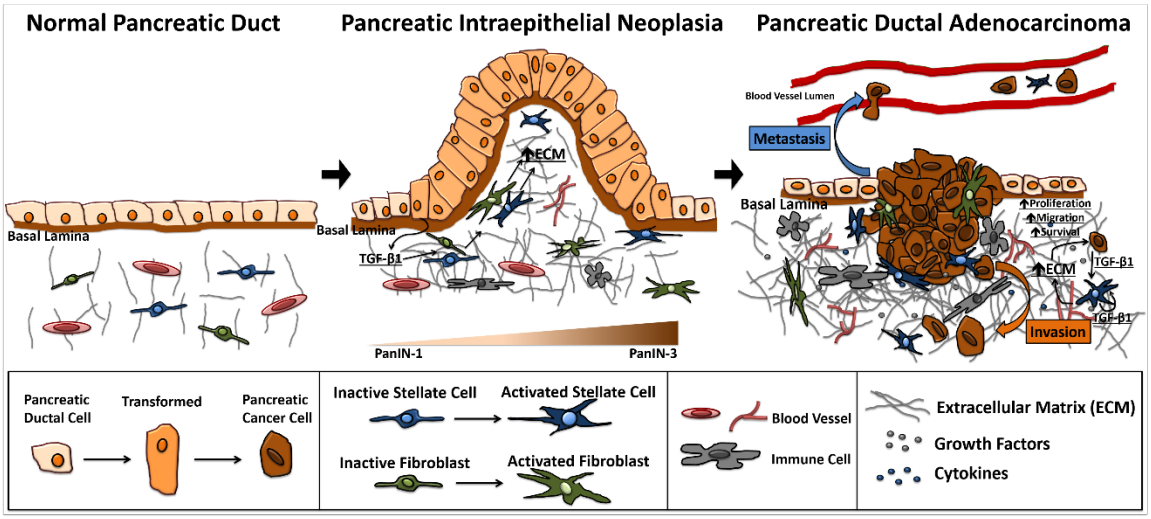

Figure 1. Pathogenesis of Pancreatic Cancer and its Associated Stroma Illustration of the progression of PDAC from normal pancreatic duct to precursor pancreatic intraepithelial neoplasm (PanIN) and ultimately to invasive/metastatic cancer (left to right). During carcinogenesis, normal ductal epithelial cells (tan cells) acquire oncogenic mutations (e.g. Kras) (light orange cells) early and develop into hyperplastic ductal lesions called PanIN which progress through various grades (PanIN-1A, PanIN-2A, PanIN-2, and PanIN-3), eventually developing into fully invasive and metastatic pancreatic cancer (dark brown cells). Pancreatic cancer cells (dark brown) and pancreatic stellate cells (blue) release TGF-β1 and other pro-inflammatory cytokines/growth factors that activate pancreatic stellate cells to produce ECM proteins and increase fibrotic stromal deposition. A close interaction between stellate cells, cancer cells, and pro-inflammatory growth factors/cytokines contribute to the PDAC progression and metastasis.

1.3 Autophagy in Pancreatic Cancer

Dense fibrotic PDAC stroma with poor intratumoral vasculature leads to a nutrient deprived, hypoxic tumor microenvironment (38). Under these harsh conditions, pancreatic cancer cells induce macroautophagy (autophagy) as a survival mechanism to maintain energy homeostasis, proliferation, and metastasis (39-41). Autophagy is the process in which cytosolic components are enveloped by double-membrane vesicles called autophagosomes that are trafficked to the lysosome for degradation/recycling (42).

Autophagy is initiated at phagophore assembly sites (PAS) on the endoplasmic reticulum (ER) (43-45) where the UNC51-like kinase (ULK) complex is recruited, consisting of ULK1, ATG13, FIP200, and ATG101 (46). This initiating event leads to the budding and elongation of a double membrane structure as ULK1 phosphorylates and activates Beclin 1 (47), which is a part of the class III PI3K complex along with ATG14, VPS15, and VPS34 (48). The activated class III PI3K complex converts phosphatidylinositol 2-phosphate (PIP2) to phosphatidylinositol 3-phosphate (PIP3), and PIP3 accumulation recruits WD-repeat protein interacting with phosphoinositides (WIPI) proteins (49). WIPI proteins recruit the ATG12/ATG5/ATG16 complex (50) which is required for the critical step of lipidating microtubule-associated protein 1 light chain 3 (LC3) to phosphatidylethanolamine on the phagophore membrane in an E3 ubiquitin ligase-like manner (51). Subsequently, sequestosome-1 (SQSTM1/p62), which binds to polyubiquitinated substrates, recruits cargo to the autophagosome by binding to lipidated LC3B to be degraded (52). The phagophore eventually encloses around the cargo and is referred to as an autophagosome. Autophagosomes are then trafficked to the lysosome, and once autophagosomes fuse with lysosomes, the hydrolases of the lysosomal

compartments degrade the internal substrates of the autophagosomes and release the basic cellular building blocks into the cytosol for recycling (42).

Recent studies document that the upregulation of autophagy can serve as a survival mechanism in various malignancies (53-61) including PDAC tumor growth and progression (39-41). Furthermore, autophagy inhibition was shown to potently sensitize pancreatic cancer cells to gemcitabine treatment (39) and increased survival (40). As a consequence, autophagy has become a therapeutic target of PDAC, and clinical trials are currently underway testing the therapeutic efficacy of lysosomotropic agent hydroxychloroquine (HCQ) as an autophagy inhibitor in combination with gemcitabine to target PDAC (ClinicalTrials.gov; NCT01506973 & NCT01978184). However, HCQ has been known to exhibit off-target effects and toxicity in a wide variety of diseases in clinical studies (62-65), suggesting a great need to understand the molecular mechanisms associated with PDAC autophagy and to develop alternative therapies that are safe and effective to target autophagy.

1.4 miRNA Biology and the miR-29 Family

miRNA are small non-coding RNAs, approximately ~20-30 nucleotides in length, and are known as powerful regulators of gene expression in eukaryotes. Since the first miRNA, lin-4, was reported by Ambros in 1993 (66), the field of miRNA biology has exploded as revelations were made that these minute RNAs had implications in a multitude of physiological processes and diseases.

miRNAs are normally transcribed as long transcripts by RNA polymerase II and are commonly embedded in the introns and exons of both coding and non-coding genes

(67). Within these long transcripts, they form a characteristic hairpin structure and are referred to as primary miRNAs (pri-miRNAs) (67). Subsequently, pri-miRNAs are processed by ribonuclease enzyme Drosha, which cleaves at the base of the hairpin (68). The liberated hairpin is referred to as precursor miRNA (pre-miRNA) which is exported out of the nucleus by exportin 5 (69) and further processed in the cytoplasm by another endonuclease, Dicer, to yield a double stranded mature miRNA (70). Finally, one of the strands of mature miRNA is loaded onto the Argonaut proteins (AGOs) to form the RNA induced silencing complex known as RISC (71). Following its association within RISC, miRNAs function through a 6-8mer sequence known as a seed sequence that binds to complementary sequences in the 3' untranslated region (UTR) of target mRNAs through canonical Watson-Crick base pairing, leading to repression of expression (67).

Several miRNAs have common seed sequences and have been known to regulate a similar repertoire of target transcripts. Accordingly, evolutionarily conserved miRNAs sharing analogous seed sequences have been organized into 87 distinct miRNA families (72). As one of these miRNA families, miR-29 consists of three paralogous members, miR-29a, miR-29b, and miR-29c. miR-29a and -29b-1 are encoded on chromosome 7q32.3, known as the miR-29a/b-1 cluster, and miR-29b-2 and -29c are found on chromosome1q32.2, designated as the miR-29c/b-2 cluster. While all three family members share a common 7nt seed sequence, there are reports of unique sequence/functional features of each miR-29 family member (Figure 2).

One of the notable differences among miR-29 family members resides within a 6 nucleotide segment that is unique to miR-29b (Figure 2). This hexanucleotide sequence present in nucleotide positions 18-23 has been functionally shown to lead to miR-29b

nuclear localization (73). In fact, the simple addition of the miR-29b nuclear localization sequence (NLS) to the 3'end of siRNAs was found to be sufficient to cause nuclear localization (73). Consistently, another report evaluating the therapeutic efficacy of miR-29b in targeting a subunit of the proteasome found that the deletion of the hexanucleotide NLS lead to cytoplasmic enrichment of miR-29b and further enhanced the downregulation of the target transcript (74). Although miR-29b's function within the nucleus has yet to be fully elucidated, this research has opened the gates to the discovery of \ other miRNAs that similarly localize to the nucleus to elicit non-canonical functions beyond binding to the 3'-UTR of mRNA transcripts in the cytoplasm (75, 76). Elucidating the role of miRNAs in the nucleus is still an active and ongoing area of research. There have been reports in which miRNAs regulate gene expression in the nucleus by inducing epigenetic changes (77) as well as through direct binding to the transcription start sites of genes to inhibit its transcription (78). A number of reviews are available on this subject matter (79, 80), but for simplicity, we will focus on the canonical/cytoplasmic function of miR-29 for the remainder of the thesis.

In addition to the hexanucleutide sequence, miR-29a has a distinct cytosine residue at position 10 (Figure 2). This difference is of particular importance as uracil residues located in nucleotide positions 9-11 of miRNAs have been found to have rapid decay/turnover (81). This tri-uracil sequence is found in both miR-29b and miR-29c, whereas the cytosine residue at nucleotide position 10 of miR-29a lends to its greater stability (81). This is consistent with pulse-chase experiments of synthetic miR-29a and -29b in HeLa cells demonstrated a longer half-life of miR-29a compared to -29b (74) as

well as numerous findings that miR-29a is the most abundantly expressed family member (82-85).

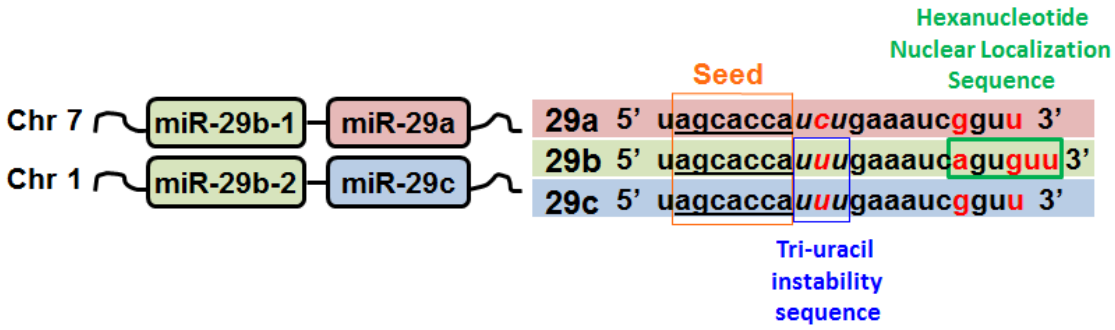

Figure 2. Schematic representation of the miR-29 family members: miR-29a, -29b, and -29c. miR-29 family members have identical seed sequences (orange box and underlined) along with similar mature miRNA sequences. However notable differences in nucleotides are indicated in red. Tri-uracil nucleotides at positions 9-11nt (blue box) present in miR-29b and -29c contribute to instability and shorter half-life, and the hexanucleotide sequence at positions 18-23nt (green box) is unique to miR-29b, leading to nuclear localization.

1.5 *In Vivo* Function of miR-29

A single miRNA family has been known to have on average >400 target transcripts that have matching, evolutionarily conserved 3'-UTR binding sites (86). Furthermore, >60% of translated genes in the human genome possess at least one miRNA binding site. Therefore, it is likely that the dysregulation of even a single miRNA can profoundly impact normal physiological processes and lead to disease. In fact, a number of *in vivo* studies in murine models have demonstrated the essential role of miR-29 in development and general physiology. Whole-body miR-29 knockout (KO) mice have a wide range of developmental defects such as premature thymic involution (87), muscle wasting (88), growth retardation, and shorter lifespan (89). In addition, liver-specific miR-29 KO mice had a robust increase in hepatic fibrosis and carcinogenesis (90) implicating its physiological relevance.

A recent report profiled miR-29a and miR-29c function in the pancreata of whole-body KO mouse models in the context of glucose regulation and diabetes (84). miR-29a KO mice had a defect in insulin secretion but interestingly, miR-29c KO mice did not (84). Similarly, miR-29a KO in an insulitis transgenic model (insHEL) resulted in diabetes, whereas wildtype (WT) mice did not (84). Taken together, miR-29a plays a vital role in proper pancreatic function and elicits a protective effect against diabetes in the context of insulitis (84). With these studies in mind, it is no surprise that miR-29 has a profound impact on cancer biology as well.

1.6 Statement of Purpose

In the context of cancer pathogenesis, miR-15a/miR-16 was the first miRNA cluster found to be aberrantly regulated, with a documented deletion of the encoding genomic region reported in chronic lymphocytic leukemia (91). Since then, dysregulated miRNA signatures have become a well-established feature of various cancers. Among dozens of miRNAs reported to be abnormally expressed in cancer, miR-29 has been recognized as one of the critical miRNAs that play a role in cancer pathogenesis.

There is a vital need for identifying novel mechanisms of PDAC fibrosis in order to develop more effective therapeutic targets that will modulate the stroma with more subtle approaches without complete ablation. miR-29 has been shown to suppress the fibrosis of various organs such as heart (92), liver (93), lung (94), kidney (95), and muscle (96), by reducing ECM deposition and inflammation. However, the role of miR-29 in the context of pancreatic fibrosis had not been established. Thus, we sought to establish miR-29's function in PSCs, the major stromal cells in PDAC stroma, to test its anti-fibrotic potential.

In addition to miR-29's role in fibrosis, a comprehensive survey of the current research work on miR-29 in cancer reveals a large body of literature reporting a significant role of miR-29 in numerous neoplastic contexts (Figure 3A). The majority of these studies have reported that miR-29 functions as a potent tumor suppressor. However, a few reports have found miR-29 to be oncogenic (Figure 3B). Therefore, additional studies are needed to better understand mechanisms of miR-29 in cancer, including pancreatic cancer. Furthermore, as current therapies for PDAC are ineffective in significantly improving overall survival (10), novel therapeutic options are desperately

needed. In view of miR-29's tumor suppressor function in various cancers, we tested its therapeutic effects in pancreatic cancer cells.

Here in this thesis, we sought to establish the pathophysiological role of miR-29 in PDAC. First, we investigated miR-29 expression levels in a murine model of pancreatic cancer and PDAC patient biopsies, as well as determined its functional effect in PSCs. Second, we went on to establish miR-29's role as a tumor suppressor in pancreatic cancer cells and identified a novel role of miR-29 in regulating PDAC autophagy. Lastly, we optimized a pancreas-specific gene delivery technique for murine models in order to provide an auspicious approach for future functional studies of miR-29 *in vivo*. Each of these studies have been organized into independent chapters which include a brief introduction to highlight the key information germane to the chapter, as well as respective methods, results, and succinct discussion sections. In this way, each chapter can be read independently with a better appreciation of key concepts for each subject matter.

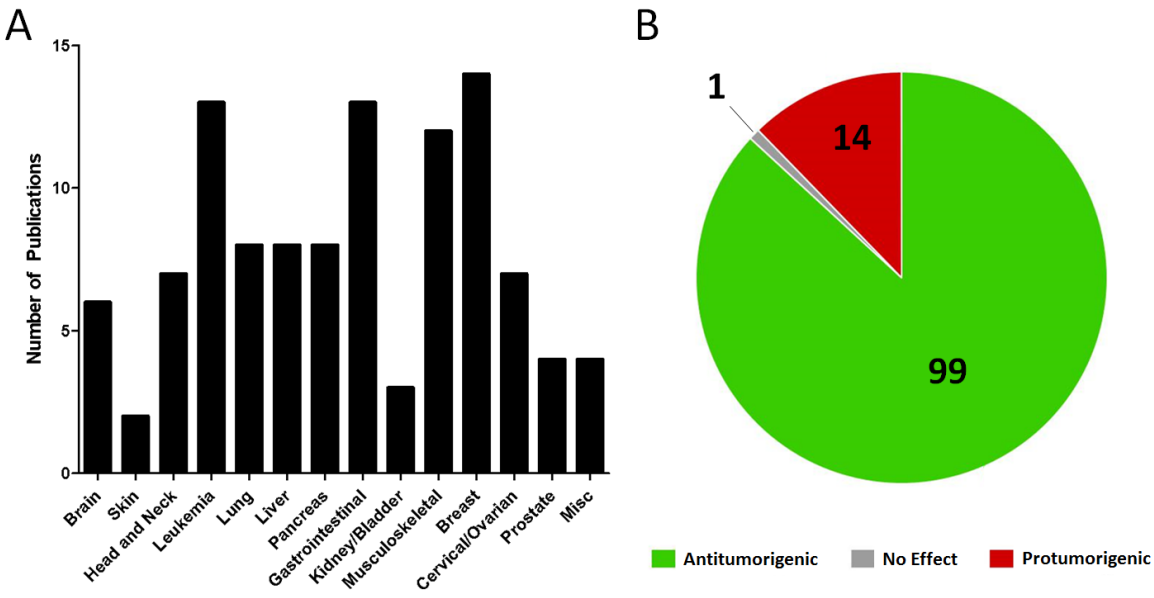

Figure 3. miR-29 studies in cancer pathogenesis.

A compilation of primary research articles (non-biomarker based) related to miR-29 in the context of cancer was carried out in order to gain insight on the role of miR-29 among cancers. (A) The bar graph indicates the number of current publications based on cancer type, with Miscellaneous (Misc) indicating studies that investigate miR-29 in a broader, multi-cancer context. (B) Pie chart with number of publications demonstrating miR-29 as a tumor suppressor (green), oncogenic (red), and no effect (grey).

Chapter 2: Pathophysiological role of microRNA-29 in pancreatic cancer stroma

2.1 Introduction

PDAC is the most lethal human cancer, with a 5-year survival rate of 6% (97) and is projected to be the second leading cause of cancer related death by 2030 (2). Dense fibrotic stroma associated with PDAC tumors is a major obstacle for drug delivery to the tumor bed (21, 98) and plays a crucial role in pancreatic cancer progression (26, 99, 100). Current, anti-stromal therapies have failed to improve tumor response to chemotherapy and patient survival (101), and they are often associated with toxicity (34). Furthermore, recent studies show that the stroma impedes tumor growth, and its complete inhibition accelerated PDAC progression (35, 36). However, reprogramming the reactive stroma through modulation of a key transcriptional regulator in stromal cells suppressed the reactive stroma and increased tumor response to chemotherapy and survival (37). These studies reinforce the critical need to understand the molecular mechanisms associated with tumor-stromal interactions for developing effective therapeutic strategies to reduce PDAC mortality.

Stroma associated with PDAC tumors is comprised of activated stellate cells/fibroblasts, immune cells, extracellular matrix, and pro-inflammatory cytokines/growth factors (12) (Figure 1). A dynamic interaction between tumor-stromal cells and the extracellular matrix has been shown to play a critical role in PDAC progression (12). A growing body of evidence suggests that PSCs are the major stromal cells responsible for fibrotic stroma. In normal pancreas, PSCs are located in the periacinar spaces and remain quiescent. In response to pancreatic injury or carcinogenesis, PSCs are activated by a number of pro-inflammatory growth factors and

cytokines, including TGF-β1, released by cancer cells, injured acinar cells (paracrine), and PSCs (autocrine). TGF-β1 serves as a key activator of quiescent PSCs, which is highly expressed in PDAC tumors and is known to play an important role in the fibrotic process associated with pancreatitis and PDAC pathogenesis (102, 103). Activated PSCs are transformed into a myofibroblast-like phenotype and secrete excessive amounts of ECM proteins such as collagen, laminin, and fibronectin, a prominent component of PDAC stroma (104). Extensive ECM deposition causes hypovascularity in PDAC tumors and attenuates drug delivery to the peritumoral milieu (14). Furthermore, PSCs closely interact with cancer cells and the ECM to promote primary tumor growth and distant metastasis (26-28, 105). However, the molecular mechanisms associated with stellate-cancer interactions remain poorly understood.

miRNAs are conserved, non-coding RNAs that regulate eukaryotic gene expression and are critical in maintaining cellular homeostasis (106). A single miRNA regulates hundreds of genes, often targeting multiple components of complex intra-cellular networks (107). Thus, misregulation of an individual miRNA can have a profound impact on cellular physiology that leads to disease(s) (108). miR-29 is known to play a paramount role in the fibrotic process of several organs (90, 93-96) and provide crucial functions downstream of pro-fibrotic signaling pathways such as TGF-β1 (109). Numerous functional studies have documented the anti-fibrotic activity of miR-29 in different tissues(110), and its restored expression reduced fibrosis by targeting ECM proteins(92), such as collagen and laminin. Additionally, a growing body of evidence implicates the role of miR-29 in cancer pathogenesis (111) and in the tumor

microenvironment (112). The role of miR-29 in pancreatic fibrosis and PDAC tumor-stromal interactions however, has yet to be delineated.

Here in this chapter, we show that the loss of miR-29a and b is a common feature of activated PSCs and fibroblasts and is associated with a significant increase in stromal ECM deposition *in vitro* and *in vivo*. Our *in vitro* miR-29 gain/loss-of-function studies directly document the role of miR-29 in PSC-mediated stromal accumulation. In addition, ectopic overexpression of miR-29a or b in PSCs decreased the stroma deposition, cancer cell viability, and colony growth when co-cultured with pancreatic cancer cells. Our findings show that miR-29 plays a critical role in regulating tumor stromal deposition and cancer growth, thus raising the possibility that modulation of miR-29 expression in PSCs may be therapeutically beneficial to normalize the reactive stroma and enhance the efficacy of chemotherapy to target PDAC.

2.2 Materials and Methods

Mice

Kras^{G12D}; *Pdx1-Cre* (KC) mice were generated as described (113). Conditional *LSL-Kras*^{G12D} mice were crossed with *Pdx1-Cre* animals to generate the KC mice. All animal housing, use, and surgical procedures were carried out in accordance with the regulatory guidelines set by Guide for the Care and Use of Laboratory Animals of the National Institutes of Health. All animal protocols were reviewed and approved by the Indiana University (IU) Animal Care and Use Committee.

Cell lines

Immortalized mouse pancreatic stellate (mPSC) cell lines (114) were a gift from Dr. Raul Urrutia at Mayo Clinic, Rochester, Minnesota. Primary human PSCs were obtained from ScienCell Research Laboratories (Carlsbad, California), grown routinely in Dulbecco's Modified Eagle Medium (DMEM) (Life Technologies, 11965-092) supplemented with 10% fetal bovine serum (FBS), 100units ml^{-1} penicillin, and 100mg ml^{-1} streptomycin. Primary human fibroblasts were purchased from Vitra Biopharma (Golden, CO), and were routinely cultured in their recommended media (VitroPlusII). Primary cancer associated fibroblasts (CAFs) isolated from PDAC patients were confirmed by α-SMA staining and authentication was performed by IDEXX-Radil (Columbia, MO). CAFs were maintained in DMEM/F-12, GlutaMAX Supplement (Life Technologies, 10565-018) plus 10% FBS, 100 units ml^{-1} penicillin, and 100mg ml^{-1} streptomycin. All primary cell lines were studied prior to reaching seven passages. Human pancreatic carcinoma cell lines Panc-1 and MIA PaCa-2 were gifts from Karen E. Pollok of Indiana University School of Medicine and IU Simon Cancer Center. Both were grown routinely in DMEM supplemented with 10% FBS, 100units ml^{-1} penicillin, and 100mg ml^{-1} streptomycin.

Patient Tissue Procurement.

This study was reviewed and approved by the Indiana University-Purdue University Indianapolis (IUPUI) Institutional Review Board (IRB) at Indianapolis, IN, USA (IUPUI IRB# 1303011057). Tissue biopsies and associated clinical data were obtained from IU Simon Cancer Tissue Bank and IU Department of Pathology. Both IU Simon Cancer Tissue Bank and IU Department of Pathology procured tissue samples and

informed consent was obtained from human subjects in compliance with IUPUI IRB policies. IUPUI IRB is accredited by the Association for the Accreditation of Human Research Protection Programs (AAHRPP). Quality and integrity of paraffin embedded or fresh pancreatic tissue biopsies was analyzed by a certified pathologist with hematoxylin and eosin staining. Control samples that were biopsied from patients with conditions unrelated to pancreatic disease or from an unaffected area of the pancreas from patients with pancreatitis were confirmed via histopathological analysis.

RNA Extractions

Total RNA was extracted from formalin fixed paraffin embedded (FFPE) tissue samples (two 10 μm thick sections) using the MagMax^{TM} FFPE total nucleic acid isolation kit (Ambion, Life Technologies, 4463365) or from frozen tissues using Rino BulletBlender beads (MidSci, CAP329) followed by Trizol (Life Technologies, 15596018) extraction. RNA was extracted from cells *in vitro* by Trizol extraction according to the manufacturer's protocols. The quantity and purity of RNA was determined by OD260/280 reading using a Nanodrop spectrophotometer.

qPCR analysis.

Mature miR-29 family member expression levels were measured by TaqMan MicroRNA Assays (Applied Biosystems) for miR-29a (ID:002112); miR-29b (ID:000413); and miR-29c (ID:000587). U6 snRNA (ID:001973) was used as a reference gene to normalize the relative amount of miRNA, and samples were analyzed using ABI 7500 real time PCR machine. Alpha smooth muscle actin (α-SMA), connective tissue growth factor (CTGF), collagen 1a1 (COL1A1), laminin (LAMC1), and fibronectin (FN1) levels were measured using gene specific qPCR primer probes purchased from

Solaris Probes. RNA samples were reverse transcribed using random primers, and α-SMA (AX-061937-00-0100); CTGF (AX-040018-00-0100); COL1A1 (AX-042068-00-0100); LAMC1 (AX-043874-00-0100); and FN1 (AX-043446-00-0100) expression levels were measured using cyclophilin B (PPIB) (AX-048843-00-0100) as an internal control. Samples were run in triplicates with 0.2 thresholds, and the ΔΔCT method was used for relative expression analysis. For miR-29 expression analysis in PDAC patient tumors, total RNA was isolated from FFPE tissue sections (two 10 μm) of normal controls (n=10) or PDAC patient tumors (n=15) with 35-80% stroma and miR-29 family expression was analyzed by qPCR as described above.

Immunoblotting

mPSCs and hPSCs were lysed in lysis buffer (50mM Hepes, 150 mM NaCl, 10% glycerol, 1% Triton-X, 1.5 mM $MgCl_2$, 1 mM EGTA, 100mM NaF, 10 mM NaPPi, Na O Vanidate, $ZnCl_2$, PMSF, protease inhibitor) and protein samples were ran through SDS-PAGE. Proteins were transferred to polyvinylidene fluoride membrane (PVDF), blocked in 10% dried non-fat milk, and subsequently probed with antibodies against collagen 1alpha1 (Santa Cruz, sc-8784-R, 1:500), collagen 3alpha1 (Santa Cruz, sc-8781, 1:500), laminin gamma-1 (Santa Cruz, sc-5584, 1:5000), fibronectin (Santa Cruz, sc-9068, 1:500), α-tubulin (Calbiochem, CP06, 1:3000), GAPDH (Millipore, MAB374, 1:10,000), and β-actin (Santa Cruz, sc-47778, 1:2000), using corresponding HRP conjugated goat anti-rabbit (Santa Cruz, sc-2004), goat anti-mouse (Santa Cruz, sc-2005), or donkey anti-goat (Santa Cruz, sc-2020) secondary antibodies. Proteins were visualized and quantified using chemiluminescent detection (GE Healthcare, Amersham ECL) and exposure to x-ray film (Thermo Scientific, CL-X Posure Film). The intensity for each band was

densitometrically quantified and normalized against loading control using ImageJ software.

Transfection

Exponentially growing mPSCs or hPSCs were seeded in 6 well plates at $1x10^5$ cells per well, serum starved for 24 hours, and treated with 10 ng/ml of TGF-β1 for 24hrs before or after transfection with 20 nM mimics using DharmaFECT®1 (Life Technologies, T-2001-01) per their protocol. For immunoblotting, cells were either transfected with 20 nM mimic control (Life Technologies, CN-001000-01), mimic-29a (Life Technologies, C-300520-05), or mimic-29b (Life Technologies, C-300520-05). For LNA transfection, $1x10^5$ serum starved and TGF-β1 treated hPSCs were transfected with 50 nM of LNA-29 (Exiqon, 450039) or LNA-control (Exiqon, 199006) using DharmaFECT®1. 24 hours post-transfection, protein was harvested and proteins in lysates were separated by gel electrophoresis and analyzed by western blot using the following antibodies: collagen 1alpha1 (Santa Cruz, sc-8784-R, 1:500), collagen 3alpha1 (Santa Cruz, sc-8781, 1:500), laminin gamma-1 (Santa Cruz, sc-5584, 1:5000), fibronectin (Santa Cruz, sc-9068, 1:500), α-tubulin (Calbiochem, CP06, 1:3000), GAPDH (Millipore, MAB374, 1:10,000), and β-actin (Santa Cruz, sc-47778, 1:2000). For studies involving siSMAD3, $1x10^5$ hPSCs/well (6-well plate) growing in culture were transfected with 50 nM non-targeting siRNA control (Life Technologies, D-001810-01-05) or siSMAD3 (Life Technologies, L-020067-00-005) using DharmaFECT®1 to inhibit endogenous SMAD3 levels in PSCs. 24 hours post-transfection, total proteins were harvested and subjected to western blot analysis to verify SMAD3 knockdown efficiency. For miR-29 expression analysis in TGF-β1-activated hPSCs transfected with siCTRL and

siSMAD3, hPSCs were transfected with 50 nM siCTRL or siSMAD3 as described. 24 hours post-transfection, cells were serum starved for 24 hours, challenged with 10 ng/ml TGF-β1 for 24 hours, and subjected to Trizol RNA isolation. miR-29 expression levels were analyzed via qPCR as described above.

Co-culture

$1x10^5$ mPSCs were transfected with either 20 nM mimic control, 20 nM mimic-29a, or 20 nM mimic-29b and plated simultaneously with 100 pancreatic cancer cells (MIA PaCa2 or Panc-1) in a 6 well plate. Co-cultures were allowed to grow for 10 days, and were fixed and stained with crystal violet solution (0.05% w/v crystal violet, 1% formaldehyde, 1x PBS, 1% MeOH) or Sirius Red. Cancer colonies greater than 50 cells were counted under phase contrast microscopy.

Collection of PSC Conditioned Media. To obtain miR-29 and control mimic transfected PSC conditioned media, exponentially growing mPSCs were seeded in a 6 well plates at $1x10^5$ cells per well, serum starved for 24 hours, and treated with 10 ng/ml of TGF-β1 for 24hrs before transfection with 20 nM control or miR-29 mimics using

DharmaFECT®1 per their protocol. 24 hours post-transfection, cells were washed twice with PBS and incubated with DMEM with 0.2% BSA for 48 hours at 37^oC. Conditioned media was collected from PSCs and centrifuged at 1500 rpm for 10min at 4^oC. Supernatant was collected and then filtered using a 0.22 μm sterile filter (Fisher Scientific, 09-719A) to eliminate any remaining suspended cells or cellular debris. In parallel, non-conditioned media control was collected from a 6 well plates with no PSCs.

Cell Viability

$1.0x10^3$ PSCs were plated per well in a 96 well plate. Cells were serum starved for 24 hours, and treated with 10 ng/ml of TGF-β1 for 24 hours before transfection with 20 nM control or miR-29 mimics using DharmaFECT®1 per their protocol. Cell viability was measured at 24, 48, 72, and 96 hours after plating the assays by adding 10 µl Cell Counting Kit-8 (Dojindo #CK04) reagent and absorbance was measured at 450 nm. For cancer cells viability,

$5.0x10^3$ pancreatic cancer cells (MIA PaCa-2 or Panc-1) were plated per well in a 96-well plate. Cancer cells were washed with PBS, and treated with PSC conditioned media for 24 and 48 hours. Cell viability was measured post-treatment by adding 10 µl of Cell Counting Kit-8 reagent and absorbance was measured at 450 nm.

Soft agar assays

24 hours post-transfection with 20 nM control or miR-29 mimics, $5.0x10^4$ mPSCs were co-seeded with $5.0x10^3$ pancreatic cancer cells (MIA PaCa-2 or Panc-1) per well in a 6 well plate containing 0.5% top agarose and 1% bottom agarose (BioRad, #162-0137). After 7 days, colonies were stained with crystal violet and were counted under low power for positive colonies (>6 cells/colony).

Histology

FFPE pancreata of KC and C57BL/6 mice or normal control and PDAC patients were sectioned (5 µm) and stained with H&E for gross histological analysis. Tissue sections were also stained with Sirius Red to estimate collagen and the degree of fibrosis. ImageJ analysis was used to quantify Sirius Red positive collagen area in the pancreatic sections (four 20X random images/animal).

Immunofluorescence

$1.0x10^5$ mouse PSCs, human PSCs or primary human fibroblasts were plated on collagen coated cover slips in 6-well plates and grown to ~80% confluency. Cells were washed with PBS, fixed in 4% paraformaldehyde at 37°C and then permeabilized with 0.25% Tween-20 in PBS (PBS-T). Subsequently, cells were blocked with 1% BSA in PBS-T at room temperature and α-SMA primary antibody (α-SMA, Novus Biologicals, NB600-531, 1:500) and secondary antibody (Goat-α-Rabbit-594, Molecular Probes, 11012, 1:500) were used to detect intracellular α-SMA levels. Slides were coversliped using VectaShield mounting medium with DAPI (H-1200).

In Situ Hybridization

FFPE pancreata of C57BL/6 control mice at 2 and 10 months (n=3/group) and KC mice at 1, 4, and 9 months (n=3/group) were sectioned and subjected to *in situ* hybridization as previously described(115). FFPE pancreatic tissue sections (5 μm) from normal control and PDAC patients (n=4/group) were also subjected to miR-29 *in situ* hybridization as described. Slides were hybridized with 50 nM 5'-biotin labeled U6 snRNA LNA probe (Exiqon, 99002-03) and 5' and 3' DIG labeled miR-29a LNA probe (Exiqon, 10000-899999-15) for 90 minutes at 55^oC. Subsequently, slides were probed with antibody against GFAP (Novus Biologic, NB300-141, 1:200) or CK19 (Abcam, ab52625, 1:200) and stained with secondary antibodies conjugated to HRP to facilitate Tyramide signal amplification (TSA) reaction: goat anti-rabbit IgG (Santa Cruz, sc-2004, 1:500-1:1000), anti-Dioxigenin (Abcam, ab6212, 1:200), and Streptavadin (Thermo Scientific, #21130, 1:5000). Slides were then stained with Hoechst NucRed™ Dead 647 (Life Technologies) to stain nuclei. 20X images were taken using DeltaVision Core

confocal microscope, projected in four channels, pseudo-colored, and merged. Corrected total cell fluorescence (CTCF) of miR-29a (green) was quantified in six or more randomly selected GFAP-positive PSCs/fibroblasts or CK19-positive epithelial cells using ImageJ analysis as previously described (116).

Statistical analysis

Student's t-test was used for statistical analysis. Data is presented as mean and error bars are represented as standard error of the mean. Statistical significance denoted as # $p< 0.08$, *$p< 0.05$, **$p< 0.01$. All experiments were repeated 3 or more times in biological replicates.

2.3 Results

TGF-β1 activates PSCs, downregulates miR-29, and increases ECM protein expression.

In PDAC, activated PSCs are the major stromal cells responsible for fibrotic stroma. In an effort to evaluate the role of miR-29, an anti-fibrotic miRNA, in PSC-mediated stromal deposition, we challenged immortalized mouse PSCs and primary human PSCs with TGF-β1, a proinflammatory growth factor that is associated with PDAC pathogenesis (102) and that is known to activate quiescent PSCs (104). Subsequently, we examined miR-29 family (-29a, -29b & -29c) expression in TGF-β1 activated mouse and human PSCs by qPCR analysis. Both mouse and human PSCs stimulated with TGF-β1 showed a significant loss of miR-29a and miR-29b compared to nascent cells, with no significant difference in miR-29c (Figure 4A, Figure 5). TGF-β1 bound TGF-β receptors form an activated heterotetramer (type I and type II) with serine/threonine kinase activity which phosphorylates downstream transcription factors, Smad2 and Smad3 proteins

(117). Upon phosphorylation and activation, pSMAD2/3 form a heterogeneous complex with SMAD4, translocates into the nucleus, and directly regulates target gene expression. To verify the activation of TGF-β1 signaling in PSCs, we examined the levels of its downstream effector molecules, pSMAD2/3. PSCs treated with TGF-β1 showed a significant increase in pSMAD2/3 levels with no difference in total SMAD2/3 expression in both mouse and human PSCs (Figure 4B, Figure 6). To further confirm TGF-β1-mediated activation of PSCs and TGF-β1 signaling, we evaluated the expression of α-SMA, a myofibroblast/PSC activation marker (104), and connective tissue growth factor (CTGF), a transcriptional target and mediator for the pro-fibrotic effects of TGF-β1. We observed a decrease in miR-29a and miR-29b expression (Figure 4A) with a concurrent increase in α-SMA (Figure 4C) and CTGF (Figure 4D) expression. Upregulation of TGF-β1 and CTGF has been well documented in human PDAC and chronic pancreatitis, a major risk factor for PDAC (102, 103, 118), and causes an increase in the accumulation of stromal ECM proteins: collagen, laminin, and fibronectin (12). Furthermore, collagen and laminin are direct targets of miR-29 (92), and fibronectin is an indirect target of miR-29 (94). We observed their significant increase in PSCs treated with TGF-β1 in conjunction with a loss of miR-29a and miR-29b (Figure 4E, Figure 7). Consistently, overexpression of miR-29 has been shown to suppress the fibrosis of various organs, including heart (92), liver (93), lung (94), kidney (95), and muscle (96) by reducing ECM deposition.

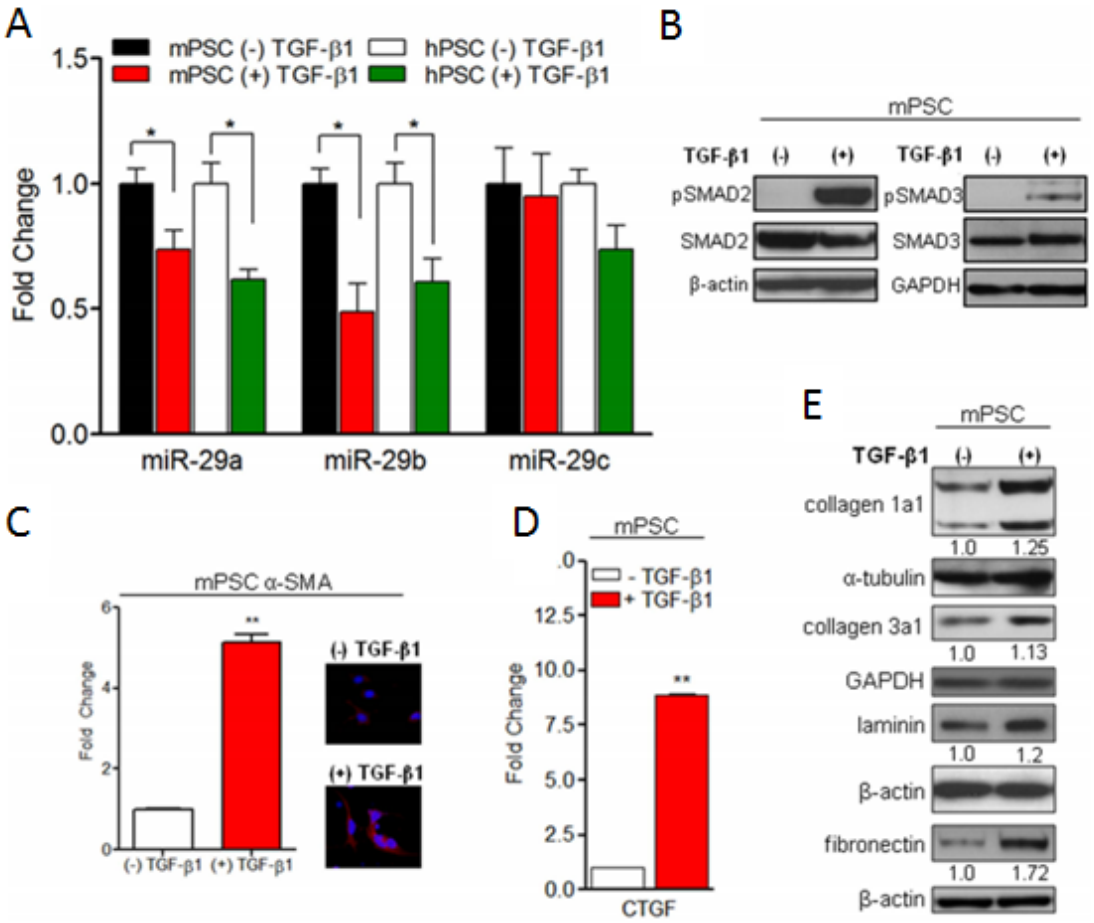

Figure 4. TGF-β1-mediated activation of PSCs leads to downregulation of miR-29 and increases ECM protein expression. Mouse PSCs (mPSCs) and human PSCs (hPSCs) were serum starved for 24hours and stimulated with 10 ng/ml of TGF-β1 for 24hours. Total RNA or protein were isolated for qPCR and western blot analysis respectively. (A) qPCR measurements of levels of miR-29 family members in nascent and TGF-β1 stimulated mPSCs and hPSCs. (B) Activation of pSMAD2/3 in TGF-β1 stimulated mPSCs. Serum starved mPSCs were treated with TGF-β1 for 6hours and protein lysates were prepared and subjected to western blot analysis using antibodies against pSMAD2/3 and total SMAD2/3, as indicated. β-actin and GAPDH were used as

loading controls. (C) Measurements of mRNA by qPCR and immunofluorescence analysis of PSC activation marker, alpha smooth muscle actin (α-SMA) in TGF-β1 stimulated mPSCs. Representative images are shown, α-SMA (red) and nuclear stain, DAPI (blue). (D) Meaures of TGF-β1 responsive gene target, connective tissue growth factor (CTGF) mRNA, in nascent and TGF-β1 stimulated mPSCs. (E) Western blot analysis of extracellular matrix proteins: collagen 1alpha1 (collagen 1a1), collagen 3alpha1 (collagen 3a1), laminin gamma-1 (laminin), and fibronectin in nascent and TGF-β1 activated mPSCs. α-tubulin, or GAPDH, or β-actin were used as loading controls. Relative quantification of band intensities, normalized to loading controls, are shown below respective blots. Experiments were repeated 3-4 times and representative data are shown. Data is presented as the mean $\pm$ standard error of the mean (SEM); n= 3; p-values determined by t-test, *$p< 0.05$, **$p< 0.01$.

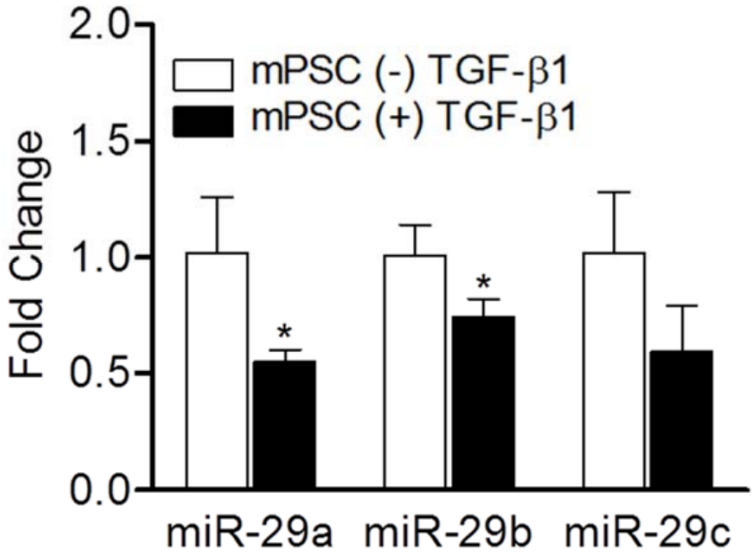

Figure 5. miR-29 expression analysis in an additional mouse PSC cell line. An additional immortalized mouse pancreatic stellate cell line (imPSC3) was serum starved, activated with 10 ng/ml TGF-β1 for 24 hours, and subjected to RNA extraction. miR-29a, miR29b, and miR-29c expression levels were analyzed by qPCR using U6 snRNA as an internal control. Data is presented as mean ± SEM; n=3, statistics generated by t-test, *$p<0.05$.

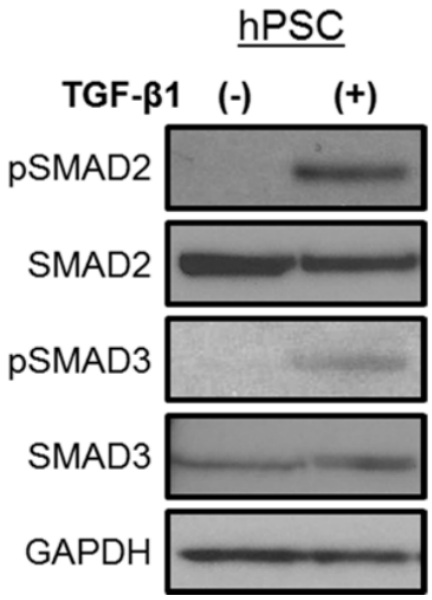

Figure 6. TGF-β1 mediated activation of human PSCs leads to an increase in pSMAD2/3 expression levels. hPSCs were serum starved for 24 hours and treated with 10 ng/ml TGF-β1 for 1 hour. Total proteins were harvested and subjected to western blot analysis of phosphorylated SMAD2/3 (pSMAD2, pSMAD3) and total SMAD2/3. GAPDH was used as a loading control.

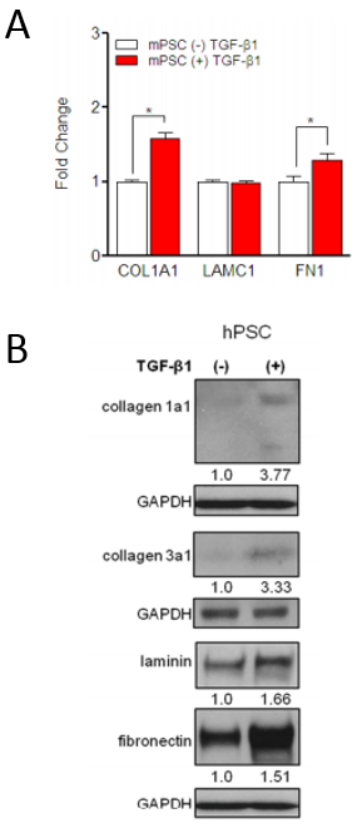

Figure 7. TGF-β1 activated PSCs exhibit increased expression of ECM components at the mRNA and protein level. (A) mPSCs were serum starved for 24 hours and then stimulated with 10 ng/ml TGF-β1 for 24 hours. Total RNA was extracted and used to quantify miR-29 targets, and collagen 1a1 (COL1A1), laminin (LAMC1), and fibronectin (FN1) mRNAs. Data is presented as mean ± SEM; n=6/group, statistics generated by t-test, *$p<0.05$. (B) Western blot analysis of ECM protein levels of collagen 1a1, collagen 3a1, laminin gamma-1 (laminin) and fibronectin in hPSCs, which were serum starved and treated with TGF-β1 for 24 hours. GAPDH was used as loading control. Relative quantification of band intensities, normalized to loading controls, are shown below respective blots.

TGF-β1 downregulates miR-29 in human fibroblasts and cancer associated fibroblasts.

In addition to PSCs, pancreatic fibroblasts are also known to play a role in the stromal reaction associated with PDAC tumors (96, 99). To understand whether the loss of miR-29 is common in TGF-β1 activation, we treated normal primary human pancreatic fibroblasts with TGF-β1 and quantified miR-29 expression levels. Similar to PSCs, TGF-β1-activated primary fibroblasts had decreased miR-29a expression compared to nascent cells (Figure 8A), suggesting that the loss of miR-29a is consistent in both activated PSCs and fibroblasts. During PDAC initiation and progression, normal pancreatic fibroblasts convert into an activated state and are known as cancer associated fibroblasts (CAFs). In addition to PSCs, CAFs have been shown to play a role in PDAC stromal deposition (99), initiation (119), progression, and metastasis (120). To determine whether TGF-β1 dependent loss of miR-29 is a common phenomenon in CAFs, we examined the effects of TGF-β1 treatment on miR-29 expression in primary CAFs isolated from PDAC patients. Similarly, CAFs challenged with TGF-β1 showed a significant decrease in the expression of miR-29 family members (Figure 8B), suggesting that the loss of miR-29 function is a common phenomenon of activated stromal cells associated with fibrotic stromal deposition.

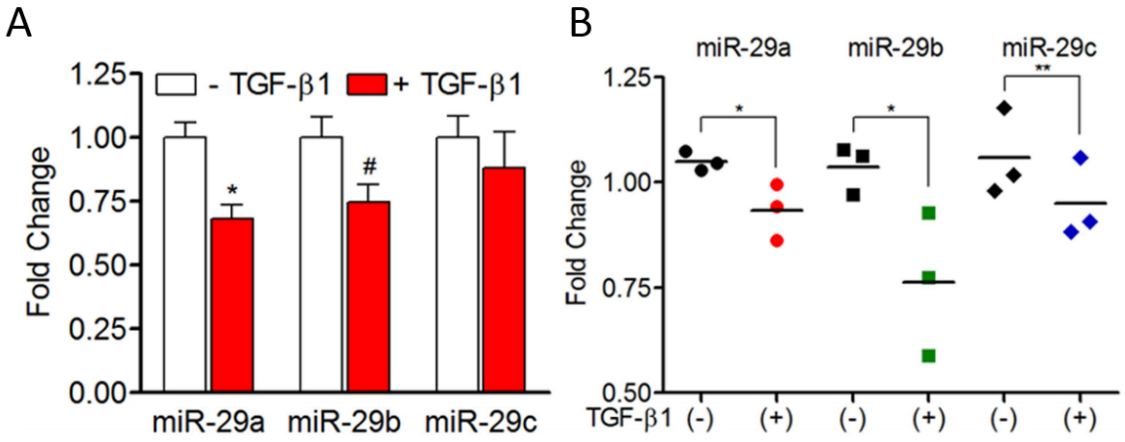

Figure 8. TGF-β1 downregulates miR-29 in human fibroblasts and cancer associated fibroblasts. Primary human pancreatic fibroblasts or cancer associated fibroblasts (CAFs) isolated from human PDAC tumors were stimulated with 10 ng/ml of TGF-β1 for 24 hours, and total RNA was isolated for miR-29 expression analysis. (A) qPCR analysis of miR-29 family members in TGF-β1 activated primary human pancreatic fibroblasts or (B) PDAC CAFs (n= 3). Data is presented as the mean ± SEM; n= 3; p-values determined by t-test, *p< 0.05, # p< 0.08, **p< 0.01. Experiments were repeated three times and representative data are shown.

Activation of *Kras*^{G12D} in the pancreas leads to loss of miR-29 and increased collagen deposition. Activating mutations in the proto-oncogene *KRAS* are common in 90%–95% of PDAC patients, and *Kras*^{G12D} is the most frequently found genetic aberration (121). In order to explore the effects of *Kras*^{G12D} on miR-29 expression, we collected pancreata from a well-characterized PDAC mouse model, KC(113), at 1-9 months of age and examined global pancreatic miR-29 expression and collagen/connective tissue deposition. We observed a significant loss of miR-29 expression in KC mice compared to C57BL/6 controls (Figure 9A) in conjunction with a significant increase in pancreatic fibrosis/collagen estimation by gross histopathological examination (H&E and Sirius Red stain) (Figure 9B) and quantification of Sirius Red positive collagen (Figure 9C).

Global loss of miR-29 expression in human PDAC tumors. To determine the miR-29 expression patterns in human PDAC tumors and establish its clinical relevance, we examined miR-29 expression in PDAC patient biopsies with 35-80% tumor stroma, assessed by Sirius Red staining, and compared them to normal patient control samples. Similar to KC mice, we observed a significant decrease in all miR-29 family members in PDAC tumor samples compared to normal patient controls (Figure 9D). Furthermore we conducted H&E and Sirius Red staining and observed a corresponding increase in fibrosis in PDAC tumor biopsies by both gross histopathological examination (Figure 10A) and quantification of Sirius Red staining (Figure 10B). Corresponding patient clinical data of each sample is provided in Table 1 and Table 2.

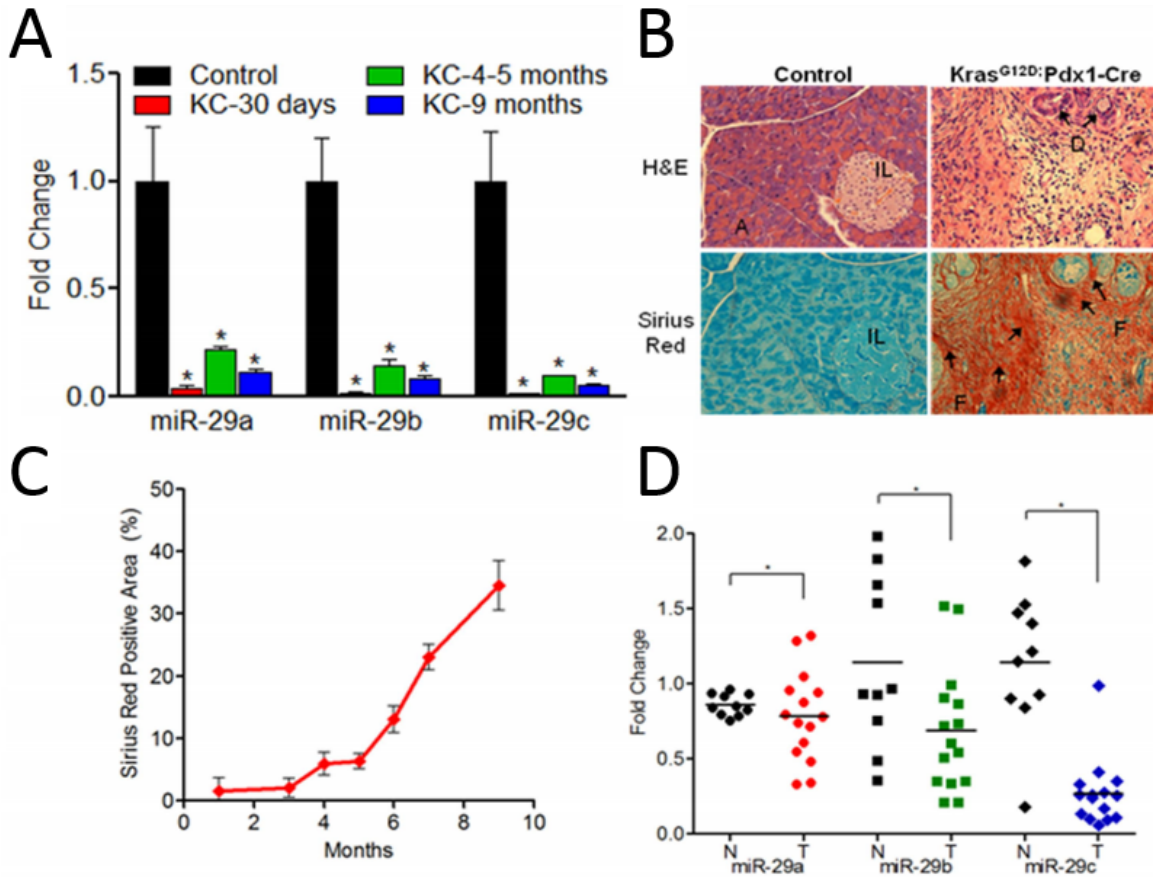

Figure 9. Global loss of miR-29 is a common phenomenon of KrasG12D-activated murine pancreata and human PDAC tumors with increased collagen deposition. (A) miR-29 expression levels in KC, PDAC mouse model. Total RNA was isolated from formalin fixed paraffin embedded (FFPE) pancreatic tissue sections of KC or C57BL/6 control mice (n= 3–5 animals/time point) and subjected to miR-29 expression analysis via qPCR. (B) Representative H&E and Sirius Red stained pancreatic sections from C57BL/6 control and KC mice (9 months). Acinar cells "A", Islets of Langerhans "IL", pancreatic ducts "D", and prominent fibrosis "F" are demonstrated in the KC animals. (C) Quantification of collagen in KC animals from 1–9 months of age. ImageJ was used to quantify Sirius Red positive collagen. Data is presented as the mean± SEM; n= 3 to 5 animals/time point; (D) miR-29 expression analysis in PDAC patient tumors. Total RNA

was isolated from FFPE sections of normal controls (n= 10) (N; solid black) or PDAC patient tumors (n= 15) with 35–80% stroma (T; red, green, or blue), and miR-29 expression was analyzed by qPCR. miR-29 family members are represented by circles (miR-29a), squares (miR-29b), and diamonds (miR-29c). For each group, the mean expression of miR-29 family members is indicated as horizontal lines. p-values determined by t-test, *$p < 0.05$.

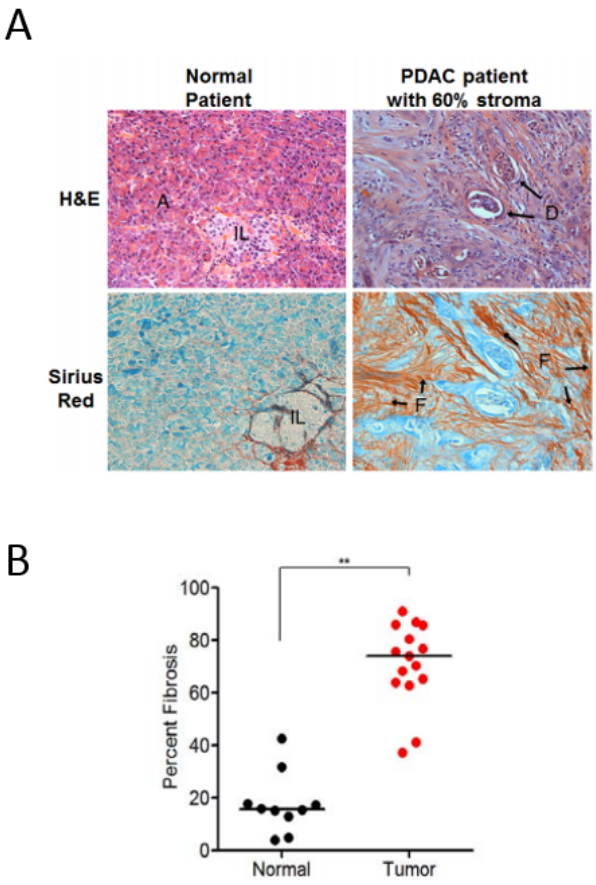

Figure 10. Pancreatic tissues from PDAC patient samples display a high degree of fibrosis. (A) Representative H&E and Sirius Red stained pancreatic sections from normal controls or PDAC patient tumors. Acinar cells "A", Islets of Langerhans "IL", pancreatic ducts "D", and prominent fibrosis "F" are demonstrated in the PDAC patients. (B) Quantification of fibrosis/collagen in normal and PDAC patients. FFPE sections from normal and PDAC patient tumors were stained with H&E for gross histological analysis and Sirius Red to estimate the degree of fibrosis/collagen. Percent fibrosis in normal patient controls (n=10) and PDAC patient tumors (n=15) was calculated using Sirius Red positive pancreatic sections (four 20X random images/patient). ImageJ was used to quantify Sirius Red positive area. The mean percentage of fibrosis/collagen for each group is shown as horizontal lines. Statistics were generated using t-test, **$p<0.01$.

Table 1: Clinical PDAC Patient Data

Patient Data

	Normal	PDAC
Pancreas		
Normal	10	0
Tumor	0	15
Sex		
Male	5	9
Female	5	6
Tumor Stage		
T0	n/a	0
T1	n/a	1
T2	n/a	1
T3	n/a	13
Tumor Grade (differentiation)		
Well	n/a	1
Moderate	n/a	10
Poor	n/a	4
Lymph Node		
Positive	1	12
Negative	3	3
Not recorded	6	0
Age		
At procedure (average)	65.2	63.7
Range	38-77	42-83
Stroma		
35-50%	n/a	10
55-80%	n/a	5

Source: Indiana University Simon Cancer Center Tissue Bank and Department of Pathology

Table 2 Clinical Sample ID and Information

Sample type	Source	Sample ID#	% of stroma	Age	Sex	Ethnicity	Tumor location in pancreas-Head/Tail	Stage	Lymph Node-Positive/negative	Lymphovascular invasion (LVI)-positive/ negative	Perineural invasion (PNI)-positive/ negative	pTumor size (T0-T5)	Tumor Grade cannot be assessed (GX) Well (G1), Moderately (G2), or Poorly (G3) differentiated	Margins negative and positive
Normal	IU Pathology	N-01		73	F	white	Head		Negative		Positive			
Normal	IU Pathology	N-02		68	M	white	Head		positive (1/9)					negative
Normal	IU Pathology	N-03		38	F	white	not specified							
Normal	IU Pathology	N-04		55	F	white	not specified							
Normal	IU Pathology	N-05		70	M	white	not specified		Negative					negative
Normal	IU Pathology	N-06		73	M	white	Head		Negative					
Normal	IUSCC	N-07		74	F	non hispanic	not specified							
Normal	IUSCC	N-08		63	M	non hispanic	not specified							
Normal	IUSCC	N-09		61	F	non hispanic	not specified							
Normal	IUSCC	N-10		77	M	non hispanic	not specified							
Tumor	IU Pathology	PDAC-01	50	64	M	white	head	pT3, N1, MX	positive (10/19)	positive	Positive	T3	Moderatly (G2)	negative
Tumor	IU Pathology	PDAC-02	80	66	M	white	Head	pT3, pN1, pMX	positive (9/11)	positive	Positive	T3	Poorly (G3)	positive
Tumor	IU Pathology	PDAC-03	70	67	M	white	Head	pT3, pN1, pMX	positive (8/13)	positive	Positive	T3	Moderatly (G2)	positive
Tumor	IU Pathology	PDAC-04	50	71	M	white	Head	pT3, N1, MX	Positive (1/12)	Negative	Positive	T3	Moderatly (G2)	negative
Tumor	IU Pathology	PDAC-05	65	68	M	white	Head	pT3, pN1, pMX	positive (9/21)	positive	Positive	T3	Well to Moderatly	positive
Tumor	IU Pathology	PDAC-06	70	69	F	black	Head	pT3, N0, MX	negative	Negative	Positive	T3	Poorly (G3)	negative
Tumor	IUSCC	PDAC-07	60	75	F	non hispanic	Head	T2, N1, MX	positive		Positive	T2	Moderatly (G2)	
Tumor	IUSCC	PDAC-08	40	54	M	non hispanic	Head	T3, N1, MX	positive		Positive	T3	Moderatly (G2)	
Tumor	IUSCC	PDAC-09	40	60	F	non hispanic	Head	T3, N1, Mx	positive		Positive	T3	Moderatly (G2)	
Tumor	IUSCC	PDAC-10	35	57	M	non hispanic	Tail	T3, N1, MX	positive	positive	Positive	T3	Moderatly (G2)	
Tumor	IUSCC	PDAC-11	40	73	F	non hispanic	Head	T1, N0, MX	negative		Positive	T1	Poorly (G3)	
Tumor	IUSCC	PDAC-12	50	83	F	non hispanic	Head	T3, N0, MX	negative		Positive	T3	Moderatly (G2)	
Tumor	IUSCC	PDAC-13	50	53	F	non hispanic	Head	T3, N1, MX		positive	Positive	T3	Moderatly (G2)	
Tumor	IUSCC	PDAC-14	50	42	M	non hispanic	Tail	T3, N1, MX		Negative	Positive	T3	Moderatly (G2)	
Tumor	IUSCC	PDAC-15	50	53	M	non hispanic	Tail	T3, N1, MX	positive	negative	Postive	T3	Poorly (G3)	

Source: Indiana University Simon Cancer Center Tissue Bank and Department of Pathology.

Table Description: “Sample type” indicates normal pancreas versus PDAC tumor biopsies. “Source” indicates the source of biopsies, either IU Pathology department (IU Pathology) or IU Simon Cancer Center (IUSCC). “Sample ID” indicates arbitrary sample name

for purposes of internal documentation. “% of stroma” indicates % area of Sirius Red positive staining as assessed by histology for respective samples. “Age”, “Sex”, “Ethnicity” are descriptors of patients at time of biopsy. “Tumor location in pancreas – Head/Tail” indicates the location in which the biopsy was taken from the patient pancreas. “Stage” indicates the grade of primary tumor (T), lymph node spread (N), and degree of metastasis (M). “Lymph Node-Positive/Negative” indicates the presence of metastatic events within the lymph node. “Lymphovascular invasion (LVI) – positive/negative” indicates presence or absence of metastatic events within patient vasculature. “Perineural invasion (PNI) – positive/negative” indicates spread of cancer near or surrounding a nerve. “pTumor size” indicates the degree of tumor growth. “Tumor Grade” indicates the degree of differentiation of cancer cells. “Margins” indicate whether the sampled biopsy encompasses the entirety of the tumor (negative) as indicated by the presence of normal tissue surrounding the tumor or only encompasses only a portion of the tumor (positive).

PSC and epithelial cell specific miR-29 loss of expression in KC mice and human PDAC tumors. As we observed global loss of miR-29 in both human PDAC tumors and KC mice, to examine PSC and epithelial cell specific miR-29 expression patterns in PDAC tumors and KC mice pancreata, we performed *in situ* hybridization of miR-29a, the most abundantly expressed miR-29 family member in PSCs, epithelial cells, and the pancreas (Figure 11). To assess PSC specific miR-29 expression, we co-stained PDAC tumors and KC mice pancreata with miR-29a and glial fibrillary acidic protein (GFAP), a cell marker of both active and inactive PSCs/fibroblasts(122). Consistent with PSCs/fibroblasts challenged with TGF-β1, GFAP- positive cells of PDAC tumors displayed a significant loss of miR-29a compared to normal patient control pancreata (Figure 12). Similarly, KC mice displayed significant loss of miR-29a in GFAP-positive cells compared to control mice at early (2-4 months) and late ages (9-10 months) (Figure 13).

To examine epithelial cell specific miR-29 expression patterns, we co-stained human PDAC tumors and KC mice pancreata with miR-29a, and Cytokeratin-19 (CK19), a cell marker specific to epithelial cells (123) . Similar to PSCs, CK19 positive epithelial cells of PDAC tumors (Figure 12C, Figure 12D) and KC mice (Figure 14) showed a significant loss of miR-29 expression compared to normal controls, indicating that the global loss of miR-29 may be attributed by both stromal PSCs and epithelial cells.

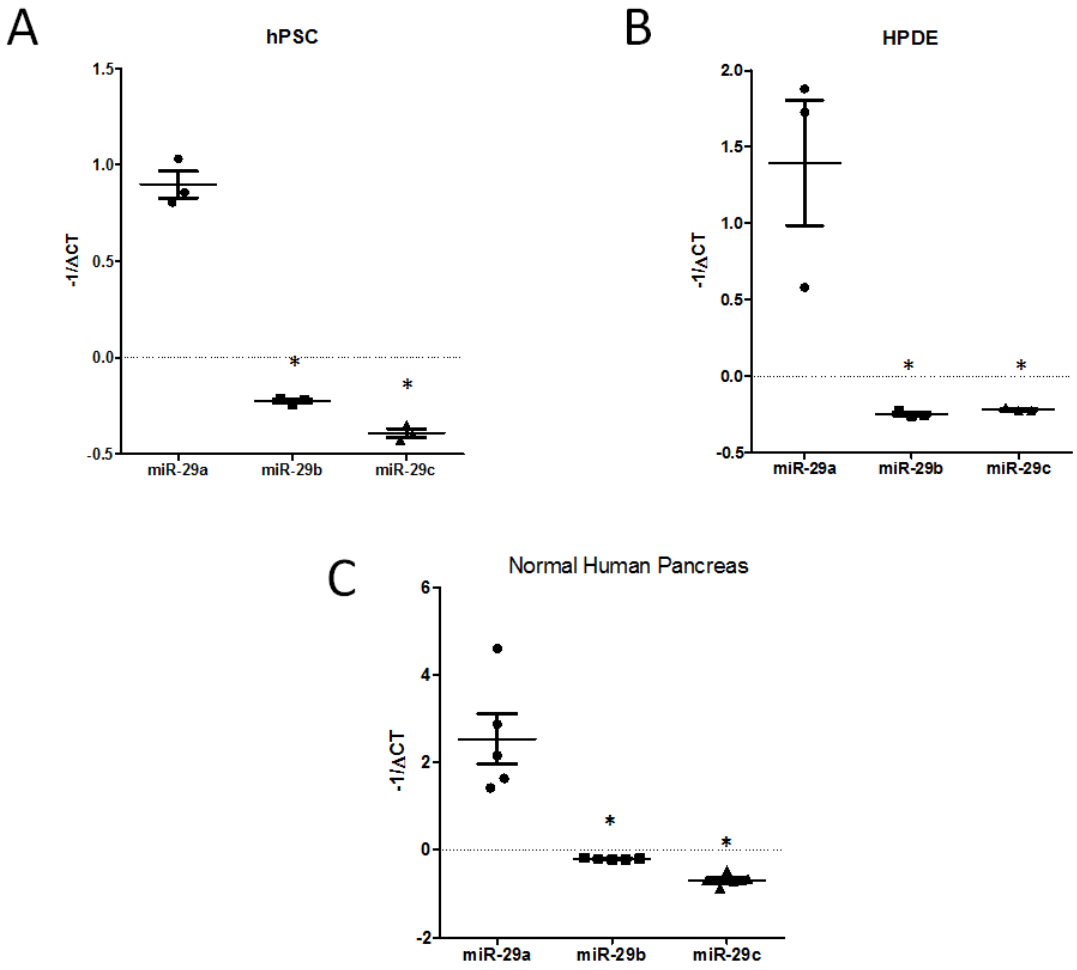

Figure 11. miR-29a is the most abundantly expressed miR-29 family member in pancreatic stellate cells, pancreatic ductal epithelial cells, and the whole pancreas. miR-29a, -29b, -29c expression was measured in RNA isolated from (A) nascent hPSCs (serum starved 24hrs), (B) pancreatic ductal epithelial cells (HPDE) (n=3), or (C) normal human pancreas (n=5), by qPCR using U6 snRNA as an internal control. Delta CT (ΔCT) was calculated for each miR-29 family member to measure relative expression levels. Boxplots represent -1/ ΔCT of miR29 expression levels in (hPSC, HPDE, or normal human pancreas,). Statistics calculated using student t-test, *$p<0.05$.

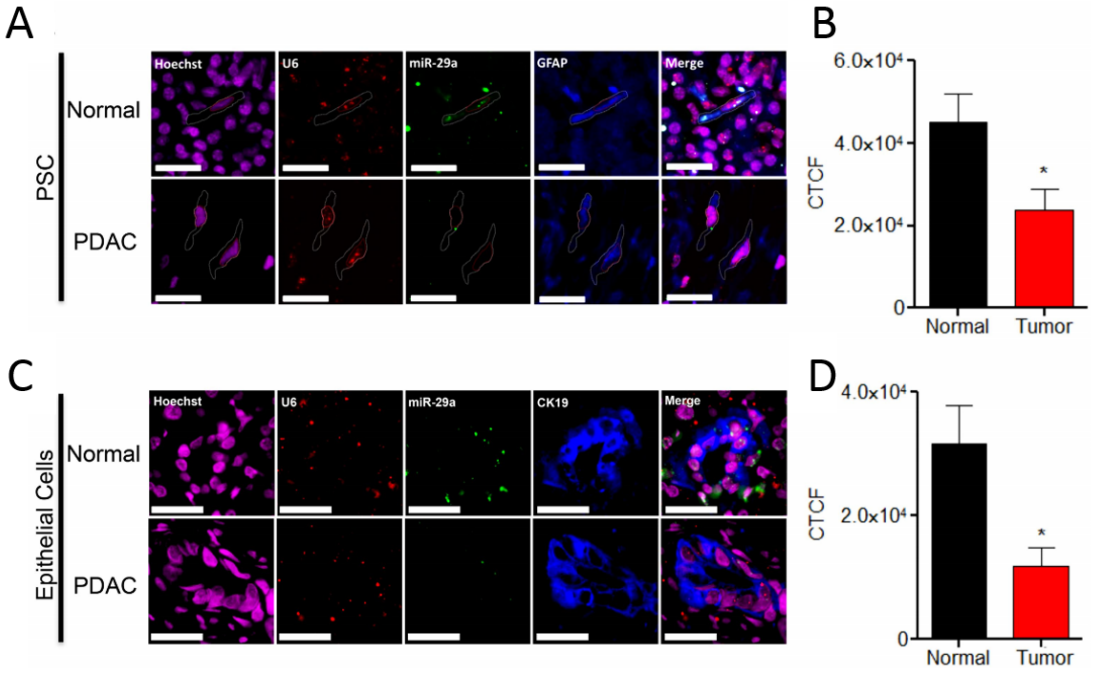

Figure 12. PSC and epithelial cell specific miR-29 loss of expression in human PDAC tumors. (A, C) In situ hybridization of miR-29 in PSCs (A) and epithelial cells (C) of normal control and PDAC patient tumors. FFPE pancreatic tissue sections from normal control and PDAC patients (n = 4/group) were subjected to miR-29a in situ hybridization. Representative images are presented as a single channel or merged (scale bar is 5 μm, 20X magnification). Hoechst nuclear stain (magenta), U6 (red), miR-29a (green), and GFAPpositive PSCs or CK19-positive epithelial cells (blue). (B, D) Corrected total cell fluorescence (CTCF) of miR29a in PDAC tumors (n = 4) compared to control patients (n = 4) was calculated for each patient averaging six or more randomly selected GFAP-positive PSCs (B) or CK19-positive epithelial cells (D) using ImageJ analysis. Data represents mean ± SEM. Statistics were generated using t-test, *$p < 0.05$.

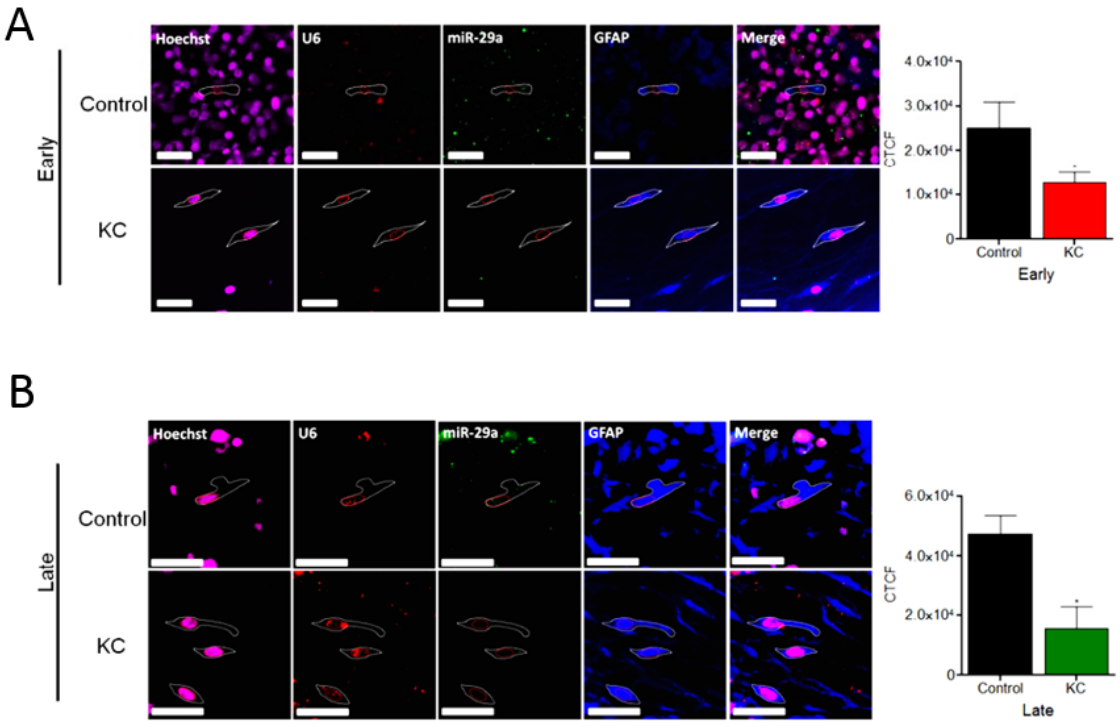

Figure 13. miR-29a is decreased in GFAP-positive PSCs in KC mice. In situ hybridization of miR-29a in pancreata of control mice (C57BL/6) and KC mice at early and late time points. FFPE pancreatic tissue sections collected at (A) early (2-4 months) and (B) late (9-10 months) time points from C57BL/6 control or KC mice (n=3/group/time point) were subjected to miR-29a in situ hybridization and images were generated using tyramide substrate amplification technique. Corrected total cell fluorescence (CTCF) of miR-29a was calculated for each animal by averaging six randomly selected GFAP-positive PSCs/fibroblasts using ImageJ analysis. Data represents the mean $\pm$ SEM; n=3; statistics generated by t-test, *$p<0.05$. Representative images are presented as a single channel, or merged (scale bar is 5 µm, 20X magnification). Hoechst Nuclear stain (magenta), U6 (red), miR-29a (green), and GFAP (blue).

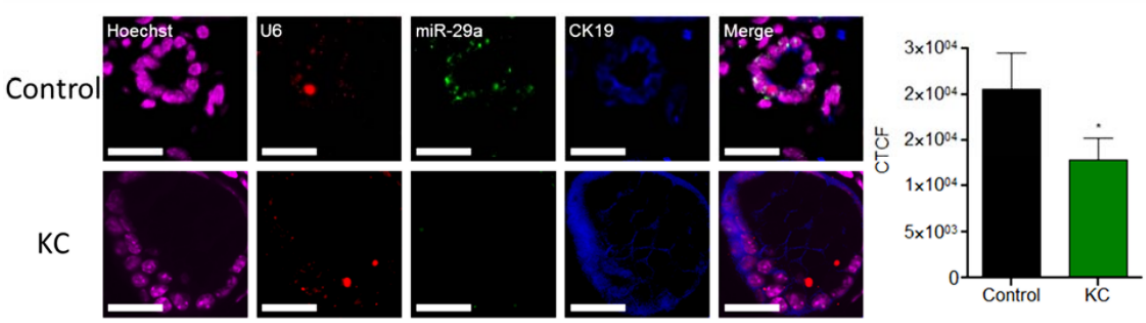

Figure 14. miR-29a is decreased in CK19-positive epithelial cells in KC mice. In situ hybridization of miR-29a in pancreata of control mice (C57BL/6) and KC mice. FFPE pancreatic tissue sections collected from 9-10 month old C57BL/6 control or KC mice (n=3/group/time point) were subjected to miR-29a in situ hybridization and images were generated using tyramide substrate amplification technique. Corrected total cell fluorescence (CTCF) of miR-29a was calculated for each animal by averaging six or more randomly selected CK19-positive epithelial cells using ImageJ analysis. Data represents the mean $\pm$ SEM; n=3; statistics generated by t-test, *$p<0.05$. Representative images are presented as a single channel, or merged (scale bar is 5 μm, 20X magnification). Hoechst Nuclear stain (magenta), U6 (red), miR-29a (green), and CK-19 Epithelial stain (blue).

Physiological role of miR-29 in PSC-mediated stromal ECM protein accumulation. Since the loss of miR-29a/b was commonly observed in PSCs/fibroblasts challenged with TGF-β1, in $Kras^{G12D}$ expressing murine pancreata, and in human PDAC biopsies, we performed *in vitro* gain/loss-of-function studies to determine the physiological role of miR-29 in PSC-mediated stromal protein expression using synthetic miR-29 mimics and miR-29 locked nucleic acids (LNAs), a miR-29 family inhibitor. To test the effect of miR-29 gain-of-function on PSC-mediated stromal accumulation, we transfected mouse and human PSCs with control, miR-29a, or b mimics, after TGF-β1 treatment, and examined ECM protein levels. We confirmed the increase of exogenous miR-29a and miR-29b in both mouse and human PSCs transfected with synthetic miR-29a/b mimics (Figure 15). As expected, we observed a significantly lower expression of direct miR-29 ECM protein targets (Figure 16A) in PSCs transfected with miR-29 mimics compared to cells transfected with control mimic (Figure 16B, Figure 17). Interestingly, in miR-29 overexpressed PSCs, we also saw a decrease in fibronectin, a major ECM protein in PDAC stroma and a known indirect target of miR-29 (94) (Figure 16B, Figure 17).

In order to better understand the underlying mechanism for miR-29-mediated fibronectin repression in TGF-β1 activated PSCs, we investigated the effect of miR-29 on TGF-β1 signaling. We observed a decrease in pSMAD2 levels in PSCs transfected with miR-29a or miR-29b compared to control mimic (Figure 16C, Figure 18), suggesting an indirect effect of miR-29 on fibronectin suppression.

For miR-29 loss-of-function studies, we transfected TGF-β1 activated PSCs with control or miR-29 LNAs and assessed the effects on stromal protein accumulation. We

confirmed the knockdown of all three miR-29 family members in PSCs transfected with miR-29 LNAs (Figure 19). Inhibition of miR-29 by LNAs led to a further increase in accumulation of ECM proteins (Figure 16D and Figure 20).

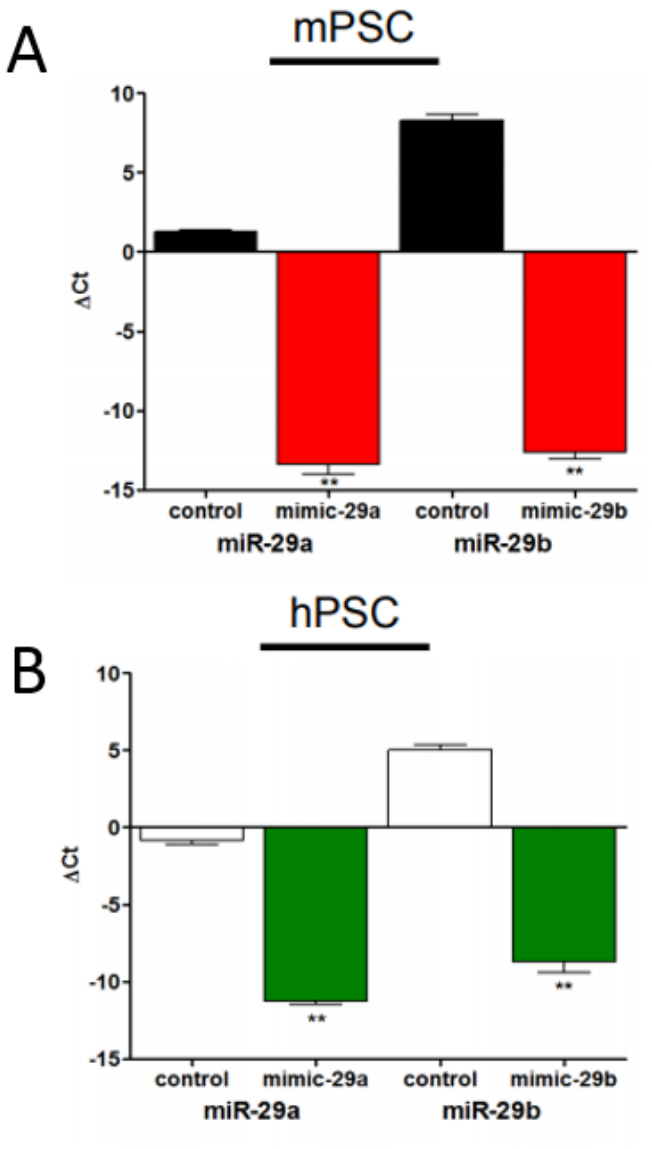

Figure 15. Mouse and human PSCs transfected with miR-29 mimics have increased exogenous miR-29a and miR-29b. (A) mPSCs and (B) hPSCs were transfected with 25 nM control, miR-29a, or miR-29b mimics. 24 hours post-transfection, RNA was extracted and miR29a and miR-29b expression levels were quantified by qPCR using U6 snRNA as an internal control. Data is presented as mean ΔCT values ± SEM; n=3, statistics calculated using student t-test, **p<0.01.

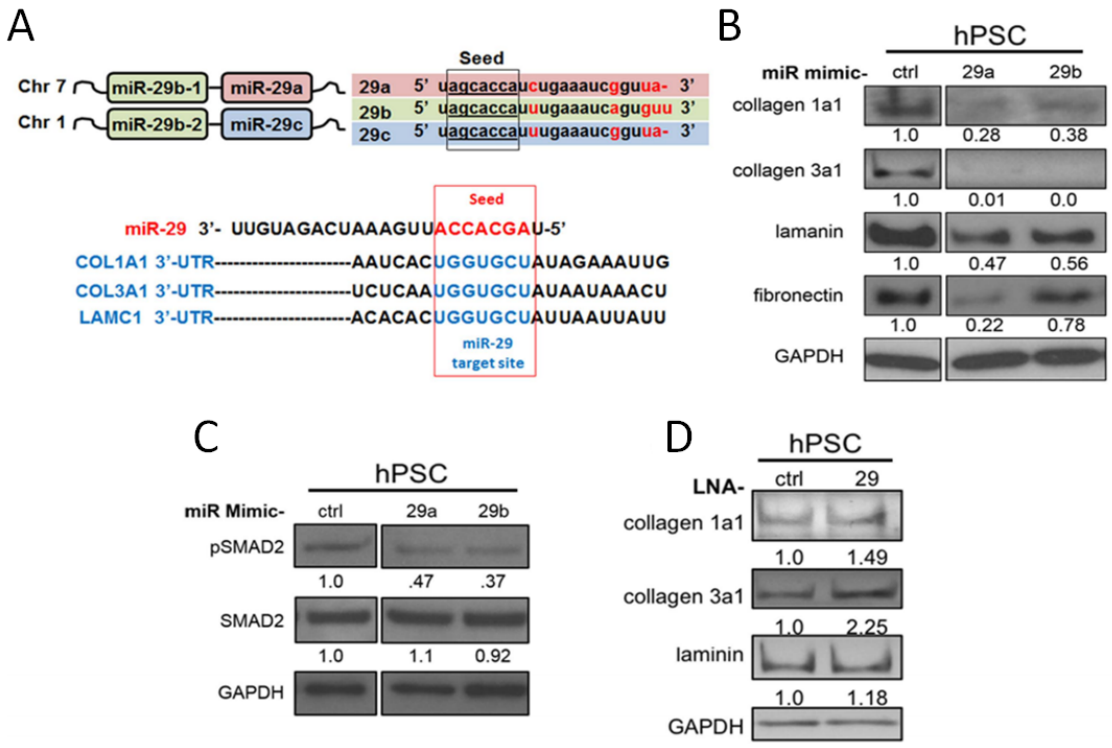

Figure 16. Physiological role of miR-29 in PSC-mediated stromal ECM protein accumulation. For miR29 gain and loss-of-function studies, serum starved and TGF-β1 (10 ng/ml, 24hours) treated PSCs were transfected with synthetic miR-29 mimics or miR-29 locked nucleic acids (LNAs), a miR-29 family inhibitor respectively. Subsequently, the effects of miR-29 gain and loss-of-function on extracellular matrix (EMC) proteins was evaluated by western blot analysis. (A) Schematic representation of the miR-29 family members, and 3′-UTR binding sites of miR-29 ECM targets. miR-29 encoding loci are located on human chromosome 7 (miR-29a/miR-29b-1) and chromosome 1 (miR-29b-2/miR-29c). All three miR29 family members (miR-29a, miR-29b, and miR-29c) have identical seed sequences. miR-29 binding sites in the 3′-UTR of ECM protein transcripts encoding collagen 1a1 (COL1A1), collagen 3a1 (COL3A1), and laminin

gamma-1 (LAMC1) are depicted. (B) Western blot analysis of ECM proteins in miR-29 gain-of-function studies of hPSCs. TGF-β1 stimulated hPSCs were transfected with 20 nM mimic control (ctrl), mimic-29a (29a), or mimic-29b (29b). 24hours post-transfection, total proteins were harvested and subjected to western blot analysis of ECM proteins (collagen 1a1, collagen 3a1, laminin, and fibronectin). (C) Western blot analysis of pSMAD2 in miR-29 overexpressed hPSCs. Serum starved and TGF-β1 treated hPSCs were transfected with miR-29 (20 nM) or control mimics (20 nM). 24 hours post-transfection, protein was harvested and subjected to western blot analysis for pSMAD2 and SMAD2. (D) Western blot of collagen 1a1, collagen 3a1, and laminin in hPSCs transfected with LNA-ctrl or miR-29 family inhibitor (LNA-29). TGF-β1 treated hPSCs were transfected with 50 nM of LNA-29 or LNA-control. 24hours post-transfection, protein was harvested and subjected to western blot analysis. Relative quantification of protein band intensities, normalized to GAPDH loading control, are shown below each blot. Each experiment was repeated three times and representative data are presented.

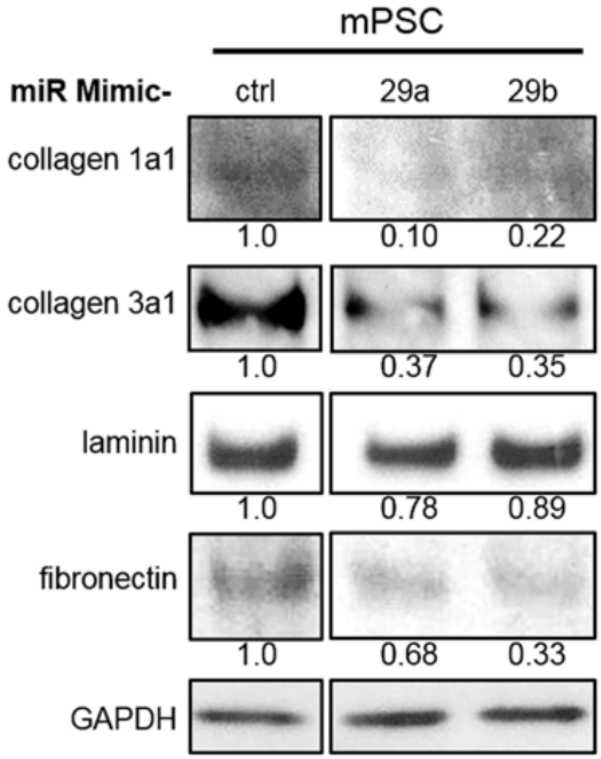

Figure 17. Ectopic expression of miR-29 mimics reduce ECM components in TGF-β1 activated mouse PSCs. Mouse PSCs were serum starved for 24 hours and activated with 10 ng/ml TGF-β1. 48 hours post-treatment, PSCs were transfected with miR-mimics (29a, 29b, or control) for 24 hours, and total proteins isolated. Western blot analysis was performed to determine the expression levels of ECM proteins (collagen 1a1, collagen 3a1, laminin gamma-1, and fibronectin) using GAPDH as a loading control. Relative quantification of protein band intensities, normalized to loading controls are shown below respective blots.

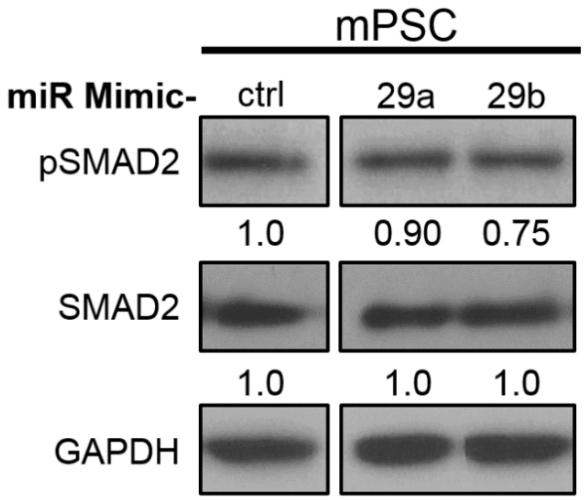

Figure 18. miR-29 suppresses SMAD2 activation in mouse PSCs. mPSCs were transfected with 25 nM miR-mimics, miR-29a (29a), miR-29b (29b), or mimic control (ctrl). Cells were then serum starved for 24 hours and activated with 10 ng/ml TGF-β1 for 24 hours. Western blot analysis of pSMAD2 and SMAD2 was performed. Relative quantity was measured using GAPDH as a loading control and are shown below respective blots.

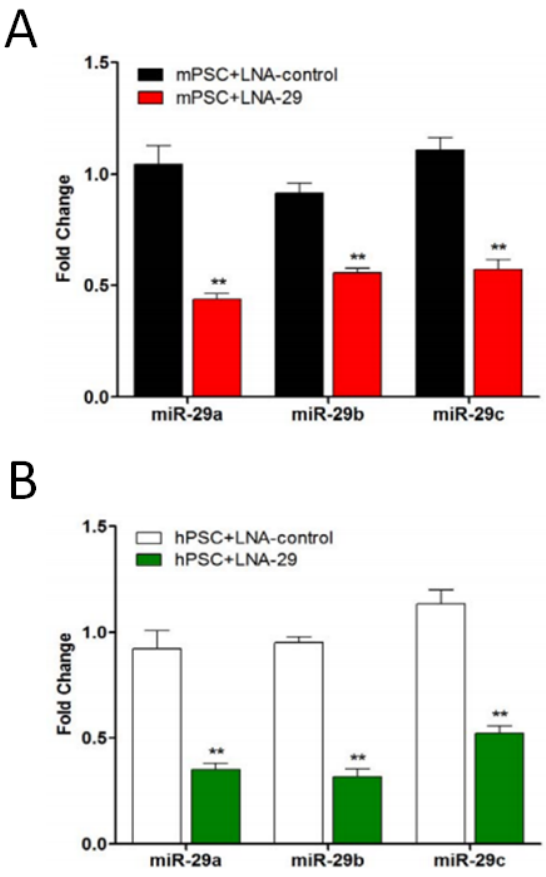

Figure 19. LNA-miR-29 efficiently knockdown all endogenous miR-29 family members (miR-29a, miR-29b, and miR-29c) in mouse and human PSCs. (A) mPSCs and (B) hPSCs were transfected with 25 nM LNA-control or LNA-miR-29 (LNA-29). 24 hours posttransfection, total RNA was isolated and miR-29 expression was quantified using qPCR analysis. Data is presented as mean $\pm$ SEM; n=3, statistics generated by student's t-test, **$p<0.01$.

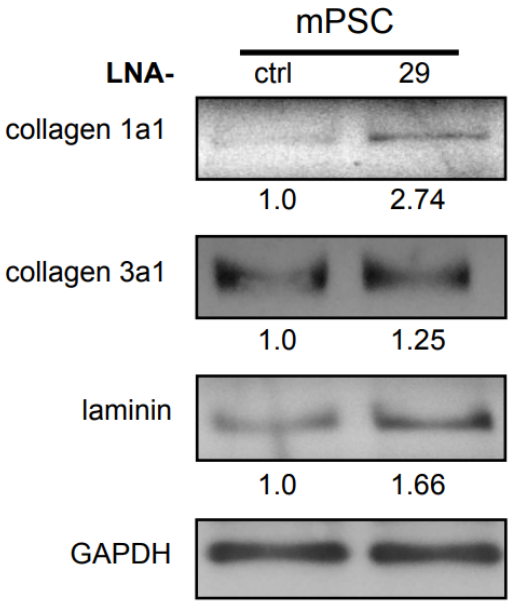

Figure 20. miR-29 knockdown increases direct miR-29 ECM target proteins in mouse PSCs. mPSCs were starved for 24 hours, activated with 10 ng/ml TGF-β1 for 24 hours, and transfected with LNA-control (ctrl) or LNA-29 (29). 24 hours post-transfection, total proteins were harvested to examine ECM proteins, collagen 1a1, collagen 3a1, and laminin gamma-1 (laminin) by western blot analysis. Measurements of GAPDH were used as a loading control. Relative quantification of band intensities normalized to loading control and are shown below respective blots.

Ectopic expression of miR-29 in PSCs reduces stromal deposition, cancer cell viability, and colony growth in co-culture. Subsequently, to evaluate the effects of miR-29 overexpression in PSCs on cancer growth, we transfected PSCs with control or miR-29 mimics and co-cultured them with pancreatic cancer cells. Direct co-culture of PSCs overexpressing miR-29a or b with pancreatic cancer cells caused a significant decrease in the ability of the cancer cells to form colonies (Figure 21A, Figure 22A) and reduced stromal deposition associated with cancer colonies (Figure 22B). To elucidate the underlying mechanism that leads to a decrease in pancreatic cancer colony formation, we evaluated the autocrine and paracrine effects of miR-29 on the viability of PSCs and pancreatic cancer cells, respectively. For autocrine effects of miR-29, we transfected PSCs with control or miR-29 mimics, and cell viability was monitored for up to 96 hours post-transfection. Overexpression of miR-29 did not reduce PSC viability compared to cells transfected with control mimics (Figure 23). To determine the paracrine effects of miR-29 on cancer cell viability, pancreatic cancer cells were cultured in conditioned media collected from PSCs transfected with control or miR-29 mimics. We observed a significant decrease in viability of pancreatic cancer cells growing in conditioned media collected from miR-29 transfected PSCs compared to PSCs transfected with control mimics (Figure 21B). Finally, to evaluate the effect of miR-29 overexpression in PSCs on anchorage independent growth of pancreatic cancer cells, we co-cultured miR-29 transfected PSCs with cancer cells in soft agar assays. We observed a decrease in anchorage independent growth of pancreatic cancer cells when co-seeded with miR-29a overexpressing PSCs compared to PSCs transfected with control mimics (Figure 24). Overall, overexpression of miR-29 in PSCs caused a decrease in stromal/ECM protein accumulation and cancer colony growth.

However, the long-term consequences of miR-29 overexpression in stromal deposition and cancer progression need to be further evaluated *in vivo.*

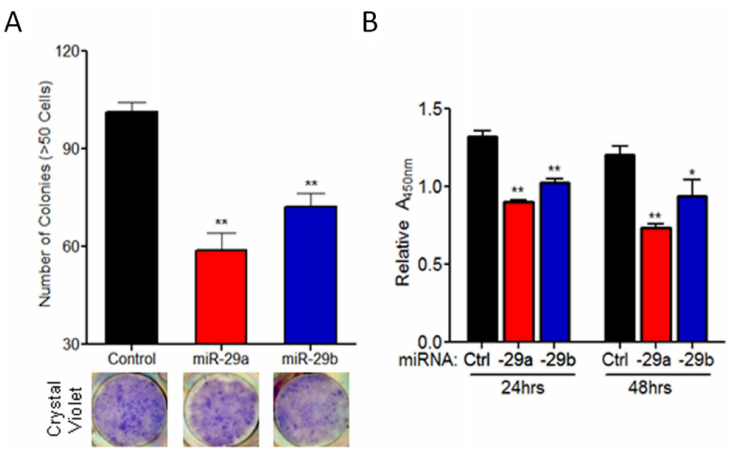

Figure 21. Ectopic expression of miR-29 in PSCs reduces cancer cells viability and cancer colony growth in co-culture. (A) Effect of miR-29 overexpression in PSCs on cancer colony growth in direct cocultures. mPSCs were transfected with 20 nM of mimic control, mimic-29a, or 29b. 24 hours post-transfection, mPSCs were plated simultaneously with 100 pancreatic cancer cells (Panc-1) in a 6-well plate. Co-cultures were allowed to grow for 10 days, fixed, and stained with crystal violet fixing solution to stain cancer cells as previously described (124) with few modifications. Cancer colonies greater than 50 cells were counted under phase contrast microscopy. Representative images of co-cultures stained with crystal violet are shown. (B) Conditioned media of PSCs expressing miR-29 show decreased effect on pancreatic cell viability. Conditioned media from mPSCs transfected with control, miR-29a, or miR-29b mimics was applied to pancreatic cancer cells (Panc-1) in a 96-well plate and viability was measured 24 and 48hours post-treatment using the Cell Counting Kit-8 assay according to manufacture protocol. Data is normalized to pancreatic cancer cells (Panc-1) treated with non-conditioned media. All experiments were repeated 3-4 times and representative data is presented. Data represents mean $\pm$ SEM. Statistics generated by t-test, *$p < 0.05$, **$p < 0.01$.

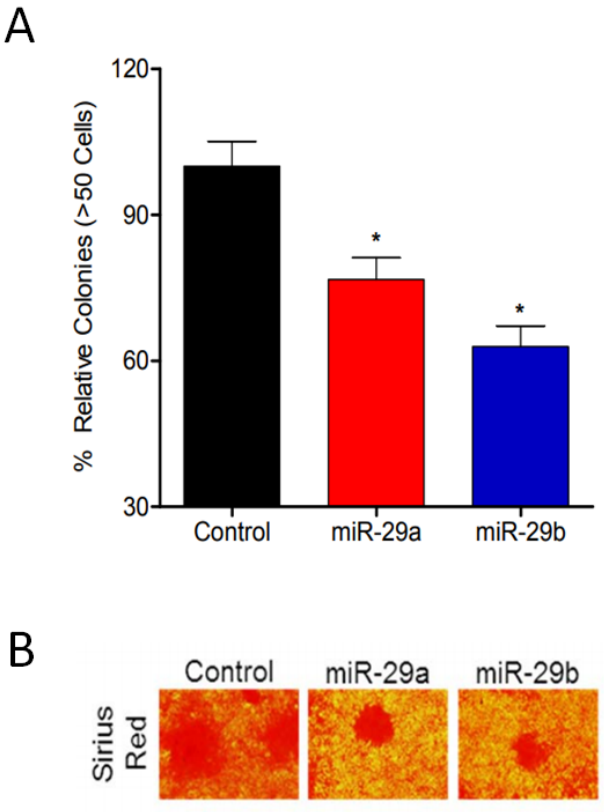

Figure 22. Ectopic expression of miR-29 in PSCs causes reduced cancer colony formation and stromal deposition in direct co-cultures. (A) mPSCs transfected with mimic control, miR-29a, or miR-29b were co-seeded in 6-well plates with MIA PaCa2 cancer cells and cultured at 37°C for 10 days. Cancer colonies were stained with crystal violet and counted. Data is presented as relative percentage of cancer colonies normalized to mimic control; mean ± SEM; n=3, statistics generated by student's t-test, *$p<0.05$. (B) Effect of miR-29 overexpression in PSCs on stromal accumulation in direct co-cultures. Mouse PSCs transfected with mimic control, miR-29a, or miR-29b, were co-seeded in 6-well plates with MIA PaCa-2 cancer cell lines, cultured at 37° for 10 days, fixed, and subjected to Sirius Red staining. Representative images of co-cultures stained with Sirius Red are shown. All experiments were repeated 3-4 times and representative data is presented.

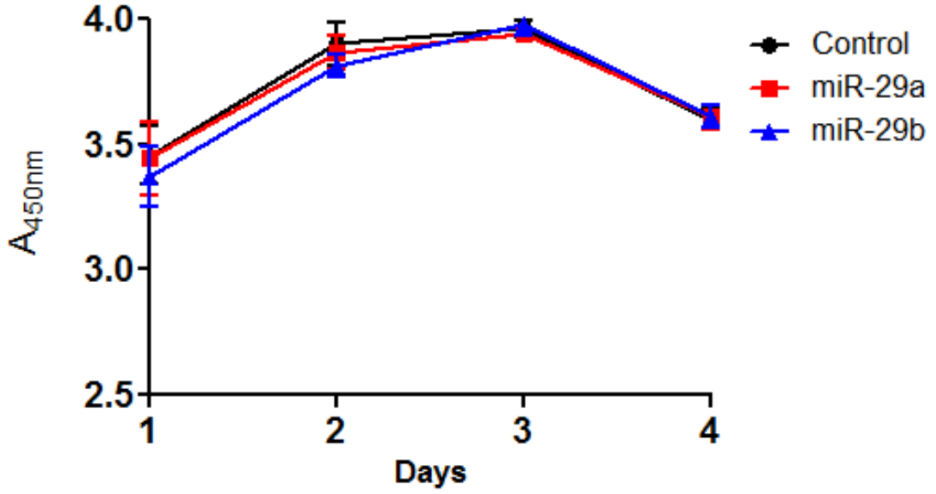

Figure 23. Ectopic miR-29 expression does not affect PSC viability. PSCs were plated into 96-well plates, serum starved 24 hours, treated with 10 ng/ml TGF-β1 for 24 hours, and then transfected with miR-control, miR-29a, or miR-29b. Cell viability was measured at 24, 48, 72, and 96 hours using the Cell Counting Kit-8 assay and absorbance was measured at 450 nm. Data is presented as average relative absorbance ± SEM; n=4-8, statistics generated by student's t-test, but were not significant.

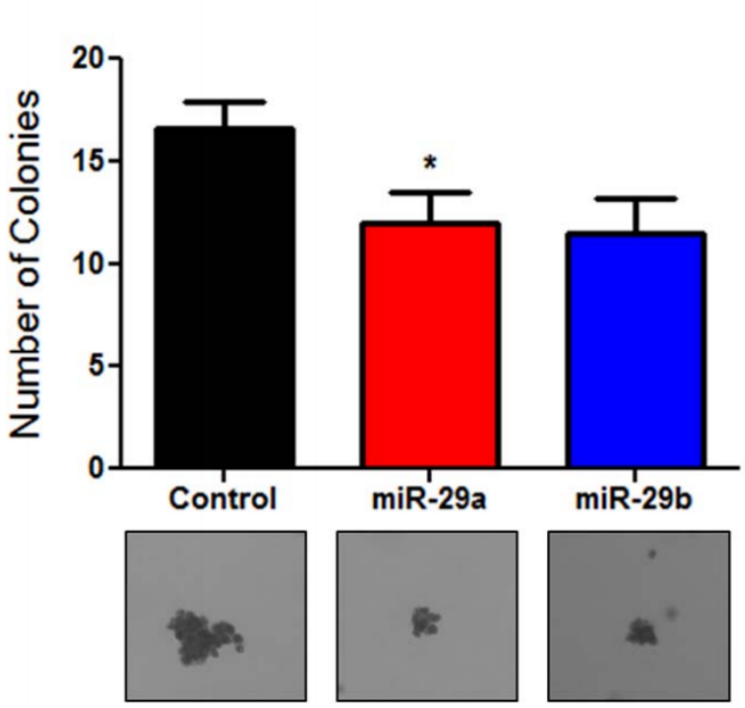

Figure 24. miR-29 decreases the effect of PSCs on anchorage independent growth of pancreatic cancer cells. mPSC transfected with mimic control, miR-29a, or miR-29b were coseeded in soft agar assay in a 6-well plate with pancreatic cancer cells (MIA PaCa-2) and were cultured at 37°C for 7 days. 500 µl of medium was supplemented every other day. Following 7 days, cells were stained with crystal violet. Cell numbers was meaured microscopically and representative images are shown. Number of colonies per well is presented as mean $\pm$ SEM; n=6, statistics generated by student's t-test, *$p<0.05$.

TGF-β1-mediated downregulation of miR-29 in PSCs is SMAD3 dependent. We next sought to identify the underlying mechanism of TGF-β1 activated loss of miR-29 in PSCs. An earlier report identified SMAD3 binding elements near the miR-29a/b-1 locus on chromosome 7 upstream of the miR-29a/b1 transcription start site (125) (Figure 25A). We subsequently knocked down SMAD3 by siRNA, a major downstream effector molecule of TGF-β1, which is known to directly regulate miR-29 expression in myoblast and renal cells (126, 127) and confirmed the loss of SMAD3 protein in transfected PSCs by western blot analysis (Figure 25B). PSCs transfected with control siRNA displayed a significant downregulation of miR-29a and miR-29b upon TGF-β1stimulation (Figure 25C). Whereas in the absence of SMAD3, PSCs no longer showed a significant change in miR-29 (Figure 25C), suggesting that the ability of TGF-β1 to suppress miR-29 expression is SMAD3 dependent. Our results, in conjunction with previous findings in muscle and kidney (95, 128) suggests that TGF-β1-mediated loss of miR-29 in PSCs may be due to the direct binding of SMAD3 to miR-29 promoter elements.

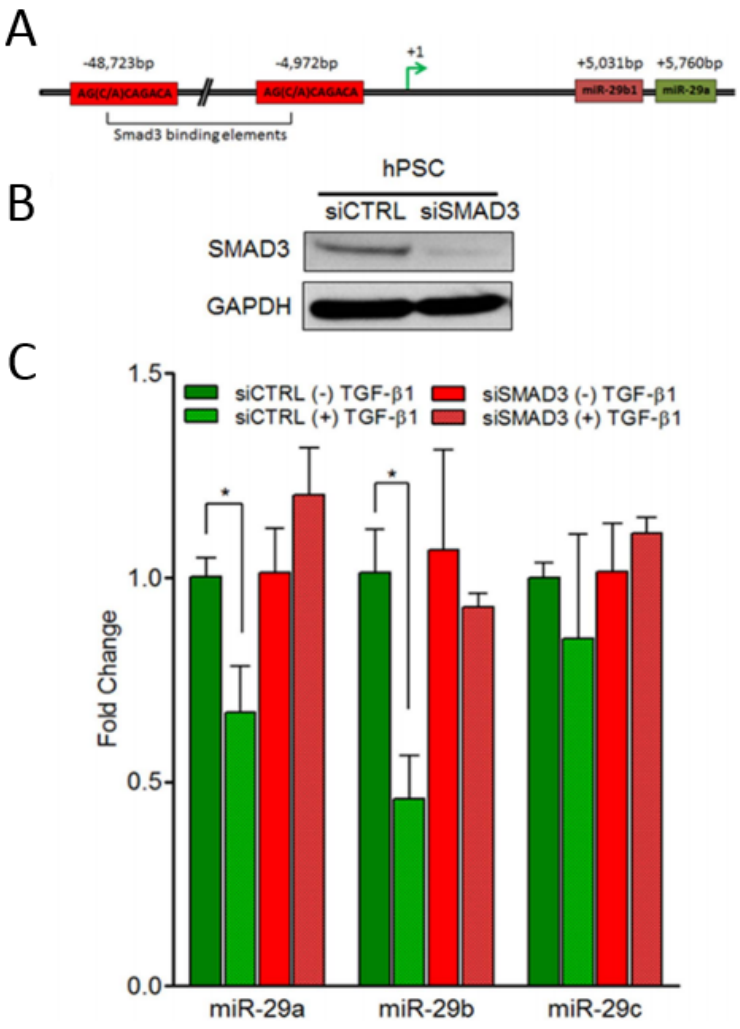

Figure 25. TGF-β1-mediated downregulation of miR-29 expression in PSCs is SMAD3 dependent. (A) Predicted SMAD3 binding sites upstream of miR-29a/b1 promoter: there are two SMAD3 binding elements (S3BE) 5 kb and 49 kb upstream of the transcription start site of the miR-29a/b1 loci on chromosome 7. SMAD3 binds specifically to CAGA boxes: AG(C/A)CAGACA and regulates neighboring gene expression. (B) siSMAD3 efficiently reduces endogenous SMAD3 protein levels in hPSCs. hPSCs growing in culture were transfected with 50 nM non-targeting siRNA (siCTRL) or siSMAD3. 24hours post-transfection, total proteins were harvested and

subjected to western blot analysis to determine SMAD3 expression levels. GAPDH was used as a loading control. (C) SMAD3 knockdown abrogates TGF-β1-mediated miR29 repression. qPCR analysis of miR-29 levels in TGF-β1-activated hPSCs transfected with siCTRL and siSMAD3. hPSCs were transfected with 50 nM siCTRL or siSMAD3. 24hours post-transfection, cells were challenged with 10 ng/ml TGF-β1 for 24 hours and subjected to qPCR for miR-29 expression levels. All experiments were repeated three times and representative data is presented. Data are presented as mean $\pm$ SEM; n= 3, statistics generated by t-test, *$p < 0.05$.

2.4 Discussion

Dense, fibrotic stroma is a histopathological hallmark of pancreatic cancer, and it precludes drug delivery to the tumor bed (21, 98). Activated PSCs are major contributors of fibrotic stromal reaction and are known to interact with cancer cells and promote PDAC tumor progression (26, 100). Quiescent PSCs normally located within the periacinar/ductal regions of the pancreas are activated in response to autocrine and paracrine pro-inflammatory cytokines/growth factors and secrete excessive amount of ECM proteins, a major component of PDAC stroma (104). TGF-β1 is a pro-tumorigenic/fibrotic growth factor secreted from cancer cells and injured acinar cells and is known to be a vital contributor of PSCs activation (28, 104). The upregulation of TGF-β1 in PDAC has been well documented and perpetuates the stromal reaction (12, 102).

Although previous studies have shown that miR-29 is reduced in TGF-β1 signaling and promotes fibrosis of various organs (126, 127), the role of miR-29 in the context of PSCs and PDAC fibrotic stroma has yet to be elucidated. In our study, we show for the first time that TGF-β1 acts as a negative regulator of miR-29 in PSCs, while simultaneously upregulating ECM proteins: collagens, laminin and fibronectin. Through qPCR analysis, we observed a predominant downregulation of miR-29a and miR-29b family members in both mouse and human PSCs upon TGF-β1-mediated activation. In muscle and kidney fibrosis, TGF-β1 is known to downregulate miR-29 expression in myoblasts (126) and renal cells (127) through SMAD3 binding elements located upstream of miR-29 promoter region and promote fibrosis. Similarly, we found that TGF-β1-mediated miR-29 repression in PSCs is SMAD3 dependent. In addition to PSCs, TGF-β1 activated pancreatic fibroblasts (99) (additional stromal cell responsible for stromal reaction), also displayed a loss of miR-29. Interestingly, we found the downregulation of all three miR-29 family members in TGF-β1 stimulated CAFs isolated from PDAC patient tumors. miR-29 family

members encoding genes reside on two different human chromosomes with miR-29a/b1 loci on Chromosome 7 and the miR-29c/b2 loci on Chromosome 1 (Fig 5a) (125), lending to the possibility that TGF-β1 may elicit downstream effects to inhibit both miR-29 encoding loci in CAFs but not in PSCs and normal pancreatic fibroblasts. Our findings implicate a differential effect of TGF-β1 in regulation of miR-29 expression in CAFs compared to PSCs/pancreatic fibroblasts that warrants further studies and may reveal differential regulatory mechanisms between miR-29 family members.

Subsequent investigation of miR-29 expression patterns in the pancreata of spontaneous tumor forming PDAC mouse model KC (113) and in PDAC patient tumor biopsies revealed similar findings of miR-29 loss of expression. We found a global decrease in expression of all three miR-29 family members in $Kras^{G12D}$ murine pancreata and human PDAC in conjunction with an increase in pancreatic fibrosis and stromal deposition associated with PDAC tumors. Although we observed a global loss of miR-29, these findings did not implicate whether the loss of miR-29 is specific to PSCs and epithelial cells associated with murine and human PDAC. Thus, we performed *in situ* hybridization to assess PSC and epithelial cell specific miR-29a expression by co-staining KC pancreata and human PDAC tumors with GFAP, a marker specific to PSCs/fibroblasts(122) and CK19, a marker specific to epithelial cells(123). Accordingly, we found a similar loss of miR-29a in PSCs of KC mice and PDAC patient samples. These findings further confirm that the loss of miR-29 is consistent in PSCs associated with PDAC stromal reaction. Nevertheless, our results do not document the underlying mechanisms for the loss of miR-29 expression in $K\text{-}Ras^{G12D}$ activated murine pancreata and human PDAC tumors, but our findings advocate for future functional studies *in vivo* to

examine miR-29 expression patterns in disease onset and progression in various etiologies associated with human PDAC.

Stromal ECM proteins such as collagens and laminin are direct miR-29 targets. These proteins in addition with fibronectin, another stromal abundant protein, interact with cancer cells and enhance tumor progression of various malignancies (129, 130) including pancreatic cancer (131). Although miR-29 has been shown to suppress fibrosis of several different organs, including heart (117), liver (93), lung (94), kidney (95), and muscle (110) by negatively regulating ECM protein expression, the function of miR-29 in PSC-mediated ECM protein expression has yet to be validated. Using miR-29 gain and loss-of-functions studies, we found that miR-29 suppresses its direct ECM targets collagen1a1, collagen 3a1, and laminin in activated PSCs. Surprisingly, we also found that miR-29 inhibits fibronectin expression, even though fibronectin does not contain canonical miR-29 binding sites within its 3'-untranslated region (Targetscan, miRanda, and PicTar). As a result, we sought to find an indirect mechanism for miR-29 mediated fibronectin inhibition in TGF-β1 activated PSCs. Interestingly, we found that ectopic expression of miR-29 in TGF-β1 activated PSCs reduced SMAD2 phosphorylation, implicating that miR-29 may act as an auto-inhibitory feedback regulator within TGF-β1 signaling. TGF-β1 is known to play a key role in PDAC pathogenesis, and its upregulation has been well documented in PDAC (102) and pancreatitis (103), a major risk factor of PDAC. As a consequence, TGF-β1 has emerged as an appealing therapeutic target, and numerous therapeutic strategies have been developed to inhibit TGF-β1 signaling via ligand inhibition and ligand/receptor interactions(132). Our findings reveal miR-29 to be a potential downstream inhibitor of TGF-β1 signaling.

In addition to the fibrotic stromal reaction, PSCs are known to interact with pancreatic cancer cells and promote tumor progression and metastasis. In our functional studies, restored expression of miR-29 in PSCs caused a decrease in cancer colony growth and stromal protein accumulation associated with co-cultures. Our data suggests that miR-29 overexpression reduced cancer colony growth by inhibiting the paracrine effects of PSCs on cancer cells, as we observed a decrease in pancreatic cancer viability. The precise mechanism associated with the paracrine effect of miR-29 overexpression in PSCs on cancer cell growth has yet to be elucidated, and future studies would further shed light on the role of miR-29 in tumor-stromal interactions. A large body of experimental evidence documents the role of extracellular matrix protein such as collagen and laminin in cancer cell proliferation and drug resistance (133-135). Although, we observed that the overexpression of miR-29 in PSCs reduced stromal accumulation associated with cancer colonies, additional studies are required to elucidate the direct mechanistic role of miR-29 in ECM-mediated pancreatic cancer progression.

As fibrotic stroma impairs the efficacy of chemotherapeutics and promotes PDAC progression, it is considered as an attractive therapeutic target in developing effective treatment strategies to target PDAC. Anti-stromal therapies to date have sought to deplete the reactive stroma. However, these approaches failed to improve patient survival and are often associated with toxicity. Furthermore, recent studies show that stroma impedes tumor growth, and its complete inhibition accelerated disease progression[10,](35). However, inactivating PSCs by modulation of a key transcriptional regulator suppressed the reactive stroma, increased tumor response to chemotherapy, and enhanced survival

(37). These findings suggest that normalizing reactive stroma is a safe and efficacious treatment strategy, as opposed to completely ablating the reactive stroma.

In our studies using *in vitro* and *in vivo* models and PDAC patient biopsies, we observed a loss of miR-29 in PSCs and fibroblasts, the critical stromal cells responsible for fibrotic stroma. Restored expression of miR-29 in PSCs suppressed major stromal protein expression (collagens, laminin and fibronectin) and inhibited cancer cell growth in co-culture. While the long-term consequences of miR-29 overexpression or miR-29 loss-of-function on PDAC progression/metastasis and its role in cancer cells and the tumor microenvironment remain to be investigated *in vivo*, our findings indicate that the efficacy of stroma-targeted therapy in PDAC may also be dictated by stromal miRNA expression and function. We anticipate that the restored expression of miR-29 in stromal cells reduces the stromal protein accumulation and cancer growth and enhances the drug delivery to the inner tumor core. Furthermore, increasing evidence indicate miR-29 plays a vital role in cancer pathogenesis (111), tumor microenvironment, and metastasis (112). In contrast to pharmacological approaches, the use of miR-29 as a therapeutic agent may be more effective in targeting reactive stroma, as a single miRNA regulates the expression of several genes associated with disease mechanisms (108). Thus, restored expression of a critical miRNA is therapeutically beneficial and targets multiple cellular pathways associated with disease processes. In our previous work, we demonstrated that the replacement of a single missing miRNA suppressed tumor progression with no toxicity and off-target effects (136).

Thus far, no studies have interrogated the relevance of miR-29 in the context of PDAC stroma. Based on our *in vitro*, *in vivo*, and clinical observations in stromal cells and

functional studies, our results indicate that miR-29 plays a critical role in stromal deposition and inhibits the pro-growth effects of PSCs on pancreatic cancer colony formation. Our findings raise the possibility that miR-29 could serve as an anti-stromal therapeutic agent in the context of PDAC. A large body of evidence demonstrates the pleiotropic role of miRNAs in fibrotic process, cancer pathogenesis and metastasis, and their potential use as therapeutic agents for cancer (136-138), fibrosis (139), and other human diseases (140). Some miRNA-based drugs have already reached clinical trials (140, 141) or are in advanced stage of pre-clinical development(142, 143), indicating the feasibility of miR-29 in prospective clinical applications. This new and substantially different approach is expected to overcome the problems associated with other means of modulating the stroma and result in an effective approach to improve drug delivery to the tumor bed. Future work aimed at determining the role of miR-29 in pancreatic cancer cells, patient survival, and its biological functions *in vivo* will allow us to further understand the role of miR-29 in PDAC development and progression and ultimately determine its prognostic and therapeutic applicability to target PDAC.

Chapter 3: Novel role of miR-29a in pancreatic cancer autophagy and its therapeutic potential

3.1 Introduction

PDAC is one of the most lethal forms of human malignancies worldwide with poor prognoses (144). In the United States, PDAC is the fourth leading cause of cancer related deaths (11) and is projected to become the second leading cause of cancer deaths by 2030 (2). PDAC is often undiagnosed until it has metastasized and these advanced tumors display resistance to existing therapeutic modalities. Although there have been recent improvements in combination chemotherapies such as Nab-Paclitaxel/Gemcitabine and FOLFIRINOX (145, 146), the overall 5-year survival rate has not exceeded 8% (11). Furthermore, PDAC has a well-characterized mutational profile that plays a key role in disease onset and progression (>90% cases with KRAS mutations and >50% with inactivating mutations in p53, CDKN2A, or SMAD4) (147), but the knowledge of these genetic perturbations has yet to yield targeted therapies. The lack of effective treatments and early detection necessitates the critical need to further dissect molecular mechanisms associated with PDAC progression to develop novel and effective therapeutic strategies for improving patient survival.

Autophagy is the process in which cells degrade internal constituents for the maintenance of cellular homeostasis and survival under stress conditions (42). When autophagy is induced, cytoplasmic components are sequestered into double-membrane vesicles called autophagosomes, which then fuse with lysosomes. Subsequently, the hydrolases of the lysosomal compartments degrade cytoplasmic cargo and release the

basic cellular building blocks into the cytosol for recycling (42). Recent studies document that the upregulation of autophagy can serve as a survival mechanism in various malignancies (39-41, 53-61), including PDAC tumor growth and progression (39-41). These reports have paved the way for therapies in clinical trials for PDAC patients that feature HCQ, a lysosomotropic agent that inhibits autophagy (clinicaltrials.gov NCT01273805). However, HCQ is associated with toxicity and off-target effects such as neuromyotoxicity (65), retinopathy (62, 63), and cardiomyopathy (64, 148).

Increasing evidence suggests that miRNA-based therapeutics have limited off-target effects and could emerge as novel therapeutic agents for various human diseases including cancer (139, 140, 142, 149-152). miRNAs are conserved small non-coding RNAs, that regulate post-transcriptional gene expression (66, 153). These small molecules are abundantly expressed in normal tissue, and are often missregulated in disease states. Restored expression of downregulated miRNAs has been suggested to be beneficial in therapeutically targeting cancer (136, 154, 155). We and others have found miR-29 to be downregulated in PDAC (85, 156, 157). Of importance, overexpression of miR-29 in stromal cells reduced the accumulation of stromal proteins and cancer colony formation in direct co-cultures (85).

In this study, we address the role of miR-29 in autophagy in pancreatic cancer cells. We found downregulation of miR-29 in a range of pancreatic cancer cell lines, and restored expression of miR-29a blocked autophagy flux by inhibiting expression of key autophagy proteins, TFEB and ATG9A. Furthermore, miR-29a overexpression sensitized chemoresistant pancreatic cancer cells to gemcitabine and reduced their invasive

potential. Our findings provide evidence for the use of miR-29a as a novel therapeutic agent to thwart autophagy and target PDAC.

3.2 Materials and Methods

Cell lines

Normal human pancreatic epithelial cell lines HPNE (ATCC, CRL-4023) and HPDE (AddexBio, T0018001) were grown in Dulbecco's Modified Eagle Medium (DMEM) (Life Technologies, 11965-092) supplemented with 10% fetal bovine serum (FBS). Panc-1 (ATCC, CRL-1469) and MIA PaCa-2 (ATCC, CRL-1420) were grown in DMEM supplemented with 10% FBS, 100units ml^{-1} penicillin, and 100mg ml^{-1} streptomycin. COLO 357 (158), AsPC-1 (ATCC, CRL-1682), and BxPC-3 (ATCC, CRL-1687) were grown in Roswell Park Memorial Institute (RPMI) 6140 (Life Technologies, 11875-093) supplemented with 10% FBS, 100units ml^{-1} penicillin, and 100mg ml^{-1} streptomycin.

RNA purification

Total RNA was extracted from cells using Trizol extraction kit (Life Technologies, 15596018) according to the manufacturer's protocol. The quantity and purity of RNA was determined by OD260/280 reading using a Nanodrop spectrophotometer.

Measurements of RNA by qPCR

Mature miR-29 family member expression and p62 mRNA expression levels were measured by TaqMan Assays (Applied Biosystems): miR-29a (ID:002112); miR-29b (ID:000413); and miR-29c (ID:000587) ; and SQSTM1/p62 (ID: 4331182). U6

snRNA (ID:001973) or ACTB (ID: 4331182) were used as a endogenous controls to normalize miR-29 expression and p62 expression respectively. Samples were analyzed using ABI 7500 Real-Time PCR machine. Samples were run in triplicates with 0.2 thresholds, and the $^{\Delta\Delta}$CT method was used for relative miR-29 expression analysis.

Western blot analyses of proteins

Total cell protein was isolated using RIPA buffer (Thermo Scientific, PI-89900) and quantified using BCA Protein Assay Kit (Pierce Biotechnology, 23225). Protein were separated by SDS-PAGE and were transferred to polyvinylidene fluoride membrane. Membranes were incubated in a solution of 10% dried non-fat milk, and then probed with primary antibodies against Caspase-3 (Novus Biological, 9662S), Procaspase-3 (Cell Signaling, 9662S), LC3B (Novus Biological, NB100-2220), SQSTM1/p62 (Thermo Scientific, H00008878-M01), LAMP-2 (Santa Cruz, sc-18822), ATG9A (ab108338), TFEB (Cell Signaling, 4240), or GAPDH (Millipore, MAB374). The membranes were then incubated with corresponding HRP conjugated goat anti-rabbit (Santa Cruz, sc-2004), goat anti-mouse (Bio-Rad, 172-1011), or donkey anti-goat (Santa Cruz, sc-2020) secondary antibodies. Proteins were visualized and quantified using chemiluminescent detection kit (GE Healthcare, Amersham ECL) and exposed to x-ray film (Thermo Scientific, CL-X Posure Film) or captured on an Amersham Imager 600 (GE Healthcare, CCD Model). The intensity for each band was densitometrically quantified and normalized against loading control using ImageJ software.

Transfection of cultured cells

Exponentially growing cancer cells were seeded in 6 well plates at $1x10^5$ cells per well or 12 well plates at $5x10^4$ per well and allowed to adhere overnight and transfected

with indicated concentrations (10 μM, 20 μM) of control (GE Dharmacon, CN-001000-01) or miR-29a (GE Dharmacon, C-300504-07) mimics, or 1 μM siRNA using siCTRL (GE Dharmacon, D-001810-10-05), siTFEB (GE Dharmacon, L-009798-00-0005), and siATG9A (GE Dharmacon, L-014294-01-0005) using DharmaFECT®1 (GE Dharmacon, T-2001-01) as per the manufacturer's protocol. Total protein or RNA was isolated at 24 hours post-transfection for western blot or qPCR analysis respectively as described above.

Migration and invasion measurements

$1x10^4$ cells (Panc-1 or MIA PaCa-2) transfected with 20 nM control or miR-29a mimics using DharmaFECT®1 were plated in triplicate in the upper chambers of 8 μm transwells (Falcon, 353097) in 100 μl serum-free media and 750 μl 10% serum containing media in the lower chamber of 24-well plates and incubated at 37°C for 24 hours. For invasion assays, 80 μl of 1:5 diluted matrigel (BD, 354234) was pre-coated in the upper chambers and allowed to solidify prior to plating cells. 24 hours post-seeding, membranes were washed twice with PBS, fixed with 4% paraformaldehyde, and stained with 0.1% crystal violet in 20% ethanol. Cells remaining in the upper chamber were carefully removed, and cells migrated/invaded on to the lower membrane were imaged and counted. For each well, 5 random fields were counted, and average number of cells per field was presented.

Measurements of cell viability, cytotoxicity, and caspase activity

$5x10^3$ pancreatic cancer cells per well (Panc-1, MIA PaCa-2, or COLO 357) were plated in 96 well plates and grown at 37°C for 24 hours. Cells were then transfected with 20 nM mimic control or miR-29a mimic using DharmaFECT®1 for 24

hours. Transfection media was then removed and replaced with complete media, and cells were allowed to recover for 24 hours and subsequently treated with varying concentrations of gemcitabine (0 μM, 0.1 μM, 1 μM, 10 μM, 100 μM). Cell viability was measured at 72 hours post-gemcitabine treatment by adding 10μl Cell Counting Kit-8 (CCK8) reagent (Dojindo, CK04) and absorbance was measured at 450 nm. For cell viability with Chloroquine (CQ) and BafilomycinA1 (BafA1) treatment, cells were treated with 25 μM CQ (Sigma Aldrich, C6628) or 10 μM BafA1 (Sigma Aldrich, B1793) in combination with 10 μM gemcitabine for 48 hours, and viability was measured using CCK8 kit as described above. For cytotoxic effects and caspase activity, pancreatic cancer cells (Panc-1, MIA PaCa-2) were transfected with mimic control or miR-29a mimic as described above and treated with 10 μM gemcitabine for 24-48 hours. For cytotoxic effects, lactate dehydrogenase release was determined using Promega CytoTox-ONE Homogeneous Membrane Integrity Assay (Promega, G7890) and fluorescence was measured at 560/590 nm. Caspase activity was determined using Promega Apo-ONE Homogenous Caspase-3/7 Assay Kit (Promega, PRG7790) with fluorescence measured at 490/530 nm.

Soft agar assays

$3x10^5$ pancreatic cancer cells per well (Panc-1 or MIA PaCa-2) were plated in 6 well plates and grown at 37°C for 24 hours. Cells were then transfected with 20 nM mimic control or miR-29a mimic using DharmaFECT®. $1.5x10^3$ pancreatic cancer cells (Panc-1 or MIA PaCa-2) transfected with control or miR-29a mimcs were plated per well in a 6 well plate containing 0.5% top agarose and 1% bottom agarose (BioRad, 162-

0137). After 20 days, colonies were stained with crystal violet and were counted under low power bright field microscopy for positive colonies.

Luciferase reporter assay

The 3'-UTR containing predicted miR-29 binding sites, both wild type and mutant, for ATG9A and TFEB were cloned into pmirGLO Dual-Luciferase miRNA Target Expression Vector (Promega, #E1330) downstream of the firefly luciferase open reading frame. $5x10^3$ pancreatic cancer cells per well (Panc-1 or MIA PaCa-2) were plated in 96 well plates and grown at 37°C for 24 hours. Cells were then co-transfected 10 nM mimic control or miR-29a mimic with 100 ng of pmirGLO Dual-Luciferase miRNA Target Expression Vector containing each respective 3'-UTR binding site using DharmaFECT Duo Transfection Reagent (GE, T-2010-02). Cells were transfected for 24 hours, and luciferase levels were measured 24 hours post-transfection using Dual-Glo® Luciferase Assay System (Promega, #E2920). Firefly luciferase luminescence was normalized to renilla luciferase activity for each transfected well.

Autophagy assays

For assessment of miR-29 effects on autophagy flux via immunoblotting, $1x10^5$ pancreatic cancer cells per well (Panc-1, MIA PaCa-2, or COLO 357) were plated in 12 well plates and grown at 37°C for 24 hours. Cells were then transfected with 10 nM control or miR-29a mimics using DharmaFECT®1. 24 hours post-transfection, cells were treated with 25 μM CQ in complete media for 3-6 hours. Subsequently, total proteins were harvested and subjected to western blot analysis as described above. Lentivirus encoding GFP-LC3B were generated using plasmid (GeneCopoepia, EX-T0824-Lv103) in HEK293 cells (ATCC, CRL-1573) via standard HEPES/Calcium Phosphate

transfection. Stable Panc-1 GFP-LC3B cells were generated by transducing exponentially growing Panc-1 cells in T-75 flask. GFP positive cells were selected by flow cytometry and were expanded for one week prior to conducting experiments. For immunofluorescence imaging, cells were fixed with 4% PFA and permeabilized using 0.1% triton and blocked using 1% BSA. Primary LAMP-2 antibody (Santa Cruz, SC18822) was incubated overnight, followed by secondary Alexa Fluor® 647 antibody (Abcam, ab150079) incubation and 10ug/mL Hoechst Nuclear Stain (Life Technologies, ab150083). Eight 0.5 micron Z-stack sections were captured using the Opera (Perkin Elmer) fluorescent microscope and final images were deconvolved and analyzed using Volocity imaging analysis software (Perkin Elmer). Quantifications for number of GFP-LC3B positive compartments and colocalization of GFP-LC3B and LAMP-2 were taken from 4 random fields with 8-10 cells per field.

Statistics

ANOVA with Tukey's post-hoc test and 2-tailed Student's *t* tests were used to test for statistical significance. $P < 0.05$ was considered statistically significant.

3.3 Results

miR-29a sensitizes chemotherapeutic resistant pancreatic cancer cell lines to gemcitabine treatment. Previously, we observed a global and epithelial-specific decrease in miR-29 expression in the pancreata of a well-characterized pancreatic cancer mouse model, LSL-$KRas^{G12D}$; Pdx1Cre, and human PDAC patients (85). To understand the function of miR-29 in pancreatic cancer cells, we initially measured the expression levels of miR-29 in five pancreatic cancer cell lines (Panc-1, MIA PaCa-2, COLO 357, BxPC-3, and AsPc-1)

compared to two normal human pancreatic ductal epithelial cell lines (HPNE and HPDE). There was a significant decrease in miR-29a and miR-29b expression in four out of five pancreatic cancer cell lines compared to normal human pancreatic ductal epithelial cells and levels of miR-29c were lower in three out of five pancreatic cancer cell lines (Figure 26A). We have previously reported that miR-29a is the most abundantly expressed miR-29 family member in the human pancreas and in pancreatic stellate cells (85) and also found that miR-29a is the most highly expressed miR-29 family member in the normal human pancreatic epithelial cell line, HPNE (Figure 27). Therefore, we focused on miR-29a for functional studies.

One of the major limitations in treating PDAC is that cancer cells acquire resistance to existing chemo and radiation therapeutic modalities, including gemcitabine (159). Furthermore, pancreatic cancer cells are surrounded by dense fibrotic stroma, which is known to impair drug delivery to the tumor core (21). Previously, we showed that overexpression of miR-29a in pancreatic stellate cells, the major stromal cells responsible for fibrotic stroma, reduced extracellular matrix protein accumulation and cancer growth in co-cultures, suggesting its potential use as a novel therapeutic agent in normalizing stromal abundance to target PDAC (85). To test the feasibility of combining miR-29a with gemcitabine, a standard therapy, we investigated the effect of miR-29a overexpression on viability of known gemcitabine resistant pancreatic cancer cell lines, Panc-1 and MIA PaCa-2 (160). Overexpression of miR-29a alone did not significantly reduce the viability of cancer cells, but the addition of gemcitabine resulted in a significant decrease at various concentrations starting at 0.1 μM (Figure 26B).

Furthermore, miR-29a did not have any additive effect on cell viability in gemcitabine sensitive PDAC cell line, COLO 357 (161), to drug treatment (Figure 28).

Evasion of cell death is a crucial event during malignant transformation of pancreatic cancer cells. Initially, we determined the cytotoxic effects of miR-29a in combination with gemcitabine on PDAC cell lines resistant to gemcitabine (Panc-1 and MIA PaCa-2) by measuring the release of lactate dehydrogenase (LDH) (162, 163). There was a significant increase in LDH from the Panc-1 and MIA PaCa-2 cells overexpressing miR-29a upon gemcitabine treatment, indicating that miR-29a increases cytotoxicity in combination with gemcitabine (Figure 26C, Figure 29). We also observed increased caspase 3/7 activity (Figure 26D, Figure 30A) and cleaved caspase-3 levels (Figure 26E, Figure 30B) in miR-29a overexpressing cancer cells upon gemcitabine treatment compared to cancer cells treated with gemcitabine alone. Taken together, these findings indicate that miR-29a sensitizes pancreatic cancer cells to gemcitabine treatment and provides compelling evidence for its use in combination with gemcitabine as a novel therapeutic strategy to target PDAC.

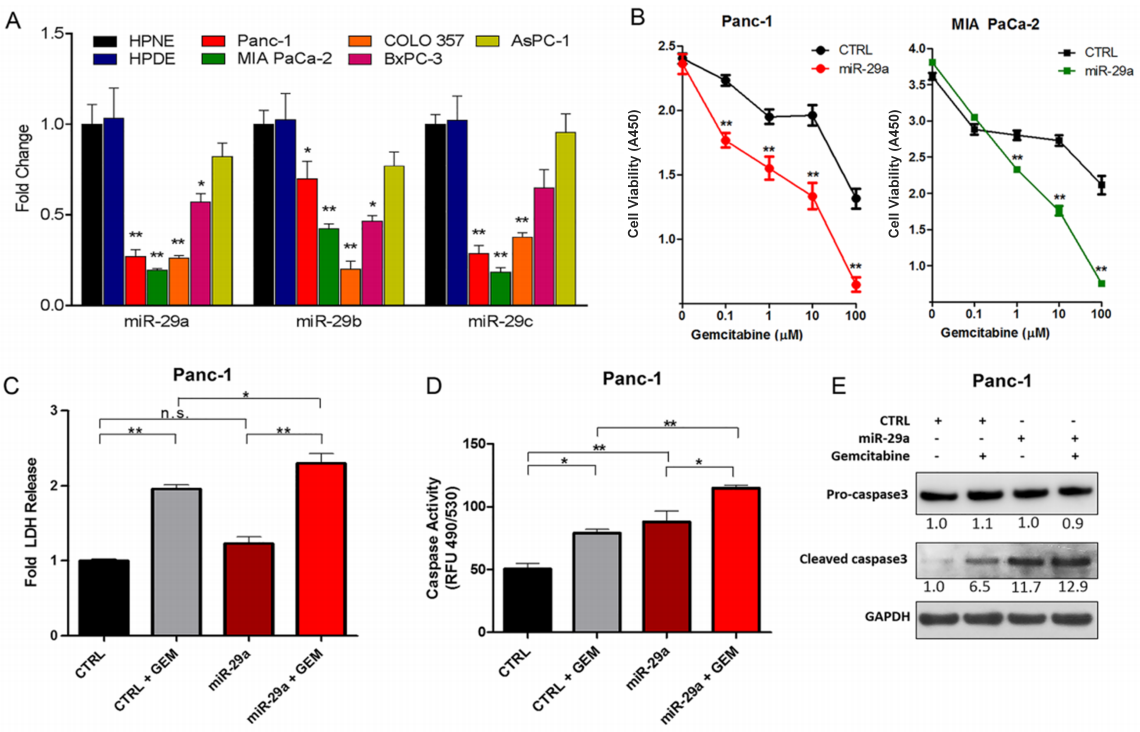

Figure 26. miR-29a increased sensitivity of chemoresistant PDAC cells to gemcitabine treatment. (A) qPCR analysis of miR29 family members in normal human ductal epithelial cell lines (HPNE and HPDE) and pancreatic cancer cell lines (Panc-1, MIA PaCa-2, COLO 357, BxPC-3, AsPC-1) (n=4). Data represented as average fold change (ΔΔCT) ± standard error of the mean (S.E.M.) (B) Pancreatic cancer cell lines (Panc-1 and MIA PaCa-2) were seeded into 96-well plates, transfected with control (CTRL) or miR-29a mimics, treated with indicated concentrations of gemcitabine (GEM) for 24 hours post-transfection, and viability was measured at 72 hours post-treatment using the Cell Counting Kit-8 (CCK-8) as a measure of viability. Average absorbance (A450) is represented (n=8) ± S.E.M. (C) Panc-1 cells were transfected with CTRL or miR-29a mimics, treated with 10μM GEM for 48 hours and lactate dehydrogenase (LDH) release was determined by substrate based activity assay (fluorescence 560/590 nm). Average relative percent cytotoxicity are represented (n=3-4) ± S.E.M. (D) Panc-1 cells

were transfected with CTRL or miR-29a mimics. 24 hours post-transfection cells were treated with 10μM GEM for 24 hours, lysed, and caspase activity was determined by absorbance using Apo-ONE Homogeneous Caspase-3/7 Assay according to manufacturer's protocol. Average relative fluorescence (RFU, 490/530 nm) are represented (n=4) ± S.E.M. (E) Panc-1 transfected with CTRL or miR-29a mimics, treated with 10μM GEM for 12 hours and 15 μg of total cell protein lysate was subjected to western blot analysis for procaspase-3, cleaved caspase-3, and GAPDH was used as loading control. Relative quantification of band intensities normalized to GAPDH are shown below respective blots. All experiments were repeated 3-4 times and representative data is presented. *$p<0.05$, **$p<0.01$, non-significant (n.s.).

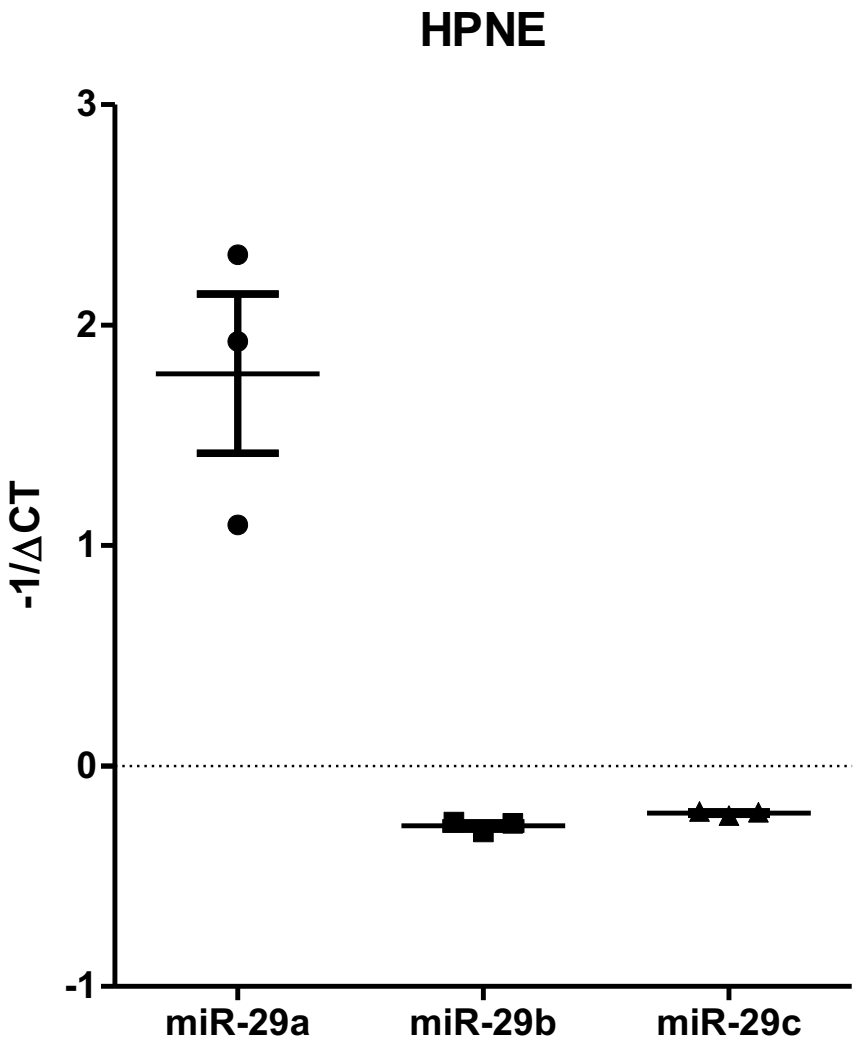

Figure 27. miR-29a is the most abundantly expressed miR-29 family member in human pancreatic normal epithelial cell line. RNA was isolated from human pancreatic normal epithelial cells (HPNE) (n=3) and miR-29a, -29b, and -29c expression levels were determined by qPCR analysis using U6 snRNA as an internal control. Delta CT (ΔCT) was calculated for each miR-29 family member to measure relative expression levels. Boxplots represent -1/ΔCT of miR-29 family expression levels. *$p<0.05$.

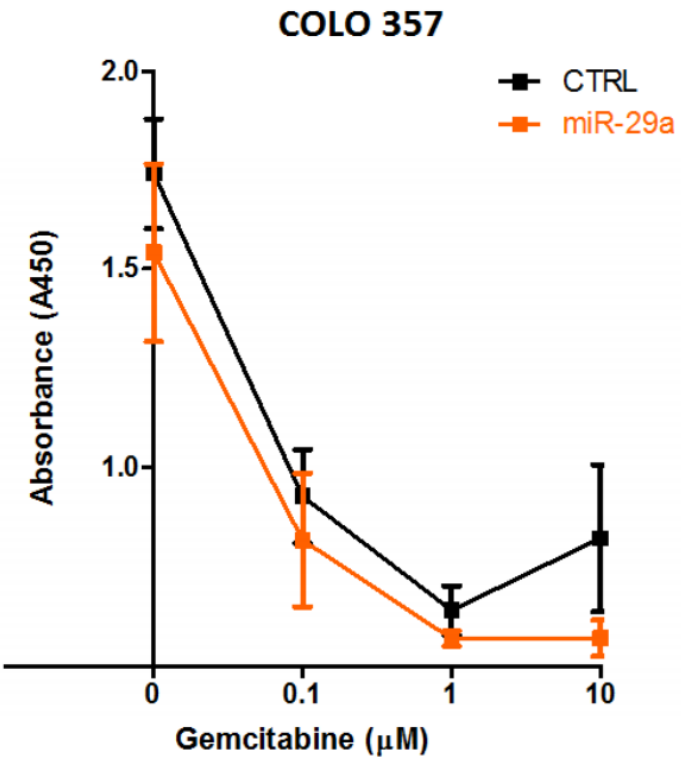

Figure 28. Effect of miR-29a overexpression and gemcitabine treatment on COLO 357 cell viability. COLO 357 were seeded into a 96-well plate, transfected for 24 hours with CTRL or miR-29a mimics, and treated with various concentrations of gemcitabine, and cell viability was measured at 72 hours post-treatment using the Cell Counting Kit-8 (CCK-8) assay according to manufacture's protocol. Average relative absorbance (A450) is presented (n=6) ± Standard Error of the Mean (S.E.M.).

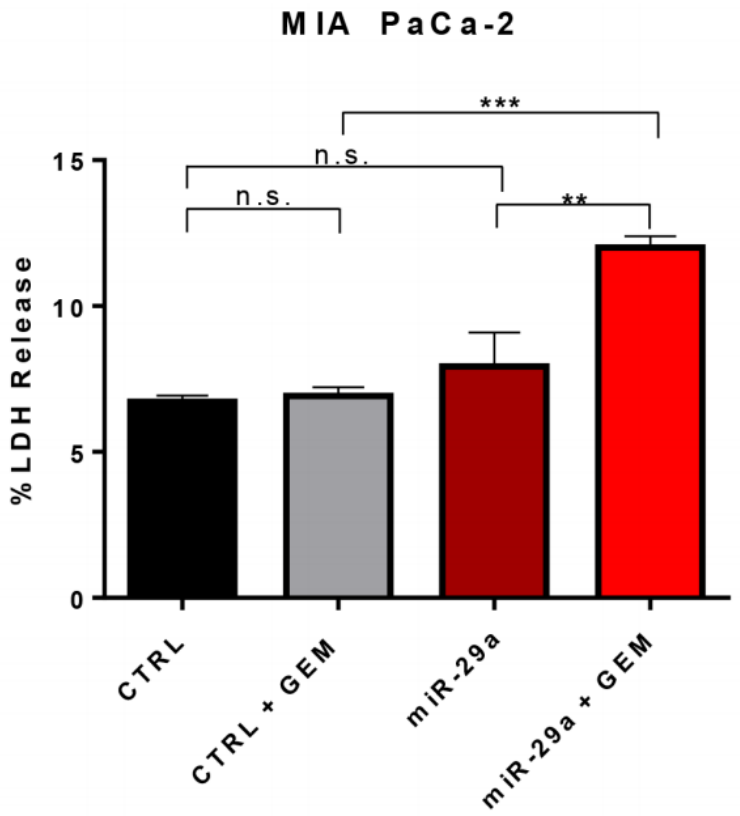

Figure 29. LDH release in MIA PaCa-2 cells treated with gemcitabine in combination with miR-29a. MIA PaCa-2 cells were transfected with CTRL or miR-29a mimics, treated with gemcitabine (GEM) for 48 hours and lactate dehydrogenase (LDH) release was determined by substrate based activity assay (fluorescence 560/590 nm). Average relative percent cytotoxicity is represented (n=4) ± S.E.M.

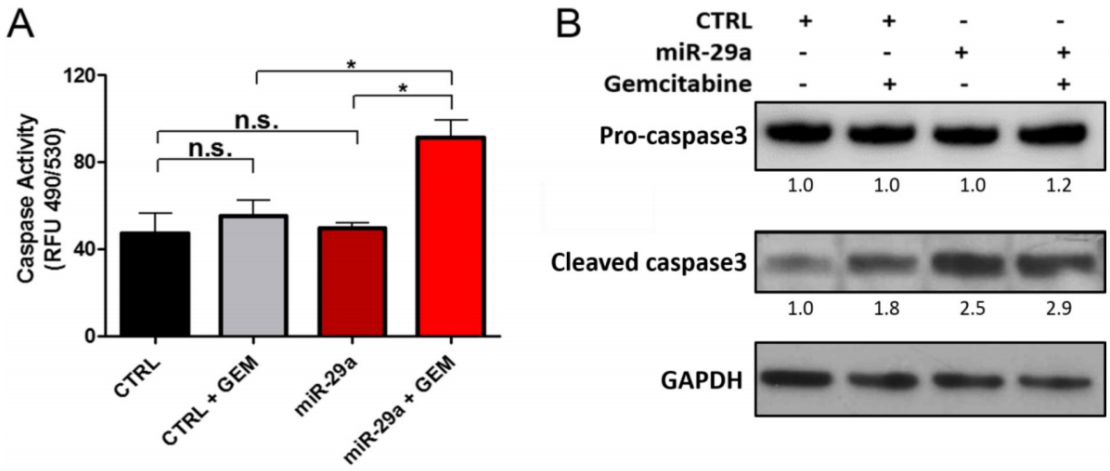

Figure 30. Caspase3/7 activity and activated caspase 3 levels in MIA PaCa-2 cells treated with gemcitabine in combination with miR-29a. MIA PaCa-2 cells were transfected with CTRL or miR-29a mimics. (A) Transfected cells were treated with 10μM gemcitabine (GEM) for 24 hours, lysed, and caspase activity was determined using Apo-ONE Homogeneous Caspase-3/7 Assay. Average fluorescence (490/530 nm) is represented (n=4) ± S.E.M. (B) Transfected cells were treated with 10μM GEM for 12 hours. Post GEM treatment, 15 μg of total protein lysate was subjected to western blot analysis for quantitation of pro-caspase 3 and cleaved caspase 3. GAPDH was used as loading control for the western blot. Relative quantification of band intensities normalized to GAPDH is shown below respective blots.

miR-29a inhibits autophagy flux in pancreatic cancer cells. Pancreatic cancer cells induce autophagy as a survival mechanism to escape gemcitabine induced cell death (39, 60, 61). Therefore, we sought to determine the effect of miR-29 on autophagy, to assess whether the increased sensitivity and cytotoxic effects of gemcitabine in chemotherapeutic resistant pancreatic cancer cells is due to alterations in autophagy. LC3B is a widely used marker to monitor autophagy levels (164). Normally, LC3B resides in the cytoplasm (LC3BI), and upon initiation of autophagy, it is conjugated with phosphatidyl-ethanolamine (LC3BII) to facilitate formation and expansion of the autophagosome membrane (165-169).

To elucidate the effects of miR-29a on PDAC autophagy, Panc-1 cells, which have high basal levels of autophagy (39), were transfected with miR-29a or mimic control and LC3B levels were assessed by western blot analysis. There was a marked increase in LC3B upon miR-29a overexpression in Panc-1 cells (Figure 31A). Similar observations were found in MIA PaCa-2 and COLO 357 cells (Figure 32). An increase in LC3B levels can indicate an upregulation of autophagy or a blockage of autophagy flux (170). We therefore examined the expression of an autophagic substrate, p62, in conjunction with LC3B. p62/SQSTM1 is efficiently degraded upon autophagy induction and serves as an indicator of autophagic turnover (170). An increase in p62 levels correlates with an inhibition in autophagy, whereas a decrease indicates induction of autophagy (171). There was a robust accumulation of p62 in miR-29a overexpressing cancer cells (Figure 31, Figure 32), suggesting that miR-29a causes a late stage blockage in autophagy flux. It is possible that the increase in p62 could be due to an indirect transcriptional upregulation rather than inhibition of autophagy. Therefore, we measured p62 transcript levels and

found no significant change (Figure 33), indicating that p62 accumulation is due to a perturbation in autophagy.

Chloroquine (CQ) is a lysosomotropic agent that inhibits autophagy by raising lysosomal pH (172). The increase in lysosomal pH permits autophagosome-lysosome fusion but prevents degradation and autolysosomal turnover (173). To further assess the effect of miR-29a on autophagy flux, miR-29a or mimic control was transiently expressed in Panc-1 cells and then treated with CQ. Our results showed a net increase in LC3BI and II and p62 accumulation in control cells upon CQ addition. However, when miR-29a is overexpressed, prior to CQ treatment, the amount of LC3B and p62 in cells subjected to a combination of miR-29a and CQ combination was as low as miR-29a alone, supporting the idea the miR-29a had already blocked autophagy (Figure 31A). These results were further recapitulated in MIA PaCa-2 and COLO 357 cells (Figure 32). Similar to CQ, BafilomycinA1 (BafA1) functions as a late stage inhibitor of autophagy by raising lysosomal pH (174) and also blocks autophagosome-lysosome fusion (175). Treatment of Panc-1 and MIA PaCa-2 with other late stage autophagy inhibitors, CQ and BafA1, resulted in p62 and LC3B accumulation similar to miR-29a overexpression (Figure 34).

Pancreatic cancer cells have been previously shown to induce autophagy and acquire resistance to chemotherapy (41, 176, 177). To verify the functional effect of miR-29a mediated blockage of autophagy flux on gemcitabine sensitization, we evaluated the effects of miR-29a on cancer cell viability in comparison with BafA1. Similar to miR-29, treatment of cancer cells with gemcitabine in combination with BafA1 decreased cancer cell viability (Panc-1 and MIA PaCa-2) compared to gemcitabine alone (Figure 31B,

Figure 35). To further elucidate the effect of miR-29a and gemcitabine combination on pancreatic cancer cell autophagy, miR-29a expressing Panc-1 and MIA PaCa-2 cells were treated with gemcitabine and LC3B and p62 proteins were measured by western blot analysis (Figure 36). Similar to previous reports of gemcitabine induced autophagy in cancer cells (176, 178), Panc-1 and MIA PaCa-2 cells treated with gemcitabine alone exhibited a marked increase in LC3BII and decrease in p62, indicating autophagy induction. However, miR-29a overexpressing cancer cells did not exhibit any net decrease in p62 with an increase in LC3B levels upon gemcitabine treatment due to a miR-29a mediated inhibition of autophagy (Figure 36). Taken together, these findings suggest that miR-29a functions as an inhibitor of late stage autophagy, which serves to sensitize chemoresistant pancreatic cancer cell lines (Panc-1 and MIA PaCa-2) to gemcitabine treatment.

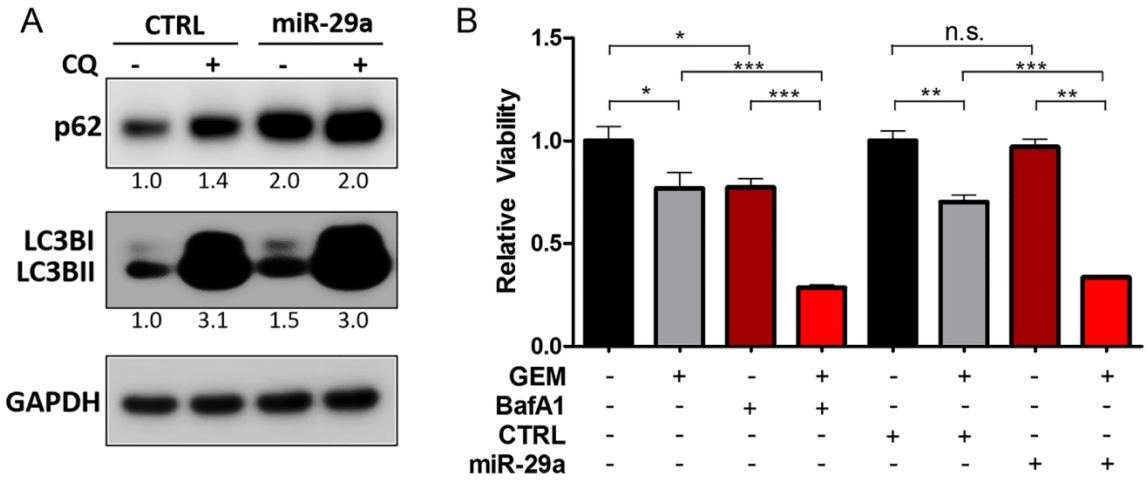

Figure 31. miR-29a overexpression causes blockage in autophagy flux. (A) Panc-1 cells were transfected with CTRL or miR-29a mimics. Following transfection, cells were treated with 25μM chloroquine (CQ) and 5 μg of total protein lysates were subjected to western blot analysis to measure p62 and LC3B. GAPDH was used as loading control. Quantification of band intensities normalized to GAPDH is shown below the respective blots. (B) Panc-1 cells were transfected with CTRL or miR-29a mimics and treated with and without 10μM GEM. In parallel, Panc-1 cells were treated with 10μM GEM alone or in combination with 10μM BafA1. 48 hours post GEM treatment, cell viability was determined using CCK-8 assay kit. Average relative absorbance (A450) normalized to respective controls is presented (n=6) ± S.E.M. All experiments were repeated 3-4 times and representative data is presented. *$p<0.05$, **$p<0.01$, and ***$p<0.001$.

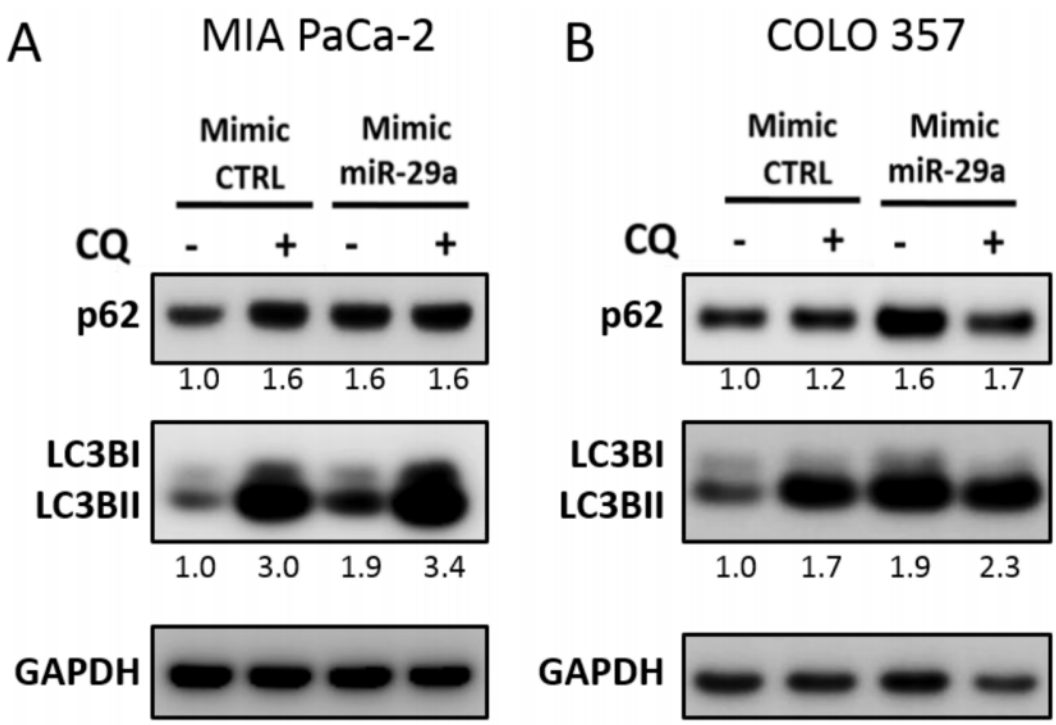

Figure 32. Overexpression of miR-29a inhibits autophagic flux in MIA PaCa-2 and COLO 357 cells. (A) MIA PaCa-2 or (B) COLO 357 pancreatic cancer cells were transfected with CTRL or miR-29a mimics. 24 hours after transfection, cells were treated with 25 μM chloroquine (CQ) for 3 hours and total protein was harvested. 5 μg of total protein lysate was subjected to western blot analysis for quantitation of p62 and LC3B. GAPDH was used as loading control. Quantification of protein band intensities normalized to GAPDH is shown below respective blots.

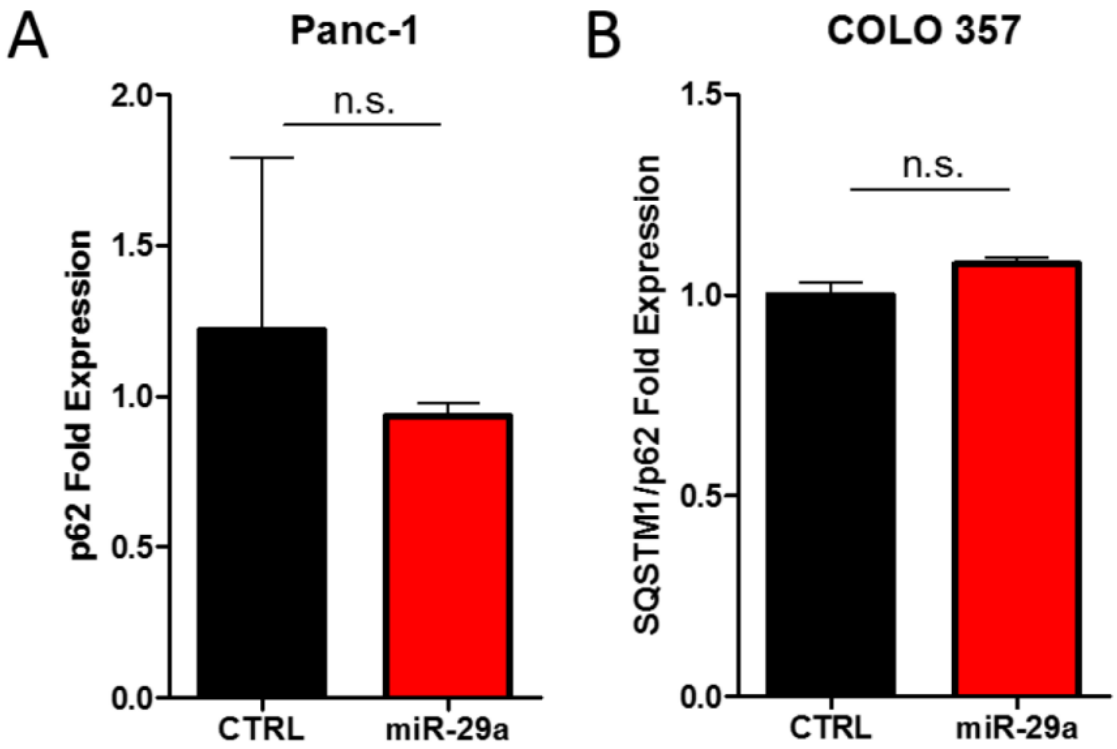

Figure 33. p62 mRNA expression is unaltered by miR-29a overexpression in Panc-1 and COLO 357 cells. (A) Panc-1 or (B) COLO 357 pancreatic cancer cells were transfected with CTRL or miR-29a mimics (n=3). 24 hours after cell transfection, total RNA was harvested and the levels of p62 gene transcripts were measured by qPCR. ACTB mRNA was used as an endogenous control. The measurments are represented as average fold change (ΔΔCT) ± S.E.M.

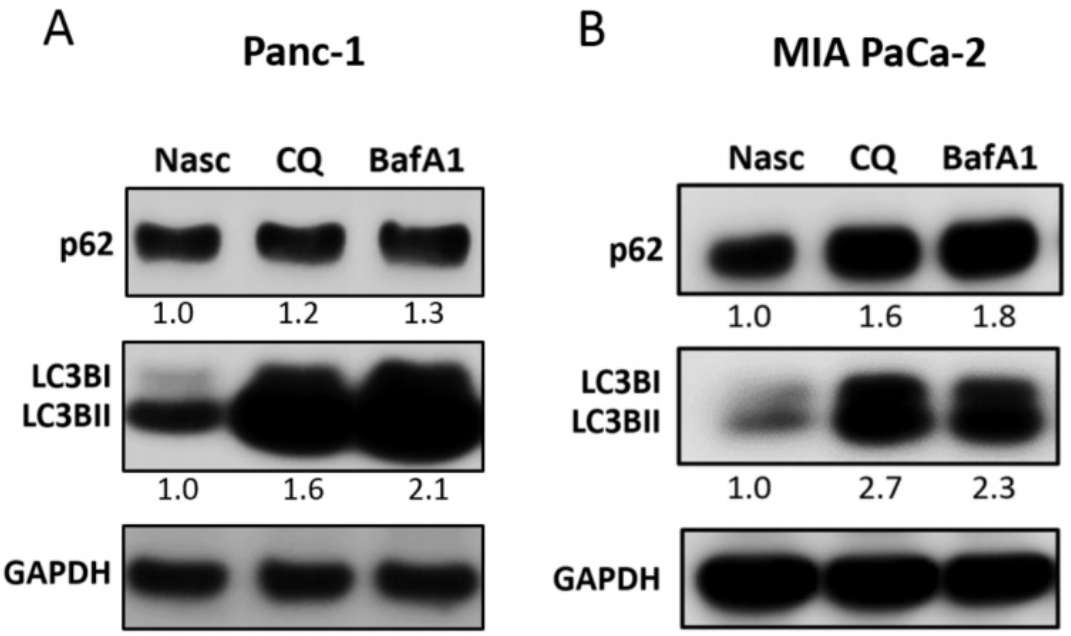

Figure 34. Effect of CQ and BafA1 on Panc-1 and MIA PaCa-2 autophagy. (A) Panc-1 or (B) MIA PaCa-2 cells were treated with either 25μM chloroquine (CQ) or 10μM bafilomycinA1 (BafA1) for 6 hours. Cells were lysed and. 5 μg of total protein was analyzed by western blot analysis to measure p62 and LC3B proteins. GAPDH was used as loading control. Quantification of protein band intensities normalized to GAPDH are shown below respective blots.

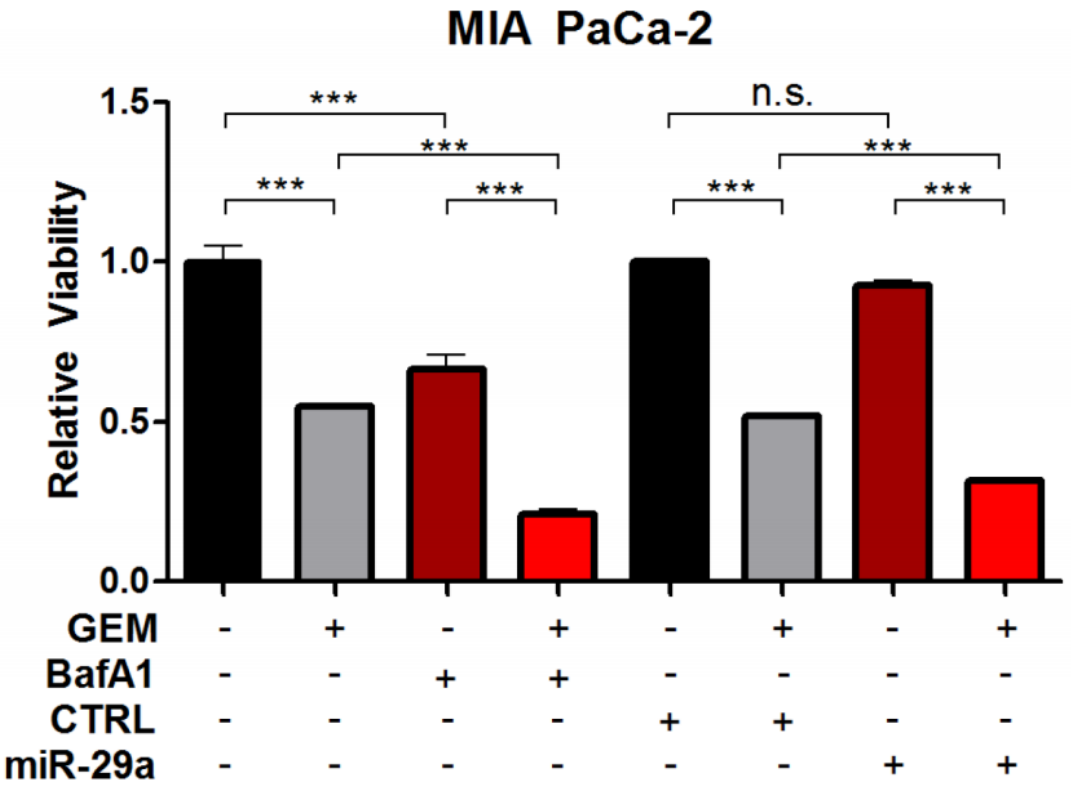

Figure 35. Effect of miR-29a, CQ, and BafA1 on sensitization of MIA PaCa-2 cells to gemcitabine treatment. MIA PaCa-2 cells were transfected with CTRL or miR-29a mimics and treated with 10μM gemcitabine (GEM). In parallel, MIA PaCa-2 cells were treated with 10μM GEM alone or in combination with 25μM CQ or 10μM BafA1. 48 hours post GEM treatment, cell viability was determined using CCK-8 assay kit. Average relative absorbance (A450) normalized to respective controls is presented (N=6) ± S.E.M. ***$p<0.001$.

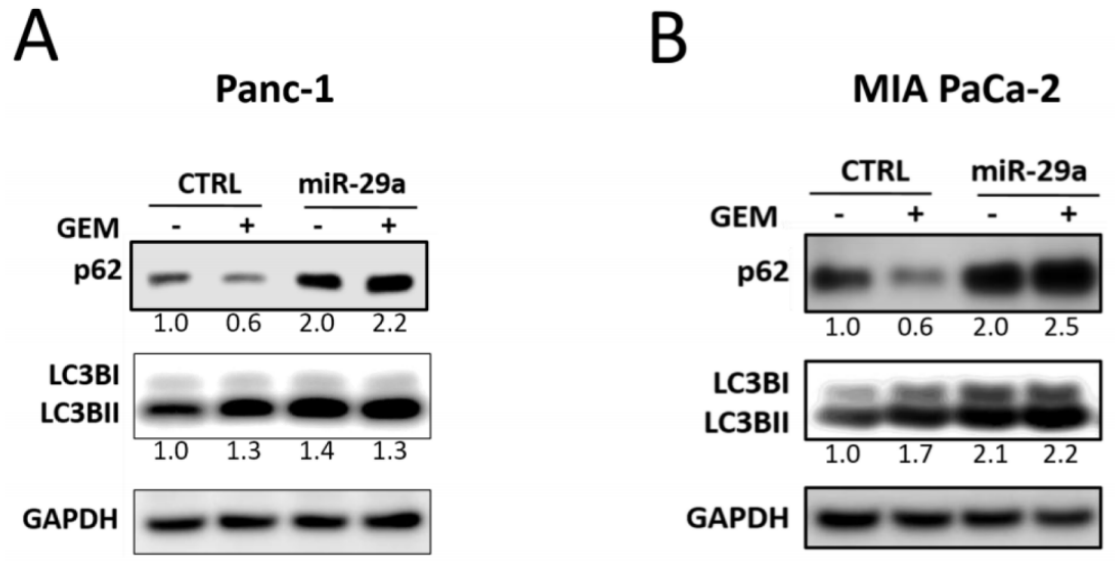

Figure 36. miR-29a blocks gemcitabine induced autophagy in Panc-1 and MIA PaCa-2. (A) Panc-1 or (B) MIA PaCa-2 cells transfected with CTRL or miR-29a mimics, were treated with or without 10μM GEM and 5 μg of total protein lysates were subjected to western blot analysis to measure p62 and LC3B proteins. GAPDH was used as loading control. Relative quantification of band intensities normalized to GAPDH are shown below respective blots.

miR-29a inhibits autophagosome-lysosome fusion. During autophagy, autophagosomes fuse with lysosomes where lysosomal hydrolases degrade the autophagosomal contents, which are recycled back into the cytoplasm (42). To understand the mechanisms by which miR-29a mediates blockage of autophagy flux, we evaluated its impact on autophagosomes and their interactions with lysosomes. Panc-1 cells stably expressing GFP-LC3B were transfected with miR-29a or control mimics, treated with 25 μM CQ, and stained with lysosomal-associated membrane protein 2 (LAMP-2), a lysosomal marker. In subsequent image analysis, we observed a two-fold increase in accumulation of autophagosomes/autophagolysosomes in miR-29a overexpressing cells (Figure 37A, Figure 37B, Figure 38, Figure 39). Furthermore, overexpression of miR-29a resulted in a >35% decrease in LC3B/LAMP-2 colocalization at basal levels and >60% decrease in miR-29a overexpressing cells treated with CQ, compared to CQ alone (Figure 37A, Figure 37C, Figure 39), indicating that miR-29a mediated blockage of autophagosome-lysosome fusion.

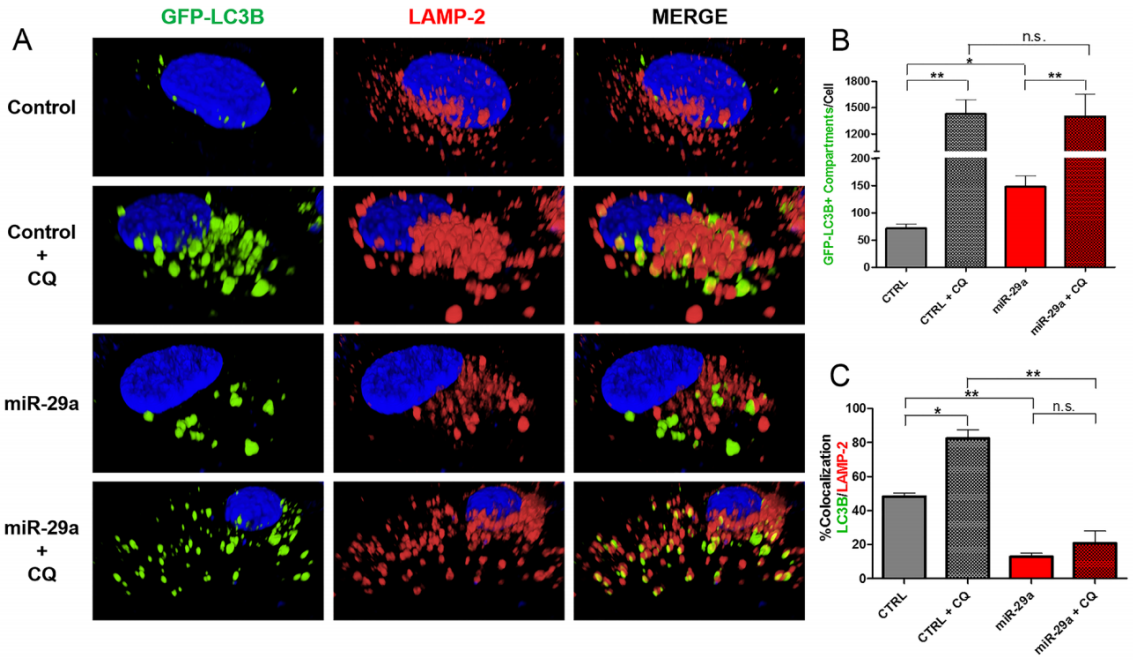

Figure 37. miR-29a inhibits autophagosome-lysosome fusion. (A) Panc-1 stably expressing GFP-LC3B were transfected with CTRL or miR-29a mimics. Following transfection, cells were treated with 25μM CQ. Cells were fixed and stained for lysosomal-associated membrane protein 2 (LAMP-2). (B) Image analysis was conducted to quantify number of GFP-LC3B positive compartments per cell, and averages are presented ± S.E.M. (C) Colocalization of GFP-LC3B and LAMP-2 was calculated based on the percentage of colocalization ± S.E.M. Experiment was repeated 3 times and representative data is presented. *p<0.05, **p<0.01, nonsignificant (n.s.).

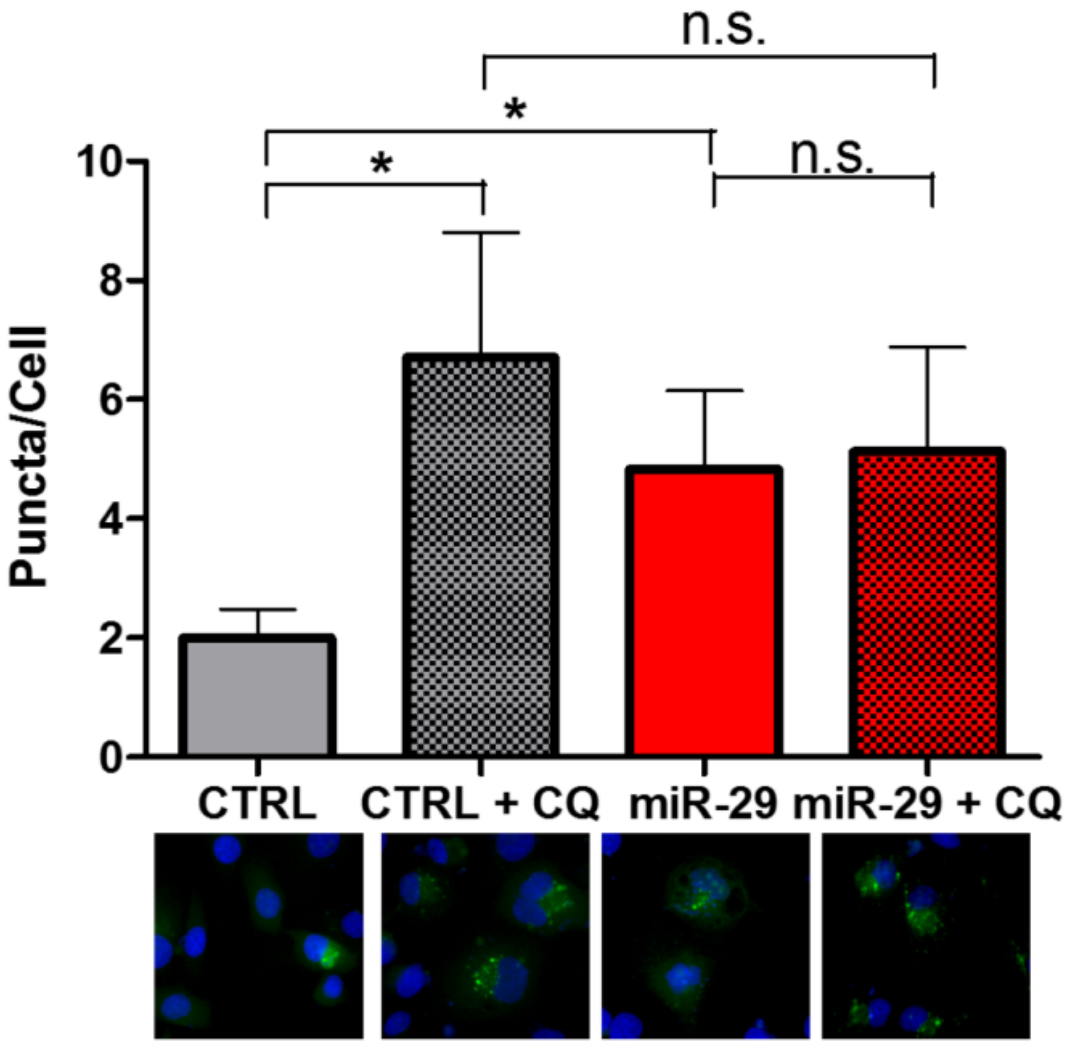

Figure 38. LC3B puncta quantification in miR-29a overexpressing Panc-1 cells.

GFP-LC3B stable Panc1 cells were transfected with CTRL or miR-29a mimics. Following transfection, cells were treated with 25μM CQ for 3 hours, fixed, and imaged. Number of GFP-LC3B positive puncta was counted and average number of GFP-LC3B positive puncta per cell (N>25 cells/group) is presented ± S.E.M (n=3). Representative images are shown below each graph. *$p<0.05$, non-significant (n.s.).

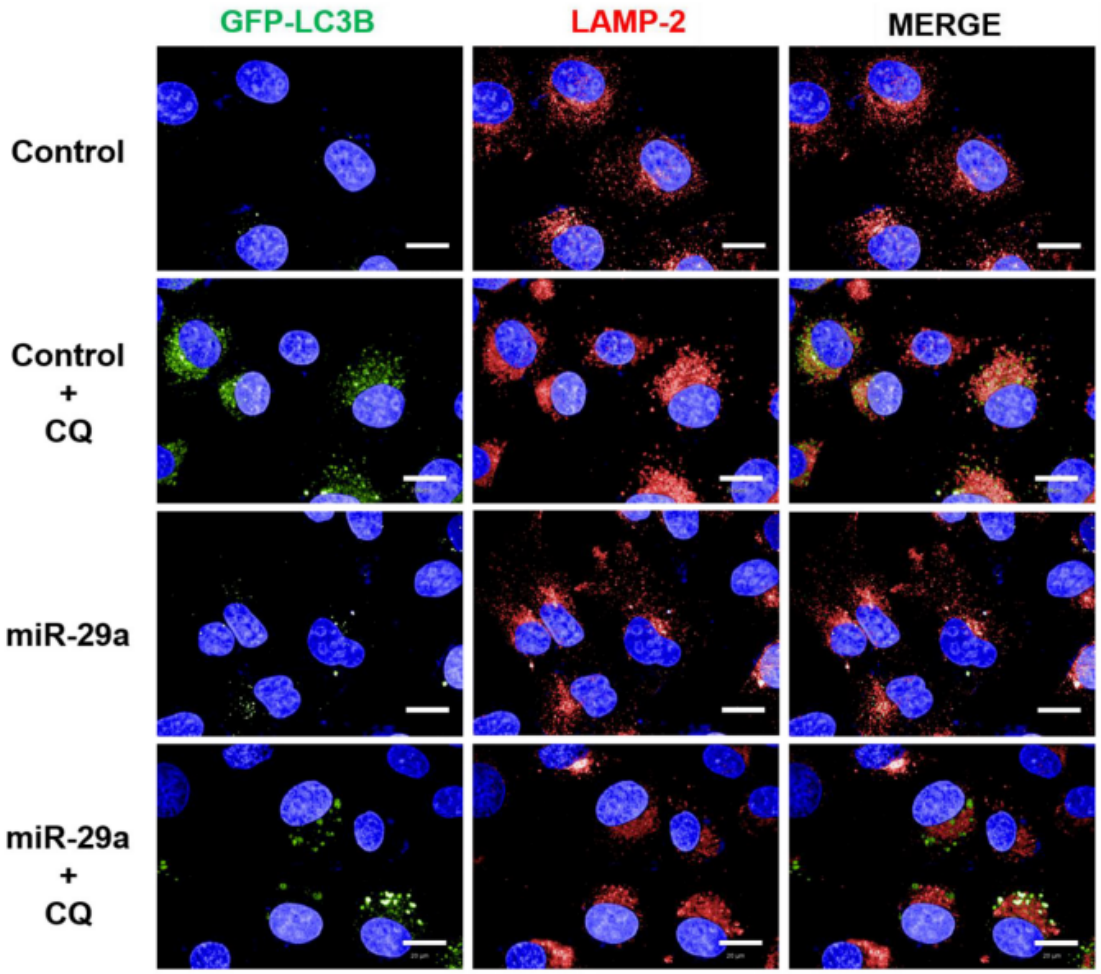

Figure 39. 2D representative images of LC3B and LAMP-2 colocalization in miR-29a overexpressing Panc-1 cells. GFP-LC3B stable Panc-1 cells were transfected with CTRL miRNA or miR-29a mimics. Following transfection, cells were treated with 25μM CQ for 3 hours, fixed, and stained for the LAMP-2 lysosomal marker (60x magnification). GFP-LC3B and LAMP-2 are presented, along with a merged image. Scale bar indicates 20μm.

miR-29a downregulates critical autophagy proteins TFEB and ATG9A. To address the mechanisms by which miR-29a mediates blockage of autophagy at late stages, we searched for potential autophagy related genes that are targeted by miR-29a using four prediction algorithms (TargetScan, PicTar, PITA, and miRanda). We found that both transcription factor EB (*TFEB*) and autophagy-related protein 9A (*ATG9A*) contain phylogenetically conserved miR-29 binding sites in their 3'-UTRs (Figure 40A). TFEB is a transcription factor and member of the MiT/TFE family, which has been shown to be an integral part of the lysosome and autophagy machinery (179). Upregulation of MiT/TFE factors has been implicated in various cancers (180-182), and a recent study documented that upregulation of TFEB contributes to increased autophagy in PDAC (182). Furthermore, knockdown of TFEB impaired growth and metabolism of PDAC cells by disrupting lysosomal catabolism in autophagy (182). Among >30 essential autophagy-related (ATG) genes (183), ATG9A is the only transmembrane protein (184) and has been shown to facilitate trafficking lipid membrane from the Golgi network and endosomes to the formation of autophagosomes (185, 186). Expression of ATG9A has been shown to be increased in some carcinomas (187, 188), but it has yet to be studied in PDAC. In our western blot analysis, overexpression of miR-29a in pancreatic cancer cells resulted in a marked repression of both TFEB and ATG9A expression (Figure 40B, Figure 41). As miRNAs regulate the expression of multiple target mRNAs, we wished to confirm that miR-29a does not alter expression of GAPDH, our endogenous control. We conducted target prediction analysis (Targetscan) and confirmed that GAPDH is not a target of miR-29a (data not shown), and we did not detect changes in Ct values for *GADPH* mRNA levels upon transfection of the miR-29a compared to control. These

findings help to insure that GAPDH was a proper loading control in our western blot analysis.

As we observed downregulation of TFEB and ATG9A in response to miR-29a overexpression, we next wished to address whether miR-29a directly repressed the expression of *TFEB* and *ATG9A* mRNAs. Luciferase reporter plasmids were constructed that included the 3'-UTR for both gene transcripts. Both 3'-UTRs contain predicted miR-29 binding sites. Wild type and mutated versions of the predicted miR-29a binding sites (Figure 40A) were include in the 3'-UTR downstream of the luciferase open reading frame. When reporter plasmids with wild type miR-29a binding sites were co-transfected with miR-29a mimics into cancer cells, there was a significant repression of luciferase activity. However, when the 3'-UTRs were mutated, miR-29a no longer has the ability to repress luciferase activity of the reporters with the TFEB and ATG9A 3-UTRs. These findings indicate that miR-29a represses *TFEB* and *ATG9A* expression by directly interacting with the predicted sites 3'-UTR sites in both autophagy genes. Consistently, we observed higher ATG9A and TFEB expression in pancreatic cancer cells that have low miR-29a expression (Panc-1 and MIA PaCa-2), compared to normal pancreatic epithelial cell line (HPNE) and cancer cell line with high miR-29 expression (AsPC-1) (Figure 42). Taken together, our data indicates that miR-29a downregulates TFEB and ATG9A through direct interactions with the 3'-UTR binding sites.

Next, we sought to determine the effects of TFEB and ATG9A depletion on PDAC autophagy using siRNA mediated knockdown of TFEB or ATG9A. Knockdown of these two genes resulted in an accumulation of LC3B and p62 similar to miR-29a overexpression (Figure 40D and Figure 43). Furthermore, knockdown of TFEB and

ATG9A led to a significant increase in accumulation of GFP-LC3B positive vesicles (Figure 44). TFEB knockdown resulted in a ~50% increase of autophagosome accumulation, whereas ATG9A knockdown caused a >100% increase in autophagosome accumulation (Figure 44A, Figure 44B). Although knockdown of TFEB blocked autophagy as indicated by an increased accumulation in p62 and LC3B (Figure 44C). We did not find a significant difference in GFP-LC3B and LAMP-2 colocalization, suggesting that the increase in GFP-LC3B positive vesicles were mostly due to accumulation of autophagolysosomes (Figure 44A, Figure 44B). Whereas, knockdown of ATG9A resulted in a robust 2-fold decrease in colocalization of LC3B and LAMP-2, demonstrating that miR-29a inhibits autophagosome-lysosome fusion predominately by deregulation of ATG9A. Taken together, our results suggest that miR-29a inhibits autophagy flux through the downregulation of TFEB and ATG9A expression, which are critical for lysosomal function and autophagosome trafficking respectively.

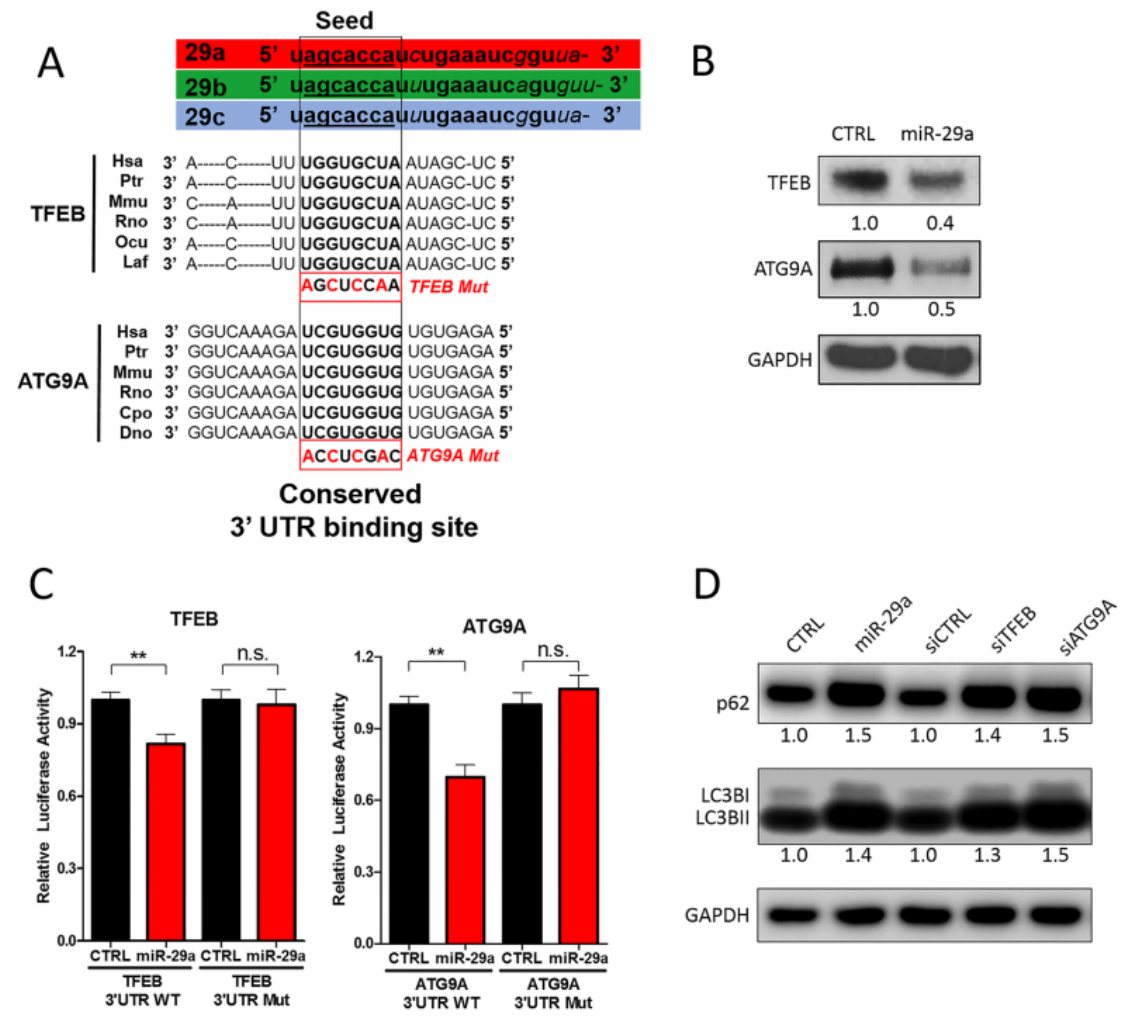

Figure 40. miR-29a downregulates TFEB and ATG9A expression to inhibit autophagy. (A) Schematic representation of the miR-29 family members and 3'-UTR binding sites of miR-29 targets as well as mutated binding sites used in Luciferase Assays: Transcription Factor EB (TFEB) and Autophagy-related protein 9A (ATG9A). All three miR-29 family members (miR-29a, miR-29b, and miR-29c) have identical seed sequences. Conserved miR-29 binding sites in the 3'-UTR of mRNA transcripts encoding

ATG9A and TFEB are depicted in bold. (B) 10 µg of total protein lysates from Panc-1 transfected with CTRL or miR-29a mimics were subjected to western blot analysis to measure the levels of TFEB, ATG9A, and GAPDH. Quantification of protein band intensities normalized to GAPDH are shown below each blot. (C) Relative firefly luciferase activity from reporter plasmid encoding *TFEB* or *ATG9A* 3'-UTRs following cotransfection into Panc-1 cells with control or miR-29a mimics. For each, either wild type (WT) and mutant (mut) reporter constructs were analyzed. All readouts were normalized to renilla luciferase activity. Average relative luminesce normalized to respective controls is presented (n=6) ± S.E.M. (D) 5 µg of total protein lysates from Panc-1 cells that were transfected with CTRL, miR-29a mimics, siCTRL, siTFEB, or siATG9A. 24 hours post-transfection, total protein was harvested and subjected to western blot analysis for p62 and LC3B proteins. GAPDH was used as loading control. Quantification of the indicated protein bands, which were normalized to GAPDH and relative to control, are shown below respective blots. All experiments were repeated 3 times and representative data is presented.

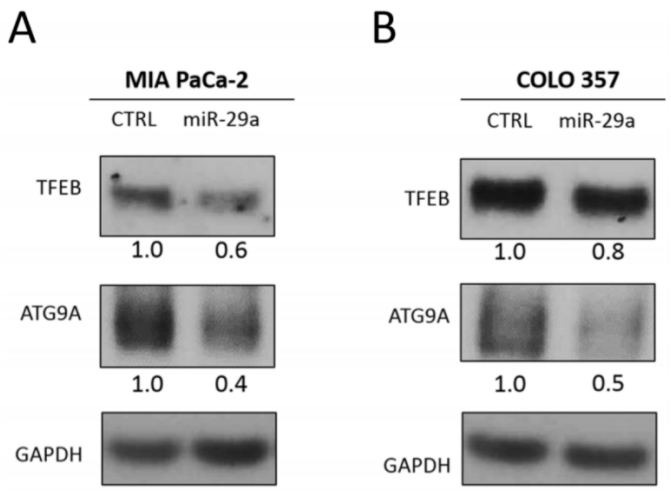

Figure 41. Effect of miR-29a overexpression on TFEB and ATG9A expression in MIA PaCa-2 and COLO 357 cells. (A) MIA PaCa-2 and (B) COLO 357 cells transfected with CTRL or miR-29a mimics. 10 µg total protein lysate was subjected to western blot to measure ATG9A and TFEB proteins. GAPDH was used as a loading control. Quantification of protein intensities normalized to GAPDH is shown below each blot.

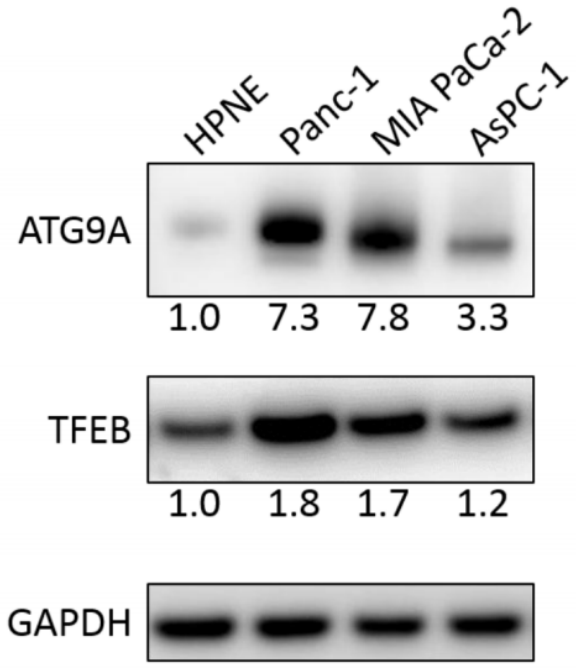

Figure 42. ATG9A and TFEB expression in HPNE, Panc-1, MIA PaCa-2, and AsPC-1. Lysates were harvested from normal epithelial cells, HPNE, and cancer cell lines, Panc-1, MIA PaCa-2, and AsPC-1. 10 µg of total protein were analyzed by SDS-PAGE and western blot analysis to measure ATG9A and TFEB proteins. GAPDH was used as loading control. Quantification of protein band intensities normalized to GAPDH is shown below each blot.

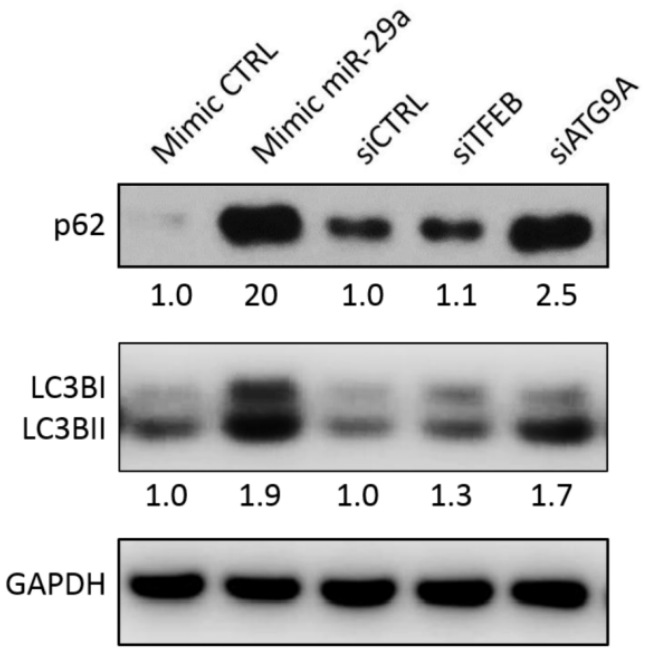

Figure 43. Effect of TFEB and ATG9A knockdown on autophagy of MIA PaCa-2 cells. MIA PaCa-2 cells were transfected with CTRL miRNA or miR-29a mimics, or with siCTRL, siTFEB, or siATG9A. 24 hours after transfection, total protein was harvested and 5 µg of each was analyzed by western blot to measure the levels of p62 and LC3B proteins. GAPDH was used as loading control. Quantification of protein band intensities normalized to respective controls is shown below each blot.

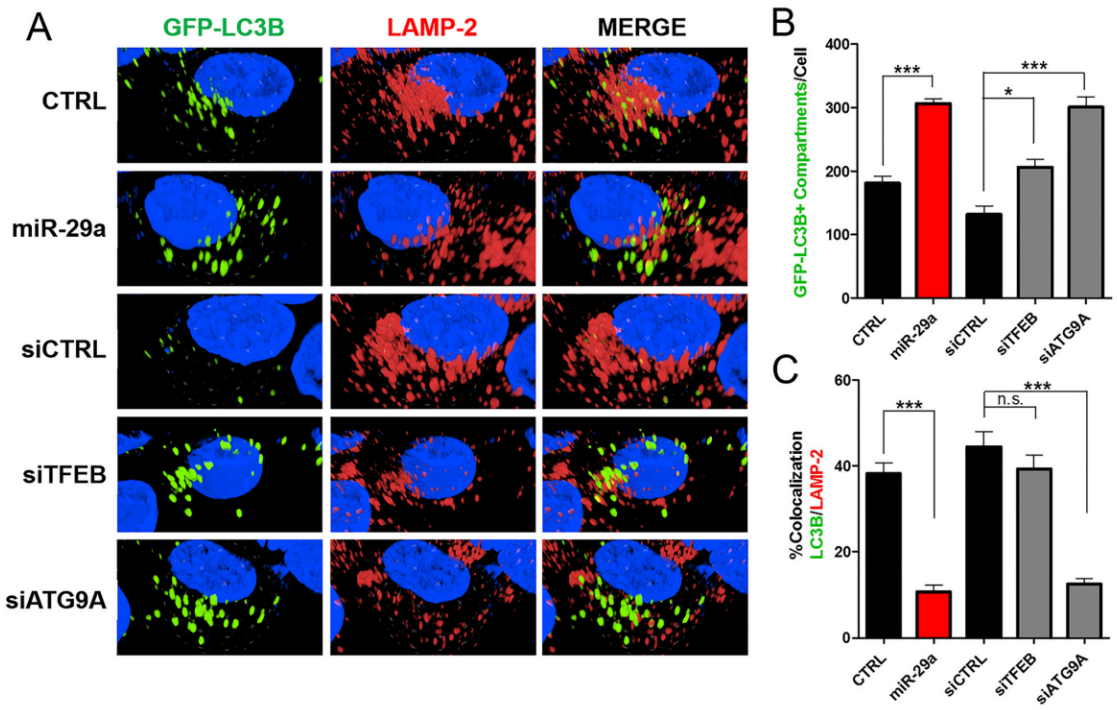

Figure 44. Knockdown of TFEB and ATG9A results in decreased autophagosomal-lysosomal fusion. (A) Panc-1 cells stably expressing GFP-LC3B were transfected with either CTRL miRNA or miR-29a mimics in cells in parallel with siCTRL, siTFEB, or siATG9A. Following transfection, cells were fixed and stained for lysosomal-associated membrane protein 2 (LAMP-2). (B) Image analysis was conducted to quantify number of GFP-LC3B positive compartments per cell, and averages are presented ± S.E.M. (C) Colocalization was calculated based on GFP-LC3B and LAMP-2 staining, and average percentage of colocalization is presented ± S.E.M. All experiments were repeated 3 times and representative data is presented. **p<0.05, **p<0.01, ***p<0.001 non-significant (n.s.).

miR-29a reduces pancreatic cancer cell invasion *in vitro.* Prior studies have also found that miR-29 is downregulated in a wide variety of carcinomas, including breast, colorectal, and prostate, and its reintroduction had anti-metastatic effects (112, 189, 190). Furthermore, increase in autophagy has been shown to enhance the invasive potential of cancer cells and promote epithelial-mesenchymal transition (EMT) (56, 57). As we observed downregulation of miR-29 in pancreatic cancer cells and its subsequent overexpression inhibited autophagy, we performed a series of *in vitro* functional studies to evaluate the effect of miR-29a on the invasive potential of pancreatic cancer cells. To determine the effect of miR-29a on cancer cell migration and invasion, Panc-1 and MIA PaCa-2 cells were transfected with control or miR-29a mimics and seeded in transwell assays. Compared to control cells, significantly fewer miR-29a overexpressing cancer cells migrated through transwell membranes and invaded through matrigel-precoated membranes (Figure 45, Figure 46).

EMT is known to enhance the migration/invasion of pancreatic cancer cells and resistance to apoptosis (191-193). As miR-29 reduced the migration and invasion potential of pancreatic cancer cells, we sought to determine its effect on EMT. As expected, overexpression of miR-29a in pancreatic cancer cells increased expression of epithelial marker, E-cadherin (192) and decreased mesenchymal marker, Vimentin (192) (Figure 45C).

We next tested the effect of miR-29a overexpression on anchorage independent growth of pancreatic cancer cells using soft agar assays. There was a significant decrease in the number of anchorage independently growing cancer colonies in miR-29a overexpressing PDAC cells compared to cells expressing control mimic (Figure 46D,

Figure 47). Our results show that miR-29a induces an anti-invasive potential as illustrated by a reduction in migration, invasion, and anchorage independent growth of pancreatic cancer cells.

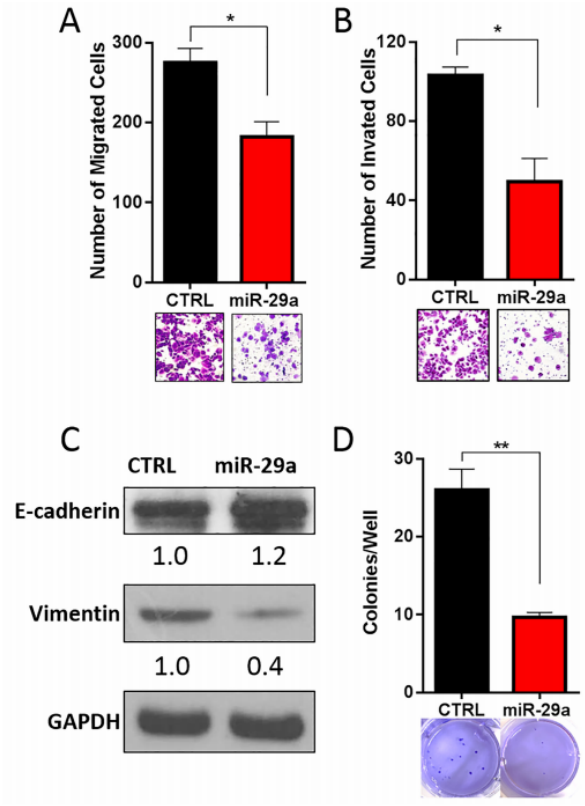

Figure 45. miR-29a inhibits invasive potential of PDAC cells. Panc-1 cells were transfected with control (CTRL) or miR-29a and plated into (A) migration and (B) invasion assays. Migration and invasion data were presented as average number of cells per 5 fields (n=3) ± S.E.M. and representative images shown below each graph. (C) 10 µg of total cell lysates from Panc-1 transfected with CTRL or miR-29a mimics were subjected to western blot analysis for epithelial marker, E-cadherin, and mesenchymal marker, Vimentin, and GAPDH was used as loading control. Quantification of protein band intensities normalized to GAPDH is shown below each blot. (D) Panc-1 cells were transfected with CTRL or miR-29a mimics and plated into soft agar assays. Data presented as average number of colonies per well (n=6) ± S.E.M. and representative images are shown below each graph. All experiments were repeated 3-4 times and representative data is presented. *$p<0.05$, **$p<0.01$.

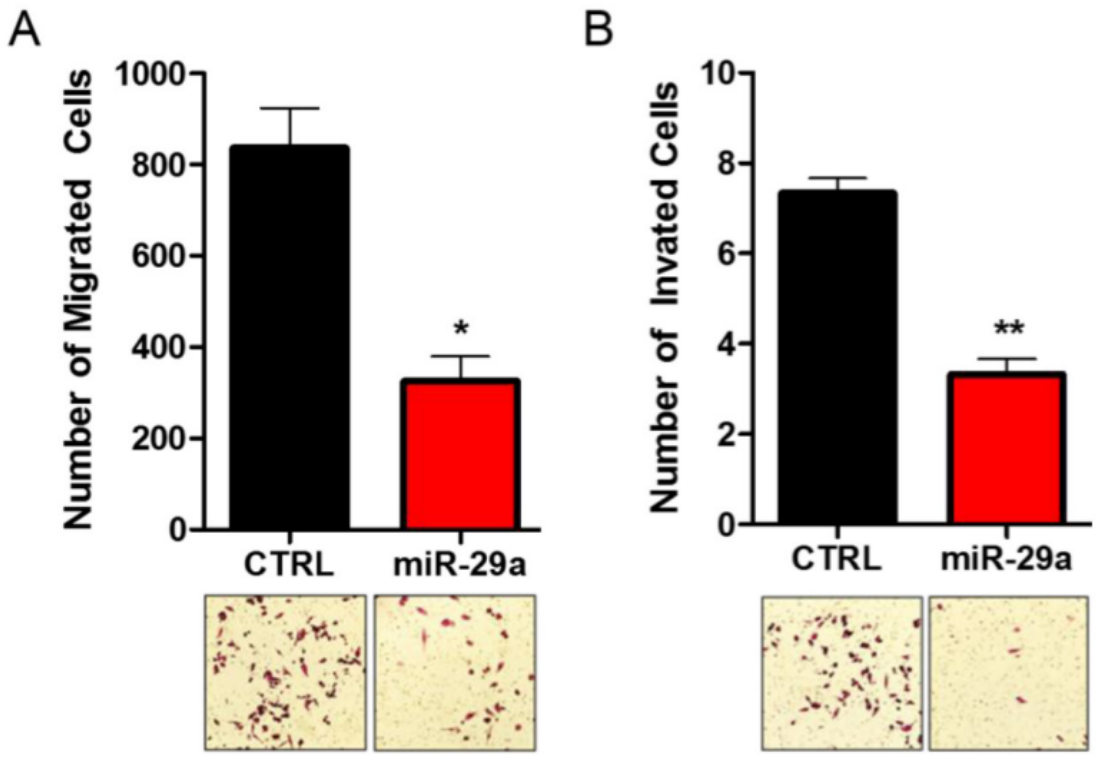

Figure 46. Effect of miR-29a overexpression on migration and invasion of MIA PaCa-2 cells. MIA PaCa-2 cells were transfected with control (CTRL) or miR-29a mimics and plated into (A) migration and (B) invasion assays. Migration and invasion data presented as average number of cells per 5 fields (n=3) ± S.E.M. with representative images below each graph. *$p<0.05$, **$p<0.01$.

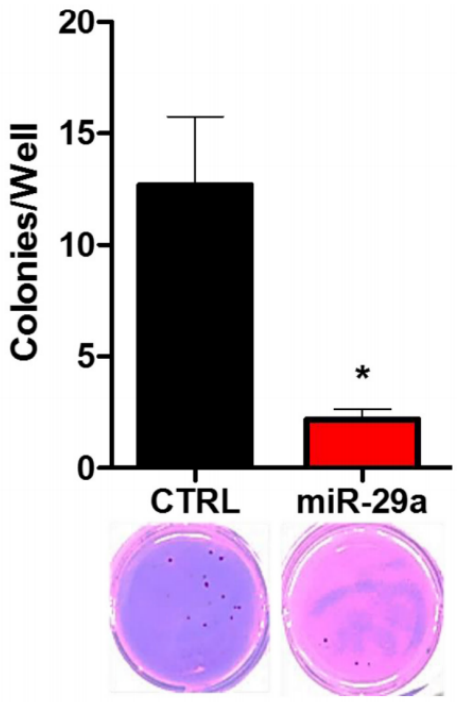

Figure 47. Effect of miR-29a overexpression on anchorage independent growth of MIA PaCa-2 cells. MIA PaCa-2 cells were transfected with control (CTRL) or miR-29a mimics and plated into soft agar assays. Representative data is presented as average ± S.E.M. (n=3). Representative images are below each graph. *$p<0.05$.

3.4 Discussion

Our study demonstrates for the first time that miR-29a functions as a potent autophagy inhibitor, and also sensitizes chemoresistant cancer cells to gemcitabine, and reduces the invasive potential of pancreatic cancer cells (Figure 48). There is an increasing body of evidence documenting a role for autophagy in cancer pathogenesis, supporting that idea that this pathway is a new therapeutic target (39-41, 53-59). We found consistent repression of miR-29 expression in pancreatic cancer cells, and overexpression of miR-29a inhibited autophagy, as illustrated by increased accumulation of autophagosomes/autophagolysosomes and autophagy markers, LC3B and p62. Furthermore, miR-29a decreased autophagosome-lysosome fusion, as shown by a significant decrease in colocalization of LC3B and LAMP-2, autophagosomal and lysosomal markers respectively. Taken together, our results suggest that miR-29a functions as a late stage autophagy inhibitor by blocking autophagosome-lysosome fusion.

To determine the mechanisms of miR-29a mediated inhibition of autophagy, we identified two critical autophagy genes, TFEB and ATG9A, which have phylogenetically conserved miR-29 binding sites in the 3'-UTRs of their encoded transcripts. As expected, overexpression of miR-29a caused a marked reduction of TFEB and ATG9A expression. TFEB, a transcription factor essential for lysosomal function, is highly activated in PDAC (179) and its knockdown reduces tumor progression and impairs autophagy due to lysosomal dysfunction (182). ATG9A is the only transmembrane ATG protein, and facilitates membrane trafficking of autophagosomes (194, 195). Upregulation of ATG9A has been well documented in other carcinomas (187, 188). Knockdown of TFEB or

ATG9A caused a late stage blockage in autophagy similar to miR-29a overexpression. Interestingly, knockdown of ATG9A or TFEB increased the accumulation of LC3B positive compartments, but only the knockdown of ATG9A blocked autophagosome-lysosome fusion. As ATG9A functions in vesicular trafficking, reduced expression of ATG9A is likely to cause perturbations in autophagosome trafficking and prevent them from fusing with lysosomes. Whereas, TFEB knockdown mediated accumulation of autophagolysosomes is likely due to defective lysosomal degradation capacity rather than a blockage of autophagosome-lysosome fusion. Collectively, our results indicate that miR-29a inhibits PDAC autophagy by downregulation of TFEB and ATG9A.

Pancreatic cancer acquires chemo-resistance by inducing autophagy (39-41). We found that miR-29a sensitized chemoresistant pancreatic cancer cells to gemcitabine treatment, decreased cancer cell viability, and enhanced gemcitabine-mediated cytotoxicity. Accordingly, upon gemcitabine treatment, miR-29a overexpression resulted in an increased LDH release (162, 163), caspase 3/7 activity, and cleaved caspase 3. CQ and BafA1 are known late stage autophagy inhibitors (172, 175). The effects of miR-29a on LC3B and p62 accumulation is similar to CQ and BafA1, suggesting that miR-29a serves as an effective late stage inhibitor of autophagy. miR-29 has been previously reported to induced cellular cytotoxicity/apoptosis by targeting anti-apoptotic protein Mcl-1 in cholangiocarcinoma (196). However, the effect of miR-29 on Mcl-1 and gemcitabine-mediated cytotoxicity is not known in pancreatic cancer cells. Further studies are required to dissect the role of Mcl-1 in this mechanistic axis.

Our functional studies demonstrate that overexpression of miR-29a inhibits pancreatic cancer cell migration and invasion through reversion of cancer cell EMT. Prior

to metastasis, tumor cells undergo EMT, a process in which cells lose epithelial characteristics and gain a mesenchymal phenotype. A recent report suggested that EMT is a characteristic feature of malignant transformation that contributes to the invasive/metastatic properties of a wide variety of cancers (197). Overexpression of miR-29a resulted in an increase in epithelial marker, E-cadherin, and reduction in mesenchymal marker, vimentin, indicating that reintroduction of miR-29a induces mesenchymal–epithelial transition (MET) in pancreatic cancer cells. However, vimentin is not a predicted miR-29 target (Targetscan), suggesting that miR-29a may induce MET transition through indirect effects rather than direct regulation of Vimentin. Of interest, autophagy has been shown to be concomitant with increased metastasis and EMT (56, 57). Our findings demonstrate similar effects in which miR-29a mediated an inhibition of autophagy in tandem with MET transition and reduction of cancer cell invasive potential. It is possible that miR-29a reduces EMT in pancreatic cancer cells by inhibition of autophagy. However, further studies are warranted to dissect the precise underlying mechanisms.

To further study the function of miR-29a, we investigated the effect of miR-29a on anchorage independent growth of pancreatic cancer cells. Epithelial cells require attachment to a substrate in order to maintain structural polarity, function, and survival (198). When this adhesion is lost, cells undergo anoikis, a form of programmed cell death induced by detachment (198, 199). Various cancers have been shown to avoid anoikis, leading to properties associated with metastasis and tumorigenesis (200). We found that overexpression of miR-29a significantly reduces the ability of pancreatic cancer cells to grow in an anchorage independent manner.

With the exception of AsPc-1, we observed consistent downregulation of all three miR-29 family members in various pancreatic cancer cell lines. AsPC-1 contains homologous deletions in SMAD4, whereas the other cancer cell lines contain wildtype SMAD4 (201). SMAD4 is a major downstream effector molecule of TGF-β1 signaling, forms a heterogeneous complex with pSMAD2/3, and regulate the target gene expression (117). We and others demonstrated that TGF-β1 downregulates miR-29 expression in other cell types through SMAD2/3/4 complex (85, 202). Perhaps homologous deletion of SMAD4 in AsPC-1 derepresses miR-29 expression. However, this mechanism needs to be validated in PDAC. Furthermore, the regulatory mechanism associated with downregulation of miR-29 has not been fully elucidated. The three miR-29 family members (miR-29a, -29b, -29c) are encoded from two co-transcribed miRNA clusters, miR-29a/b1 and 29c/b2 located on Chromosome 7 and 1 respectively. Both miR-29 loci have promoter regions containing c-Myc (203) and SMAD3 (202) binding sites. It would be of interest to determine if c-Myc or SMAD4 regulates miR-29 expression in pancreatic cancer cells, as both of them have been indicated to play a critical role in PDAC (204, 205).

The downregulation and anti-tumorigenic effects of miR-29 have been reported in a wide variety of cancers (112, 189, 190). Furthermore, autophagy has been implicated in a number of carcinomas to promote metastasis (54) and induce chemoresistance (206-208). It would be of interest to evaluate the role of miR-29 in autophagy of other cancers, as this would shed light on whether the mechanism of autophagy inhibition that we have discovered is ubiquitous in cancer pathogenesis or idiosyncratic to pancreatic cancer. Furthermore, our findings need to be validated *in vivo* to translate our findings into the

clinic. Nevertheless, our studies reveal a novel role of miR-29a in PDAC autophagy and provide evidence for its use as an autophagy inhibitor and novel therapeutic agent in combination with gemcitabine, to target PDAC.

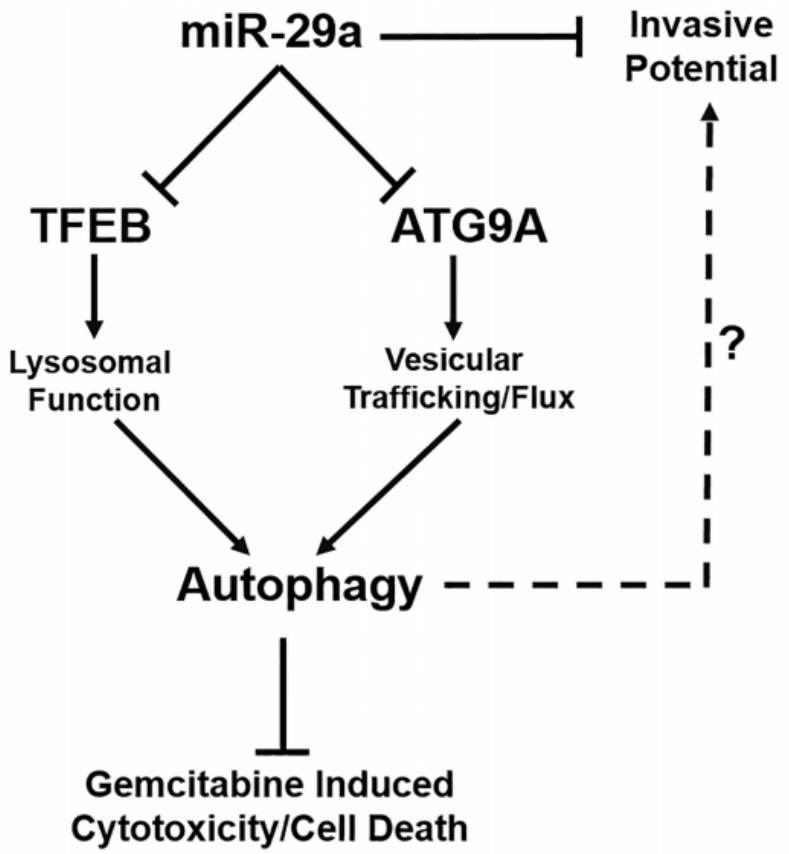

Figure 48. Schematic diagram representing the role of miR-29a in PDAC autophagy and metastasis. miR-29a overexpression in pancreatic cancer cells decreases invasive potential and inhibits autophagy flux through downregulation of TFEB and ATG9A, resulting in increased sensitivity to GEM treatment. miR-29a may serve as a potential novel anti-autophagic/invasive agent to target PDAC.

Chapter 4: Safety and Efficacy of AAV Retrograde Pancreatic Ductal Gene Delivery in Normal and Pancreatic Cancer Mice

4.1 Introduction

The pancreas is a primary site of origin for a wide variety of diseases including diabetes, pancreatic cancer, and pancreatitis (209). PDAC has the worst prognosis among pancreatic diseases (210, 211). In the United States, it is the third leading cause of cancer deaths and is projected to become the second leading cause of cancer related deaths in just over a decade (2). Although combination chemotherapies such as Nab-Paclitaxel/Gemcitabine and FOLFIRINOX (145, 146) modestly improves survival, the overall 5-year survival rate has not exceeded 8% for the last 30 years (212). Furthermore, PDAC has a well-characterized mutational profile that plays a key role in disease onset and progression (147), but the knowledge of these genetic perturbations has yet to yield effective, targeted therapies. A combination of novel gene/cell based therapeutic strategies with conventional chemo-radiation therapies may improve the survival rate of this deadly cancer.

Pre-clinical animal models, particularly genetically engineered mouse models (GEMMs) of PDAC, have played a pivotal role in understanding the pathobiology of oncogenes/tumor suppressors and in developing new therapeutic strategies (113, 213-217). Importantly, large-scale deep sequencing data and The Cancer Genome Atlas (TCGA) are identifying new genetic aberrations associated with PDAC pathogenesis(218-220). Developing pre-clinical mouse models for new oncogenic mutations and/or in combination with well-characterized genetic mutations associated with PDAC progression is a daunting process that typically takes several years. Genome

editing tools such as CRISPR/Cas9 in combination with targeted gene delivery could serve as a potential surrogate to transgenic mouse models to study *in vivo* gene function (221-224). However, because of its anatomical location, targeted pancreatic gene delivery without safety concerns, particularly pancreatitis, is a major challenge for *in vivo* gene delivery.

A wide range of non-viral and viral gene delivery systems have been exploited to target the pancreas for therapeutic purposes and functional studies (225). Non-viral liposomes and nanoparticles have been commonly employed to deliver conjugated drugs/chemotherapy or therapeutic genes. However, a major limitation with non-viral delivery methods is low efficacy, and they require repeated delivery to achieve therapeutic benefit (226, 227). Viral vectors have been shown to be more efficacious to achieve long-term gene expression with limited off-target effects. Among the viral vectors, integrating lentiviral vectors target the pancreas efficiently (exocrine and endocrine) with no immune response (228). However, insertional mutagenesis is a major concern and limits its use for *in vivo* delivery (229, 230). By comparison recombinant adenovirus (rAd) or adeno-associated virus (rAAV) are predominately episomal, and both still achieve efficient *in vivo* pancreatic delivery (231, 232). Ad vector mediated pancreatic gene transfer is transient in nature due to potent host immune responses and vector mediated cytotoxicity (233-235). On the other hand, non-integrating AAV vectors are particularly promising in efficiently targeting the whole pancreas (236-238). Also both have the potential to target specific cell types in the pancreas (239-241) and pancreatic neoplasms(242), and both do not elicit humoral responses or alterations in physiological pancreatic functions (236-238, 242, 243). AAV vectors contain a single-

stranded (ss) DNA genome, with a packaging capacity of ~4.8 kb, and are able to mediate long-term transgene expression because of their lack of pathogenicity and low immunogenicity(244-246). In addition, ssAAV vectors have been engineered to contain a double-stranded (ds) DNA genome (hairpin) to circumvent the requirement for second strand DNA synthesis, a requisite for transgene expression, and are self-complementary (sc) AAV viral vectors (247, 248). Improved scAAV vectors were shown to be more efficacious in *in vivo* gene delivery (249).

Determining an ideal delivery route with limited off-target effects is another critical component to target the pancreas efficiently. A wide range of gene delivery routes have been exploited such as direct pancreatic injections (233, 238, 250), intraperitoneal (242, 251), systemic delivery (252, 253) and in conjunction with clamped hepatic circulation (236), celiac/hepatic artery (254), and retrograde ductal delivery via pancreaticobiliary ductal infusion (224, 231, 237, 243), or catheterizing the cystic duct through the gallbladder/common bile duct (228, 236). Among several AAV serotypes tested, AAV8 and AAV9 have been shown to be well-suited for systemic delivery (255, 256), and AAV6 has been shown to transduce the normal pancreas very efficiently via retrograde pancreatic ductal delivery (236). Accumulating evidence documents the use of AAV to deliver therapeutic molecules/genes to neoplasms, including pancreatic tumors (242, 257), and tissues undergoing rapid degeneration and regeneration (258, 259). However, a comprehensive study on ideal serotype, route, vector dose, and safety profile to target the pancreas with limited off-target effects and in the context of cancer is not well established using scAAV vectors. In this study, we have investigated the use of three scAAV serotypes (AAV6, AAV8,

and AAV9) to target the pancreas via systemic delivery or retrograde targeted ductal delivery and optimized the vector dose to maximize pancreatic gene expression. In addition, we evaluated the effect of ductal delivery mediated pressure on pancreatitis and use of AAV to target the pancreas in a PDAC mouse model driven by $Kras^{G12D}$, a common Kras mutation found in PDAC. We demonstrate that retrograde intraductal delivery of $5x10^{11}$ scAAV6.GFP vg/animal transduces the pancreas with >80% transduction efficiency, without causing fibrosis or inflammation. Furthermore, we have also shown that scAAV6 transduces acini, epithelial, and stromal cells in a PDAC mouse model with persistent long-term gene expression and does not adversely affect PDAC progression.

4.2 Materials and Methods

AAV vector production

A self-complementary recombinant AAV vector encoding a green fluorescent protein expressing under ubiquitous EF1α promoter has been previously described (136). Recombinant AAV vectors were produced by a standard triple transfection calcium phosphate precipitation method using HEK293 cells (ATCC, CRL-1573). The production plasmids were: (i) scAAV.GFP (ii) rep2-cap6/8/9 modified AAV helper plasmid encoding the cap serotype 6, or 8 or 9, and (iii) an adenovirus type 5 helper plasmid (pAdhelper) expressing adenovirus E2A, E4, ORF6, and VA I/II RNA genes. Purification was accomplished from clarified HEK293 cell lysates by sequential iodixanol gradient purification and ion exchange column chromatography using a linear NaCl salt gradient for particle elution. Vector genome (vg) titers were determined by quantitative

polymerase chain reaction (qPCR) using EF1 primer and probe set as previously described (136, 260).

AAV transduction efficiency

Fresh tissues were harvested and fixed in 4% paraformaldehyde followed by overnight incubation in 30% sucrose and then embedded in OCT. Tissue blocks were cut into 6 μm sections using Leica cryostat. Transduction efficiency was determined by counting the number of GFP^+ and negative acinar, ductal cells, PSCs, or islets using four random 20x GFP and DAPI overlay images. To further quantify transduction efficiently, GFP transgene qPCR was performed on total DNA isolated from pancreatic and liver tissues. Total tissue DNA was isolated using the Gentra Puregene kit (Qiagen) according to the manufacturer's instructions. 60 ng of DNA (10,000 cell equivalents) was used as PCR template in triplicate reactions and vg numbers were extrapolated from a linearized plasmid standard. Vector genome/cell calculations assume 6 pg of total DNA per cell using GFP primer and probe set as previously described (136).

Whole organ pancreatic GFP expression

At necropsy, the abdominal cavity was opened, and the whole pancreas was imaged for GFP expression using a LEICA dissecting fluorescent microscope.

H&E, Masson's trichrome/Sirius Red staining

After formalin fixation, specimens were dehydrated through a graded series of ethanols, cleared in two changes of xylenes and infiltrated through 3 changes of melted paraffin. The specimens are then embedded in melted paraffin and allowed to harden. Thin sections (~5 μm) were cut using a rotary microtome equipped with disposable steel knives. Sections were flattened on a heated water bath, floated onto

microscope slides and dried. Serial sections were de-paraffinized and stained for Hematoxylin and Eosin (H&E), Masson's trichrome staining (Sigma-Aldrich, HT15-1KT) and Picro-Sirius Red to detect pancreatic fibrosis following standard histological procedures or as per the manufactures instructions. Similarly, serial frozen sections (~5-7μm) were stained for H&E.

B220-immunohistochemistry

Antigen retrieval was performed at high pH in the Dako Link PT module. After treating with a protein block (Dako) for 10 min, slides were incubated with CD45 primary antibody (clone B220BD Pharmingen, BD-550286, 1:50) for 60 min followed by biotinylated-anti-rat IgG (Jackson Immuno-Research) for 30 min, and finally with LSAB2-SA-HRP (Dako) for 30 min. The chromogen was developed with DAB (Dako). All steps were separated by tris buffer (Dako) washes and performed at room temperature. All histological stains were performed by histology cores at IU School of Medicine.

PanIN analysis in KC mice

Using a standard H&E slide, small clusters of abnormal ducts were looked at as a first target. Using the Johns Hopkins School of Medicine classification system (261), clusters of abnormal ducts were classified into PanIN grades 0 (normal), 1-A, 1-B, 2, and 3. Each duct in the cluster was scored and PanIN size analysis was done using the Aperio Imagescope system.

Fibrosis and immune response quantification

The slides were analyzed using Aperio Imagescope and the FDA approved algorithm with few a modifications. The entire pancreatic tissue was analyzed, with the

exclusion of vessels, lymph nodes, and peri-pancreatic fat. *Trichrome*: FDA approved algorithm was altered to detect blue against a red background. Hue value was altered from 0.1 (Brown) to 0.62 (Blue), hue width was altered from 0.5 to 0.4, and color saturation was altered from 0.04 to 0.005. *Sirius Red:* Hue value was altered from 0.1 (Brown) to 0.85 (Red) and hue width was not changed. Color saturation was altered from 0.04 to 0.6. The intensity threshold was lowered from 175 to 100. *B220:* A pathologist reviewed the slides and determined the quantity of cells that were B220 positive.

Immunostaining

Serial frozen sections (5-7 μm) were rehydrated in PBS, permeabilized with 0.5% Triton X solution, blocked with 10% BSA, and probed with either α-SMA antibody (Novus Biologic, NB500-631, 1:200), CK19 antibody (Abcam, ab52625, 1:200), insulin antibody (Cell Signaling, 4590S, 1:200), or α-Amylase (Cell Signaling, 3796S, 1:200) overnight at 4^{o}C. Epitope retrieval was performed using 1x sodium citrate buffer followed by Triton X permeabilization. Subsequently, slides were stained with secondary antibody Alexa Fluor 594 goat anti-rabbit IgG (Life Technologies, A11037, 1:1000). Slides were mounted with Vectashield antifade mounting medium with DAPI (Vector Laboratories, H-1200) and coverslips were sealed.

GFP Immunohistochemistry

Paraffin embedded tissues were sectioned (5 μm) and epitope retrieval was performed using heat-induced epitope retrieval (HIER) with 10 mM citrate buffer. Endogenous peroxidase activity was blocked using 3% H2O2 in methanol and subsequently blocked with 0.5% BSA. Primary antibody, mouse anti-GFP (Cell Signaling, #2955, 1:200), was applied and incubated overnight at 4^{o}C. Secondary anti-

mouse IgG was utilized from Vectastain mouse IgG ABC kit (Vector Labs, PK-6102) and developed with peroxidase substrate solution consisted of 0.05% DAB and 0.01% H_2O_2 in PBS via the manufacturer's protocol. Sections were counterstained in Gill No. 1 hematoxylin (Leica Biosystems, 3801520), cleared, and mounted with a resin-based mounting medium.

Retrograde Pancreatic Ductal Delivery

Mice were sedated using isoflurane with 1.5-3% oxygen, the abdominal cavity was opened, and a customized catheter was inserted into the cystic duct through a small opening at the bottom of the gallbladder. The catheter was then advanced into the common bile duct and secured in place with a micro clamp around the bile duct and catheter to prevent vector reflux into the liver. A micro clamp was placed on the sphincter of Oddi to avoid leakage of the vector into the duodenum, and 100µl of AAV vector containing the GFP transgene or PBS (vehicle control) was slowly infused into the pancreatic duct through the catheter. Successful administration was documented by uniform swelling of the gland. The micro clamps used to temporarily block liver infusion and duodenum leakage were released 5 min after the infusion was completed. The catheter was then removed, the inner abdominal cavity was closed with absorbable sutures, and the outer skin was closed with wound clips. Post-surgery, mice were placed on a heating pad to maintain body temperature during recovery. Once the animals recovered, they were returned to their cages. Mice were treated subcutaneously with Carprofen (5-10mg/kg) to prevent post-operative discomfort.

Mice

KC mice were generated as described (113). Conditional *LSL-Kras*^{G12D} mice were crossed with *Pdx1-Cre* animals to generate the KC mice. All animal housing, use, and surgical procedures were carried out in accordance with the regulatory guidelines set by Guide for the Care and Use of Laboratory Animals of the National Institutes of Health. All animal protocols were reviewed and approved by the Indiana University (IU) and The Research Institute at Nationwide Children's Hospital Animal Care and Use Committees.

Statistical analysis

Student's t-test and Analysis of Variance with Tukey post-hoc analysis was used for statistical analysis. Data is presented as mean and error bars are represented as standard error of the mean.

4.3 Results

Comparison of scAAV8 and scAAV9 serotypes to target the pancreas via systemic delivery

In both clinical and pre-clinical settings, either direct injection or systemic delivery to the target tissue are preferred routes of administration for therapeutic purposes because of their ease of use. As direct injection of the pancreas would be more invasive and may not achieve uniform gene expression in the entire pancreas, for our initial studies, we elected systemic delivery. Previously, systemic delivery of ssAAV serotype 8 and 9 (AAV8 and AAV9) has been demonstrated to modestly transduce the pancreas (255, 256). scAAV vectors are known to transduce target tissues with higher efficiency compared to ssAAV vectors (249). To test the ideal serotype for systemic delivery, scAAV viral vector expressing green fluorescent

protein (GFP) under EF1α promoter (scAAV.GFP) (Figure 49A) was packaged using AAV8 and AAV9 serotypes, and $1x10^{12}$ vg/animal were delivered systemically (n=3 mice/group) to normal C57BL/6 mice, and animals were sacrificed at 3 weeks post-vector administration. As documented by fluorescence microscopy for GFP expression, AAV9 showed modestly higher pancreatic transduction efficiency (14.6% ± 2.5 Standard Error of the Mean - S.E.M.) compared to AAV8 (11.5 % ± 0.2 S.E.M.) (Figure 49B) with some off targets (Figure 50).

To test the ideal dose for achieving maximum pancreatic transduction efficiency via systemic delivery of scAAV9.GFP, we compared three different doses ranging from $1x10^{12}$-$5x10^{12}$ vg/animal. Although increase in vector dose improved transduction percentages, none of the tested doses reached >45% pancreatic transduction efficiency (Figure 49C, Figure 49D). This level of gene expression may be sufficient to develop therapeutic strategies for non-neoplastic tissues, but in the context of cancer, optimal transduction efficiency is preferred for therapeutic benefit and functional studies. Further dose increase via systemic delivery may improve transduction efficiency, but producing large quantities of clinical vectors for dosing adult PDAC patients without causing toxicity with high dose may be challenging.

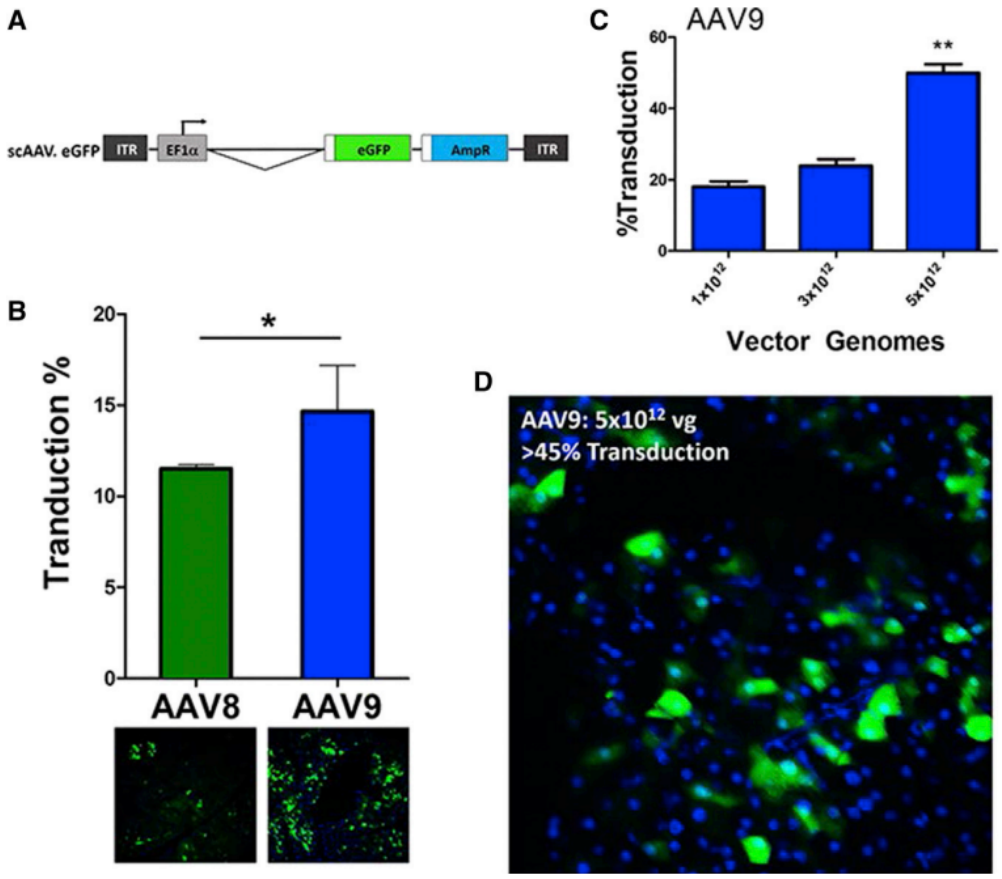

Figure 49. Comparison of scAAV8 and AAV9 to Target the Pancreas via Systemic Delivery. (A) Schematic of the scAAV.GFP vector. (B) Quantification of GFP expression in C57BL/6 mice administered 1 x 10^{12} vg/animal of scAAV8.GFP and scAAV9.GFP via tail vein injection (n = 3/group), as determined by percentage GFP+ acinar cells. A representative image of global pancreatic GFP expression is shown below each graph column; 6 mm frozen tissue sections. (C) Quantification of GFP expression in C57BL/6 mice administered scAAV9.GFP at various doses via tail vein injection (n = 3/group), as determined by percentage GFP+ acinar cells. (D) Representative global pancreatic GFP expression of C57BL/6 mice dosed with 5 x 10^{12} vg scAAV9.GFP 3 weeks post-vector administration. 20X magnification. Data represent mean ± SEM; *p < 0.05.

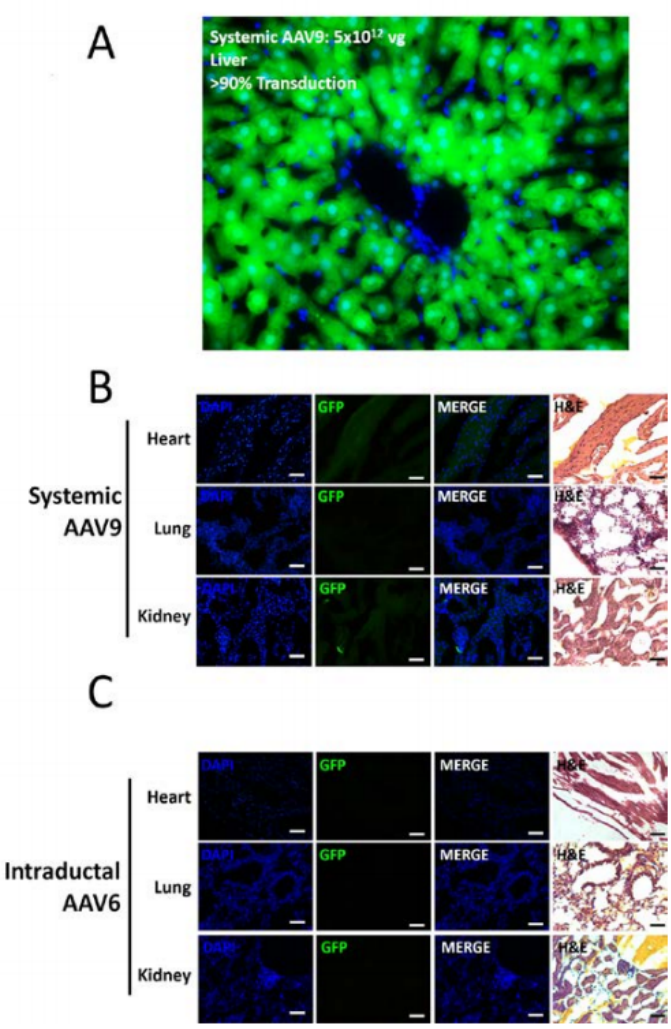

Figure 50. Assessment of off-target effects for AAV9 systemic delivery and AAV6 retrograde pancreatic intraductal delivery. Multiple organs were harvested from mice that were systemically dosed with scAAV9.GFP at $5x10^{12}$ vg/animal and (A) global representative image of liver GFP expression via florescence microscopy is presented, as well as (B) heart, lung, and kidney, with H&E stained serial sections (20X magnification, scale bar 50 μm). (C) Heart, lung, and kidney of mice intraductally dosed with scAAV6.GFP at $5x10^{11}$ vg/animal were harvested and serial sections were taken to assess global GFP expression determined via florescence microscopy and H&E staining for heart, lung, and kidney (20X magnification, scale bar 50 μm).

Retrograde intraductal infusion of scAAV6 transduces the pancreas uniformly and efficiently.

A wide range of gene delivery methods were previously evaluated to directly target the pancreas such as retrograde pancreatic ductal delivery by direct injection of the distal common bile duct (224, 237), cannulation of the common bile duct through the gallbladder/cystic duct, and intravenous injection coupled with liver blockage (236). Although each of these methods were shown to be effective to transduce the whole pancreas or various cell types of the pancreas (acini, islet of Langerhans, and ductal cells), we elected retrograde ductal delivery via cannulation of the common bile duct to evaluate its safety profile and use in cancer settings using scAAV vectors.

Initially to optimize the conditions for cannulation and retrograde ductal delivery, we dosed a cohort of mice with Evans Blue dye. As elaborated in the methods section, a customized 10 mm catheter was advanced through the gallbladder and cystic duct to the common bile duct (Figure 51A). A micro clamp is placed on the bile duct and sphincter of Oddi to prevent vector leakage into the liver and small intestine, and 100 µl of Evans Blue was injected over 2-3 minutes to target the pancreas. We observed a uniform distribution of Evans Blue in the entire pancreas (Figure 51A).

Subsequently, to test the efficacy of rAAV to target the pancreas, in our initial studies, we packaged scAAV.GFP with the AAV6 serotype, which has been shown to efficiently target the pancreas (236, 237). We administered $1x10^{11}$ vg/animal of scAAV6.GFP via retrograde ductal delivery, and animals were sacrificed three weeks later for global pancreatic GFP expression analysis. As documented under direct

fluorescence, scAAV6 transduced the pancreas with uniform GFP expression (Figure 51B).

Identification of an AAV serotype to efficiently target the pancreas via retrograde intraductal infusion.

Single-stranded AAV 6, 8, and 9 serotype vectors have been shown to transduce the pancreas efficiently via retrograde pancreatic intraductal delivery (262). However, the efficiency of scAAV vectors has not yet been determined. To address this question, we compared scAAV.GFP serotypes 6, 8, and 9, and dosed a cohort of C57BL/6 mice for each serotype (n=3-4 mice/group) with $1x10^{11}$ vg/animal via retrograde pancreatic ductal delivery. At 3 weeks post-vector infusion, animals were sacrificed, and pancreata were collected from each animal to compare GFP transduction efficiency. As documented by fluorescent microscopy, scAAV6 and scAAV9 transduced acinar cells (exocrine cells) more efficiently with 53% ± 3.8 S.E.M. and 52% ± 2.7 S.E.M., respectively (Figure 51C) compared to scAAV8 (21.7% ± 5.9 S.E.M.). Similarly, scAAV6 transduced ductal cells (48.2% ± 10.25 S.E.M.) more efficiently compared to scAAV8 (12.1% ± 3.2 S.E.M.) and scAAV9 (13.6% ± 3.7 S.E.M.) (Figure 51D). Furthermore, scAAV6 transduced pancreatic islet cells with relatively higher efficiency (82.1% ± 3.1 S.E.M.) compared to scAAV8 (16.3% ± 3.1 S.E.M) and scAAV9 (30.5% ± 5.0 S.E.M) (Figure 51E). To achieve maximum pancreatic transduction via intraductal delivery, we dosed a cohort of mice (n=3-5 mice/group), with three escalating doses ($1x10^{11}$, $3x10^{11}$, and $5x10^{11}$ vg/animal) using scAAV6.GFP. Quantification of the transduced exocrine acinar cells

showed an increase in transduction percentages and with maximum gene expression achieved at $5x10^{11}$ vg (Figure 51F).

As scAAV6 and scAAV9 showed comparable transduction efficiency at the lowest dose (10^{11} vg/animal), to determine maximum pancreatic gene expression in this model, we compared the transduction efficiency of AAV6 and AAV9 at a dose of $5x10^{11}$ vg/animal. AAV6 had statistically significant higher pancreatic GFP expression (86% ± 2.4 S.E.M.) compared to AAV9 (75% ±1 S.E.M.) (Figure 52A, Figure 52B)**.** We also examined GFP expression in the livers of these mice (a common off-target of intraductally dosed mice (243, 262)), and AAV9 has relatively higher liver transduction percentages compared to AAV6 (Figure 52A). To further confirm this observation, we quantified transduced vector genomes of the pancreas and liver by quantitative real-time PCR (qPCR). AAV6 had more specificity in targeting the pancreas with more vector genomes compared to AAV9. Whereas AAV9 had relatively very high vector genome copies in the liver compared to AAV6 (Figure 52C). We further tested this phenomenon in animals dosed with $5x10^{11}$ vg/animal of AAV6 and AAV9 and found that AAV6 has more specificity in transducing the pancreas compared to AAV9 (Table 3). scAAV6 mediated GFP expression was not found in any other tissues in the body including heart, lung, and kidney (Figure 50C). Finally, to test the effect of murine gender on AAV6 mediated pancreatic transduction, we dosed a cohort of C57BL/6 males and females with $5x10^{11}$ vg of scAAV6.GFP (n=3 mice/group) and found that the gender did not have a significant effect on pancreatic transduction (Figure 52D).

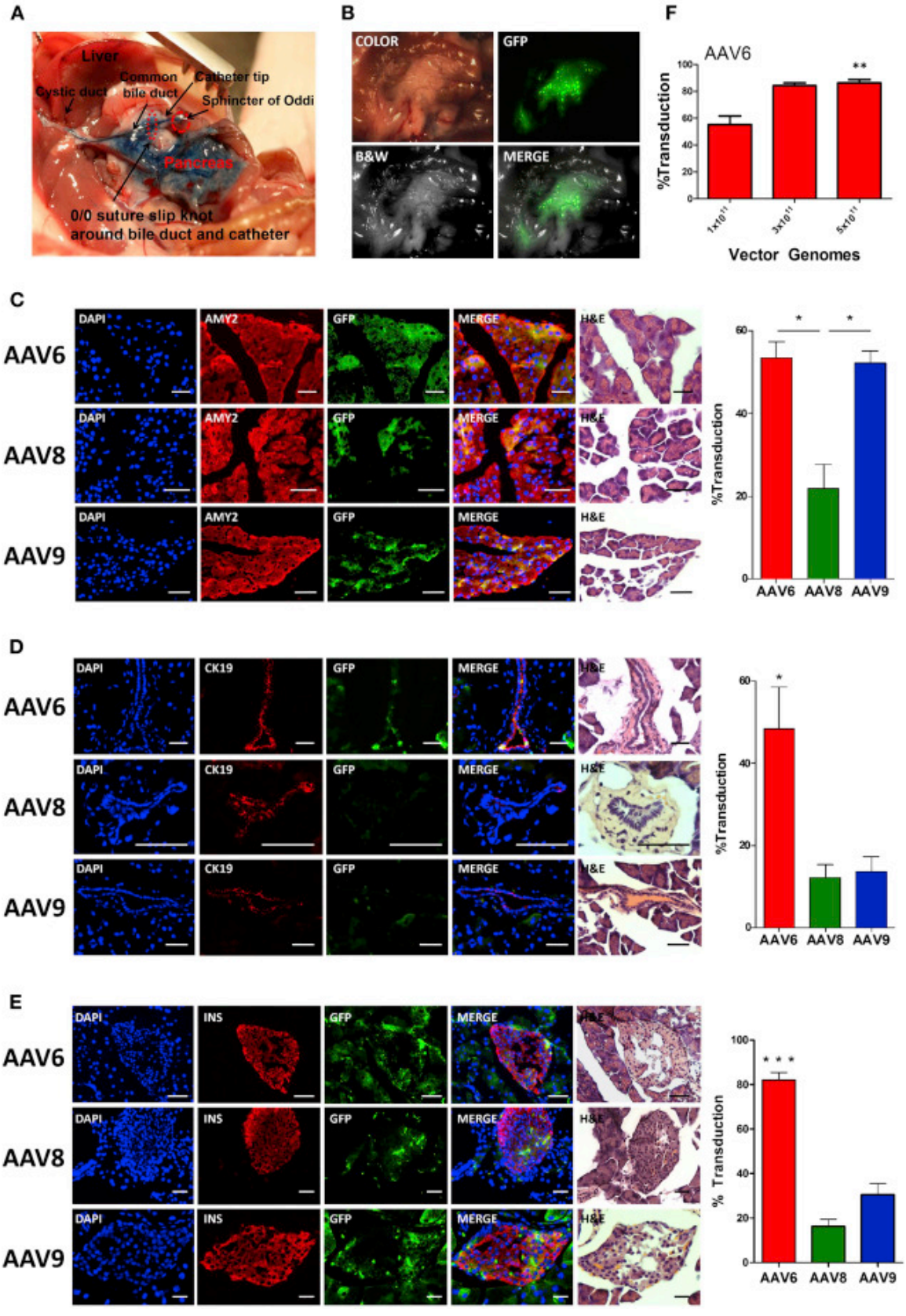
A
Liver
Common bile duct
Catheter tip
Cystic duct
Sphincter of Oddi
Pancreas
0/0 suture slip knot around bile duct and catheter
B
COLOR
GFP
B&W
MERGE
F
AAV6
%Transduction
Vector Genomes
C
AAV6
AAV8
AAV9
DAPI
AMY2
GFP
MERGE
H&E
%Transduction
D
CK19
E
INS
% Transduction

Figure 51. Optimization of Retrograde Intraductal Infusion via Catheterizing the Common Bile Duct through the Gallbladder and Cystic Duct. (A) Uniform Evans Blue dye delivery to the entire pancreas via the retrograde intraductal infusion procedure. (B) A C57BL/6 mouse was dosed with 1 x 10^{11} vg of scAAV6.GFP via retrograde intraductal infusion, and pancreatic GFP expression was observed via direct fluorescence. (C–E) A cohort of C57BL/6 mice was dosed with scAAV6.GFP, 8, or 9 at 1 x 10^{11} vg/animal (n = 3–4/group). Serial sections of frozen (6 mm) pancreatic tissue collected 3 weeks post-vector infusion were stained for (C) amylase (AMY2, acinar cells), (D) Cytokeratin 19 (CK19, ductal cells), or (E) insulin (INS, islets) or with H&E to quantify cell-specific GFP transduction percentages. GFP, green; AMY2, CK19, or INS, red; DAPI, blue; 20X magnification; scale bar, 50 mm; representative images are presented. (F) A cohort of C57BL/6 mice was intraductally infused with different doses of scAAV6.GFP (n = 4–6/group), and the percentage of GFP+ acinar cells was determined. Data represent mean ± SEM, *$p < 0.05$, **$p < 0.01$, ***$p < 0.001$.

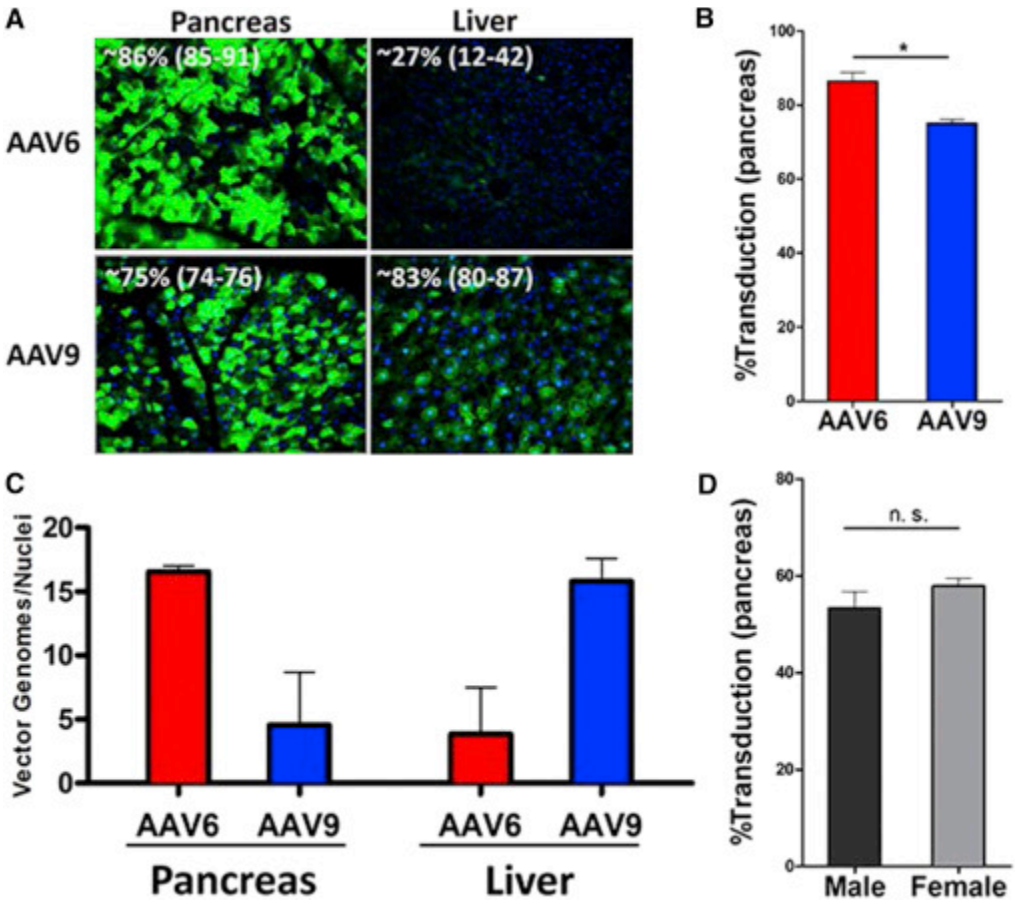

Figure 52. scAAV6 Has Increased Specificity in Transducing the Pancreas Compared with scAAV9 C57BL/6 mice were dosed with scAAV6.GFP or scAAV9.GFP at 5 x 10^{11} vg/animal. (A) Pancreatic and liver GFP+ expression was determined via fluorescence microscopy. Representative pancreatic and liver images are shown for each serotype at 20 magnification. (B) Quantification of pancreatic and liver transduction was determined by the percentage of GFP+ acinar cells and hepatocytes, respectively. (C) DNA was isolated from pancreata and livers of scAAV6.GFP or scAAV9.GFP retrograde intraductally infused C57BL/6 mice and subjected to qPCR analysis for AAV genome copy numbers. Data represent mean ± SEM. *$p < 0.05$. (D) Quantification of pancreatic GFP expression was determined in male and female C57BL/6 mice dosed with 5 x 10^{11} vg of scAAV6.GFP.

	AAV6		AAV9	
	Liver	Pancreas	Liver	Pancreas
Mouse 1	7.5	16.1	17.6	8.7
Mouse 2	0.2	17	14	0.4
Average	**3.9**	**16.6**	**15.8**	**4.6**

Table 3. Comparison of scAAV6 and scAAV9 pancreatic transduction efficiency via retrograde intraductal delivery (vector genomes/nuclei) C57BL/6 mice were dosed with scAAV6.GFP or scAAV9.GFP at 5x1011 vector genomes (vg)/ animal and vg per cell was determined by qPCR.

AAV6 targets and shows long-term gene expression in acinar, epithelial, and stromal cells in PDAC mice.

To test the feasibility of using scAAV6 to target the pancreas of PDAC mice, we dosed a cohort of a well-characterized PDAC mouse model, KC, with scAAV6.GFP at 1 month of age via intraductal delivery. As documented via fluorescence microscopy and immunohistochemistry for GFP, scAAV6 transduced KC mice pancreata efficiently at 3 weeks post-vector administration (Figure 53). To test AAV mediated long-term gene expression, we collected the pancreata of scAAV6.GFP intraductally dosed KC mice at 5 months post-infusion and found persistent GFP expression (Figure 54, Table 2) in acinar, epithelial/cancer, islet, and pancreatic stellate cells (PSCs). scAAV6 transduced PSCs (28.5% ± 4.7 S.E.M.) and PanIN)/ducts (7.6% ± 2.6 S.E.M.) with relatively lower efficiency compared to acinar cells (55.0% ± 16.5 S.E.M.) and islets cells (41.5% ± 5.5 S.E.M.) (Figure 54, Table 4). The efficiency of scAAV6 to target neoplastic tissues needs to be further optimized through understanding mechanisms associated with AAV6 transduction in the various pancreatic compartments. Nevertheless, our findings provide the evidence that persistent gene expression can be achieved in proliferating epithelial and stromal cells in the context of a genetically engineered mouse model of pancreatic cancer.

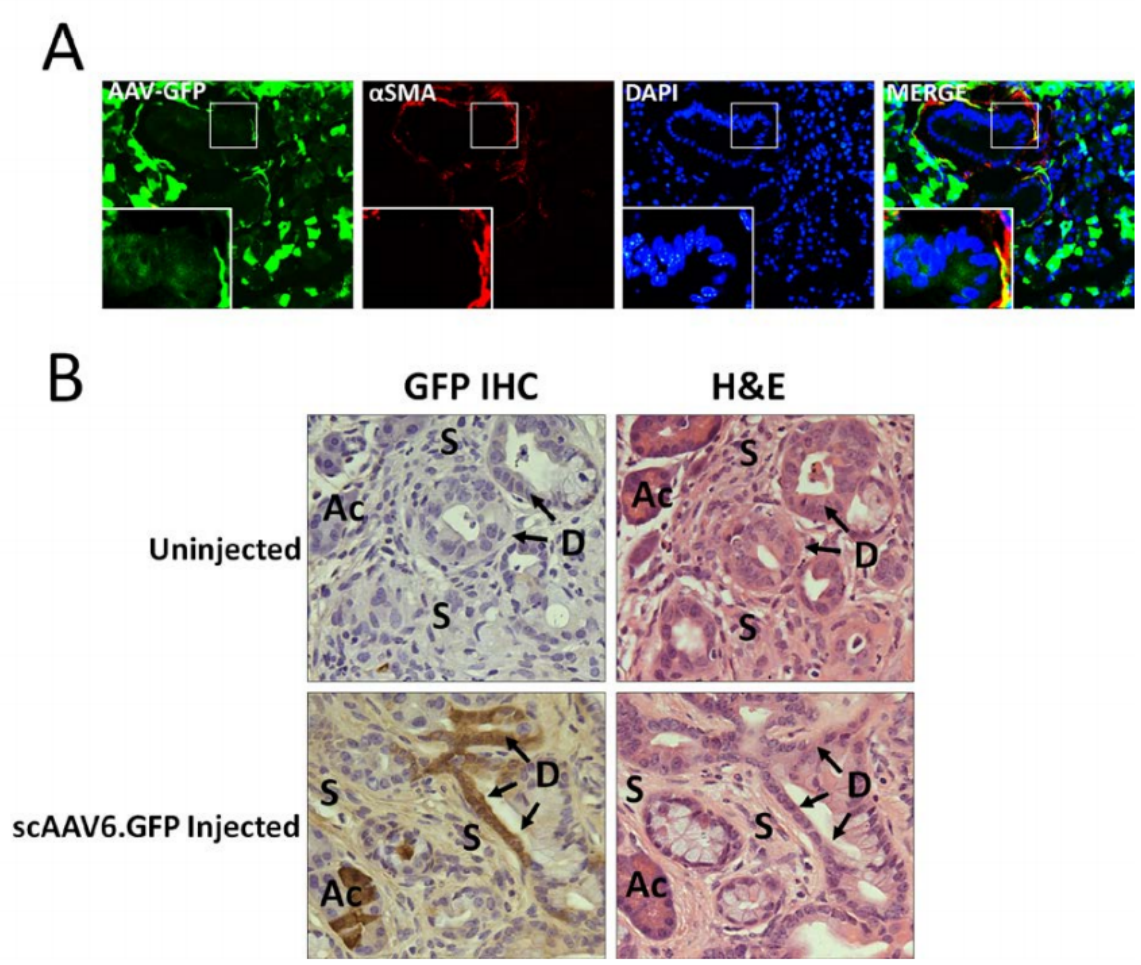

Figure 53. Retrograde pancreatic intraductal delivery of scAAV6 targets KC mice pancreata at early timepoint (3 weeks post-injection). KC mice were intraductally infused with $5x10^{11}$vg of scAAV6.GFP and pancreata was collected at 3 weeks post-vector administration for early timepoint and were either (A) stained with α-SMA (red) and DAPI (blue) to assess GFP expression via fluorescent microscopy (60X inset) or (B) subjected to immunohistochemistry (IHC) for GFP expression and hematoxylin and eosin (H&E) staining (20X). Acinar cells (Ac), pancreatic ducts (D), and stromal compartments (S) are indicated.

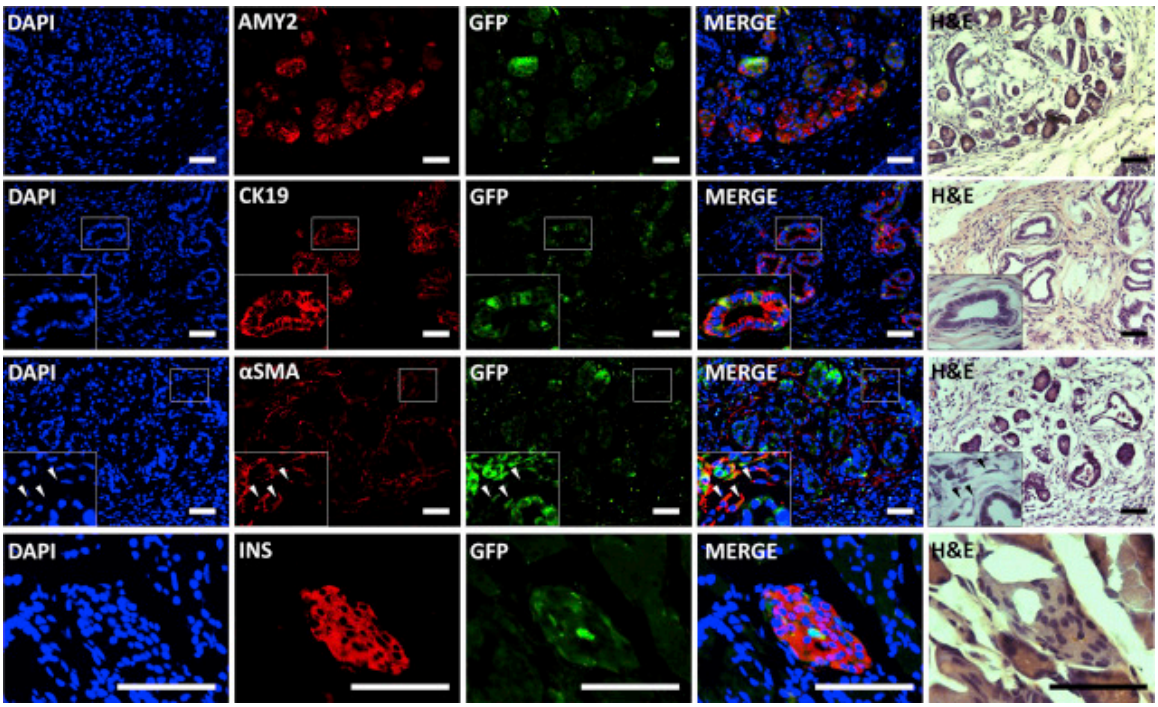

Figure 54. Retrograde Pancreatic Intraductal Delivery of scAAV6 Targets Acinar, Epithelial, and Stromal Cells and Shows Long-Term Gene Expression in PDAC Mice. 5 x 10^{11}vg of scAAV6.GFP was dosed in 1-month-old KC mice, and pancreata were collected 5 months post-delivery for the late time point and stained for amylase (AMY2), CK19, α-SMA, or insulin (INS) to identify acinar cells, ductal cells, PSCs, and islet cells, respectively. Serial sections were stained with H&E, and representative images are presented. GFP, green; AMY2, CK19, α-SMA, or INS, red; DAPI, blue; 20 magnification; scale bars, 50 mm; inset, 40; arrows indicate α-SMA^+/GFP^+ PSCs.

KC Compartment %Transduction	
Acini (AMY2)	55.0% ± 17 S.E.M.
Epithelial Cells (CK19)	7.6% ± 2.6 S.E.M.
PSCs (α-SMA)	28.5% ± 4.7 S.E.M.
Islets (INS)	41.5% ± 5.5 S.E.M.

Table 4. Percentage Longterm GFP expression Retrograde Pancreatic Intraductal Delivery of scAAV6

Retrograde intraductal delivery is safe with no evidence of pancreatitis in normal pancreata nor enhanced disease progression in PDAC mice.

Increase in pancreatic intraductal pressure is known to cause inflammation/pancreatitis, a known risk factor for PDAC (263-265). To evaluate the effect of intraductal delivery mediated pressure on pancreatic inflammation, we dosed a cohort of C57BL/6 mice with PBS and monitored serum pancreatitis markers, amylase and lipase (266-268). We observed a rapid increase in amylase and lipase levels at 3 hours post-vector delivery which resolved within a day of intraductal infusion (Figure 55A, Figure 55B). By histopathological examination, there was minimal to no pancreatic inflammation seen at various timepoints (Figure 55C), except for a detectable peri-pancreatic fat lymphoid response in a few mice at 2-5 days post-infusion (Figure 55D). We also stained pancreata with the B cell marker (B220) to monitor lymphoid responses. Normal mice were negative for B220 at all timepoints, 1-15 days post-infusion (Figure 55C; Table 5). In addition, to evaluate the effect of intraductal mediated pressure on pancreatic fibrosis, we stained pancreata of C57BL/6 mice with trichrome (Figure 55C) and found no significant increase in pancreatic fibrosis in intraductally dosed mice compared to non-injected control mice (Figure 55E).

Finally, to evaluate the effect of intraductal delivery mediated inflammation on PDAC progression, we performed histopathological analysis in KC mice dosed with PBS or scAAV6.GFP at 5 months post-infusion. As shown in Figures 56A-C, there was no significant difference in the size and number of PanIN grades between intraductally infused KC mice and controls. Furthermore, intraductually infused KC mice were

negative for B220 staining <1% (Table 6), and there was no significant increase in pancreatic fibrosis based on trichrome staining (Figure 56C).

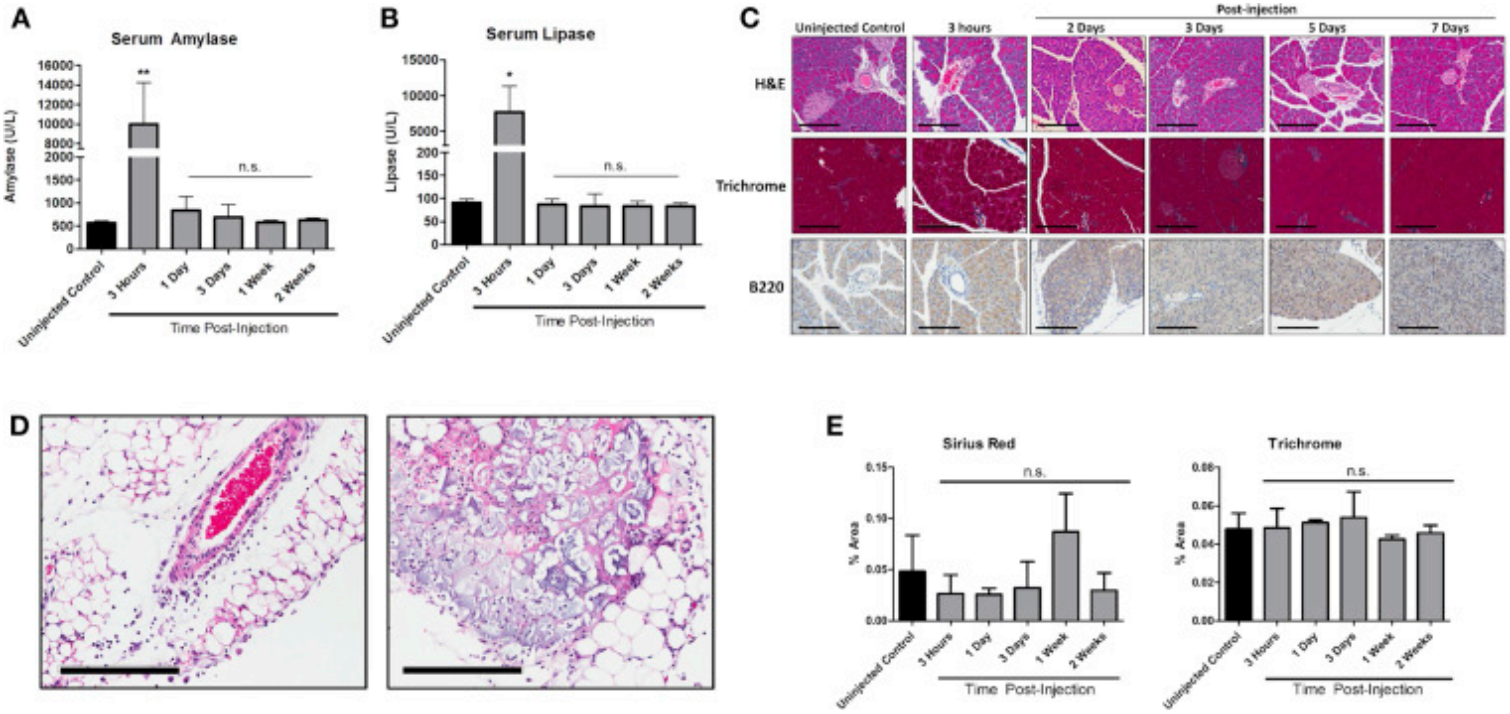

Figure 55. Retrograde Pancreatic Intraductal Delivery Is Safe and Does Not Induce Chronic Pancreatitis. (A and B) Serum samples collected from intraductally dosed (100 mL PBS) C57BL/6 mice were analyzed for (A) amylase and (B) lipase. Data represent mean ± SEM; *$p < 0.05$; **$p < 0.01$; n.s., non-significant. (C) Representative H&E, trichrome, and B220 images; 20 magnification; scale bars, 200 mm. (D) Representative fat lymphoid responses observed at early time points (1–3 days, H&E). Scale bars, 200 mm, 20 magnification. (E) Mean Sirius Red- or trichrome-positive area (percent) of pancreatic tissue in retrograde pancreatic intraductally injected C57BL/6 (1–14 days post-infusion) mice (n = 3–4 mice/time point). Data represent mean ± SEM.

	Group	% Positive	Histology Notes
1	Uninjected Control	2-3%	peripancreatic lymph node, peripancreatic fascia
2	Uninjected Control	1-2%	peripancreatic lymph node, peripancreatic fascia
3	Uninjected Control	1-2%	peripancreatic lymph node, peripancreatic fascia
5	PBS	2-3%	peripancreatic lymph node, peripancreatic fascia
6	PBS	1-2%	peripancreatic lymph node, peripancreatic fascia
7	scAAV6 EF1αGFP	2-3%	peripancreatic lymph node, peripancreatic fascia
8	scAAV6 EF1αGFP	2-3%	peripancreatic lymph node, peripancreatic fascia
9	scAAV6 EF1αGFP	1-2%	peripancreatic lymph node, peripancreatic fascia

Table 5. Histological analysis of B cell activation (B220) in retrograde pancreatic intraductally infused KC mice. Pancreata collected from intraductally dosed (100µl PBS or scAAV6.GFP) KC mice at 5 months post-infusion were analyzed for B220 staining. Histological descriptions by a pathologist are provided for individual animals.

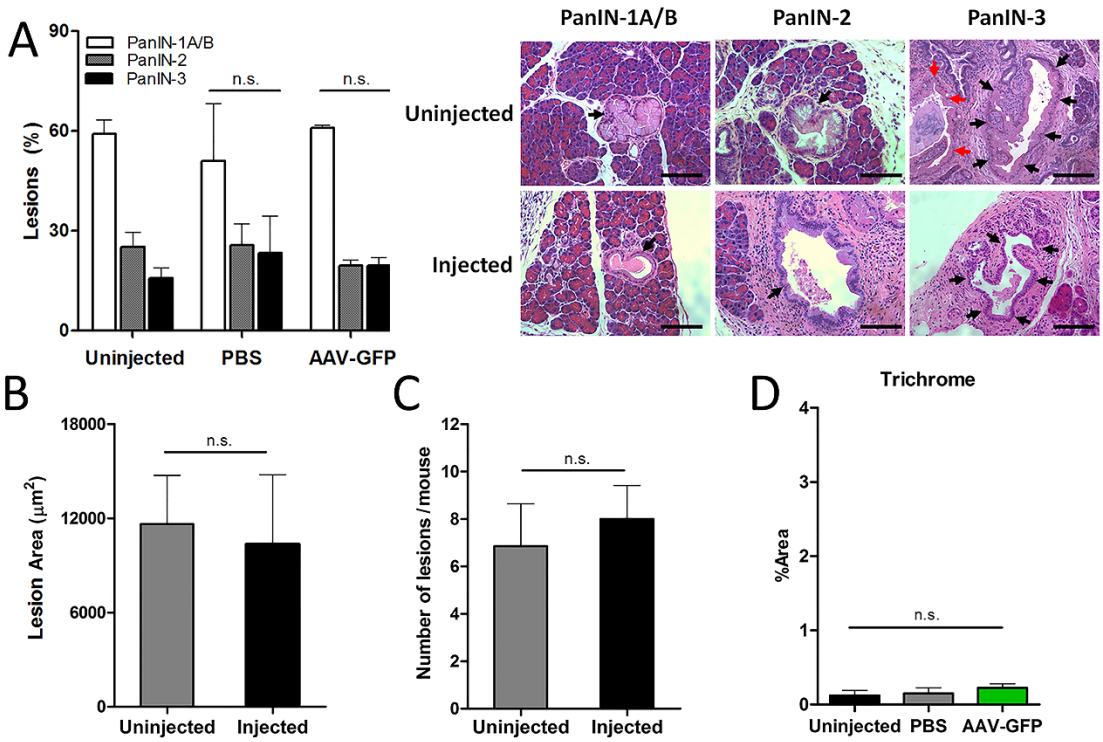

Figure 56. Retrograde Pancreatic Intraductal Delivery has No Effect on PDAC Progression in KC mice. Pancreata collected from KC mice at 5-months post-infusion (100 µl of PBS or 5x1011vg scAAV6.GFP) was analyzed and compared against un-injected control mice for (A) PanIN grades (1A/B, 2, & 3) (n=3-5 mice/group) and representative images for each PanIN grade are shown indicated by black arrows. Adjacent PanIN-3 lesion is indicated by red arrows. 20X magnification, Scale bar 100µm, (B) Average area of PanIN lesions and (C) number of PanIN lesions per mouse are presented (n=5-7 mice/group). (D) Trichrome staining positive percentage area was quantified (n=3-5 mice/group). Data represents mean ± S.E.M. p-values determined by t-test, n.s.: non-significant.

4.4 Discussion

Previously, numerous non-viral and viral mediated delivery methods were employed to deliver therapeutic molecules/genes to the pancreas via direct (233, 238), systemic (253, 254), intraperitoneal (242), and retrograde ductal delivery (224, 228, 236). Among various vector systems and routes of administration, retrograde ductal delivery of AAV demonstrated efficient pancreatic gene expression (236, 237, 243). However, the safety and efficacy of retrograde ductal delivery on the development of pancreatitis, a known risk factor for PDAC, and use of AAV in cancer settings has not been well established. Here in the current study, we compared the use of different AAV serotypes for efficient delivery to the pancreas via intravenous (AAV8 and AAV9) or retrograde pancreatic ductal delivery (AAV6, AAV8, and AAV9) using double-stranded scAAV vectors expressing GFP under a ubiquitous promoter, EF1α. Our results indicate that retrograde pancreatic ductal delivery of scAAV6 via catheterizing the common bile duct through the gall bladder/cystic duct transduces various cell types of the pancreas, such as acini, ducts, and islets, efficiently compared to scAAV8 and scAAV9 without inducing pancreatitis. Furthermore, as a proof-of-concept, we showed that retrograde pancreatic ductal delivery of scAAV6 transduces acini, epithelial, and stromal cells in a pre-clinical PDAC mouse model and demonstrated persistent gene expression up to 5 months post-infusion.

Although direct pancreatic targeted delivery is very robust and achieves maximum gene expression, because of retroperitoneal location of the pancreas, a less invasive systemic gene delivery is a preferred method of choice in clinical settings. In an attempt to identify a serotype that can be used to efficiently target the pancreas via

systemic delivery, we compared pancreatic transduction efficiency of scAAV8 and scAAV9. scAAV9 showed relatively higher pancreatic transduction efficiency compared scAAV8 via systemic gene delivery. However, maximum acinar gene expression was <60% in spite of high scAAV9 dose, $5x10^{12}$ vg/animal. Previous reports indicate that systemic delivery of ssAAV9 transduces pancreas robustly at a relatively low vector dose ($1.8x10^{12}$ vg/animal) (256). Perhaps, the lower transduction percentage observed in gene expression could be due to the use of an endogenous promoter, EF1α, compared to the CMV promoter used in previous studies (256). We used scAAV9 compared to the ssAAV9, which are known to transduce more efficiently compared to ssAAV(249). In spite of utilizing scAAV vectors, pancreatic transduction efficiency via systemic delivery was significantly lower compared to previous reports that used ssAAV vectors. Perhaps the low pancreatic transduction percentage via systemic delivery may fulfill the required gene expression levels for studies involving pancreatic origin diseases such as diabetes, where restoration of a few functional copies of a gene may have a functional/therapeutic effect.

Similar to previous reports using ssAAV (236, 237, 243), our observations demonstrate that efficient pancreatic transduction can be achieved via retrograde pancreatic ductal delivery of scAAV, a surgical procedure that parallels the clinical endoscopic retrograde cholangiopancreatography (ERCP) in humans. Among the three AAV serotypes tested via pancreatic ductal delivery, AAV6 transduced the whole pancreas and various pancreatic compartments (acini, ducts, islets) more efficiently compared to AAV8 and AAV9. Transduction efficiency of intraductal mediated delivery of AAV6 via EF1α promoter in various pancreatic compartments is comparable to

previous reports using CMV promoter (237). In addition, AAV6 has relatively minimal liver transduction, a common off-target of intraductally dosed mice (236, 243). AAV9 had comparable pancreatic targeting efficiency to AAV6, but showed higher liver transduction. The increase in liver transduction with AAV9 may be due to the higher abundance of receptors and/or co-receptors to AAV9 in hepatocytes or increased circulation residence and is consistent with a previous report indicating that AAV9 transduces the liver more efficiently upon systemic injections compared to AAV6 (256). As the liver is a common site for metastasis in pancreatic cancer, AAV9 may be more appealing for gene delivery at later disease stages in a metastatic context.

Our results also demonstrate that retrograde pancreatic ductal delivery is safe and does not induce pancreatitis in mice. Although we observed transient increase in pancreatitis markers at ~1 day post-infusion, amylase and lipase levels resolved within 24 hours. Furthermore, no significant increase of lymphoid proliferation or fibrosis was observed by histopathological examination in intraductally infused mice. Pancreatitis is a known risk factor for PDAC, and patients with chronic or acute pancreatitis have a higher risk of developing cancer and can experience enhanced cancer progression. To test the safety of intraductal mediated delivery in cancer settings, we evaluated the PanIN progression in a well characterized PDAC mouse model dosed with PBS and scAAV6.GFP and found no effect on cancer progression.

Finally, to test the potential use of scAAV to target the pancreatic neoplasm via retrograde delivery, we dosed 1 month old KC mice, a $Kras^{G12D}$ driven PDAC mouse model, with scAAV6.GFP and found efficient transduction in acinar and ductal cells (primary cells of origin for PDAC) and PSCs, the major cells responsible for PDAC

stromal accumulation(38, 85). Furthermore, we observed long-term GFP expression in amylase$^+$ acini, CK19$^+$ ductal, and α-SMA$^+$ stromal cells at 6 months of age, a timepoint at which KC mice develop more advanced PanIN2-3 lesions (113). In addition to our work, a recent report demonstrated the use of capsid optimized scAAV8 to target pancreatic neoplasm via intraperitoneal administration (242). Although capsid optimized AAV8 has limited off-target effects compared to WT AAV8, there was a robust gene expression in the liver comparable to the pancreas which could be improved in combination with the retrograde pancreatic targeted delivery we employed here to efficiently target the pancreas.

Our current research and recent reports from others (242) indicate the potential applicability of AAV to deliver therapeutic molecules/genes to various compartments of PDAC and impact tumor progression. Similarly, previous reports indicate that ductal delivery of AAV in combination with cell specific promoters serves as an excellent surrogate for pancreatic cell lineage studies (239-241). Another potential application of this work is using AAV as a non-integrating delivery vehicle for genome editing mediated functional studies. The latest developments in genome sequencing technologies are rapidly unravelling new genes underlying various human diseases (269). However, alternative and more rapid methods to transgenic mouse models are required for *in vivo* characterization of new genes in order to quickly translate basic research findings into the clinic (223).

Genome editing tools such as CRISPR/Cas9 have become useful to study gene function (270-272). In fact, surrogate use of retrograde pancreatic targeted delivery of Cre-recombinase or CRISPR/Cas9 via integrating adeno and lentiviral vectors has been

elegantly demonstrated to lead to the development of PDAC mouse models (224). AAV mediated pancreatic targeted delivery described here in combination with cell specific promoters is amenable to genome editing technologies to study *in vivo* gene function and will aid in accelerating basic research findings into the clinic. The AAV platform is more attractive as its safety profile and ideal serotypes are well established to target various tissues. Although viral vectors may not replace mouse models, they will serve as great tools to further advance pre-clinical research by studying the gene function alone or in combination with known genetic causes. The retrograde ductal delivery will be a useful tool in studying the gene function of non-coding RNAs, such as miRNAs. Often a single miRNA has several family members (92, 273, 274) that are expressed in a tissue and cell specific manner. Developing a tissue/cell specific mouse models for individual miRNA family members in combination with underlying disease related genetic mutations is a daunting process. Using a similar method described here, miRNA families can be inhibited by developing AAV vectors for miRNA inhibition strategies such as Tough Decoys (TuDs), anatagomirs, etc. Proof-of-concept studies suggest the use of viral vectors to inhibit endogenous miRNAs (275-277). Similarly, delivering synthetic miRNA duplexes, for therapeutic purposes has potential limitations associated with half-life and requires repeated administration (278). Evidence suggests the use of AAV for *in vivo* delivery of therapeutic miRNA with no toxicity (136, 279).

In summary, our study demonstrates that scAAV6 targets both normal and neoplastic pancreas via retrograde ductal delivery. Our previous work and that of others supports the use of AAV vectors to target a wide variety of neoplasms (136, 155, 257, 280-283) and target tissues undergoing multiple cycles of degeneration-

regeneration (284-286). However, a number of pre-clinical studies need to be performed before this method reaches clinical settings due to the fact that AAV is a non-integrating vector and its expression is lost in rapidly proliferating neoplastic tissue. First, transduction efficacy in KC mice needs to be evaluated in animals dosed at early stages of PanIN-1A/B development at <2 months of age versus more advanced stages of PanIN-2-3 lesions at ~9 months of age (113). Second, transduction efficiency and long-term gene expression need to be evaluated in a more aggressive PDAC mouse model that recapitulate the aggressive form of human disease such as $Kras^{G12D}$; $P53^{R172H}$; PDX1-Cre, etc (215). Third, further refinements to the gene transfer vector will be necessary to allow for cell-specific targeting of pancreatic tumors, similar to previous reports (239-241). Fourth, the underlying mechanisms for efficient scAAV6 pancreatic transduction in neoplastic tissues and AAV receptor profiling in various pancreatic compartments and cancer cells needs to be evaluated, particularly in order to further optimize transduction efficiency of neoplastic tissue. Fifth, the present study also points out the limitations of AAV to achieve high levels of long-term gene expression in rapidly dividing neoplastic tissue. Nevertheless, our results point out the potential use of AAV in early stages of cancer development, where transient therapeutic gene expression may have an impact on the disease progression and could be used to treat patients with pancreatitis, PDAC patients prophylactically, or as an adjunct therapy. Furthermore, targeted AAV mediated *in vivo* gene delivery to various pancreatic compartments will serve as a great tool in pre-clinical functional studies.

Chapter 5: Summary and Future Directions

Our work provides proof-of-concept evidence for the use of miR-29 as an anti-fibrotic and tumor suppressor agent in PDAC. However, several open-ended questions still remain.

5.1 The Role of miR-29 in PDAC Stroma

Our findings show that miR-29 plays a critical role in regulating tumor stromal deposition and cancer growth. Thus, raising the possibility that modulation of miR-29 expression in PSCs may be therapeutically beneficial in cancer. Nevertheless, some groups have reported pancreatic stroma acts to restrain tumor growth, not promote it (35, 36). A subtler approach of converting activated PSCs to quiescence led to a more promising therapeutic outcome, in contrast to complete stromal ablation (37). Consistent with this more nuanced tactic, we would expect that miR-29 restoration in PSCs would result in hampered ECM production but not the complete depletion of existing stromal proteins. Furthermore, our findings demonstrate that miR-29 overexpression in PSCs leads to decreased cancer growth in co-culture without affecting the intrinsic viability of PSCs themselves. However, the effect of miR-29 on PSC activation has not been assessed. In addition to increased α-SMA expression, the loss of retinol lipid droplets is a critical hallmark of activated PSCs (287). A simple experiment of assessing α-SMA expression and Vitamin A droplets within miR-29 overexpressing PSCs could determine if miR-29 reverts activated PSCs to quiescent ones, similar to calcipotriol treatment. If this holds true, miR-29 could also serve as a more tactical way to normalize the reactive stroma and enhance the efficacy of chemotherapy to target PDAC.

5.2 The Role of miR-29 in PDAC Autophagy

miR-29 has been shown to play a significant role in regulating autophagy. Initial studies in bovine cells infected with virus revealed endogenous bovine miR-29 had an anti-viral, protective effect within the host cell by upregulating miR-29b, leading to the targeting of ATG14 and ATG9A. As bovine diarrhea virus (BVDV) utilizes host cell autophagy machinery as a means of promoting viral replication, miR-29b mediated inhibition of autophagy led to a decrease in BVDV replication (288).

We have shown that miR-29a has a similar effect in inhibiting pancreatic cancer cell autophagy. This is of interest as previous reports demonstrated that pancreatic cancer cells heavily upregulate autophagy for survival and autophagy facilitates chemoresistance against gemcitabine (39). Similarly, we found that miR-29a overexpression led to increased gemcitabine sensitization in chemoresistant cell lines along with a concurrent late stage blockage of autophagy mediated through TFEB and ATG9A downregulation.

Interestingly, miR-29b overexpression has also been shown to cause a decrease in TFEB expression in multiple myeloma (289). Although the authors postulated that this was an indirect effect of miR-29 mediated repression of HDAC4, it may be possible they were observing a direct targeting of TFEB by miR-29b as well. In contrast to our findings, the earlier study went on to show that miR-29b in myeloma cells had no impact on autophagy flux (289). These results indicate that miR-29 inhibition of autophagy may be context dependent or differ between miR-29a and -29b family members. Further investigations are warranted to determine the ubiquity of miR-29 mediated autophagy inhibition across various cancer types, as well as determine if miR-29 family members have different impacts on autophagy.

Finally, a recent report indicated that autophagy plays a critical role in PSCs as well (290). PDAC cells were shown to induce autophagy in PSCs, which in turn catabolize their internal components and secrete alanine to further fuel cancer cell proliferation (290). In addition to testing the effect of miR-29 on autophagy in other cancers, it would be interesting to determine if restoration of miR-29 in activated PSCs could also inhibit autophagy. As we observed that miR-29 inhibits the pro-growth effects of PSC conditioned media on cancer cells, perhaps miR-29 mediated autophagy inhibition in PSCs lend an explanation to our observations. Further studies are necessary to determine if this holds true.

5.3 Mechanisms of miR-29 in Pancreatic Cancer Cell Migration Potential

Metastasis occurs when cancer cells undergo epithelial-mesenchymal transition (EMT), a cellular reprogramming event in which epithelial cells revert to a pseudo-stem cell state that is characterized by a loss of polarity and increased migratory behavior (291). EMT plays a vital role in normal physiology during development as well as in wound healing, but it is also exhibited in cancer metastasis where a subset of tumor cells disseminate to distant organ sites beyond the site of origination. As a defining signature of Stage IV cancer, metastasis is regarded as a major cause of cancer mortality (292). This is largely because by the time a cancer has metastasized, surgical resection is typically no longer a viable option, and metastatic tumors are often refractory to conventional therapies.

miR-29 has been well-established to inhibit migration/metastasis in various cancers through direct inhibition of a several pro-metastatic targets (112, 293-298)

including in pancreatic cancer (156, 157, 296). Consistent with these outcomes, we find that miR-29 inhibits migration/invasion *in vitro* and facilitates mesenchymal-epithelial transition (MET), as indicated by an increase in E-cadherin and reduction in Vimentin. However, we have not yet identified the exact mechanism by which miR-29 inhibits the migratory potential of pancreatic cancer cells.

Although a few mechanisms have been proposed, all three reports offered different hypotheses for which miR-29 target downregulation leads to reduced migration/invasion in PDAC (MMP2, MUC1, ITGB1) (156, 157, 296). This is further complicated by the fact that a single miRNA may simultaneously regulate a number of genes within multiple intracellular networks (107). Many of the current miRNA studies rely upon target prediction algorithms. It could be possible that miR-29 mediates these effects through all three targets, in combination or through other targets that have yet to be discovered. These incongruities demand the need for a better, systematic approach to understanding mechanisms in miR-29.

One potential method to resolving this issue could be accomplished by first identifying direct miR-29 targets through quick cross-linking, ligation, and sequencing of hybrids (qCLASH), followed by a comprehensive CRISPR-based functional genomic screen of target miR-29 binding sites identified in qCLASH. qCLASH is a new technique by which direct miRNA binding sites of target transcripts can be detected with a higher degree of confidence through crosslinking/Ago-IP in conjunction with ligating the miRNA to the target binding site and subjecting it to deep-sequencing (299). Confidence in this dataset could be tested by conducting an enrichment analysis for predicted targets from algorithms such as Targetscan (72). Once these *de novo* binding sites have been

identified, a custom, pooled CRISPR library can be made, utilizing Cas9 fused to GFP (300) with gRNAs designed to delete specific miR-29 binding sites identified via qCLASH. Subsequently, stable cells would be collected based on GFP expression, transfected with either negative control or miR-29 mimic, and subjected to transwell migration assay. Following a 24-hour migration period, the DNA of migrated cells would be isolated, subjected to deep-sequencing, and the presence of gRNAs in miR-29 overexpressing cells but not in control would indicate the most functionally relevant miR-29 targets. Following validation of the top-ranking candidate genes as proof-of-concept for this approach, the experiment could be repeated in a number of other pancreatic cancer cell lines to select targets that overlap between the greatest numbers of cell lines. This would provide an extensive dataset where the entire miR-29 targetome could be functionally tested in a high-throughput and unbiased manner.

5.4 The Need for miR-29 *In Vivo* Validation

Although our findings clearly demonstrate miR-29's anti-fibrotic potential in PSCs and tumor suppressor function in cancer cells, much of this work was conducted *in vitro* and requires further validation to see if these findings translate *in vivo*. We have established a method of functionally studying the role of miR-29 *in vivo* via optimized intraductal delivery method of scAAV6, which demonstrated a high degree of transduction efficiency. We currently possess an AAV vector that expresses miR-29a under a ubiquitous EF1α promoter. Utilizing this parental vector, we will create two different rAAV vectors by replacing the EF1α promoter with an α-SMA or PDX-1 promoter for PSC- and cancer cell-specific expression respectively. We will package

rAAV vectors with AAV6 serotype and dose GEMMs of PDAC via intraductal delivery to study the functional effects of miR-29 restoration on stromal compartment and cancer cells and determine its impact on tumor progression and survival. The results of these *in vivo* studies will provide valuable insights on the role of miR-29 in pancreatic cancer, and test its therapeutic potential through a clinically translational surgical delivery method.

In contrast to the expected outcomes of our studies, the loss of miR-29 was recently reported to have no impact on pancreatic acinar carcinoma (301). However, these findings should be admonished due to several pitfalls. First, miRNAs regulate gene expression in a cell-type-specific manner, and this study employed a whole-body miR-29 KO which limits the ability to isolate miR-29 function within the model system. As the authors conceded, crossing whole-body miR-29 KO mice with viral SV40 T antigen driven acinar cancer model is not as physiologically relevant as other more commonly used GEMMs of pancreatic cancer (113, 215). Finally, pancreatic acinar carcinoma comprises a small percentage of patients compared to pancreatic ductal adenocarcinoma (302). Nevertheless, these incongruities demand the need for further studies to better understand these seemingly unexpected results. In contrast to this study, our intraductal delivery technique showed limited off-target effects and will provide a more refined method of elucidating miR-29 function in specific cell types of PDAC.

5.5 The Pragmatism of miRNA-Based Therapies

Since the discovery of the first miRNA, the area of miRNA research has rapidly expanded and moved beyond basic biology into therapeutic use. Within only the past two decades, >2,000 patent documents related to miRNAs have been published (303). Even

so, the development of miRNA therapeutics lags behind many other forms of treatment including RNAi based drugs (304). Recent setbacks were made when the first miRNA based clinical trial that tested the therapeutic effect of miR-34 (MRX34) in cancer was halted at Phase I due to immune-related side-effects (305). However, these adverse events may have not been due to miR-34 itself, but rather caused by the method of delivery (e.g. liposomes) or immunostimulation induced by double-stranded RNA (305, 306).

Nevertheless, the promise of miRNA-based therapies has remained appealing as indicated by the numerous miRNA based therapies that are still actively being pursued within the pipelines of several biotech companies (304). In fact, miR-29 mimic, MRG-201, is currently being tested in Phase I clinical trials via intradermal injection (ClinicalTrials.gov; NCT02603224). As new and improved modes of gene delivery are being developed and tested (307-309), it may be just a matter of time before additional therapeutic delivery methods will be available for miR-29 to be tested in cancer.

5.6 Controversies of miR-29 in Cancer

Although miR-29 may seem to show a high degree of promise as a potent tumor suppressor, the minority of studies reporting miR-29 as an oncogene are still grounds for circumspection and must be strongly taken into consideration. The drastically opposing effects of miR-29 reported even within the same cancer types, such as breast cancer (310-313) and pancreatic cancer (156, 157, 314, 315), is confounding.

Genomic heterogeneity is a well-known feature of cancer and exists between tumors of different patients and is even evident within the same tumor (316). In recent years, there has been a paradigm shift towards classifying cancers based on genetics

rather than in the context of anatomical location. In fact, Pembrolizumab was the first recently FDA approved cancer therapy on the basis of the patients' tumor gene expression profile instead of the cancer's originating tissue-type. As miRNAs function in a context dependent manner (317-320), the discrepancies of miR-29 function and alternative mechanisms of action may be due to a lack of contextualizing miR-29 against specific genetic backgrounds. Most of the current miR-29-related literature in cancer frequently generalizes the function of miR-29 within the framework of organ-based stratification without acknowledging the genetic background of the cells and biopsies. This may be due to the fact that utilizing a traditional, reductionist approach in biology to factor in so many various genetic variables is a daunting, if not impossible, task.

Recent advancements of high-throughput technologies such as proteomics, next generation sequencing, single cell sequencing, and functional genomics has facilitated a more refined insight into global gene regulation, as well as provided a more systematic approach to testing the function of genes on a large scale. The accumulation of large genomic databases (e.g. The Cell Atlas, TCGA, Project Achilles) has allowed for a greater degree of resolution in studying the effects of heterogeneity associated with cancer. Perhaps utilizing these comprehensive methods of Integrative Omics and Systems Biology will provide a more auspicious approach to better understanding miR-29's function in the context of cancer.

In fact, some systematic studies have already been conducted for miR-29. For example, Chris Sander's group analyzed miRNA expression across 10 cancer types in the TCGA database to determine commonalities in miRNA-target networks (321). They noted that, "miR-29a was generally downregulated… in tumors of most cancer types as

compared with representative normal samples." (321). Other analogous analyses utilizing comprehensive approaches find similarly consistent results of miR-29 as a tumor suppressor (322, 323). With time, further methodical studies employing these techniques in an unbiased fashion will rectify the disputed role of miR-29 as tumor suppressor versus tumor promoter.

5.7 Concluding Remarks

The multifaceted function of miR-29 lends concern to claiming it as a panacea for PDAC. The dichotomous role of miR-29 as tumor suppressor versus oncogene may be context dependent. However, at the current moment, miR-29 is well-documented as a tumor suppressor, with >85% of all miR-29/cancer-related studies demonstrating miR-29 inhibiting various oncogenes (Figure 1B). It will be of interest to see if future studies that investigate the function of miR-29 in a more comprehensive and systematic manner will resolve these disputes and elucidate a more refined perspective on miR-29's role in PDAC. In spite of the contrasting reports, our findings clearly demonstrate miR-29 is a potent anti-fibrotic agent and tumor suppressor in PDAC. Further follow up studies, as proposed in the discussion section, will provide a more thorough understanding of miR-29's role in pancreatic tumor-stromal interactions and cancer biology and may serve as the foundation for the future use of miR-29 as a novel therapeutic agent for PDAC.

References

1. The Lancet O. Pancreatic cancer: cause for optimism? Lancet Oncol. 2016;17(7):845. doi: 10.1016/S1470-2045(16)30234-0. PubMed PMID: 27396632.
2. Rahib L, Smith BD, Aizenberg R, Rosenzweig AB, Fleshman JM, Matrisian LM. Projecting cancer incidence and deaths to 2030: the unexpected burden of thyroid, liver, and pancreas cancers in the United States. Cancer research. 2014;74(11):2913-21. doi: 10.1158/0008-5472.CAN-14-0155. PubMed PMID: 24840647.
3. Shenoi PM. Ototoxicity of absorbable gelatin sponge. Proc R Soc Med. 1973;66(2):193-6. PubMed PMID: 4541382; PMCID: PMC1644504.
4. ACS. Cancer Facts & Figure. 2015.
5. Ryan DP, Hong TS, Bardeesy N. Pancreatic adenocarcinoma. The New England journal of medicine. 2014;371(11):1039-49. doi: 10.1056/NEJMra1404198. PubMed PMID: 25207767.
6. Cid-Arregui A, Juarez V. Perspectives in the treatment of pancreatic adenocarcinoma. World journal of gastroenterology : WJG. 2015;21(31):9297-316. doi: 10.3748/wjg.v21.i31.9297. PubMed PMID: 26309356; PMCID: 4541382.
7. Paulson AS, Tran Cao HS, Tempero MA, Lowy AM. Therapeutic advances in pancreatic cancer. Gastroenterology. 2013;144(6):1316-26. doi: 10.1053/j.gastro.2013.01.078. PubMed PMID: 23622141.
8. Heinemann V, Hertel LW, Grindey GB, Plunkett W. Comparison of the cellular pharmacokinetics and toxicity of 2',2'-difluorodeoxycytidine and 1-beta-D-arabinofuranosylcytosine. Cancer research. 1988;48(14):4024-31. Epub 1988/07/15. PubMed PMID: 3383195.
9. Huang P, Chubb S, Hertel LW, Grindey GB, Plunkett W. Action of 2',2'-difluorodeoxycytidine on DNA synthesis. Cancer research. 1991;51(22):6110-7. Epub 1991/11/15. PubMed PMID: 1718594.
10. Kleeff J, Korc M, Apte M, La Vecchia C, Johnson CD, Biankin AV, Neale RE, Tempero M, Tuveson DA, Hruban RH, Neoptolemos JP. Pancreatic cancer. Nat Rev Dis Primers. 2016;2:16022. Epub 2016/05/10. doi: 10.1038/nrdp.2016.22. PubMed PMID: 27158978.
11. Siegel RL, Miller KD, Jemal A. Cancer statistics, 2016. CA: a cancer journal for clinicians. 2016;66(1):7-30. doi: 10.3322/caac.21332. PubMed PMID: 26742998.
12. Korc M. Pancreatic cancer-associated stroma production. American journal of surgery. 2007;194(4 Suppl):S84-6. Epub 2007/12/06. doi: 10.1016/j.amjsurg.2007.05.004. PubMed PMID: 17903452; PMCID: 2094116.
13. Chu GC, Kimmelman AC, Hezel AF, DePinho RA. Stromal biology of pancreatic cancer. Journal of cellular biochemistry. 2007;101(4):887-907. doi: 10.1002/jcb.21209. PubMed PMID: 17266048.
14. Feig C, Gopinathan A, Neesse A, Chan DS, Cook N, Tuveson DA. The pancreas cancer microenvironment. Clin Cancer Res. 2012;18(16):4266-76. doi: 10.1158/1078-0432.CCR-11-3114. PubMed PMID: 22896693; PMCID: PMC3442232.
15. Hidalgo M, Von Hoff DD. Translational therapeutic opportunities in ductal adenocarcinoma of the pancreas. Clin Cancer Res. 2012;18(16):4249-56. doi: 10.1158/1078-0432.CCR-12-1327. PubMed PMID: 22896691.

16. Xu Z, Pothula SP, Wilson JS, Apte MV. Pancreatic cancer and its stroma: a conspiracy theory. World journal of gastroenterology : WJG. 2014;20(32):11216-29. doi: 10.3748/wjg.v20.i32.11216. PubMed PMID: 25170206; PMCID: PMC4145760.
17. Wilson JS, Pirola RC, Apte MV. Stars and stripes in pancreatic cancer: role of stellate cells and stroma in cancer progression. Front Physiol. 2014;5:52. doi: 10.3389/fphys.2014.00052. PubMed PMID: 24592240; PMCID: PMC3924046.
18. Andoh A, Takaya H, Saotome T, Shimada M, Hata K, Araki Y, Nakamura F, Shintani Y, Fujiyama Y, Bamba T. Cytokine regulation of chemokine (IL-8, MCP-1, and RANTES) gene expression in human pancreatic periacinar myofibroblasts. Gastroenterology. 2000;119(1):211-9. PubMed PMID: 10889171.
19. Shek FW, Benyon RC, Walker FM, McCrudden PR, Pender SL, Williams EJ, Johnson PA, Johnson CD, Bateman AC, Fine DR, Iredale JP. Expression of transforming growth factor-beta 1 by pancreatic stellate cells and its implications for matrix secretion and turnover in chronic pancreatitis. Am J Pathol. 2002;160(5):1787-98. PubMed PMID: 12000730; PMCID: PMC1850856.
20. Erkan M, Reiser-Erkan C, Michalski CW, Deucker S, Sauliunaite D, Streit S, Esposito I, Friess H, Kleeff J. Cancer-stellate cell interactions perpetuate the hypoxia-fibrosis cycle in pancreatic ductal adenocarcinoma. Neoplasia. 2009;11(5):497-508. PubMed PMID: 19412434; PMCID: PMC2671860.
21. Olive KP, Jacobetz MA, Davidson CJ, Gopinathan A, McIntyre D, Honess D, Madhu B, Goldgraben MA, Caldwell ME, Allard D, Frese KK, Denicola G, Feig C, Combs C, Winter SP, Ireland-Zecchini H, Reichelt S, Howat WJ, Chang A, Dhara M, Wang L, Ruckert F, Grutzmann R, Pilarsky C, Izeradjene K, Hingorani SR, Huang P, Davies SE, Plunkett W, Egorin M, Hruban RH, Whitebread N, McGovern K, Adams J, Iacobuzio-Donahue C, Griffiths J, Tuveson DA. Inhibition of Hedgehog signaling enhances delivery of chemotherapy in a mouse model of pancreatic cancer. Science. 2009;324(5933):1457-61. doi: 10.1126/science.1171362. PubMed PMID: 19460966; PMCID: PMC2998180.
22. Masamune A, Kikuta K, Watanabe T, Satoh K, Hirota M, Shimosegawa T. Hypoxia stimulates pancreatic stellate cells to induce fibrosis and angiogenesis in pancreatic cancer. Am J Physiol Gastrointest Liver Physiol. 2008;295(4):G709-17. doi: 10.1152/ajpgi.90356.2008. PubMed PMID: 18669622.
23. Wormann SM, Diakopoulos KN, Lesina M, Algul H. The immune network in pancreatic cancer development and progression. Oncogene. 2014;33(23):2956-67. doi: 10.1038/onc.2013.257. PubMed PMID: 23851493.
24. Protti MP, De Monte L. Immune infiltrates as predictive markers of survival in pancreatic cancer patients. Front Physiol. 2013;4:210. doi: 10.3389/fphys.2013.00210. PubMed PMID: 23950747; PMCID: PMC3738865.
25. Neesse A, Algul H, Tuveson DA, Gress TM. Stromal biology and therapy in pancreatic cancer: a changing paradigm. Gut. 2015;64(9):1476-84. doi: 10.1136/gutjnl-2015-309304. PubMed PMID: 25994217.
26. Xu Z, Vonlaufen A, Phillips PA, Fiala-Beer E, Zhang X, Yang L, Biankin AV, Goldstein D, Pirola RC, Wilson JS, Apte MV. Role of pancreatic stellate cells in pancreatic cancer metastasis. Am J Pathol. 2010;177(5):2585-96. Epub 2010/10/12. doi: 10.2353/ajpath.2010.090899. PubMed PMID: 20934972; PMCID: 2966814.

27. Ikenaga N, Ohuchida K, Mizumoto K, Cui L, Kayashima T, Morimatsu K, Moriyama T, Nakata K, Fujita H, Tanaka M. CD10+ pancreatic stellate cells enhance the progression of pancreatic cancer. Gastroenterology. 2010;139(3):1041-51, 51 e1-8. doi: 10.1053/j.gastro.2010.05.084. PubMed PMID: 20685603.
28. Bachem MG, Schunemann M, Ramadani M, Siech M, Beger H, Buck A, Zhou S, Schmid-Kotsas A, Adler G. Pancreatic carcinoma cells induce fibrosis by stimulating proliferation and matrix synthesis of stellate cells. Gastroenterology. 2005;128(4):907-21. Epub 2005/04/13. PubMed PMID: 15825074.
29. Thompson CB, Shepard HM, O'Connor PM, Kadhim S, Jiang P, Osgood RJ, Bookbinder LH, Li X, Sugarman BJ, Connor RJ, Nadjsombati S, Frost GI. Enzymatic depletion of tumor hyaluronan induces antitumor responses in preclinical animal models. Mol Cancer Ther. 2010;9(11):3052-64. doi: 10.1158/1535-7163.MCT-10-0470. PubMed PMID: 20978165.
30. Whatcott CJ, Han H, Von Hoff DD. Orchestrating the Tumor Microenvironment to Improve Survival for Patients With Pancreatic Cancer: Normalization, Not Destruction. Cancer J. 2015;21(4):299-306. doi: 10.1097/PPO.0000000000000140. PubMed PMID: 26222082.
31. Jacobetz MA, Chan DS, Neesse A, Bapiro TE, Cook N, Frese KK, Feig C, Nakagawa T, Caldwell ME, Zecchini HI, Lolkema MP, Jiang P, Kultti A, Thompson CB, Maneval DC, Jodrell DI, Frost GI, Shepard HM, Skepper JN, Tuveson DA. Hyaluronan impairs vascular function and drug delivery in a mouse model of pancreatic cancer. Gut. 2013;62(1):112-20. doi: 10.1136/gutjnl-2012-302529. PubMed PMID: 22466618; PMCID: PMC3551211.
32. Kozono S, Ohuchida K, Eguchi D, Ikenaga N, Fujiwara K, Cui L, Mizumoto K, Tanaka M. Pirfenidone inhibits pancreatic cancer desmoplasia by regulating stellate cells. Cancer research. 2013;73(7):2345-56. doi: 10.1158/0008-5472.CAN-12-3180. PubMed PMID: 23348422.
33. Ji T, Li S, Zhang Y, Lang J, Ding Y, Zhao X, Zhao R, Li Y, Shi J, Hao J, Zhao Y, Nie G. An MMP-2 Responsive Liposome Integrating Antifibrosis and Chemotherapeutic Drugs for Enhanced Drug Perfusion and Efficacy in Pancreatic Cancer. ACS Appl Mater Interfaces. 2016;8(5):3438-45. doi: 10.1021/acsami.5b11619. PubMed PMID: 26759926.
34. Amakye D, Jagani Z, Dorsch M. Unraveling the therapeutic potential of the Hedgehog pathway in cancer. Nat Med. 2013;19(11):1410-22. doi: 10.1038/nm.3389. PubMed PMID: 24202394.
35. Rhim AD, Oberstein PE, Thomas DH, Mirek ET, Palermo CF, Sastra SA, Dekleva EN, Saunders T, Becerra CP, Tattersall IW, Westphalen CB, Kitajewski J, Fernandez-Barrena MG, Fernandez-Zapico ME, Iacobuzio-Donahue C, Olive KP, Stanger BZ. Stromal Elements Act to Restrain, Rather Than Support, Pancreatic Ductal Adenocarcinoma. Cancer cell. 2014. doi: 10.1016/j.ccr.2014.04.021. PubMed PMID: 24856585.
36. Ozdemir BC, Pentcheva-Hoang T, Carstens JL, Zheng X, Wu CC, Simpson TR, Laklai H, Sugimoto H, Kahlert C, Novitskiy SV, De Jesus-Acosta A, Sharma P, Heidari P, Mahmood U, Chin L, Moses HL, Weaver VM, Maitra A, Allison JP, LeBleu VS, Kalluri R. Depletion of Carcinoma-Associated Fibroblasts and Fibrosis Induces Immunosuppression and Accelerates Pancreas Cancer with Reduced Survival. Cancer cell. 2014. doi: 10.1016/j.ccr.2014.04.005. PubMed PMID: 24856586.

37. Sherman MH, Yu RT, Engle DD, Ding N, Atkins AR, Tiriac H, Collisson EA, Connor F, Van Dyke T, Kozlov S, Martin P, Tseng TW, Dawson DW, Donahue TR, Masamune A, Shimosegawa T, Apte MV, Wilson JS, Ng B, Lau SL, Gunton JE, Wahl GM, Hunter T, Drebin JA, O'Dwyer PJ, Liddle C, Tuveson DA, Downes M, Evans RM. Vitamin D receptor-mediated stromal reprogramming suppresses pancreatitis and enhances pancreatic cancer therapy. Cell. 2014;159(1):80-93. doi: 10.1016/j.cell.2014.08.007. PubMed PMID: 25259922; PMCID: PMC4177038.
38. Kota J, Hancock J, Kwon J, Korc M. Pancreatic cancer: Stroma and its current and emerging targeted therapies. Cancer letters. 2017;391:38-49. doi: 10.1016/j.canlet.2016.12.035. PubMed PMID: 28093284.
39. Yang S, Wang X, Contino G, Liesa M, Sahin E, Ying H, Bause A, Li Y, Stommel JM, Dell'antonio G, Mautner J, Tonon G, Haigis M, Shirihai OS, Doglioni C, Bardeesy N, Kimmelman AC. Pancreatic cancers require autophagy for tumor growth. Genes & development. 2011;25(7):717-29. doi: 10.1101/gad.2016111. PubMed PMID: 21406549; PMCID: 3070934.
40. Yang A, Rajeshkumar NV, Wang X, Yabuuchi S, Alexander BM, Chu GC, Von Hoff DD, Maitra A, Kimmelman AC. Autophagy is critical for pancreatic tumor growth and progression in tumors with p53 alterations. Cancer discovery. 2014;4(8):905-13. doi: 10.1158/2159-8290.CD-14-0362. PubMed PMID: 24875860; PMCID: 4125497.
41. Yang MC, Wang HC, Hou YC, Tung HL, Chiu TJ, Shan YS. Blockade of autophagy reduces pancreatic cancer stem cell activity and potentiates the tumoricidal effect of gemcitabine. Molecular cancer. 2015;14(1):179. doi: 10.1186/s12943-015-0449-3. PubMed PMID: 26458814; PMCID: 4603764.
42. He C, Klionsky DJ. Regulation mechanisms and signaling pathways of autophagy. Annual review of genetics. 2009;43:67-93. doi: 10.1146/annurev-genet-102808-114910. PubMed PMID: 19653858; PMCID: 2831538.
43. Hayashi-Nishino M, Fujita N, Noda T, Yamaguchi A, Yoshimori T, Yamamoto A. A subdomain of the endoplasmic reticulum forms a cradle for autophagosome formation. Nature cell biology. 2009;11(12):1433-7. Epub 2009/11/10. doi: 10.1038/ncb1991. PubMed PMID: 19898463.
44. Yla-Anttila P, Vihinen H, Jokitalo E, Eskelinen EL. 3D tomography reveals connections between the phagophore and endoplasmic reticulum. Autophagy. 2009;5(8):1180-5. Epub 2009/10/27. PubMed PMID: 19855179.
45. Hamasaki M, Furuta N, Matsuda A, Nezu A, Yamamoto A, Fujita N, Oomori H, Noda T, Haraguchi T, Hiraoka Y, Amano A, Yoshimori T. Autophagosomes form at ER-mitochondria contact sites. Nature. 2013;495(7441):389-93. Epub 2013/03/05. doi: 10.1038/nature11910. PubMed PMID: 23455425.
46. Alers S, Loffler AS, Wesselborg S, Stork B. Role of AMPK-mTOR-Ulk1/2 in the regulation of autophagy: cross talk, shortcuts, and feedbacks. Mol Cell Biol. 2012;32(1):2-11. Epub 2011/10/26. doi: 10.1128/MCB.06159-11. PubMed PMID: 22025673; PMCID: PMC3255710.
47. Russell RC, Tian Y, Yuan H, Park HW, Chang YY, Kim J, Kim H, Neufeld TP, Dillin A, Guan KL. ULK1 induces autophagy by phosphorylating Beclin-1 and activating VPS34 lipid kinase. Nature cell biology. 2013;15(7):741-50. Epub 2013/05/21. doi: 10.1038/ncb2757. PubMed PMID: 23685627; PMCID: PMC3885611.

48. Kang R, Zeh HJ, Lotze MT, Tang D. The Beclin 1 network regulates autophagy and apoptosis. Cell death and differentiation. 2011;18(4):571-80. Epub 2011/02/12. doi: 10.1038/cdd.2010.191. PubMed PMID: 21311563; PMCID: PMC3131912.
49. Proikas-Cezanne T, Takacs Z, Donnes P, Kohlbacher O. WIPI proteins: essential PtdIns3P effectors at the nascent autophagosome. Journal of cell science. 2015;128(2):207-17. Epub 2015/01/09. doi: 10.1242/jcs.146258. PubMed PMID: 25568150.
50. Dooley HC, Razi M, Polson HE, Girardin SE, Wilson MI, Tooze SA. WIPI2 links LC3 conjugation with PI3P, autophagosome formation, and pathogen clearance by recruiting Atg12-5-16L1. Mol Cell. 2014;55(2):238-52. Epub 2014/06/24. doi: 10.1016/j.molcel.2014.05.021. PubMed PMID: 24954904; PMCID: PMC4104028.
51. Fujita N, Itoh T, Omori H, Fukuda M, Noda T, Yoshimori T. The Atg16L complex specifies the site of LC3 lipidation for membrane biogenesis in autophagy. Molecular biology of the cell. 2008;19(5):2092-100. Epub 2008/03/07. doi: 10.1091/mbc.E07-12-1257. PubMed PMID: 18321988; PMCID: PMC2366860.
52. Pankiv S, Clausen TH, Lamark T, Brech A, Bruun JA, Outzen H, Overvatn A, Bjorkoy G, Johansen T. p62/SQSTM1 binds directly to Atg8/LC3 to facilitate degradation of ubiquitinated protein aggregates by autophagy. The Journal of biological chemistry. 2007;282(33):24131-45. Epub 2007/06/21. doi: 10.1074/jbc.M702824200. PubMed PMID: 17580304.
53. Apel A, Herr I, Schwarz H, Rodemann HP, Mayer A. Blocked autophagy sensitizes resistant carcinoma cells to radiation therapy. Cancer research. 2008;68(5):1485-94. doi: 10.1158/0008-5472.CAN-07-0562. PubMed PMID: 18316613.
54. Li J, Yang B, Zhou Q, Wu Y, Shang D, Guo Y, Song Z, Zheng Q, Xiong J. Autophagy promotes hepatocellular carcinoma cell invasion through activation of epithelial-mesenchymal transition. Carcinogenesis. 2013;34(6):1343-51. doi: 10.1093/carcin/bgt063. PubMed PMID: 23430956.
55. Fels DR, Ye J, Segan AT, Kridel SJ, Spiotto M, Olson M, Koong AC, Koumenis C. Preferential cytotoxicity of bortezomib toward hypoxic tumor cells via overactivation of endoplasmic reticulum stress pathways. Cancer research. 2008;68(22):9323-30. doi: 10.1158/0008-5472.CAN-08-2873. PubMed PMID: 19010906; PMCID: 3617567.
56. Claerhout S, Verschooten L, Van Kelst S, De Vos R, Proby C, Agostinis P, Garmyn M. Concomitant inhibition of AKT and autophagy is required for efficient cisplatin-induced apoptosis of metastatic skin carcinoma. International journal of cancer. 2010;127(12):2790-803. doi: 10.1002/ijc.25300. PubMed PMID: 21351258.
57. Akalay I, Janji B, Hasmim M, Noman MZ, Andre F, De Cremoux P, Bertheau P, Badoual C, Vielh P, Larsen AK, Sabbah M, Tan TZ, Keira JH, Hung NT, Thiery JP, Mami-Chouaib F, Chouaib S. Epithelial-to-mesenchymal transition and autophagy induction in breast carcinoma promote escape from T-cell-mediated lysis. Cancer research. 2013;73(8):2418-27. doi: 10.1158/0008-5472.CAN-12-2432. PubMed PMID: 23436798.
58. Kanzawa T, Germano IM, Komata T, Ito H, Kondo Y, Kondo S. Role of autophagy in temozolomide-induced cytotoxicity for malignant glioma cells. Cell death and differentiation. 2004;11(4):448-57. doi: 10.1038/sj.cdd.4401359. PubMed PMID: 14713959.

59. Li M, Jiang X, Liu D, Na Y, Gao GF, Xi Z. Autophagy protects LNCaP cells under androgen deprivation conditions. Autophagy. 2008;4(1):54-60. PubMed PMID: 17993778.
60. Hashimoto D, Blauer M, Hirota M, Ikonen NH, Sand J, Laukkarinen J. Autophagy is needed for the growth of pancreatic adenocarcinoma and has a cytoprotective effect against anticancer drugs. European journal of cancer. 2014;50(7):1382-90. doi: 10.1016/j.ejca.2014.01.011. PubMed PMID: 24503026.
61. Donadelli M, Dando I, Zaniboni T, Costanzo C, Dalla Pozza E, Scupoli MT, Scarpa A, Zappavigna S, Marra M, Abbruzzese A, Bifulco M, Caraglia M, Palmieri M. Gemcitabine/cannabinoid combination triggers autophagy in pancreatic cancer cells through a ROS-mediated mechanism. Cell death & disease. 2011;2:e152. doi: 10.1038/cddis.2011.36. PubMed PMID: 21525939; PMCID: 3122066.
62. Ma X, Yan L, He L, He D, Lu H. Ocular fundus manifestation of two patients following long-term chloroquine therapy: a case report. Diagn Pathol. 2010;5:20. doi: 10.1186/1746-1596-5-20. PubMed PMID: 20346186; PMCID: PMC2859853.
63. Nogueira HM, Gama RD. Images in clinical medicine. Bull's-eye maculopathy. The New England journal of medicine. 2009;360(21):2224. doi: 10.1056/NEJMicm0708021. PubMed PMID: 19458367.
64. Veinot JP, Mai KT, Zarychanski R. Chloroquine related cardiac toxicity. J Rheumatol. 1998;25(6):1221-5. PubMed PMID: 9632091.
65. Estes ML, Ewing-Wilson D, Chou SM, Mitsumoto H, Hanson M, Shirey E, Ratliff NB. Chloroquine neuromyotoxicity. Clinical and pathologic perspective. Am J Med. 1987;82(3):447-55. Epub 1987/03/01. PubMed PMID: 3826099.
66. Lee RC, Feinbaum RL, Ambros V. The C. elegans heterochronic gene lin-4 encodes small RNAs with antisense complementarity to lin-14. Cell. 1993;75(5):843-54. PubMed PMID: 8252621.
67. Lee Y, Kim M, Han J, Yeom KH, Lee S, Baek SH, Kim VN. MicroRNA genes are transcribed by RNA polymerase II. EMBO J. 2004;23(20):4051-60. Epub 2004/09/17. doi: 10.1038/sj.emboj.7600385. PubMed PMID: 15372072; PMCID: PMC524334.
68. Lee Y, Ahn C, Han J, Choi H, Kim J, Yim J, Lee J, Provost P, Radmark O, Kim S, Kim VN. The nuclear RNase III Drosha initiates microRNA processing. Nature. 2003;425(6956):415-9. Epub 2003/09/26. doi: 10.1038/nature01957. PubMed PMID: 14508493.
69. Lund E, Guttinger S, Calado A, Dahlberg JE, Kutay U. Nuclear export of microRNA precursors. Science. 2004;303(5654):95-8. Epub 2003/11/25. doi: 10.1126/science.1090599. PubMed PMID: 14631048.
70. Grishok A, Pasquinelli AE, Conte D, Li N, Parrish S, Ha I, Baillie DL, Fire A, Ruvkun G, Mello CC. Genes and mechanisms related to RNA interference regulate expression of the small temporal RNAs that control C. elegans developmental timing. Cell. 2001;106(1):23-34. Epub 2001/07/20. PubMed PMID: 11461699.
71. Pratt AJ, MacRae IJ. The RNA-induced silencing complex: a versatile gene-silencing machine. J Biol Chem. 2009;284(27):17897-901. Epub 2009/04/04. doi: 10.1074/jbc.R900012200. PubMed PMID: 19342379; PMCID: PMC2709356.

72. Agarwal V, Bell GW, Nam JW, Bartel DP. Predicting effective microRNA target sites in mammalian mRNAs. eLife. 2015;4. doi: 10.7554/eLife.05005. PubMed PMID: 26267216; PMCID: 4532895.
73. Hwang HW, Wentzel EA, Mendell JT. A hexanucleotide element directs microRNA nuclear import. Science. 2007;315(5808):97-100. doi: 10.1126/science.1136235. PubMed PMID: 17204650.
74. Jagannathan S, Vad N, Vallabhapurapu S, Vallabhapurapu S, Anderson KC, Driscoll JJ. MiR-29b replacement inhibits proteasomes and disrupts aggresome+autophagosome formation to enhance the antimyeloma benefit of bortezomib. Leukemia. 2015;29(3):727-38. doi: 10.1038/leu.2014.279. PubMed PMID: 25234165; PMCID: 4360212.
75. Jeffries CD, Fried HM, Perkins DO. Nuclear and cytoplasmic localization of neural stem cell microRNAs. Rna. 2011;17(4):675-86. doi: 10.1261/rna.2006511. PubMed PMID: 21363885; PMCID: 3062178.
76. Khudayberdiev SA, Zampa F, Rajman M, Schratt G. A comprehensive characterization of the nuclear microRNA repertoire of post-mitotic neurons. Frontiers in molecular neuroscience. 2013;6:43. doi: 10.3389/fnmol.2013.00043. PubMed PMID: 24324399; PMCID: 3840315.
77. Morris KV, Chan SW, Jacobsen SE, Looney DJ. Small interfering RNA-induced transcriptional gene silencing in human cells. Science. 2004;305(5688):1289-92. Epub 2004/08/07. doi: 10.1126/science.1101372. PubMed PMID: 15297624.
78. Janowski BA, Huffman KE, Schwartz JC, Ram R, Hardy D, Shames DS, Minna JD, Corey DR. Inhibiting gene expression at transcription start sites in chromosomal DNA with antigene RNAs. Nat Chem Biol. 2005;1(4):216-22. Epub 2006/01/13. doi: 10.1038/nchembio725. PubMed PMID: 16408038.
79. Liang H, Zhang J, Zen K, Zhang CY, Chen X. Nuclear microRNAs and their unconventional role in regulating non-coding RNAs. Protein & cell. 2013;4(5):325-30. doi: 10.1007/s13238-013-3001-5. PubMed PMID: 23584808; PMCID: 4883050.
80. Roberts TC. The MicroRNA Biology of the Mammalian Nucleus. Molecular therapy Nucleic acids. 2014;3:e188. doi: 10.1038/mtna.2014.40. PubMed PMID: 25137140; PMCID: 4221600.
81. Zhang Z, Zou J, Wang GK, Zhang JT, Huang S, Qin YW, Jing Q. Uracils at nucleotide position 9-11 are required for the rapid turnover of miR-29 family. Nucleic acids research. 2011;39(10):4387-95. doi: 10.1093/nar/gkr020. PubMed PMID: 21288881; PMCID: 3105410.
82. Tumaneng K, Schlegelmilch K, Russell RC, Yimlamai D, Basnet H, Mahadevan N, Fitamant J, Bardeesy N, Camargo FD, Guan KL. YAP mediates crosstalk between the Hippo and PI(3)K-TOR pathways by suppressing PTEN via miR-29. Nat Cell Biol. 2012;14(12):1322-9. Epub 2012/11/13. doi: 10.1038/ncb2615. PubMed PMID: 23143395; PMCID: PMC4019071.
83. Liu Y, Taylor NE, Lu L, Usa K, Cowley AW, Jr., Ferreri NR, Yeo NC, Liang M. Renal medullary microRNAs in Dahl salt-sensitive rats: miR-29b regulates several collagens and related genes. Hypertension. 2010;55(4):974-82. Epub 2010/03/03. doi: 10.1161/HYPERTENSIONAHA.109.144428. PubMed PMID: 20194304; PMCID: PMC2862728.

84. Dooley J, Garcia-Perez JE, Sreenivasan J, Schlenner SM, Vangoitsenhoven R, Papadopoulou AS, Tian L, Schonefeldt S, Serneels L, Deroose C, Staats KA, Van der Schueren B, De Strooper B, McGuinness OP, Mathieu C, Liston A. The microRNA-29 Family Dictates the Balance Between Homeostatic and Pathological Glucose Handling in Diabetes and Obesity. Diabetes. 2016;65(1):53-61. Epub 2015/12/24. doi: 10.2337/db15-0770. PubMed PMID: 26696639; PMCID: PMC4876765.
85. Kwon JJ, Nabinger SC, Vega Z, Sahu SS, Alluri RK, Abdul-Sater Z, Yu Z, Gore J, Nalepa G, Saxena R, Korc M, Kota J. Pathophysiological role of microRNA-29 in pancreatic cancer stroma. Scientific reports. 2015;5:11450. doi: 10.1038/srep11450. PubMed PMID: 26095125; PMCID: 4476113.
86. Friedman RC, Farh KK, Burge CB, Bartel DP. Most mammalian mRNAs are conserved targets of microRNAs. Genome Res. 2009;19(1):92-105. Epub 2008/10/29. doi: 10.1101/gr.082701.108. PubMed PMID: 18955434; PMCID: PMC2612969.
87. Papadopoulou AS, Dooley J, Linterman MA, Pierson W, Ucar O, Kyewski B, Zuklys S, Hollander GA, Matthys P, Gray DH, De Strooper B, Liston A. The thymic epithelial microRNA network elevates the threshold for infection-associated thymic involution via miR-29a mediated suppression of the IFN-alpha receptor. Nat Immunol. 2011;13(2):181-7. Epub 2011/12/20. doi: 10.1038/ni.2193. PubMed PMID: 22179202; PMCID: PMC3647613.
88. Cushing L, Costinean S, Xu W, Jiang Z, Madden L, Kuang P, Huang J, Weisman A, Hata A, Croce CM, Lu J. Disruption of miR-29 Leads to Aberrant Differentiation of Smooth Muscle Cells Selectively Associated with Distal Lung Vasculature. PLoS Genet. 2015;11(5):e1005238. Epub 2015/05/29. doi: 10.1371/journal.pgen.1005238. PubMed PMID: 26020233; PMCID: PMC4447351.
89. Smith KM, Guerau-de-Arellano M, Costinean S, Williams JL, Bottoni A, Mavrikis Cox G, Satoskar AR, Croce CM, Racke MK, Lovett-Racke AE, Whitacre CC. miR-29ab1 deficiency identifies a negative feedback loop controlling Th1 bias that is dysregulated in multiple sclerosis. J Immunol. 2012;189(4):1567-76. Epub 2012/07/10. doi: 10.4049/jimmunol.1103171. PubMed PMID: 22772450; PMCID: PMC3411895.
90. Kogure T, Costinean S, Yan I, Braconi C, Croce C, Patel T. Hepatic miR-29ab1 expression modulates chronic hepatic injury. Journal of cellular and molecular medicine. 2012;16(11):2647-54. doi: 10.1111/j.1582-4934.2012.01578.x. PubMed PMID: 22469499; PMCID: 3923513.
91. Calin GA, Dumitru CD, Shimizu M, Bichi R, Zupo S, Noch E, Aldler H, Rattan S, Keating M, Rai K, Rassenti L, Kipps T, Negrini M, Bullrich F, Croce CM. Frequent deletions and down-regulation of micro- RNA genes miR15 and miR16 at 13q14 in chronic lymphocytic leukemia. Proc Natl Acad Sci U S A. 2002;99(24):15524-9. Epub 2002/11/16. doi: 10.1073/pnas.242606799. PubMed PMID: 12434020; PMCID: PMC137750.
92. van Rooij E, Sutherland LB, Thatcher JE, DiMaio JM, Naseem RH, Marshall WS, Hill JA, Olson EN. Dysregulation of microRNAs after myocardial infarction reveals a role of miR-29 in cardiac fibrosis. Proc Natl Acad Sci U S A. 2008;105(35):13027-32. doi: 10.1073/pnas.0805038105. PubMed PMID: 18723672; PMCID: 2529064.
93. Kwiecinski M, Elfimova N, Noetel A, Tox U, Steffen HM, Hacker U, Nischt R, Dienes HP, Odenthal M. Expression of platelet-derived growth factor-C and insulin-like growth factor I in hepatic stellate cells is inhibited by miR-29. Laboratory investigation; a

journal of technical methods and pathology. 2012;92(7):978-87. doi: 10.1038/labinvest.2012.70. PubMed PMID: 22565577.
94. Xiao J, Meng XM, Huang XR, Chung AC, Feng YL, Hui DS, Yu CM, Sung JJ, Lan HY. miR-29 inhibits bleomycin-induced pulmonary fibrosis in mice. Molecular therapy : the journal of the American Society of Gene Therapy. 2012;20(6):1251-60. doi: 10.1038/mt.2012.36. PubMed PMID: 22395530; PMCID: 3369297.
95. Wang B, Komers R, Carew R, Winbanks CE, Xu B, Herman-Edelstein M, Koh P, Thomas M, Jandeleit-Dahm K, Gregorevic P, Cooper ME, Kantharidis P. Suppression of microRNA-29 expression by TGF-beta1 promotes collagen expression and renal fibrosis. Journal of the American Society of Nephrology : JASN. 2012;23(2):252-65. doi: 10.1681/ASN.2011010055. PubMed PMID: 22095944; PMCID: 3269175.
96. Wang H, Garzon R, Sun H, Ladner KJ, Singh R, Dahlman J, Cheng A, Hall BM, Qualman SJ, Chandler DS, Croce CM, Guttridge DC. NF-kappaB-YY1-miR-29 regulatory circuitry in skeletal myogenesis and rhabdomyosarcoma. Cancer cell. 2008;14(5):369-81. doi: 10.1016/j.ccr.2008.10.006. PubMed PMID: 18977326; PMCID: 3829205.
97. Siegel R, Ma J, Zou Z, Jemal A. Cancer statistics, 2014. CA: a cancer journal for clinicians. 2014;64(1):9-29. Epub 2014/01/09. doi: 10.3322/caac.21208. PubMed PMID: 24399786.
98. Provenzano PP, Cuevas C, Chang AE, Goel VK, Von Hoff DD, Hingorani SR. Enzymatic targeting of the stroma ablates physical barriers to treatment of pancreatic ductal adenocarcinoma. Cancer cell. 2012;21(3):418-29. doi: 10.1016/j.ccr.2012.01.007. PubMed PMID: 22439937; PMCID: 3371414.
99. Hwang RF, Moore T, Arumugam T, Ramachandran V, Amos KD, Rivera A, Ji B, Evans DB, Logsdon CD. Cancer-associated stromal fibroblasts promote pancreatic tumor progression. Cancer research. 2008;68(3):918-26. doi: 10.1158/0008-5472.CAN-07-5714. PubMed PMID: 18245495; PMCID: 2519173.
100. Vonlaufen A, Joshi S, Qu C, Phillips PA, Xu Z, Parker NR, Toi CS, Pirola RC, Wilson JS, Goldstein D, Apte MV. Pancreatic stellate cells: partners in crime with pancreatic cancer cells. Cancer research. 2008;68(7):2085-93. Epub 2008/04/03. doi: 10.1158/0008-5472.CAN-07-2477. PubMed PMID: 18381413.
101. Andersen DK, Andren-Sandberg A, Duell EJ, Goggins M, Korc M, Petersen GM, Smith JP, Whitcomb DC. Pancreatitis-diabetes-pancreatic cancer: summary of an NIDDK-NCI workshop. Pancreas. 2013;42(8):1227-37. Epub 2013/10/25. doi: 10.1097/MPA.0b013e3182a9ad9d. PubMed PMID: 24152948; PMCID: 3878448.
102. Friess H, Yamanaka Y, Buchler M, Ebert M, Beger HG, Gold LI, Korc M. Enhanced expression of transforming growth factor beta isoforms in pancreatic cancer correlates with decreased survival. Gastroenterology. 1993;105(6):1846-56. PubMed PMID: 8253361.
103. Friess H, Lu Z, Riesle E, Uhl W, Brundler AM, Horvath L, Gold LI, Korc M, Buchler MW. Enhanced expression of TGF-betas and their receptors in human acute pancreatitis. Annals of surgery. 1998;227(1):95-104. PubMed PMID: 9445116; PMCID: 1191178.
104. Apte MV, Haber PS, Darby SJ, Rodgers SC, McCaughan GW, Korsten MA, Pirola RC, Wilson JS. Pancreatic stellate cells are activated by proinflammatory

cytokines: implications for pancreatic fibrogenesis. Gut. 1999;44(4):534-41. Epub 1999/03/17. PubMed PMID: 10075961; PMCID: 1727467.
105. Lonardo E, Frias-Aldeguer J, Hermann PC, Heeschen C. Pancreatic stellate cells form a niche for cancer stem cells and promote their self-renewal and invasiveness. Cell cycle. 2012;11(7):1282-90. doi: 10.4161/cc.19679. PubMed PMID: 22421149.
106. Ambros V. microRNAs: tiny regulators with great potential. Cell. 2001;107(7):823-6. Epub 2002/01/10. PubMed PMID: 11779458.
107. Boudreau RL, Jiang P, Gilmore BL, Spengler RM, Tirabassi R, Nelson JA, Ross CA, Xing Y, Davidson BL. Transcriptome-wide discovery of microRNA binding sites in human brain. Neuron. 2014;81(2):294-305. doi: 10.1016/j.neuron.2013.10.062. PubMed PMID: 24389009; PMCID: 4108341.
108. Mendell JT, Olson EN. MicroRNAs in stress signaling and human disease. Cell. 2012;148(6):1172-87. doi: 10.1016/j.cell.2012.02.005. PubMed PMID: 22424228; PMCID: 3308137.
109. Bowen T, Jenkins RH, Fraser DJ. MicroRNAs, transforming growth factor beta-1, and tissue fibrosis. The Journal of pathology. 2013;229(2):274-85. Epub 2012/10/09. doi: 10.1002/path.4119. PubMed PMID: 23042530.
110. Vettori S, Gay S, Distler O. Role of MicroRNAs in Fibrosis. The open rheumatology journal. 2012;6:130-9. Epub 2012/07/18. doi: 10.2174/1874312901206010130. PubMed PMID: 22802911; PMCID: 3396185.
111. Jamieson NB, Morran DC, Morton JP, Ali A, Dickson EJ, Carter CR, Sansom OJ, Evans TR, McKay CJ, Oien KA. MicroRNA molecular profiles associated with diagnosis, clinicopathologic criteria, and overall survival in patients with resectable pancreatic ductal adenocarcinoma. Clin Cancer Res. 2012;18(2):534-45. doi: 10.1158/1078-0432.CCR-11-0679. PubMed PMID: 22114136.
112. Chou J, Lin JH, Brenot A, Kim JW, Provot S, Werb Z. GATA3 suppresses metastasis and modulates the tumour microenvironment by regulating microRNA-29b expression. Nat Cell Biol. 2013;15(2):201-13. doi: 10.1038/ncb2672. PubMed PMID: 23354167; PMCID: 3660859.
113. Hingorani SR, Petricoin EF, Maitra A, Rajapakse V, King C, Jacobetz MA, Ross S, Conrads TP, Veenstra TD, Hitt BA, Kawaguchi Y, Johann D, Liotta LA, Crawford HC, Putt ME, Jacks T, Wright CV, Hruban RH, Lowy AM, Tuveson DA. Preinvasive and invasive ductal pancreatic cancer and its early detection in the mouse. Cancer cell. 2003;4(6):437-50. PubMed PMID: 14706336.
114. Mathison A, Liebl A, Bharucha J, Mukhopadhyay D, Lomberk G, Shah V, Urrutia R. Pancreatic stellate cell models for transcriptional studies of desmoplasia-associated genes. Pancreatology : official journal of the International Association of Pancreatology. 2010;10(4):505-16. doi: 10.1016/S1424-3903(10)80035-3. PubMed PMID: 20847583; PMCID: 3214918.
115. Sempere LF, Korc M. A method for conducting highly sensitive microRNA in situ hybridization and immunohistochemical analysis in pancreatic cancer. Methods in molecular biology. 2013;980:43-59. doi: 10.1007/978-1-62703-287-2_4. PubMed PMID: 23359149.
116. Burgess A, Vigneron S, Brioudes E, Labbe JC, Lorca T, Castro A. Loss of human Greatwall results in G2 arrest and multiple mitotic defects due to deregulation of the cyclin B-Cdc2/PP2A balance. Proceedings of the National Academy of Sciences of the

United States of America. 2010;107(28):12564-9. doi: 10.1073/pnas.0914191107. PubMed PMID: 20538976; PMCID: 2906566.
117. Massague J. TGFbeta signalling in context. Nature reviews Molecular cell biology. 2012;13(10):616-30. doi: 10.1038/nrm3434. PubMed PMID: 22992590; PMCID: 4027049.
118. Aikawa T, Gunn J, Spong SM, Klaus SJ, Korc M. Connective tissue growth factor-specific antibody attenuates tumor growth, metastasis, and angiogenesis in an orthotopic mouse model of pancreatic cancer. Mol Cancer Ther. 2006;5(5):1108-16. doi: 10.1158/1535-7163.MCT-05-0516. PubMed PMID: 16731742.
119. Bhowmick NA, Chytil A, Plieth D, Gorska AE, Dumont N, Shappell S, Washington MK, Neilson EG, Moses HL. TGF-beta signaling in fibroblasts modulates the oncogenic potential of adjacent epithelia. Science. 2004;303(5659):848-51. doi: 10.1126/science.1090922. PubMed PMID: 14764882.
120. Karagiannis GS, Poutahidis T, Erdman SE, Kirsch R, Riddell RH, Diamandis EP. Cancer-associated fibroblasts drive the progression of metastasis through both paracrine and mechanical pressure on cancer tissue. Molecular cancer research : MCR. 2012;10(11):1403-18. doi: 10.1158/1541-7786.MCR-12-0307. PubMed PMID: 23024188.
121. Almoguera C, Shibata D, Forrester K, Martin J, Arnheim N, Perucho M. Most human carcinomas of the exocrine pancreas contain mutant c-K-ras genes. Cell. 1988;53(4):549-54. PubMed PMID: 2453289.
122. Omary MB, Lugea A, Lowe AW, Pandol SJ. The pancreatic stellate cell: a star on the rise in pancreatic diseases. The Journal of clinical investigation. 2007;117(1):50-9. doi: 10.1172/JCI30082. PubMed PMID: 17200706; PMCID: 1716214.
123. Schussler MH, Skoudy A, Ramaekers F, Real FX. Intermediate filaments as differentiation markers of normal pancreas and pancreas cancer. Am J Pathol. 1992;140(3):559-68. PubMed PMID: 1372155; PMCID: 1886166.
124. Mantoni TS, Lunardi S, Al-Assar O, Masamune A, Brunner TB. Pancreatic stellate cells radioprotect pancreatic cancer cells through beta1-integrin signaling. Cancer research. 2011;71(10):3453-8. Epub 2011/05/12. doi: 10.1158/0008-5472.CAN-10-1633. PubMed PMID: 21558392; PMCID: PMC3097171.
125. Noetel A, Kwiecinski M, Elfimova N, Huang J, Odenthal M. microRNA are Central Players in Anti- and Profibrotic Gene Regulation during Liver Fibrosis. Frontiers in physiology. 2012;3:49. PubMed PMID: 22457651.
126. Zhou L, Wang L, Lu L, Jiang P, Sun H, Wang H. Inhibition of miR-29 by TGF-beta-Smad3 signaling through dual mechanisms promotes transdifferentiation of mouse myoblasts into myofibroblasts. PloS one. 2012;7(3):e33766. doi: 10.1371/journal.pone.0033766. PubMed PMID: 22438993; PMCID: 3306299.
127. Qin W, Chung AC, Huang XR, Meng XM, Hui DS, Yu CM, Sung JJ, Lan HY. TGF-beta/Smad3 signaling promotes renal fibrosis by inhibiting miR-29. Journal of the American Society of Nephrology : JASN. 2011;22(8):1462-74. doi: 10.1681/ASN.2010121308. PubMed PMID: 21784902; PMCID: 3148701.
128. Wang L, Zhou L, Jiang P, Lu L, Chen X, Lan H, Guttridge DC, Sun H, Wang H. Loss of miR-29 in myoblasts contributes to dystrophic muscle pathogenesis. Molecular therapy : the journal of the American Society of Gene Therapy. 2012;20(6):1222-33. doi: 10.1038/mt.2012.35. PubMed PMID: 22434133; PMCID: 3369280.

129. Kenny HA, Chiang C-Y, White EA, Schryver EM, Habis M, Romero IL, Ladanyi A, Penicka CV, George J, Matlin K, Montag A, Wroblewski K, Yamada SD, Mazar AP, Bowtell D, Lengyel E. Mesothelial cells promote early ovarian cancer metastasis through fibronectin secretion. The Journal of clinical investigation. 2014;124(10):4614-28. PubMed PMID: 25202979.
130. Fernandez-Garcia B, Eiro N, Marin L, Gonzalez-Reyes S, Gonzalez LO, Lamelas ML, Vizoso FJ. Expression and prognostic significance of fibronectin and matrix metalloproteases in breast cancer metastasis. Histopathology. 2014;64(4):512-22. PubMed PMID: 24117661.
131. Schwarz RE, Awasthi N, Konduri S, Caldwell L, Cafasso D, Schwarz MA. Antitumor effects of EMAP II against pancreatic cancer through inhibition of fibronectin-dependent proliferation. Cancer Biol Ther. 2010;9(8):632-9. PubMed PMID: 20212356.
132. Neuzillet C, de Gramont A, Tijeras-Raballand A, de Mestier L, Cros J, Faivre S, Raymond E. Perspectives of TGF-beta inhibition in pancreatic and hepatocellular carcinomas. Oncotarget. 2014;5(1):78-94. PubMed PMID: 24393789.
133. Ohlund D, Franklin O, Lundberg E, Lundin C, Sund M. Type IV collagen stimulates pancreatic cancer cell proliferation, migration, and inhibits apoptosis through an autocrine loop. BMC cancer. 2013;13:154. doi: 10.1186/1471-2407-13-154. PubMed PMID: 23530721; PMCID: 3618250.
134. Armstrong T, Packham G, Murphy LB, Bateman AC, Conti JA, Fine DR, Johnson CD, Benyon RC, Iredale JP. Type I collagen promotes the malignant phenotype of pancreatic ductal adenocarcinoma. Clin Cancer Res. 2004;10(21):7427-37. doi: 10.1158/1078-0432.CCR-03-0825. PubMed PMID: 15534120.
135. Grzesiak JJ, Ho JC, Moossa AR, Bouvet M. The integrin-extracellular matrix axis in pancreatic cancer. Pancreas. 2007;35(4):293-301. doi: 10.1097/mpa.0b013e31811f4526. PubMed PMID: 18090233.
136. Kota J, Chivukula RR, O'Donnell KA, Wentzel EA, Montgomery CL, Hwang HW, Chang TC, Vivekanandan P, Torbenson M, Clark KR, Mendell JR, Mendell JT. Therapeutic microRNA delivery suppresses tumorigenesis in a murine liver cancer model. Cell. 2009;137(6):1005-17. doi: 10.1016/j.cell.2009.04.021. PubMed PMID: 19524505; PMCID: 2722880.
137. Esquela-Kerscher A, Trang P, Wiggins JF, Patrawala L, Cheng A, Ford L, Weidhaas JB, Brown D, Bader AG, Slack FJ. The let-7 microRNA reduces tumor growth in mouse models of lung cancer. Cell cycle. 2008;7(6):759-64. PubMed PMID: 18344688.
138. Kumar MS, Erkeland SJ, Pester RE, Chen CY, Ebert MS, Sharp PA, Jacks T. Suppression of non-small cell lung tumor development by the let-7 microRNA family. Proceedings of the National Academy of Sciences of the United States of America. 2008;105(10):3903-8. Epub 2008/03/01. doi: 10.1073/pnas.0712321105. PubMed PMID: 18308936; PMCID: 2268826.
139. Chau BN, Xin C, Hartner J, Ren S, Castano AP, Linn G, Li J, Tran PT, Kaimal V, Huang X, Chang AN, Li S, Kalra A, Grafals M, Portilla D, MacKenna DA, Orkin SH, Duffield JS. MicroRNA-21 promotes fibrosis of the kidney by silencing metabolic pathways. Science translational medicine. 2012;4(121):121ra18. doi: 10.1126/scitranslmed.3003205. PubMed PMID: 22344686; PMCID: 3672221.

140. Janssen HL, Reesink HW, Lawitz EJ, Zeuzem S, Rodriguez-Torres M, Patel K, van der Meer AJ, Patick AK, Chen A, Zhou Y, Persson R, King BD, Kauppinen S, Levin AA, Hodges MR. Treatment of HCV infection by targeting microRNA. The New England journal of medicine. 2013;368(18):1685-94. doi: 10.1056/NEJMoa1209026. PubMed PMID: 23534542.
141. Therapeutics. M. Mirna Therapuetics is First to Advance MicroRNA into the Clinic for Cancer. www.mirnarx.com (accessed May 13, 2013).
142. Xue W, Dahlman JE, Tammela T, Khan OF, Sood S, Dave A, Cai W, Chirino LM, Yang GR, Bronson R, Crowley DG, Sahay G, Schroeder A, Langer R, Anderson DG, Jacks T. Small RNA combination therapy for lung cancer. Proceedings of the National Academy of Sciences of the United States of America. 2014;111(34):E3553-61. doi: 10.1073/pnas.1412686111. PubMed PMID: 25114235; PMCID: 4151750.
143. Kasinski AL, Kelnar K, Stahlhut C, Orellana E, Zhao J, Shimer E, Dysart S, Chen X, Bader AG, Slack FJ. A combinatorial microRNA therapeutics approach to suppressing non-small cell lung cancer. Oncogene. 2014. doi: 10.1038/onc.2014.282. PubMed PMID: 25174400.
144. Torre LA, Bray F, Siegel RL, Ferlay J, Lortet-Tieulent J, Jemal A. Global cancer statistics, 2012. CA: a cancer journal for clinicians. 2015;65(2):87-108. doi: 10.3322/caac.21262. PubMed PMID: 25651787.
145. Von Hoff DD, Ervin T, Arena FP, Chiorean EG, Infante J, Moore M, Seay T, Tjulandin SA, Ma WW, Saleh MN, Harris M, Reni M, Dowden S, Laheru D, Bahary N, Ramanathan RK, Tabernero J, Hidalgo M, Goldstein D, Van Cutsem E, Wei X, Iglesias J, Renschler MF. Increased survival in pancreatic cancer with nab-paclitaxel plus gemcitabine. The New England journal of medicine. 2013;369(18):1691-703. doi: 10.1056/NEJMoa1304369. PubMed PMID: 24131140.
146. Conroy T, Desseigne F, Ychou M, Bouche O, Guimbaud R, Becouarn Y, Adenis A, Raoul JL, Gourgou-Bourgade S, de la Fouchardiere C, Bennouna J, Bachet JB, Khemissa-Akouz F, Pere-Verge D, Delbaldo C, Assenat E, Chauffert B, Michel P, Montoto-Grillot C, Ducreux M, Groupe Tumeurs Digestives of U, Intergroup P. FOLFIRINOX versus gemcitabine for metastatic pancreatic cancer. The New England journal of medicine. 2011;364(19):1817-25. doi: 10.1056/NEJMoa1011923. PubMed PMID: 21561347.
147. Ryan DP, Hong TS, Bardeesy N. Pancreatic adenocarcinoma. The New England journal of medicine. 2014;371(22):2140-1. doi: 10.1056/NEJMc1412266. PubMed PMID: 25427123.
148. Tonnesmann E, Kandolf R, Lewalter T. Chloroquine cardiomyopathy - a review of the literature. Immunopharmacology and immunotoxicology. 2013;35(3):434-42. doi: 10.3109/08923973.2013.780078. PubMed PMID: 23635029.
149. Kasinski AL, Kelnar K, Stahlhut C, Orellana E, Zhao J, Shimer E, Dysart S, Chen X, Bader AG, Slack FJ. A combinatorial microRNA therapeutics approach to suppressing non-small cell lung cancer. Oncogene. 2015;34(27):3547-55. doi: 10.1038/onc.2014.282. PubMed PMID: 25174400; PMCID: 4345154.
150. Krzeszinski JY, Wei W, Huynh H, Jin Z, Wang X, Chang TC, Xie XJ, He L, Mangala LS, Lopez-Berestein G, Sood AK, Mendell JT, Wan Y. miR-34a blocks osteoporosis and bone metastasis by inhibiting osteoclastogenesis and Tgif2. Nature.

2014;512(7515):431-5. doi: 10.1038/nature13375. PubMed PMID: 25043055; PMCID: 4149606.
151. Daige CL, Wiggins JF, Priddy L, Nelligan-Davis T, Zhao J, Brown D. Systemic delivery of a miR34a mimic as a potential therapeutic for liver cancer. Molecular cancer therapeutics. 2014;13(10):2352-60. doi: 10.1158/1535-7163.MCT-14-0209. PubMed PMID: 25053820.
152. Pramanik D, Campbell NR, Karikari C, Chivukula R, Kent OA, Mendell JT, Maitra A. Restitution of tumor suppressor microRNAs using a systemic nanovector inhibits pancreatic cancer growth in mice. Mol Cancer Ther. 2011;10(8):1470-80. doi: 10.1158/1535-7163.MCT-11-0152. PubMed PMID: 21622730; PMCID: 3154495.
153. Wightman B, Ha I, Ruvkun G. Posttranscriptional regulation of the heterochronic gene lin-14 by lin-4 mediates temporal pattern formation in C. elegans. Cell. 1993;75(5):855-62. PubMed PMID: 8252622.
154. Bader AG, Brown D, Winkler M. The promise of microRNA replacement therapy. Cancer research. 2010;70(18):7027-30. doi: 10.1158/0008-5472.CAN-10-2010. PubMed PMID: 20807816; PMCID: 2940943.
155. Hsu SH, Wang B, Kota J, Yu J, Costinean S, Kutay H, Yu L, Bai S, La Perle K, Chivukula RR, Mao H, Wei M, Clark KR, Mendell JR, Caligiuri MA, Jacob ST, Mendell JT, Ghoshal K. Essential metabolic, anti-inflammatory, and anti-tumorigenic functions of miR-122 in liver. The Journal of clinical investigation. 2012;122(8):2871-83. doi: 10.1172/JCI63539. PubMed PMID: 22820288; PMCID: 3408748.
156. Zou Y, Li J, Chen Z, Li X, Zheng S, Yi D, Zhong A, Chen J. miR-29c suppresses pancreatic cancer liver metastasis in an orthotopic implantation model in nude mice and affects survival in pancreatic cancer patients. Carcinogenesis. 2015;36(6):676-84. doi: 10.1093/carcin/bgv027. PubMed PMID: 25863127.
157. Trehoux S, Lahdaoui F, Delpu Y, Renaud F, Leteurtre E, Torrisani J, Jonckheere N, Van Seuningen I. Micro-RNAs miR-29a and miR-330-5p function as tumor suppressors by targeting the MUC1 mucin in pancreatic cancer cells. Biochimica et biophysica acta. 2015;1853(10 Pt A):2392-403. doi: 10.1016/j.bbamcr.2015.05.033. PubMed PMID: 26036346.
158. Morgan RT, Woods LK, Moore GE, Quinn LA, McGavran L, Gordon SG. Human cell line (COLO 357) of metastatic pancreatic adenocarcinoma. International journal of cancer Journal international du cancer. 1980;25(5):591-8. PubMed PMID: 6989766.
159. Long J, Zhang Y, Yu X, Yang J, LeBrun DG, Chen C, Yao Q, Li M. Overcoming drug resistance in pancreatic cancer. Expert opinion on therapeutic targets. 2011;15(7):817-28. doi: 10.1517/14728222.2011.566216. PubMed PMID: 21391891; PMCID: 3111812.
160. Pan X, Arumugam T, Yamamoto T, Levin PA, Ramachandran V, Ji B, Lopez-Berestein G, Vivas-Mejia PE, Sood AK, McConkey DJ, Logsdon CD. Nuclear factor-kappaB p65/relA silencing induces apoptosis and increases gemcitabine effectiveness in a subset of pancreatic cancer cells. Clinical cancer research : an official journal of the American Association for Cancer Research. 2008;14(24):8143-51. doi: 10.1158/1078-0432.CCR-08-1539. PubMed PMID: 19088029; PMCID: 4403242.
161. Arnold NB, Arkus N, Gunn J, Korc M. The histone deacetylase inhibitor suberoylanilide hydroxamic acid induces growth inhibition and enhances gemcitabine-

induced cell death in pancreatic cancer. Clin Cancer Res. 2007;13(1):18-26. doi: 10.1158/1078-0432.CCR-06-0914. PubMed PMID: 17200334.
162. Korzeniewski C, Callewaert DM. An enzyme-release assay for natural cytotoxicity. Journal of immunological methods. 1983;64(3):313-20. PubMed PMID: 6199426.
163. Decker T, Lohmann-Matthes ML. A quick and simple method for the quantitation of lactate dehydrogenase release in measurements of cellular cytotoxicity and tumor necrosis factor (TNF) activity. Journal of immunological methods. 1988;115(1):61-9. PubMed PMID: 3192948.
164. Mann SS, Hammarback JA. Molecular characterization of light chain 3. A microtubule binding subunit of MAP1A and MAP1B. The Journal of biological chemistry. 1994;269(15):11492-7. PubMed PMID: 7908909.
165. Ichimura Y, Kirisako T, Takao T, Satomi Y, Shimonishi Y, Ishihara N, Mizushima N, Tanida I, Kominami E, Ohsumi M, Noda T, Ohsumi Y. A ubiquitin-like system mediates protein lipidation. Nature. 2000;408(6811):488-92. doi: 10.1038/35044114. PubMed PMID: 11100732.
166. Kabeya Y, Mizushima N, Ueno T, Yamamoto A, Kirisako T, Noda T, Kominami E, Ohsumi Y, Yoshimori T. LC3, a mammalian homologue of yeast Apg8p, is localized in autophagosome membranes after processing. The EMBO journal. 2000;19(21):5720-8. doi: 10.1093/emboj/19.21.5720. PubMed PMID: 11060023; PMCID: 305793.
167. He H, Dang Y, Dai F, Guo Z, Wu J, She X, Pei Y, Chen Y, Ling W, Wu C, Zhao S, Liu JO, Yu L. Post-translational modifications of three members of the human MAP1LC3 family and detection of a novel type of modification for MAP1LC3B. The Journal of biological chemistry. 2003;278(31):29278-87. doi: 10.1074/jbc.M303800200. PubMed PMID: 12740394.
168. Tanida I, Ueno T, Kominami E. Human light chain 3/MAP1LC3B is cleaved at its carboxyl-terminal Met121 to expose Gly120 for lipidation and targeting to autophagosomal membranes. The Journal of biological chemistry. 2004;279(46):47704-10. doi: 10.1074/jbc.M407016200. PubMed PMID: 15355958.
169. Wu J, Dang Y, Su W, Liu C, Ma H, Shan Y, Pei Y, Wan B, Guo J, Yu L. Molecular cloning and characterization of rat LC3A and LC3B--two novel markers of autophagosome. Biochemical and biophysical research communications. 2006;339(1):437-42. doi: 10.1016/j.bbrc.2005.10.211. PubMed PMID: 16300744.
170. Zhang XJ, Chen S, Huang KX, Le WD. Why should autophagic flux be assessed? Acta pharmacologica Sinica. 2013;34(5):595-9. doi: 10.1038/aps.2012.184. PubMed PMID: 23474710; PMCID: 4002868.
171. Mizushima N, Yoshimori T. How to interpret LC3 immunoblotting. Autophagy. 2007;3(6):542-5. PubMed PMID: 17611390.
172. Poole B, Ohkuma S. Effect of weak bases on the intralysosomal pH in mouse peritoneal macrophages. The Journal of cell biology. 1981;90(3):665-9. PubMed PMID: 6169733; PMCID: 2111912.
173. Shintani T, Klionsky DJ. Autophagy in health and disease: a double-edged sword. Science. 2004;306(5698):990-5. doi: 10.1126/science.1099993. PubMed PMID: 15528435; PMCID: 1705980.
174. van Schalkwyk DA, Chan XW, Misiano P, Gagliardi S, Farina C, Saliba KJ. Inhibition of Plasmodium falciparum pH regulation by small molecule indole derivatives

results in rapid parasite death. Biochemical pharmacology. 2010;79(9):1291-9. doi: 10.1016/j.bcp.2009.12.025. PubMed PMID: 20067768.
175. Mauvezin C, Nagy P, Juhasz G, Neufeld TP. Autophagosome-lysosome fusion is independent of V-ATPase-mediated acidification. Nature communications. 2015;6:7007. doi: 10.1038/ncomms8007. PubMed PMID: 25959678; PMCID: 4428688.
176. Mukubou H, Tsujimura T, Sasaki R, Ku Y. The role of autophagy in the treatment of pancreatic cancer with gemcitabine and ionizing radiation. International journal of oncology. 2010;37(4):821-8. PubMed PMID: 20811703.
177. Donohue E, Thomas A, Maurer N, Manisali I, Zeisser-Labouebe M, Zisman N, Anderson HJ, Ng SS, Webb M, Bally M, Roberge M. The autophagy inhibitor verteporfin moderately enhances the antitumor activity of gemcitabine in a pancreatic ductal adenocarcinoma model. Journal of Cancer. 2013;4(7):585-96. doi: 10.7150/jca.7030. PubMed PMID: 24069069; PMCID: 3781989.
178. Wu HM, Shao LJ, Jiang ZF, Liu RY. Gemcitabine-Induced Autophagy Protects Human Lung Cancer Cells from Apoptotic Death. Lung. 2016;194(6):959-66. Epub 2016/11/04. doi: 10.1007/s00408-016-9936-6. PubMed PMID: 27604425.
179. Settembre C, Di Malta C, Polito VA, Garcia Arencibia M, Vetrini F, Erdin S, Erdin SU, Huynh T, Medina D, Colella P, Sardiello M, Rubinsztein DC, Ballabio A. TFEB links autophagy to lysosomal biogenesis. Science. 2011;332(6036):1429-33. doi: 10.1126/science.1204592. PubMed PMID: 21617040; PMCID: 3638014.
180. Argani P. MiT family translocation renal cell carcinoma. Seminars in diagnostic pathology. 2015;32(2):103-13. doi: 10.1053/j.semdp.2015.02.003. PubMed PMID: 25758327.
181. Giatromanolaki A, Sivridis E, Mitrakas A, Kalamida D, Zois CE, Haider S, Piperidou C, Pappa A, Gatter KC, Harris AL, Koukourakis MI. Autophagy and lysosomal related protein expression patterns in human glioblastoma. Cancer Biol Ther. 2014;15(11):1468-78. doi: 10.4161/15384047.2014.955719. PubMed PMID: 25482944; PMCID: 4622979.
182. Perera RM, Stoykova S, Nicolay BN, Ross KN, Fitamant J, Boukhali M, Lengrand J, Deshpande V, Selig MK, Ferrone CR, Settleman J, Stephanopoulos G, Dyson NJ, Zoncu R, Ramaswamy S, Haas W, Bardeesy N. Transcriptional control of autophagy-lysosome function drives pancreatic cancer metabolism. Nature. 2015;524(7565):361-5. doi: 10.1038/nature14587. PubMed PMID: 26168401.
183. Klionsky DJ, Cregg JM, Dunn WA, Jr., Emr SD, Sakai Y, Sandoval IV, Sibirny A, Subramani S, Thumm M, Veenhuis M, Ohsumi Y. A unified nomenclature for yeast autophagy-related genes. Developmental cell. 2003;5(4):539-45. PubMed PMID: 14536056.
184. Yen WL, Klionsky DJ. Atg27 is a second transmembrane cycling protein. Autophagy. 2007;3(3):254-6. PubMed PMID: 17297289.
185. Young AR, Chan EY, Hu XW, Kochl R, Crawshaw SG, High S, Hailey DW, Lippincott-Schwartz J, Tooze SA. Starvation and ULK1-dependent cycling of mammalian Atg9 between the TGN and endosomes. Journal of cell science. 2006;119(Pt 18):3888-900. doi: 10.1242/jcs.03172. PubMed PMID: 16940348.
186. Orsi A, Razi M, Dooley HC, Robinson D, Weston AE, Collinson LM, Tooze SA. Dynamic and transient interactions of Atg9 with autophagosomes, but not membrane

integration, are required for autophagy. Molecular biology of the cell. 2012;23(10):1860-73. doi: 10.1091/mbc.E11-09-0746. PubMed PMID: 22456507; PMCID: 3350551.
187. Tang JY, Hsi E, Huang YC, Hsu NC, Chen YK, Chu PY, Chai CY. ATG9A overexpression is associated with disease recurrence and poor survival in patients with oral squamous cell carcinoma. Virchows Archiv : an international journal of pathology. 2013;463(6):737-42. doi: 10.1007/s00428-013-1482-5. PubMed PMID: 24085552.
188. Dai F, Zhang Y, Chen Y. Involvement of miR-29b signaling in the sensitivity to chemotherapy in patients with ovarian carcinoma. Human pathology. 2014;45(6):1285-93. doi: 10.1016/j.humpath.2014.02.008. PubMed PMID: 24767251.
189. Ru P, Steele R, Newhall P, Phillips NJ, Toth K, Ray RB. miRNA-29b suppresses prostate cancer metastasis by regulating epithelial-mesenchymal transition signaling. Mol Cancer Ther. 2012;11(5):1166-73. doi: 10.1158/1535-7163.MCT-12-0100. PubMed PMID: 22402125.
190. Wang B, Li W, Liu H, Yang L, Liao Q, Cui S, Wang H, Zhao L. miR-29b suppresses tumor growth and metastasis in colorectal cancer via downregulating Tiam1 expression and inhibiting epithelial-mesenchymal transition. Cell death & disease. 2014;5:e1335. doi: 10.1038/cddis.2014.304. PubMed PMID: 25032858; PMCID: 4123095.
191. Yang AD, Camp ER, Fan F, Shen L, Gray MJ, Liu W, Somcio R, Bauer TW, Wu Y, Hicklin DJ, Ellis LM. Vascular endothelial growth factor receptor-1 activation mediates epithelial to mesenchymal transition in human pancreatic carcinoma cells. Cancer research. 2006;66(1):46-51. doi: 10.1158/0008-5472.CAN-05-3086. PubMed PMID: 16397214.
192. Rasheed ZA, Yang J, Wang Q, Kowalski J, Freed I, Murter C, Hong SM, Koorstra JB, Rajeshkumar NV, He X, Goggins M, Iacobuzio-Donahue C, Berman DM, Laheru D, Jimeno A, Hidalgo M, Maitra A, Matsui W. Prognostic significance of tumorigenic cells with mesenchymal features in pancreatic adenocarcinoma. Journal of the National Cancer Institute. 2010;102(5):340-51. doi: 10.1093/jnci/djp535. PubMed PMID: 20164446; PMCID: 2831049.
193. Hotz B, Arndt M, Dullat S, Bhargava S, Buhr HJ, Hotz HG. Epithelial to mesenchymal transition: expression of the regulators snail, slug, and twist in pancreatic cancer. Clin Cancer Res. 2007;13(16):4769-76. doi: 10.1158/1078-0432.CCR-06-2926. PubMed PMID: 17699854.
194. Reggiori F, Tooze SA. Autophagy regulation through Atg9 traffic. The Journal of cell biology. 2012;198(2):151-3. doi: 10.1083/jcb.201206119. PubMed PMID: 22826119; PMCID: 3410426.
195. Webber JL, Young AR, Tooze SA. Atg9 trafficking in Mammalian cells. Autophagy. 2007;3(1):54-6. PubMed PMID: 17102588.
196. Mott JL, Kobayashi S, Bronk SF, Gores GJ. mir-29 regulates Mcl-1 protein expression and apoptosis. Oncogene. 2007;26(42):6133-40. doi: 10.1038/sj.onc.1210436. PubMed PMID: 17404574; PMCID: 2432524.
197. Lamouille S, Xu J, Derynck R. Molecular mechanisms of epithelial-mesenchymal transition. Nature reviews Molecular cell biology. 2014;15(3):178-96. doi: 10.1038/nrm3758. PubMed PMID: 24556840; PMCID: 4240281.

198. Taddei ML, Giannoni E, Fiaschi T, Chiarugi P. Anoikis: an emerging hallmark in health and diseases. The Journal of pathology. 2012;226(2):380-93. doi: 10.1002/path.3000. PubMed PMID: 21953325.
199. Frisch SM, Francis H. Disruption of epithelial cell-matrix interactions induces apoptosis. The Journal of cell biology. 1994;124(4):619-26. PubMed PMID: 8106557; PMCID: 2119917.
200. Horbinski C, Mojesky C, Kyprianou N. Live free or die: tales of homeless (cells) in cancer. Am J Pathol. 2010;177(3):1044-52. doi: 10.2353/ajpath.2010.091270. PubMed PMID: 20639456; PMCID: 2928938.
201. Sun C, Yamato T, Furukawa T, Ohnishi Y, Kijima H, Horii A. Characterization of the mutations of the K-ras, p53, p16, and SMAD4 genes in 15 human pancreatic cancer cell lines. Oncology reports. 2001;8(1):89-92. PubMed PMID: 11115575.
202. Noetel A, Kwiecinski M, Elfimova N, Huang J, Odenthal M. microRNA are Central Players in Anti- and Profibrotic Gene Regulation during Liver Fibrosis. Frontiers in physiology. 2012;3:49. doi: 10.3389/fphys.2012.00049. PubMed PMID: 22457651; PMCID: 3307137.
203. Mott JL, Kurita S, Cazanave SC, Bronk SF, Werneburg NW, Fernandez-Zapico ME. Transcriptional suppression of mir-29b-1/mir-29a promoter by c-Myc, hedgehog, and NF-kappaB. Journal of cellular biochemistry. 2010;110(5):1155-64. doi: 10.1002/jcb.22630. PubMed PMID: 20564213; PMCID: 2922950.
204. Schild C, Wirth M, Reichert M, Schmid RM, Saur D, Schneider G. PI3K signaling maintains c-myc expression to regulate transcription of E2F1 in pancreatic cancer cells. Molecular carcinogenesis. 2009;48(12):1149-58. doi: 10.1002/mc.20569. PubMed PMID: 19603422.
205. Rajurkar M, De Jesus-Monge WE, Driscoll DR, Appleman VA, Huang H, Cotton JL, Klimstra DS, Zhu LJ, Simin K, Xu L, McMahon AP, Lewis BC, Mao J. The activity of Gli transcription factors is essential for Kras-induced pancreatic tumorigenesis. Proceedings of the National Academy of Sciences of the United States of America. 2012;109(17):E1038-47. doi: 10.1073/pnas.1114168109. PubMed PMID: 22493246; PMCID: 3340052.
206. Ding ZB, Hui B, Shi YH, Zhou J, Peng YF, Gu CY, Yang H, Shi GM, Ke AW, Wang XY, Song K, Dai Z, Shen YH, Fan J. Autophagy activation in hepatocellular carcinoma contributes to the tolerance of oxaliplatin via reactive oxygen species modulation. Clinical cancer research : an official journal of the American Association for Cancer Research. 2011;17(19):6229-38. doi: 10.1158/1078-0432.CCR-11-0816. PubMed PMID: 21825039.
207. Yoon JH, Ahn SG, Lee BH, Jung SH, Oh SH. Role of autophagy in chemoresistance: regulation of the ATM-mediated DNA-damage signaling pathway through activation of DNA-PKcs and PARP-1. Biochemical pharmacology. 2012;83(6):747-57. doi: 10.1016/j.bcp.2011.12.029. PubMed PMID: 22226932.
208. Sui X, Chen R, Wang Z, Huang Z, Kong N, Zhang M, Han W, Lou F, Yang J, Zhang Q, Wang X, He C, Pan H. Autophagy and chemotherapy resistance: a promising therapeutic target for cancer treatment. Cell death & disease. 2013;4:e838. doi: 10.1038/cddis.2013.350. PubMed PMID: 24113172; PMCID: 3824660.

209. Dimastromatteo J, Brentnall T, Kelly KA. Imaging in pancreatic disease. Nat Rev Gastroenterol Hepatol. 2017;14(2):97-109. doi: 10.1038/nrgastro.2016.144. PubMed PMID: 27826137.
210. Eliasson M, Talback M, Rosen M. Improved survival in both men and women with diabetes between 1980 and 2004--a cohort study in Sweden. Cardiovasc Diabetol. 2008;7:32. Epub 2008/10/22. doi: 10.1186/1475-2840-7-32. PubMed PMID: 18937871; PMCID: PMC2586621.
211. Xiao AY, Tan ML, Wu LM, Asrani VM, Windsor JA, Yadav D, Petrov MS. Global incidence and mortality of pancreatic diseases: a systematic review, meta-analysis, and meta-regression of population-based cohort studies. Lancet Gastroenterol Hepatol. 2016;1(1):45-55. Epub 2017/04/14. doi: 10.1016/S2468-1253(16)30004-8. PubMed PMID: 28404111.
212. Siegel RL, Miller KD, Jemal A. Cancer Statistics, 2017. CA: a cancer journal for clinicians. 2017;67(1):7-30. doi: 10.3322/caac.21387. PubMed PMID: 28055103.
213. Mazur PK, Siveke JT. Genetically engineered mouse models of pancreatic cancer: unravelling tumour biology and progressing translational oncology. Gut. 2012;61(10):1488-500. doi: 10.1136/gutjnl-2011-300756. PubMed PMID: 21873467.
214. Morris JPt, Wang SC, Hebrok M. KRAS, Hedgehog, Wnt and the twisted developmental biology of pancreatic ductal adenocarcinoma. Nat Rev Cancer. 2010;10(10):683-95. doi: 10.1038/nrc2899. PubMed PMID: 20814421; PMCID: PMC4085546.
215. Hingorani SR, Wang L, Multani AS, Combs C, Deramaudt TB, Hruban RH, Rustgi AK, Chang S, Tuveson DA. Trp53R172H and KrasG12D cooperate to promote chromosomal instability and widely metastatic pancreatic ductal adenocarcinoma in mice. Cancer cell. 2005;7(5):469-83. doi: 10.1016/j.ccr.2005.04.023. PubMed PMID: 15894267.
216. Grippo PJ, Tuveson DA. Deploying mouse models of pancreatic cancer for chemoprevention studies. Cancer Prev Res (Phila). 2010;3(11):1382-7. doi: 10.1158/1940-6207.CAPR-10-0258. PubMed PMID: 21045161; PMCID: PMC3242034.
217. Carriere C, Gore AJ, Norris AM, Gunn JR, Young AL, Longnecker DS, Korc M. Deletion of Rb accelerates pancreatic carcinogenesis by oncogenic Kras and impairs senescence in premalignant lesions. Gastroenterology. 2011;141(3):1091-101. doi: 10.1053/j.gastro.2011.05.041. PubMed PMID: 21699781; PMCID: PMC3163782.
218. Biankin AV, Waddell N, Kassahn KS, Gingras MC, Muthuswamy LB, Johns AL, Miller DK, Wilson PJ, Patch AM, Wu J, Chang DK, Cowley MJ, Gardiner BB, Song S, Harliwong I, Idrisoglu S, Nourse C, Nourbakhsh E, Manning S, Wani S, Gongora M, Pajic M, Scarlett CJ, Gill AJ, Pinho AV, Rooman I, Anderson M, Holmes O, Leonard C, Taylor D, Wood S, Xu Q, Nones K, Fink JL, Christ A, Bruxner T, Cloonan N, Kolle G, Newell F, Pinese M, Mead RS, Humphris JL, Kaplan W, Jones MD, Colvin EK, Nagrial AM, Humphrey ES, Chou A, Chin VT, Chantrill LA, Mawson A, Samra JS, Kench JG, Lovell JA, Daly RJ, Merrett ND, Toon C, Epari K, Nguyen NQ, Barbour A, Zeps N, Australian Pancreatic Cancer Genome I, Kakkar N, Zhao F, Wu YQ, Wang M, Muzny DM, Fisher WE, Brunicardi FC, Hodges SE, Reid JG, Drummond J, Chang K, Han Y, Lewis LR, Dinh H, Buhay CJ, Beck T, Timms L, Sam M, Begley K, Brown A, Pai D, Panchal A, Buchner N, De Borja R, Denroche RE, Yung CK, Serra S, Onetto N, Mukhopadhyay D, Tsao MS, Shaw PA, Petersen GM, Gallinger S, Hruban RH, Maitra A,

Iacobuzio-Donahue CA, Schulick RD, Wolfgang CL, Morgan RA, Lawlor RT, Capelli P, Corbo V, Scardoni M, Tortora G, Tempero MA, Mann KM, Jenkins NA, Perez-Mancera PA, Adams DJ, Largaespada DA, Wessels LF, Rust AG, Stein LD, Tuveson DA, Copeland NG, Musgrove EA, Scarpa A, Eshleman JR, Hudson TJ, Sutherland RL, Wheeler DA, Pearson JV, McPherson JD, Gibbs RA, Grimmond SM. Pancreatic cancer genomes reveal aberrations in axon guidance pathway genes. Nature. 2012;491(7424):399-405. doi: 10.1038/nature11547. PubMed PMID: 23103869; PMCID: PMC3530898.
219. Waddell N, Pajic M, Patch AM, Chang DK, Kassahn KS, Bailey P, Johns AL, Miller D, Nones K, Quek K, Quinn MC, Robertson AJ, Fadlullah MZ, Bruxner TJ, Christ AN, Harliwong I, Idrisoglu S, Manning S, Nourse C, Nourbakhsh E, Wani S, Wilson PJ, Markham E, Cloonan N, Anderson MJ, Fink JL, Holmes O, Kazakoff SH, Leonard C, Newell F, Poudel B, Song S, Taylor D, Waddell N, Wood S, Xu Q, Wu J, Pinese M, Cowley MJ, Lee HC, Jones MD, Nagrial AM, Humphris J, Chantrill LA, Chin V, Steinmann AM, Mawson A, Humphrey ES, Colvin EK, Chou A, Scarlett CJ, Pinho AV, Giry-Laterriere M, Rooman I, Samra JS, Kench JG, Pettitt JA, Merrett ND, Toon C, Epari K, Nguyen NQ, Barbour A, Zeps N, Jamieson NB, Graham JS, Niclou SP, Bjerkvig R, Grutzmann R, Aust D, Hruban RH, Maitra A, Iacobuzio-Donahue CA, Wolfgang CL, Morgan RA, Lawlor RT, Corbo V, Bassi C, Falconi M, Zamboni G, Tortora G, Tempero MA, Australian Pancreatic Cancer Genome I, Gill AJ, Eshleman JR, Pilarsky C, Scarpa A, Musgrove EA, Pearson JV, Biankin AV, Grimmond SM. Whole genomes redefine the mutational landscape of pancreatic cancer. Nature. 2015;518(7540):495-501. doi: 10.1038/nature14169. PubMed PMID: 25719666; PMCID: PMC4523082.
220. Ying H, Dey P, Yao W, Kimmelman AC, Draetta GF, Maitra A, DePinho RA. Genetics and biology of pancreatic ductal adenocarcinoma. Genes Dev. 2016;30(4):355-85. doi: 10.1101/gad.275776.115. PubMed PMID: 26883357; PMCID: PMC4762423.
221. Li X, Wu R, Ventura A. The present and future of genome editing in cancer research. Hum Genet. 2016;135(9):1083-92. doi: 10.1007/s00439-016-1713-3. PubMed PMID: 27432158.
222. Tschaharganeh DF, Lowe SW, Garippa RJ, Livshits G. Using CRISPR/Cas to study gene function and model disease in vivo. FEBS J. 2016;283(17):3194-203. doi: 10.1111/febs.13750. PubMed PMID: 27149548; PMCID: PMC5120361.
223. Chira S, Gulei D, Hajitou A, Zimta AA, Cordelier P, Berindan-Neagoe I. CRISPR/Cas9: Transcending the Reality of Genome Editing. Mol Ther Nucleic Acids. 2017;7:211-22. Epub 2017/06/19. doi: 10.1016/j.omtn.2017.04.001. PubMed PMID: 28624197; PMCID: PMC5415201.
224. Chiou SH, Winters IP, Wang J, Naranjo S, Dudgeon C, Tamburini FB, Brady JJ, Yang D, Gruner BM, Chuang CH, Caswell DR, Zeng H, Chu P, Kim GE, Carpizo DR, Kim SK, Winslow MM. Pancreatic cancer modeling using retrograde viral vector delivery and in vivo CRISPR/Cas9-mediated somatic genome editing. Genes Dev. 2015;29(14):1576-85. doi: 10.1101/gad.264861.115. PubMed PMID: 26178787; PMCID: PMC4526740.
225. Yu X, Zhang Y, Chen C, Yao Q, Li M. Targeted drug delivery in pancreatic cancer. Biochimica et biophysica acta. 2010;1805(1):97-104. doi: 10.1016/j.bbcan.2009.10.001. PubMed PMID: 19853645; PMCID: PMC2815202.

226. Ramamoorth M, Narvekar A. Non viral vectors in gene therapy- an overview. J Clin Diagn Res. 2015;9(1):GE01-6. doi: 10.7860/JCDR/2015/10443.5394. PubMed PMID: 25738007; PMCID: PMC4347098.
227. Al-Dosari MS, Gao X. Nonviral gene delivery: principle, limitations, and recent progress. AAPS J. 2009;11(4):671-81. doi: 10.1208/s12248-009-9143-y. PubMed PMID: 19834816; PMCID: PMC2782077.
228. Doiron B, Hu W, Norton L, DeFronzo RA. Lentivirus shRNA Grb10 targeting the pancreas induces apoptosis and improved glucose tolerance due to decreased plasma glucagon levels. Diabetologia. 2012;55(3):719-28. doi: 10.1007/s00125-011-2414-z. PubMed PMID: 22222503.
229. Montini E, Cesana D, Schmidt M, Sanvito F, Bartholomae CC, Ranzani M, Benedicenti F, Sergi LS, Ambrosi A, Ponzoni M, Doglioni C, Di Serio C, von Kalle C, Naldini L. The genotoxic potential of retroviral vectors is strongly modulated by vector design and integration site selection in a mouse model of HSC gene therapy. The Journal of clinical investigation. 2009;119(4):964-75. doi: 10.1172/JCI37630. PubMed PMID: 19307726; PMCID: PMC2662564.
230. Heckl D, Schwarzer A, Haemmerle R, Steinemann D, Rudolph C, Skawran B, Knoess S, Krause J, Li Z, Schlegelberger B, Baum C, Modlich U. Lentiviral vector induced insertional haploinsufficiency of Ebf1 causes murine leukemia. Molecular therapy : the journal of the American Society of Gene Therapy. 2012;20(6):1187-95. doi: 10.1038/mt.2012.59. PubMed PMID: 22472950; PMCID: PMC3369288.
231. Raper SE, DeMatteo RP. Adenovirus-mediated in vivo gene transfer and expression in normal rat pancreas. Pancreas. 1996;12(4):401-10. PubMed PMID: 8740409.
232. Ayuso E, Chillon M, Agudo J, Haurigot V, Bosch A, Carretero A, Otaegui PJ, Bosch F. In vivo gene transfer to pancreatic beta cells by systemic delivery of adenoviral vectors. Hum Gene Ther. 2004;15(8):805-12. doi: 10.1089/1043034041648426. PubMed PMID: 15319037.
233. Wang AY, Peng PD, Ehrhardt A, Storm TA, Kay MA. Comparison of adenoviral and adeno-associated viral vectors for pancreatic gene delivery in vivo. Hum Gene Ther. 2004;15(4):405-13. doi: 10.1089/104303404322959551. PubMed PMID: 15053865.
234. Sigalla J, David A, Anegon I, Fiche M, Huvelin JM, Boeffard F, Cassard A, Soulillou JP, Le Mauff B. Adenovirus-mediated gene transfer into isolated mouse adult pancreatic islets: normal beta-cell function despite induction of an anti-adenovirus immune response. Hum Gene Ther. 1997;8(13):1625-34. doi: 10.1089/hum.1997.8.13-1625. PubMed PMID: 9322095.
235. McClane SJ, Chirmule N, Burke CV, Raper SE. Characterization of the immune response after local delivery of recombinant adenovirus in murine pancreas and successful strategies for readministration. Hum Gene Ther. 1997;8(18):2207-16. doi: 10.1089/hum.1997.8.18-2207. PubMed PMID: 9449374.
236. Wang Z, Zhu T, Rehman KK, Bertera S, Zhang J, Chen C, Papworth G, Watkins S, Trucco M, Robbins PD, Li J, Xiao X. Widespread and stable pancreatic gene transfer by adeno-associated virus vectors via different routes. Diabetes. 2006;55(4):875-84. PubMed PMID: 16567506.
237. Xiao X, Guo P, Prasadan K, Shiota C, Peirish L, Fischbach S, Song Z, Gaffar I, Wiersch J, El-Gohary Y, Husain SZ, Gittes GK. Pancreatic cell tracing, lineage tagging

and targeted genetic manipulations in multiple cell types using pancreatic ductal infusion of adeno-associated viral vectors and/or cell-tagging dyes. Nat Protoc. 2014;9(12):2719-24. Epub 2014/10/31. doi: 10.1038/nprot.2014.183. PubMed PMID: 25356582; PMCID: PMC4734891.
238. Cheng H, Wolfe SH, Valencia V, Qian K, Shen L, Phillips MI, Chang LJ, Zhang YC. Efficient and persistent transduction of exocrine and endocrine pancreas by adeno-associated virus type 8. J Biomed Sci. 2007;14(5):585-94. Epub 2007/03/28. doi: 10.1007/s11373-007-9159-1. PubMed PMID: 17387636.
239. Guo P, Xiao X, El-Gohary Y, Criscimanna A, Prasadan K, Rymer C, Shiota C, Wiersch J, Gaffar I, Esni F, Gittes GK. Specific transduction and labeling of pancreatic ducts by targeted recombinant viral infusion into mouse pancreatic ducts. Laboratory investigation; a journal of technical methods and pathology. 2013;93(11):1241-53. Epub 2013/10/09. doi: 10.1038/labinvest.2013.113. PubMed PMID: 24100509.
240. Xiao X, Gaffar I, Guo P, Wiersch J, Fischbach S, Peirish L, Song Z, El-Gohary Y, Prasadan K, Shiota C, Gittes GK. M2 macrophages promote beta-cell proliferation by up-regulation of SMAD7. Proceedings of the National Academy of Sciences of the United States of America. 2014;111(13):E1211-20. Epub 2014/03/19. doi: 10.1073/pnas.1321347111. PubMed PMID: 24639504; PMCID: PMC3977272.
241. Xiao X, Prasadan K, Guo P, El-Gohary Y, Fischbach S, Wiersch J, Gaffar I, Shiota C, Gittes GK. Pancreatic duct cells as a source of VEGF in mice. Diabetologia. 2014;57(5):991-1000. Epub 2014/02/19. doi: 10.1007/s00125-014-3179-y. PubMed PMID: 24535231; PMCID: PMC3986695.
242. Chen M, Maeng K, Nawab A, Francois RA, Bray JK, Reinhard MK, Boye SL, Hauswirth WW, Kaye FJ, Aslanidi G, Srivastava A, Zajac-Kaye M. Efficient Gene Delivery and Expression in Pancreas and Pancreatic Tumors by Capsid-Optimized AAV8 Vectors. Hum Gene Ther Methods. 2017;28(1):49-59. doi: 10.1089/hgtb.2016.089. PubMed PMID: 28125909.
243. Loiler SA, Tang Q, Clarke T, Campbell-Thompson ML, Chiodo V, Hauswirth W, Cruz P, Perret-Gentil M, Atkinson MA, Ramiya VK, Flotte TR. Localized gene expression following administration of adeno-associated viral vectors via pancreatic ducts. Molecular therapy : the journal of the American Society of Gene Therapy. 2005;12(3):519-27. doi: 10.1016/j.ymthe.2005.04.017. PubMed PMID: 15979413.
244. Kota J, Handy CR, Haidet AM, Montgomery CL, Eagle A, Rodino-Klapac LR, Tucker D, Shilling CJ, Therlfall WR, Walker CM, Weisbrode SE, Janssen PM, Clark KR, Sahenk Z, Mendell JR, Kaspar BK. Follistatin gene delivery enhances muscle growth and strength in nonhuman primates. Science translational medicine. 2009;1(6):6ra15. doi: 10.1126/scitranslmed.3000112. PubMed PMID: 20368179; PMCID: PMC2852878.
245. Bennett J, Wellman J, Marshall KA, McCague S, Ashtari M, DiStefano-Pappas J, Elci OU, Chung DC, Sun J, Wright JF, Cross DR, Aravand P, Cyckowski LL, Bennicelli JL, Mingozzi F, Auricchio A, Pierce EA, Ruggiero J, Leroy BP, Simonelli F, High KA, Maguire AM. Safety and durability of effect of contralateral-eye administration of AAV2 gene therapy in patients with childhood-onset blindness caused by RPE65 mutations: a follow-on phase 1 trial. Lancet. 2016;388(10045):661-72. doi: 10.1016/S0140-6736(16)30371-3. PubMed PMID: 27375040.
246. Hastie E, Samulski RJ. Adeno-associated virus at 50: a golden anniversary of discovery, research, and gene therapy success--a personal perspective. Hum Gene Ther.

2015;26(5):257-65. doi: 10.1089/hum.2015.025. PubMed PMID: 25807962; PMCID: PMC4442590.
247. McCarty DM, Monahan PE, Samulski RJ. Self-complementary recombinant adeno-associated virus (scAAV) vectors promote efficient transduction independently of DNA synthesis. Gene Ther. 2001;8(16):1248-54. doi: 10.1038/sj.gt.3301514. PubMed PMID: 11509958.
248. McCarty DM, Fu H, Monahan PE, Toulson CE, Naik P, Samulski RJ. Adeno-associated virus terminal repeat (TR) mutant generates self-complementary vectors to overcome the rate-limiting step to transduction in vivo. Gene Ther. 2003;10(26):2112-8. doi: 10.1038/sj.gt.3302134. PubMed PMID: 14625565.
249. McCarty DM. Self-complementary AAV vectors; advances and applications. Molecular therapy : the journal of the American Society of Gene Therapy. 2008;16(10):1648-56. doi: 10.1038/mt.2008.171. PubMed PMID: 18682697.
250. McClane SJ, Hamilton TE, Burke CV, Raper SE. Functional consequences of adenovirus-mediated murine pancreatic gene transfer. Hum Gene Ther. 1997;8(6):739-46. doi: 10.1089/hum.1997.8.6-739. PubMed PMID: 9113513.
251. Rehman KK, Trucco M, Wang Z, Xiao X, Robbins PD. AAV8-mediated gene transfer of interleukin-4 to endogenous beta-cells prevents the onset of diabetes in NOD mice. Molecular therapy : the journal of the American Society of Gene Therapy. 2008;16(8):1409-16. doi: 10.1038/mt.2008.116. PubMed PMID: 18560422; PMCID: PMC3560428.
252. Shimony N, Bendayan M, Elkin G, Ben-nun-Shaul O, Abd-El-Latif M, Scherzer P, Arbel O, Ziv E, Krasny L, Pizov G, Oppenheim A, Haviv YS. Pancreatic acinar and islet cell infection by low-dose SV40 administration. Pancreas. 2008;36(4):411-6. doi: 10.1097/MPA.0b013e31815d349b. PubMed PMID: 18437088.
253. Phillips N, Kay MA. Characterization of vector-based delivery of neurogenin-3 in murine diabetes. Hum Gene Ther. 2014;25(7):651-61. doi: 10.1089/hum.2013.206. PubMed PMID: 24635696; PMCID: PMC4098120.
254. Griffin MA, Restrepo MS, Abu-El-Haija M, Wallen T, Buchanan E, Rokhlina T, Chen YH, McCray PB, Jr., Davidson BL, Divekar A, Uc A. A novel gene delivery method transduces porcine pancreatic duct epithelial cells. Gene Ther. 2014;21(2):123-30. doi: 10.1038/gt.2013.62. PubMed PMID: 24257348; PMCID: PMC3946305.
255. Nakai H, Fuess S, Storm TA, Muramatsu S, Nara Y, Kay MA. Unrestricted hepatocyte transduction with adeno-associated virus serotype 8 vectors in mice. J Virol. 2005;79(1):214-24. doi: 10.1128/JVI.79.1.214-224.2005. PubMed PMID: 15596817; PMCID: PMC538708.
256. Inagaki K, Fuess S, Storm TA, Gibson GA, McTiernan CF, Kay MA, Nakai H. Robust systemic transduction with AAV9 vectors in mice: efficient global cardiac gene transfer superior to that of AAV8. Molecular therapy : the journal of the American Society of Gene Therapy. 2006;14(1):45-53. doi: 10.1016/j.ymthe.2006.03.014. PubMed PMID: 16713360; PMCID: PMC1564441.
257. GuhaSarkar D, Su Q, Gao G, Sena-Esteves M. Systemic AAV9-IFNbeta gene delivery treats highly invasive glioblastoma. Neuro Oncol. 2016;18(11):1508-18. Epub 2016/05/20. doi: 10.1093/neuonc/now097. PubMed PMID: 27194146; PMCID: PMC5063516.

258. Mendell JR, Sahenk Z, Malik V, Gomez AM, Flanigan KM, Lowes LP, Alfano LN, Berry K, Meadows E, Lewis S, Braun L, Shontz K, Rouhana M, Clark KR, Rosales XQ, Al-Zaidy S, Govoni A, Rodino-Klapac LR, Hogan MJ, Kaspar BK. A phase 1/2a follistatin gene therapy trial for becker muscular dystrophy. Molecular therapy : the journal of the American Society of Gene Therapy. 2015;23(1):192-201. doi: 10.1038/mt.2014.200. PubMed PMID: 25322757; PMCID: PMC4426808.
259. Mendell JR, Rodino-Klapac LR, Rosales XQ, Coley BD, Galloway G, Lewis S, Malik V, Shilling C, Byrne BJ, Conlon T, Campbell KJ, Bremer WG, Taylor LE, Flanigan KM, Gastier-Foster JM, Astbury C, Kota J, Sahenk Z, Walker CM, Clark KR. Sustained alpha-sarcoglycan gene expression after gene transfer in limb-girdle muscular dystrophy, type 2D. Ann Neurol. 2010;68(5):629-38. doi: 10.1002/ana.22251. PubMed PMID: 21031578; PMCID: PMC2970162.
260. Clark KR, Liu X, McGrath JP, Johnson PR. Highly purified recombinant adeno-associated virus vectors are biologically active and free of detectable helper and wild-type viruses. Hum Gene Ther. 1999;10(6):1031-9. doi: 10.1089/10430349950018427. PubMed PMID: 10223736.
261. Hruban RH, Adsay NV, Albores-Saavedra J, Compton C, Garrett ES, Goodman SN, Kern SE, Klimstra DS, Kloppel G, Longnecker DS, Luttges J, Offerhaus GJ. Pancreatic intraepithelial neoplasia: a new nomenclature and classification system for pancreatic duct lesions. Am J Surg Pathol. 2001;25(5):579-86. PubMed PMID: 11342768.
262. Jimenez V, Ayuso E, Mallol C, Agudo J, Casellas A, Obach M, Munoz S, Salavert A, Bosch F. In vivo genetic engineering of murine pancreatic beta cells mediated by single-stranded adeno-associated viral vectors of serotypes 6, 8 and 9. Diabetologia. 2011;54(5):1075-86. doi: 10.1007/s00125-011-2070-3. PubMed PMID: 21311856.
263. Sato T, Miyashita E, Yamauchi H, Matsuno S. The role of surgical treatment for chronic pancreatitis. Annals of surgery. 1986;203(3):266-71. PubMed PMID: 2420294; PMCID: PMC1251088.
264. Sherman S, Lehman GA. ERCP- and endoscopic sphincterotomy-induced pancreatitis. Pancreas. 1991;6(3):350-67. PubMed PMID: 1713676.
265. Laukkarinen JM, Van Acker GJ, Weiss ER, Steer ML, Perides G. A mouse model of acute biliary pancreatitis induced by retrograde pancreatic duct infusion of Na-taurocholate. Gut. 2007;56(11):1590-8. Epub 2007/06/27. doi: 10.1136/gut.2007.124230. PubMed PMID: 17591621; PMCID: PMC2095649.
266. Wildi S, Kleeff J, Mayerle J, Zimmermann A, Bottinger EP, Wakefield L, Buchler MW, Friess H, Korc M. Suppression of transforming growth factor beta signalling aborts caerulein induced pancreatitis and eliminates restricted stimulation at high caerulein concentrations. Gut. 2007;56(5):685-92. doi: 10.1136/gut.2006.105833. PubMed PMID: 17135311; PMCID: PMC1942167.
267. Testoni PA, Bagnolo F, Caporuscio S, Lella F. Serum amylase measured four hours after endoscopic sphincterotomy is a reliable predictor of postprocedure pancreatitis. Am J Gastroenterol. 1999;94(5):1235-41. doi: 10.1111/j.1572-0241.1999.01072.x. PubMed PMID: 10235200.
268. Braganza JM, Lee SH, McCloy RF, McMahon MJ. Chronic pancreatitis. Lancet. 2011;377(9772):1184-97. doi: 10.1016/S0140-6736(10)61852-1. PubMed PMID: 21397320.

269. Hyman DM, Taylor BS, Baselga J. Implementing Genome-Driven Oncology. Cell. 2017;168(4):584-99. doi: 10.1016/j.cell.2016.12.015. PubMed PMID: 28187282.
270. Kannan R, Ventura A. The CRISPR revolution and its impact on cancer research. Swiss Med Wkly. 2015;145:w14230. doi: 10.4414/smw.2015.14230. PubMed PMID: 26661454.
271. Dow LE. Modeling Disease In Vivo With CRISPR/Cas9. Trends Mol Med. 2015;21(10):609-21. doi: 10.1016/j.molmed.2015.07.006. PubMed PMID: 26432018; PMCID: PMC4592741.
272. Kato T, Takada S. In vivo and in vitro disease modeling with CRISPR/Cas9. Brief Funct Genomics. 2017;16(1):13-24. doi: 10.1093/bfgp/elw031. PubMed PMID: 27497066.
273. Han YC, Vidigal JA, Mu P, Yao E, Singh I, Gonzalez AJ, Concepcion CP, Bonetti C, Ogrodowski P, Carver B, Selleri L, Betel D, Leslie C, Ventura A. An allelic series of miR-17 approximately 92-mutant mice uncovers functional specialization and cooperation among members of a microRNA polycistron. Nature genetics. 2015;47(7):766-75. doi: 10.1038/ng.3321. PubMed PMID: 26029871; PMCID: 4485521.
274. Concepcion CP, Bonetti C, Ventura A. The microRNA-17-92 family of microRNA clusters in development and disease. Cancer J. 2012;18(3):262-7. doi: 10.1097/PPO.0b013e318258b60a. PubMed PMID: 22647363; PMCID: PMC3592780.
275. Xie J, Ameres SL, Friedline R, Hung JH, Zhang Y, Xie Q, Zhong L, Su Q, He R, Li M, Li H, Mu X, Zhang H, Broderick JA, Kim JK, Weng Z, Flotte TR, Zamore PD, Gao G. Long-term, efficient inhibition of microRNA function in mice using rAAV vectors. Nat Methods. 2012;9(4):403-9. doi: 10.1038/nmeth.1903. PubMed PMID: 22388288; PMCID: PMC3420816.
276. He X, Xie J, Zhang D, Su Q, Sai X, Bai R, Chen C, Luo X, Gao G, Pan W. Recombinant adeno-associated virus-mediated inhibition of microRNA-21 protects mice against the lethal schistosome infection by repressing both IL-13 and transforming growth factor beta 1 pathways. Hepatology. 2015;61(6):2008-17. doi: 10.1002/hep.27671. PubMed PMID: 25546547; PMCID: PMC4441614.
277. Sicard F, Gayral M, Lulka H, Buscail L, Cordelier P. Targeting miR-21 for the therapy of pancreatic cancer. Molecular therapy : the journal of the American Society of Gene Therapy. 2013;21(5):986-94. Epub 2013/03/14. doi: 10.1038/mt.2013.35. PubMed PMID: 23481326; PMCID: PMC3666633.
278. van Rooij E, Kauppinen S. Development of microRNA therapeutics is coming of age. EMBO Mol Med. 2014;6(7):851-64. doi: 10.15252/emmm.201100899. PubMed PMID: 24935956; PMCID: PMC4119351.
279. Knabel MK, Ramachandran K, Karhadkar S, Hwang HW, Creamer TJ, Chivukula RR, Sheikh F, Clark KR, Torbenson M, Montgomery RA, Cameron AM, Mendell JT, Warren DS. Systemic Delivery of scAAV8-Encoded MiR-29a Ameliorates Hepatic Fibrosis in Carbon Tetrachloride-Treated Mice. PloS one. 2015;10(4):e0124411. doi: 10.1371/journal.pone.0124411. PubMed PMID: 25923107; PMCID: PMC4414421.
280. Ma HI, Hueng DY, Shui HA, Han JM, Wang CH, Lai YH, Cheng SY, Xiao X, Chen MT, Yang YP. Intratumoral decorin gene delivery by AAV vector inhibits brain glioblastomas and prolongs survival of animals by inducing cell differentiation. Int J Mol Sci. 2014;15(3):4393-414. doi: 10.3390/ijms15034393. PubMed PMID: 24625664; PMCID: PMC3975403.

281. Wu QJ, Gong CY, Luo ST, Zhang DM, Zhang S, Shi HS, Lu L, Yan HX, He SS, Li DD, Yang L, Zhao X, Wei YQ. AAV-mediated human PEDF inhibits tumor growth and metastasis in murine colorectal peritoneal carcinomatosis model. BMC cancer. 2012;12:129. doi: 10.1186/1471-2407-12-129. PubMed PMID: 22462776; PMCID: PMC3338360.
282. Crommentuijn MH, Kantar R, Noske DP, Vandertop WP, Badr CE, Wurdinger T, Maguire CA, Tannous BA. Systemically administered AAV9-sTRAIL combats invasive glioblastoma in a patient-derived orthotopic xenograft model. Mol Ther Oncolytics. 2016;3:16017. doi: 10.1038/mto.2016.17. PubMed PMID: 27382645; PMCID: PMC4916948.
283. Streck CJ, Dickson PV, Ng CY, Zhou J, Hall MM, Gray JT, Nathwani AC, Davidoff AM. Antitumor efficacy of AAV-mediated systemic delivery of interferon-beta. Cancer Gene Ther. 2006;13(1):99-106. doi: 10.1038/sj.cgt.7700878. PubMed PMID: 16052229.
284. Wang B, Li J, Xiao X. Adeno-associated virus vector carrying human minidystrophin genes effectively ameliorates muscular dystrophy in mdx mouse model. Proceedings of the National Academy of Sciences of the United States of America. 2000;97(25):13714-9. doi: 10.1073/pnas.240335297. PubMed PMID: 11095710; PMCID: 17641.
285. Haidet AM, Rizo L, Handy C, Umapathi P, Eagle A, Shilling C, Boue D, Martin PT, Sahenk Z, Mendell JR, Kaspar BK. Long-term enhancement of skeletal muscle mass and strength by single gene administration of myostatin inhibitors. Proceedings of the National Academy of Sciences of the United States of America. 2008;105(11):4318-22. doi: 10.1073/pnas.0709144105. PubMed PMID: 18334646; PMCID: PMC2393740.
286. Rodino-Klapac LR, Janssen PM, Shontz KM, Canan B, Montgomery CL, Griffin D, Heller K, Schmelzer L, Handy C, Clark KR, Sahenk Z, Mendell JR, Kaspar BK. Micro-dystrophin and follistatin co-delivery restores muscle function in aged DMD model. Hum Mol Genet. 2013;22(24):4929-37. doi: 10.1093/hmg/ddt342. PubMed PMID: 23863459; PMCID: PMC3895965.
287. Bachem MG, Schneider E, Gross H, Weidenbach H, Schmid RM, Menke A, Siech M, Beger H, Grunert A, Adler G. Identification, culture, and characterization of pancreatic stellate cells in rats and humans. Gastroenterology. 1998;115(2):421-32. PubMed PMID: 9679048.
288. Fu Q, Shi H, Ni W, Shi M, Meng L, Zhang H, Ren Y, Guo F, Wang P, Qiao J, Jia B, Chen C. Lentivirus-mediated Bos taurus bta-miR-29b overexpression interferes with bovine viral diarrhoea virus replication and viral infection-related autophagy by directly targeting ATG14 and ATG9A in Madin-Darby bovine kidney cells. The Journal of general virology. 2015;96(Pt 1):85-94. doi: 10.1099/vir.0.067140-0. PubMed PMID: 25234643.
289. Amodio N, Stamato MA, Gulla AM, Morelli E, Romeo E, Raimondi L, Pitari MR, Ferrandino I, Misso G, Caraglia M, Perrotta I, Neri A, Fulciniti M, Rolfo C, Anderson KC, Munshi NC, Tagliaferri P, Tassone P. Therapeutic Targeting of miR-29b/HDAC4 Epigenetic Loop in Multiple Myeloma. Molecular cancer therapeutics. 2016;15(6):1364-75. doi: 10.1158/1535-7163.MCT-15-0985. PubMed PMID: 27196750.
290. Sousa CM, Biancur DE, Wang X, Halbrook CJ, Sherman MH, Zhang L, Kremer D, Hwang RF, Witkiewicz AK, Ying H, Asara JM, Evans RM, Cantley LC, Lyssiotis

CA, Kimmelman AC. Pancreatic stellate cells support tumour metabolism through autophagic alanine secretion. Nature. 2016;536(7617):479-83. Epub 2016/08/12. doi: 10.1038/nature19084. PubMed PMID: 27509858; PMCID: PMC5228623.
291. Heerboth S, Housman G, Leary M, Longacre M, Byler S, Lapinska K, Willbanks A, Sarkar S. EMT and tumor metastasis. Clin Transl Med. 2015;4:6. Epub 2015/04/09. doi: 10.1186/s40169-015-0048-3. PubMed PMID: 25852822; PMCID: PMC4385028.
292. Chaffer CL, Weinberg RA. A perspective on cancer cell metastasis. Science. 2011;331(6024):1559-64. doi: 10.1126/science.1203543. PubMed PMID: 21436443.
293. Gong J, Li J, Wang Y, Liu C, Jia H, Jiang C, Wang Y, Luo M, Zhao H, Dong L, Song W, Wang F, Wang W, Zhang J, Yu J. Characterization of microRNA-29 family expression and investigation of their mechanistic roles in gastric cancer. Carcinogenesis. 2014;35(2):497-506. doi: 10.1093/carcin/bgt337. PubMed PMID: 24130168.
294. Tan M, Wu J, Cai Y. Suppression of Wnt signaling by the miR-29 family is mediated by demethylation of WIF-1 in non-small-cell lung cancer. Biochemical and biophysical research communications. 2013;438(4):673-9. doi: 10.1016/j.bbrc.2013.07.123. PubMed PMID: 23939044.
295. Wang X, Liu S, Cao L, Zhang T, Yue D, Wang L, Ping Y, He Q, Zhang C, Wang M, Chen X, Gao Q, Wang D, Zhang Z, Wang F, Yang L, Li J, Huang L, Zhang B, Zhang Y. miR-29a-3p suppresses cell proliferation and migration by downregulating IGF1R in hepatocellular carcinoma. Oncotarget. 2017;8(49):86592-603. doi: 10.18632/oncotarget.21246. PubMed PMID: 29156819; PMCID: 5689709.
296. Lu Y, Hu J, Sun W, Li S, Deng S, Li M. MiR-29c inhibits cell growth, invasion, and migration of pancreatic cancer by targeting ITGB1. OncoTargets and therapy. 2016;9:99-109. doi: 10.2147/OTT.S92758. PubMed PMID: 26766915; PMCID: 4699545.
297. Koshizuka K, Kikkawa N, Hanazawa T, Yamada Y, Okato A, Arai T, Katada K, Okamoto Y, Seki N. Inhibition of integrin beta1-mediated oncogenic signalling by the antitumor microRNA-29 family in head and neck squamous cell carcinoma. Oncotarget. 2018;9(3):3663-76. Epub 2018/02/10. doi: 10.18632/oncotarget.23194. PubMed PMID: 29423074; PMCID: PMC5790491.
298. He B, Xiao YF, Tang B, Wu YY, Hu CJ, Xie R, Yang X, Yu ST, Dong H, Zhao XY, Li JL, Yang SM. hTERT mediates gastric cancer metastasis partially through the indirect targeting of ITGB1 by microRNA-29a. Scientific reports. 2016;6:21955. Epub 2016/02/24. doi: 10.1038/srep21955. PubMed PMID: 26903137; PMCID: PMC4763288.
299. Gay LA, Sethuraman S, Thomas M, Turner PC, Renne R. Modified Cross-Linking, Ligation, and Sequencing of Hybrids (qCLASH) Identifies Kaposi's Sarcoma-Associated Herpesvirus MicroRNA Targets in Endothelial Cells. J Virol. 2018;92(8). Epub 2018/02/02. doi: 10.1128/JVI.02138-17. PubMed PMID: 29386283; PMCID: PMC5874430.
300. Wang T, Yu H, Hughes NW, Liu B, Kendirli A, Klein K, Chen WW, Lander ES, Sabatini DM. Gene Essentiality Profiling Reveals Gene Networks and Synthetic Lethal Interactions with Oncogenic Ras. Cell. 2017;168(5):890-903 e15. Epub 2017/02/07. doi: 10.1016/j.cell.2017.01.013. PubMed PMID: 28162770; PMCID: PMC5445660.
301. Dooley J, Lagou V, Garcia-Perez JE, Himmelreich U, Liston A. miR-29a-deficiency does not modify the course of murine pancreatic acinar carcinoma.

Oncotarget. 2017;8(16):26911-7. Epub 2017/05/04. doi: 10.18632/oncotarget.15850. PubMed PMID: 28460473; PMCID: PMC5432306.
302. Klimstra DS. Nonductal neoplasms of the pancreas. Mod Pathol. 2007;20 Suppl 1:S94-112. Epub 2007/05/09. doi: 10.1038/modpathol.3800686. PubMed PMID: 17486055.
303. van Rooij E, Purcell AL, Levin AA. Developing microRNA therapeutics. Circulation research. 2012;110(3):496-507. doi: 10.1161/CIRCRESAHA.111.247916. PubMed PMID: 22302756.
304. Chakraborty C, Sharma AR, Sharma G, Doss CGP, Lee SS. Therapeutic miRNA and siRNA: Moving from Bench to Clinic as Next Generation Medicine. Molecular therapy Nucleic acids. 2017;8:132-43. doi: 10.1016/j.omtn.2017.06.005. PubMed PMID: 28918016; PMCID: 5496203.
305. Slabakova E, Culig Z, Remsik J, Soucek K. Alternative mechanisms of miR-34a regulation in cancer. Cell death & disease. 2017;8(10):e3100. doi: 10.1038/cddis.2017.495. PubMed PMID: 29022903; PMCID: 5682661.
306. Robbins M, Judge A, Ambegia E, Choi C, Yaworski E, Palmer L, McClintock K, MacLachlan I. Misinterpreting the therapeutic effects of small interfering RNA caused by immune stimulation. Human gene therapy. 2008;19(10):991-9. doi: 10.1089/hum.2008.131. PubMed PMID: 18713023.
307. Wang H, Jiang Y, Peng H, Chen Y, Zhu P, Huang Y. Recent progress in microRNA delivery for cancer therapy by non-viral synthetic vectors. Adv Drug Deliv Rev. 2015;81:142-60. Epub 2014/12/03. doi: 10.1016/j.addr.2014.10.031. PubMed PMID: 25450259.
308. Riley MK, Vermerris W. Recent Advances in Nanomaterials for Gene Delivery-A Review. Nanomaterials (Basel). 2017;7(5). Epub 2017/04/30. doi: 10.3390/nano7050094. PubMed PMID: 28452950; PMCID: PMC5449975.
309. Herrera-Carrillo E, Liu YP, Berkhout B. Improving miRNA Delivery by Optimizing miRNA Expression Cassettes in Diverse Virus Vectors. Hum Gene Ther Methods. 2017;28(4):177-90. Epub 2017/07/18. doi: 10.1089/hgtb.2017.036. PubMed PMID: 28712309; PMCID: PMC5568016.
310. Duhachek-Muggy S, Zolkiewska A. ADAM12-L is a direct target of the miR-29 and miR-200 families in breast cancer. BMC Cancer. 2015;15:93. Epub 2015/04/18. doi: 10.1186/s12885-015-1108-1. PubMed PMID: 25886595; PMCID: PMC4352249.
311. Zhu J, Xiong G, Fu H, Evers BM, Zhou BP, Xu R. Chaperone Hsp47 Drives Malignant Growth and Invasion by Modulating an ECM Gene Network. Cancer research. 2015;75(8):1580-91. doi: 10.1158/0008-5472.CAN-14-1027. PubMed PMID: 25744716; PMCID: 4401637.
312. Cittelly DM, Finlay-Schultz J, Howe EN, Spoelstra NS, Axlund SD, Hendricks P, Jacobsen BM, Sartorius CA, Richer JK. Progestin suppression of miR-29 potentiates dedifferentiation of breast cancer cells via KLF4. Oncogene. 2013;32(20):2555-64. Epub 2012/07/04. doi: 10.1038/onc.2012.275. PubMed PMID: 22751119; PMCID: PMC4236860.
313. Cochrane DR, Jacobsen BM, Connaghan KD, Howe EN, Bain DL, Richer JK. Progestin regulated miRNAs that mediate progesterone receptor action in breast cancer. Molecular and cellular endocrinology. 2012;355(1):15-24. doi: 10.1016/j.mce.2011.12.020. PubMed PMID: 22330642; PMCID: 4716679.

314. Kwon JJ, Willy JA, Quirin KA, Wek RC, Korc M, Yin XM, Kota J. Novel role of miR-29a in pancreatic cancer autophagy and its therapeutic potential. Oncotarget. 2016;7(44):71635-50. doi: 10.18632/oncotarget.11928. PubMed PMID: 27626694; PMCID: 5342107.
315. Sun XJ, Liu BY, Yan S, Jiang TH, Cheng HQ, Jiang HS, Cao Y, Mao AW. MicroRNA-29a Promotes Pancreatic Cancer Growth by Inhibiting Tristetraprolin. Cellular physiology and biochemistry : international journal of experimental cellular physiology, biochemistry, and pharmacology. 2015;37(2):707-18. doi: 10.1159/000430389. PubMed PMID: 26356262.
316. Dagogo-Jack I, Shaw AT. Tumour heterogeneity and resistance to cancer therapies. Nat Rev Clin Oncol. 2018;15(2):81-94. Epub 2017/11/09. doi: 10.1038/nrclinonc.2017.166. PubMed PMID: 29115304.
317. Flynt AS, Lai EC. Biological principles of microRNA-mediated regulation: shared themes amid diversity. Nature reviews Genetics. 2008;9(11):831-42. doi: 10.1038/nrg2455. PubMed PMID: 18852696; PMCID: 2729318.
318. Bartel DP, Chen CZ. Micromanagers of gene expression: the potentially widespread influence of metazoan microRNAs. Nature reviews Genetics. 2004;5(5):396-400. doi: 10.1038/nrg1328. PubMed PMID: 15143321.
319. Brenner JL, Jasiewicz KL, Fahley AF, Kemp BJ, Abbott AL. Loss of individual microRNAs causes mutant phenotypes in sensitized genetic backgrounds in C. elegans. Current biology : CB. 2010;20(14):1321-5. doi: 10.1016/j.cub.2010.05.062. PubMed PMID: 20579881; PMCID: 2946380.
320. Erhard F, Haas J, Lieber D, Malterer G, Jaskiewicz L, Zavolan M, Dolken L, Zimmer R. Widespread context dependency of microRNA-mediated regulation. Genome Res. 2014;24(6):906-19. doi: 10.1101/gr.166702.113. PubMed PMID: 24668909; PMCID: PMC4032855.
321. Jacobsen A, Silber J, Harinath G, Huse JT, Schultz N, Sander C. Analysis of microRNA-target interactions across diverse cancer types. Nature structural & molecular biology. 2013;20(11):1325-32. doi: 10.1038/nsmb.2678. PubMed PMID: 24096364; PMCID: 3982325.
322. Plaisier CL, Pan M, Baliga NS. A miRNA-regulatory network explains how dysregulated miRNAs perturb oncogenic processes across diverse cancers. Genome Res. 2012;22(11):2302-14. doi: 10.1101/gr.133991.111. PubMed PMID: 22745231; PMCID: 3483559.
323. Park SY, Lee JH, Ha M, Nam JW, Kim VN. miR-29 miRNAs activate p53 by targeting p85 alpha and CDC42. Nature structural & molecular biology. 2009;16(1):23-9. doi: 10.1038/nsmb.1533. PubMed PMID: 19079265.

Curriculum Vitae

Jason Jae-Hyuk Kwon

Education

Bachelor of Arts, Biology: Wabash College, Crawfordsville, IN - 2011

Ph.D. in Medical & Molecular Genetics: IU/IUPUI Indianapolis, IN - 2018

Honors, Awards, Fellowships Research and Training Experience

2017 IBMG - IUSM Travel Grant Recipient

Poster Presentation – AACR Annual Meeting, Chicago, IL, April 2018

F31 Predoctoral Ruth L. Kirschstein National Research Service Award (NRSA)

National Cancer Institute (NCI), National Institutes of Health (NIH), September 2017 – Present

Cagiantas Scholarship

Indiana University BioMedical Gateway Program - Cagiantas Scholarship, September 2016 – August 2017

2016 IBMG - IUSM Travel Grant Recipient

Autophagy in Stress, Development, and Disease – Gordon Research Conference, Ventura, CA, March 2016

Cancer Biology Training Program Fellowship

Indiana University Simon Cancer Center, September 2015 – August 2016

1st Place - Best Science by Graduate Student

2015 IU Simon Cancer Center Annual Cancer Research Day, Indianapolis, IN, June 2015

1st Place - Pre-doctoral Poster Presentation

Indiana Health and Industry Forum – Regulatory Pathways for Regenerative Medicine Symposium, Indianapolis, IN, May 2015

2015 IU Simon Cancer Center - AACR Travel Grant Recipient

Poster Presentation - AACR Annual Meeting, Philadelphia, PA, April 2015

Cole Lecture Series - Invited Speaker

MicroRNA and Cancer. Wabash College, September 2013

Professional Experience

2016-2017 Student Representative - Medical and Molecular Genetics Department

Indiana University School of Medicine, Indianapolis, IN

2016-2017 Grant Reviewer – IBMG Travel Grant Committee

Indiana University School of Medicine, Indianapolis, IN

Summer 2011 Research Intern

Korean Research Institute of Biological Sciences and Biotechnology, Dajeon, Korea

2009 – 2011 Lab Teaching Assistant

Wabash College, Crawfordsville, IN

Summer 2009 Research Intern

IU School of Medicine: Dept. of Molecular Biology and Pathology, Indianapolis, IN

Summer 2009 Lab Assistant Instructor (Methods in Molec Bio and Pathology [G890]

IU School of Medicine: Dept. of Molecular Biology and Pathology, Indianapolis, IN

Presentations

Kwon JJ, Nabinger SC, Vega Z, Sahu SS, Saxena R, Korc M, and Kota J. Role and potential use of microRNA-29 to target the pancreatic cancer stoma. Submitted abstract and accepted Poster Presentation for 17th Annual Meeting of the American Society of Gene and Cell Therapy, Washington, DC, May 2014

Kwon JJ, Nabinger SC, Vega Z, Sahu SS, Saxena R, Korc M, and Kota J. Role and potential use of microRNA-29 to target the pancreatic cancer stoma. Poster Presentation for 2014 IU Simon Cancer Center Annual Cancer Research Day, Indianapolis, IN, June 2014

Kwon JJ, Nabinger SC, Alluri RK, Vega Z, Sahu SS, Sater Z, Yu Z, Gore AJ, Nalepa G, Saxena R, Korc M, and Kota J. Pathophysiological role of microRNA-29 in pancreatic cancer stroma. Poster Presentation for 106th AACR Annual Meeting, Philadelphia, PA, April 2015

Kwon JJ, Nabinger SC, Alluri RK, Vega Z, Sahu SS, Sater Z, Yu Z, Gore AJ, Nalepa G, Saxena R, Korc M, and Kota J. Pathophysiological role of microRNA-29 in pancreatic cancer stroma.

Poster Presentation for Indiana Health and Industry Forum – Regulatory Pathways for Regenerative Medicine Symposium, Indianapolis, IN, May 2015

Kwon JJ, Willy JA, Wek RC, Korc M, Yin XM, and Kota J. 2016. Novel role of miR-29 in pancreatic cancer autophagy and its therapeutic potential. Autophagy in Stress, Development, and Disease – Gordon Research Conference, Ventura, CA, March 2016

Kwon JJ, Quirin K, Aljoufi A, Nafiseh A, and Kota J. Restoration of MYC-repressed miR-29 in pancreatic cancer cells leads to increased reactive oxygen species and gemcitabine sensitization. AACR Annual Meeting, Washington DC, April 2017

Publications

Quirin KA*, **Kwon JJ***, Aljoufi A, Temm CJ, Jacobsen M, Sandusky GE, Shontz K, Chicoine LG, Clark KR, Mendell JT, Kota J. (2017). Safety and efficacy of AAV retrograde pancreatic ductal gene delivery in normal and pancreatic cancer mice. Molecular Therapy: Methods & Clinical Development. PMID: 29349096 **Equal Contributions* - Cover page featured image

Kota J, Hancock J, **Kwon JJ**, and Korc M. (2017). Pancreatic Cancer: Stroma and its current and emerging targeted therapies. Cancer Letters. PMID: 28093284

Yarlagadda S, Thota A, Bansal R, **Kwon JJ**, Korc M, Kota J. (2016). Methods for microRNA profiling in cancer. Epigenetics and Gene Expression in cancer, inflammatory and immune diseases. Springer Methods in Pharmacology and Toxicology book series. ISSN: 15572153

Kwon JJ, Willy JA, Wek RC, Korc M, Yin XM, and Kota J. (2016). Novel role of miR-29 in pancreatic cancer autophagy and its therapeutic potential. Oncotarget 11928. PMID: 27626694

Kwon JJ*, Nabinger CS*, Alluri KR, Vega Z, Sahu SS, Sater AZ, Yu Z, Gore A J, Nalepa G, Saxena R, Korc M, Kota J (2015). Pathophysiological role of microRNA-29 in pancreatic cancer stroma. Scientific Reports 5:11450. PMCID: PMC4476113. **Equal Contributions*